Continuous Myoelectric Prediction of Future Ankle Kinematics and Kinetics for the Control of Active Powered Prostheses

Erika Virginia Zabre González
Marquette University

CONTINUOUS MYOELECTRIC PREDICTION OF FUTURE ANKLE KINEMATICS AND KINETICS FOR THE CONTROL OF ACTIVE POWERED PROSTHESES

by

Erika Virginia Zabre González, B.S.

A Dissertation submitted to the Faculty of the Graduate School,
Marquette University,
in Partial Fulfillment of the Requirements for
the Degree of Doctor of Philosophy

Milwaukee, Wisconsin

December 2022

ABSTRACT
CONTINUOUS MYOELECTRIC PREDICTION OF FUTURE ANKLE KINEMATICS AND KINETICS FOR THE CONTROL OF ACTIVE POWERED PROSTHESES

Erika Virginia Zabre González, B.S.

Marquette University, 2022

The purpose of this dissertation is to develop a continuous predictive model of gait that incorporates user intent, vis-à-vis surface electromyography (EMG) signals of the lower limb, to continuously predict future ankle kinematics and kinetics across multiple terrains and their transitions for the control of an active ankle-foot prosthesis. Continuously predicting variations in gait, particularly during transitions and noncyclic activities, is limited in lower limb prostheses. Despite performance improvements in active lower limb prostheses, there remains a need for robust and accurate control that incorporates direct user intent (e.g., myoelectric control) to limit physical and cognitive demands and provide more natural gait across terrains. Efforts to use EMG signals have mainly focused on discrete control approaches that are reactive to changes in terrain, can introduce undesirable delays, and limit the amputee's control over the prosthesis. A nonlinear autoregressive neural network with exogenous (external) inputs (NARX) was used to continuously predict desired ankle angle and moment of the sound limb of transtibial amputees using EMG of the prosthetic side and sound-limb shank velocity as inputs. The approach of mapping prosthetic-side EMG with sound-limb ankle dynamics is a step forward to establish a more normal gait by overlaying the dynamics of the sound limb onto the prosthesis to create symmetric gait patterns. The autoregressive model accurately predicted (up to 142 ms ahead of time) ankle dynamics using natural patterns of either within-socket residual shank or thigh EMG of the prosthetic side across ambulation conditions (level walking, stair ascent, and stair descent) and staircase transitions. Importantly, the model leveraged EMG and shank velocity inputs to a similar degree for the prediction of gait, enabling accurate responses to noncyclic events. The NARX model also had the ability to characterize the normal range of ankle dynamics of able-bodied individuals using either shank or thigh muscle activity. The use of natural, yet altered in amputees, muscle activity with information about limb state, coupled with a closed-loop predictive design, could provide intuitive user-driven and robust prosthetic control capable of counteracting delays and proactively modifying gait in response to observed changes in terrain. The model provides opportunities for continuous myoelectric control using different muscle groups and takes an important step toward continuous real-time feedback control of active lower limb prostheses and robotic systems.

This dissertation is dedicated to
the memory of My Mother Irene Virginia González Herrera,
whose love and support are deeply missed every day of my life.

ACKNOWLEDGMENTS

Erika Virginia Zabre González, B.S.

I would like to express my gratitude to my dissertation advisor Dr. Scott Beardsley for his trust, guidance, and encouragement, especially when I needed to hear that my work was exceptional. In addition, I want to thank him, Dr. Barbara Silver-Thorn, Dr. Philip Voglewede, and Dr. Sara Koehler, part of my dissertation committee, for making me feel like colleagues, and not just a student, by promoting an environment of horizontality and respect that allowed me to evolve into the researcher I am today. I would also like to thank Dr. Andrew Starsky for agreeing to be part of my committee and making me think beyond the specifics of my project.

I would like to extend my appreciation to Tom Current for his insights on prosthetic fabrication, his time spent perfecting the fabrication of the test sockets, and his assistance during data collection. Testing of the amputee volunteers would not have been possible without him. Special thanks to Tom Silman for helping me set up the research part of Human Performance Lab and the unconditional and countless hours spent in the machine shop. Thanks to Dr. Gerald Harris for his assistance during the integration of the gait analysis system, for inviting me to be part of this own projects, and for always being interested in my progress. I am grateful to Dr. Brian Schmit for seeing my potential and providing funding opportunities.

I would like to acknowledge Dr. Lara Riem, Max Stillings, and Molly Erickson for their technical assistance with data collection and gait analysis, and every undergraduate student who contributed to this project. I would like to recognize the study volunteers for their invaluable time, even if that meant going home sore.

The endless love, support, and encouragement of my friends, love ones, and family were instrumental to complete this achievement. Jacqueline R., Uriel M., and Abdiel Q., my support away from home, thank you for your immeasurable care throughout these years, your words of reassurance, and for proofreading my documents at four in the morning; I could always count on you. I want to honor my father Cesar Zabre, my sister Andrea Carolina, my brother Cesar Manuel, and my grandmother Guadalupe with this dissertation. All their sacrifices have allowed me to accomplish one of the highest accolades of my education and professional development. And, I can finally answer their persistent question of “When are you going to finish?” with “Ya!”

TABLE OF CONTENTS

LIST OF TABLES

LIST OF FIGURES

CHAPTER 1: INTRODUCTION AND BACKGROUND

1.1 INTRODUCTION

Advances in robotic systems and human interface design have facilitated the development of rehabilitation devices, including state-of-the-art active ankle-foot prostheses (Sun et al., 2014; Au et al., 2009; Grimmer et al., 2016; Culver et al., 2018). For successful rehabilitation of lower limb amputees, prostheses seek to mimic the biomechanical patterns of gait that occur during daily living activities. In spite of these advancements, most lower limb amputees develop altered muscle activity and biomechanical patterns of gait to maintain stability and compensate for limitations in the prosthesis (Herr & Grabowski, 2012; S. Huang & Ferris, 2012; Seyedali et al., 2012). Despite performance improvements in active (i.e., able to generate power during propulsion) lower limb prostheses over passive designs, there remains a need for robust and accurate control techniques that incorporate user intent to limit physical and cognitive demands and provide a more natural gait across terrains (e.g., level ground, stairs, ramps) and environmental conditions.

Continuously predicting variations in gait, particularly during transitions (e.g., between terrains) and noncyclic activities, is limited in commercially available lower limb prostheses. Electromyography (EMG) measurements of muscle activity and kinematic analyses of the lower limb suggest that timing in the local patterns of muscle activity is a key discriminant of gait while traversing different types of terrains (Lencioni et al., 2019; Wentink et al., 2013, 2014). The integration of EMG signals in a continuous predictive model of gait could provide intuitive and robust prosthetic control by

counteracting delays (e.g., sensing, signal processing, and actuation), and proactively (rather than reactively as in current prostheses) modifying gait in response to unexpected perturbations and upcoming changes in terrain.

Continuous gait models have been proposed to eliminate the need for a discrete state-based control to differentiate joint motion and terrains, and in the case of myoelectric control, to reduce cognitive and physical demands on the user and eliminate the need for high quality, independent muscle signals (Farmer et al., 2014; J. Chen et al., 2018; Gupta et al., 2020; Ardestani et al., 2014; Keleş & Yucesoy, 2020). Ankle kinematics and kinetics, common targets for impedance control of ankle-foot prostheses, have been continuously estimated using surface EMG signals, in an effort to incorporate direct user intention. However, simultaneous estimation of both ankle kinematics and kinetics across multiple types of terrain, including transitions between them, has not been demonstrated. Moreover, almost all models characterize ankle dynamics using a reactive (i.e., next time-step estimate) rather than a predictive (i.e., several steps into the future) approach.

The purpose of this dissertation is to develop a continuous predictive model of gait that incorporates user intent, vis-à-vis surface EMG of the lower limb, to continuously predict future ankle kinematics and kinetics across multiple terrains and the transitions between them for the control of an active ankle-foot prosthesis. The proposed model was characterized to examine its ability to predict the normal range of ankle dynamics associated with healthy ambulation, to determine the feasibility of using natural patterns of residual EMG within the prosthetic socket from transtibial amputees, and to

identify alternative proximal sources of EMG signals further from the ankle joint and shank.

This chapter establishes a foundation on the topics related to this work by providing an overview of the changes in gait and muscle activity following lower limb amputation, the current state of lower limb prostheses and myoelectric control, and a review of continuous gait models for the estimation of ankle dynamics.

1.2 AMPUTEE POPULATION

1.2.1 Prevalence and Leading Causes of Limb Amputation

The estimated number of people with limb amputation worldwide varies from source to source since detailed records are not kept in many countries. The prevalence of limb amputation has been reported to vary by age, geographical region, and leading cause (e.g., dysvascular disease, trauma, cancer, war). Trauma (e.g., road accidents, falls) is the leading cause of amputations in low income countries [e.g., Iran, Tanzania, South Asia countries; (Rouhani & Mohajerzadeh, 2013; Shaw et al., 2018)] whereas dysvascular disease (including peripheral arterial disease and diabetes) is the primary cause of amputations in high income countries [e.g., United States, England, Canada; (Ahmad et al., 2014; Imam et al., 2017)]. In 2017, the World Health Organization estimated that 0.5% of the world population required a prosthesis or an orthosis with the global incidence of limb loss estimated between 7.6 and 13 million people (World Health Organization, 2017). However, the 2017 Global Burden of Disease study estimated that globally, approximately 58 million people were living with a limb amputation due to trauma alone (McDonald et al., 2021). Regardless of region and cause, the most frequent

level of amputation is transtibial (below-the-knee, 47%), followed by transfemoral amputations (above-the-knee, 31%) (World Health Organization et al., 2004).

In the United States, nearly 1.2 million hospital discharges involved some type of limb loss or limb congenital deficiency between 1988 and 1996 (Dillingham et al., 2002). In 1996 alone, 115,000 to 159,000 people underwent a lower limb amputation with the vast majority (95%) related to dysvascular disease (including peripheral arterial disease and diabetes) (Dillingham et al., 2002; Owings & Kozak, 1998). With the absence of recent national statistics, Ziegler- Graham et al. estimated the prevalence of limb loss to be 1.6 million in 2005 and projected the future amputee population to increase to 3.6 million by 2050 (Ziegler-Graham et al., 2008). In the 2005 estimate, dysvascular disease (including peripheral arterial disease and diabetes) accounted for 54% of total body amputations while trauma and cancer accounted for 45% and 1%, respectively. For the same year, it was estimated that a total of 1 million people had some sort of lower limb amputation, with over half being major amputations (transtibial and transfemoral). Over the coming decades, the number of people requiring a lower limb prosthesis is expected to increase due to the progressive aging and growing of the world's population, the rising number of dysvascular and diabetic cases, and the increasing number of road accidents and cancer cases.

1.2.2 Gait and Muscle Activity of Lower Limb Amputees

A hallmark of human locomotion is that it continuously adapts to changes in the environment to maintain balance, reacts to unpredictable perturbations in gait and balance, and predictively adjusts walking patterns to changes in the terrain (Choi &

Bastian, 2007; Pearson, 2000), which are major challenges to lower limb amputees. Amputees often develop altered muscle activity and biomechanical patterns of gait to maintain stability and compensate for limitations in the prosthesis (Herr & Grabowski, 2012; S. Huang & Ferris, 2012; Seyedali et al., 2012; Silver-Thorn et al., 2012). Gait asymmetries between the sound and prosthetic limb are primarily attributed to limitations in the prostheses and are a major concern in achieving normal, symmetric gait (Bateni & Olney, 2002; Pröbsting et al., 2020; Schmalz et al., 2007; Sinitski et al., 2012). The practical need to adapt to such asymmetries often leads to differences in kinematics and kinetics of the sound limb when compared to able-bodied controls (Grabowski & D'Andrea, 2013; Rábago & Wilken, 2016). In transtibial amputees, peak plantarflexion moment from commercially available ankle-foot prostheses differs from that of able-bodied individuals by as much as 28% during level walking (Ferris et al., 2012; Pröbsting et al., 2020; Rábago & Wilken, 2016; Sinitski et al., 2012), 41% during stair descent (Aldridge et al., 2012; Schmalz et al., 2007; Sinitski et al., 2012; Vack et al., 1999), and 50% during stair descent (Schmalz et al., 2007; Sinitski et al., 2012). Moreover, timing differences relative to the desired profile were present in the peak moments of those commercial prostheses. While the influence of push-off has not been linked to fall risk (Müller et al., 2019), limb asymmetry and offsets in the timing of push-off have been associated with increased metabolic rates, excessive limb loading, osteoarthritis, back pain, and can affect gait stability and stride variability among lower limb amputees (Hill & Herr, 2013; Kulkarni et al., 2005; Miller et al., 2001; Montgomery & Grabowski, 2018; Morgenroth et al., 2011).

Human locomotion is achieved by anticipatory changes in EMG activation (and corresponding muscle contraction) and the subsequent joint and segment movements by means of coordinated synergies of the upper limbs, trunk, and lower limbs (Dietz et al., 1987; Hirschfeld & Forssberg, 1991). As a result of these synergies, EMG activity from the residual shank muscles and *intact* (residual for transfemoral amputees) thigh muscles of the prosthetic side of amputees possess information about ankle motion during gait. In the case of transtibial amputees, muscle activity of the residual shank muscles is directly and strongly coupled to ankle dynamics due to its proximity to the ankle joint. However, the biomechanical coupling can be disrupted by surgical techniques and the cause of amputation (Brown et al., 2014; Clites et al., 2018). In contrast, thigh muscles are indirectly coupled to ankle biomechanics due to the increased number of degrees of freedom associated with the knee joint.

Several studies have shown that good quality and consistent EMG signals can be recorded within-socket from residual muscles of transtibial and transfemoral amputees (Hefferman et al., 2015; S. Huang & Ferris, 2012; Kannape & Herr, 2014; Silver-Thorn et al., 2012). Although amputees are able to activate their residual muscles, EMG patterns are different from those of healthy individuals and highly variable across amputees due to atrophy and changes in muscular attachment points after amputation (S. Huang & Ferris, 2012; Seyedali et al., 2012). Within-socket EMG signal variability can be sensitive to physiological and skin-electrode interface changes (e.g., motion artifacts, electrode location variation, fatigue, sweat accumulation, socket alignment, limb volume, pressure distribution) because residual muscles are subject to weight bearing conditions and daily donning/doffing of the prosthesis introduces disturbances (Wagner et al., 2020;

Hefferman et al., 2015; Nakamura & Hahn, 2017). Although the use of embedded electrodes in the socket or liner minimizes design complexity and facilitates donning and doffing of the prosthesis, it can compromise socket suspension and user comfort. In the case of transtibial amputees, besides poor intersegmental synergies, *intact* thigh muscle activity of the prosthetic side has been shown to be less variable than residual muscles and more similar to normal muscle activation patterns (S. Huang & Ferris, 2012; Seyedali et al., 2012) providing more reliable signals. Furthermore, the acquisition of EMG signals outside the socket may enhance long-term comfort, and reduce motion artifacts that occur within-socket during repeated loading and unloading of the prosthesis during gait.

1.3 LOWER LIMB PROSTHESES

Accommodation, balance, and joint motion are major requirements for lower limb prostheses to mimic biomechanical movement patterns and restore normal gait. During daily activities, lower limb prostheses need to accommodate different types of surfaces (e.g., concrete, gravel) and terrains (e.g., stairs, ramps) and the noncyclic movements that occur during the transition between terrains. Terrain accommodation and shock absorption during heel strike will then reduce the risk of stumbling and weight-bearing forces. To mimic normal biomechanical patterns, lower limb prostheses need to achieve the physiological range of joint motion and provide propulsion to limit the metabolic energy expenditure needed to maintain gait.

1.3.1 Passive and Semi-Active Lower Limb Prostheses

Current lower limb prostheses can be classified into passive, semi-active, and active designs. Commercial passive and semi-active lower limb prostheses are widely available. Passive prostheses use materials and elements with fixed spring and damping properties, and can range from simple designs such as the SACH (solid-ankle cushion-heel) foot to complex designs such as ESR (energy-storing-and-returning) feet. Passive prostheses are designed to either be compliant to increase shock absorption at heel strike and accommodate various terrains, or to be stiff and act as a leaf spring to provide some propulsion, but usually not both. Semi-active lower limb prostheses (previously categorized as *powered*) improve gait by adjusting their mechanical properties with minimal actuation. Some examples of semi-active ankle-foot prostheses include the Proprio Foot® (Ossur, Reykjavík, Iceland) and the Meridium (Ottobock, Duderstadt, Germany), which utilize a microprocessor to dynamically alter the behavior of the prosthesis and react to changes in the environment. However, they do not provide additional power to directly propel the user's movement. Ultimately, passive and semi-active lower limb prostheses are unable to meet the needs to restore normal gait of lower limb amputees.

1.3.2 Active Powered Lower Limb Prostheses

Active powered lower limb prostheses can enhance amputee ambulation by adding power into different phases of the gait cycle, power that has been lost due to amputation of the lower limb muscles. The terms *active* and *powered* have been used interchangeably in the research community for prostheses that are able to generate power

during propulsion. Developing control algorithms for active lower limb prostheses is challenging and impacts the level of human adaptation to the device. Controllers for active lower limb prostheses range from closed-loop finite state machines (FSMs) driven by electromechanical sensors intrinsic to the prosthesis [e.g., inertial sensors, position encoders; (Au et al., 2009; Cherelle et al., 2016; Shultz & Goldfarb, 2018; Sun et al., 2014; Q. Wang et al., 2014)], to continuous proportional myoelectric control [based on the amplitude of EMG signals; (Dawley et al., 2013; Hoover et al., 2012; S. Huang et al., 2016; S. Huang & Huang, 2018, 2019)], as well as hybrid strategies combining electromechanical and myoelectric signals (Au et al., 2008; M. Liu et al., 2017; Spanias et al., 2018; J. Wang et al., 2013; Kannape & Herr, 2014, 2016).

Currently, there are several active ankle-foot prostheses, at different stages of development and commercialization. The Empower (Ottobock, Duderstadt, Germany) is currently the only commercially available active ankle-foot prosthesis. The BiOM's (the preceding model of the Empower) controller uses FSM to identify the current state of the prosthesis during gait and select among low-level controllers. The system is capable of providing push-off power [torque (i.e., moment) control], varying joint stiffness during stance phase (impedance control), and completing toe clearance during swing (position control) (Au et al., 2009). In a research setting, myoelectric control in combination with FSM has been implemented to switch from level walking to stair descent using the residual tibialis anterior and gastrocnemius muscles (Au et al., 2008), and implemented as FSM-based proportional control, via the residual gastrocnemius, to modulate torque gain during level walking (J. Wang et al., 2013) and stair ascent push-off (Kannape & Herr, 2014).

The Vanderbilt-Goldfarb active ankle-foot prosthesis employs an impedance-based supervisory FSM controller to switch between four activity controllers (standing, walking, stair ascent, and stair descent) where the ankle behavior within each activity is controlled by separate sets of FSMs (Culver et al., 2018; Shultz et al., 2016). Experiments with a single transtibial amputee showed that the prosthesis provided benefits (ascent power assistance, descent power dissipation and bilateral shock absorption) over passive designs during stair ambulation and that the amputee was able to intentionally switch between activities but with some difficulty. Similarly, Cherelle et al., Zheng and Shen and Wang et al. have used FSM-based impedance (stiffness, damping) controllers to actuate their ankle-foot prostheses (Cherelle et al., 2014, 2016; Q. Wang et al., 2014; Zheng & Shen, 2015).

The Walk-Run Ankle is the latest generation of the SPARKy (Spring Ankle with Regenerative Kinetics) and is advertised as Ruggedized Odyssey Ankle (SpringActive, Tempe, Arizona, United States). The Walk-Run Ankle controller uses the phase planes of the angular velocity and acceleration of the tibia to continuously control standing, walking, and running using predefined lookup tables (gait selection, gait cycle percent determination, angle and moment motor trajectories) from experimental gait studies of able-bodied individuals. Using the latest design and complete controller, the system was validated with an able-bodied individual using an orthosis fixed parallel to the prosthesis (Grimmer et al., 2016) and with a transtibial amputee during constant-speed treadmill walking (Grimmer et al., 2017). Running was achieved in transtibial amputees using the SPARKy (Hitt et al., 2010) and a preliminary version of the Ruggedized Odyssey Ankle (Ward et al., 2015).

The Michigan-Ferris ankle-foot prosthesis is the only design that has validated continuous proportional myoelectric control (S. Huang et al., 2016). During gait, the inflation pressure of pneumatic artificial plantarflexor muscles is proportional to the contraction of the residual gastrocnemius. Using this system, transtibial amputees were able to control ankle plantarflexion during level treadmill walking only when given an explicit muscle contraction goal via real-time visual feedback. Over time, volitional actuation of the prosthesis became physically and cognitively demanding for the amputee caused by the need to constantly attend to the visual feedback and intentional muscle contraction.

The Marquette-Voglewede active ankle-foot can be controlled by state-based and continuous control algorithms. In the state-based controller, a FSM determines the phases and sub-phases of the gait cycle, and as a consequence, selects between moment or position control to regulate the motor's behavior (Sun & Voglewede, 2012). This controller design was tested with a transtibial amputee during level ground walking (Sun et al., 2014). Although it outperformed a passive prosthesis during push-off, the prosthesis was not able to fully return to neutral position due to delays in the microcontroller and the actuation following sensor signaling of the swing phase (max. 50 ms). This limitation can be eliminated by incorporating a continuous predictive model to signal user intent before the swing phase. For that reason, a predictive stiffness controller was developed and bench tested to control the prosthesis continuously (Klein & Voglewede, 2018). Other active ankle-foot prototypes developed by Ficanha et al. and Yu et al. have reported similar time delays of 40 ms for the system delay between the input and output of a two degrees of freedom cable-driven prosthesis (Ficanha et al.,

2016), and a maximum of 40 ms for the pull-in response time of a bypass restriction valve of an electrohydrostatic-based prosthesis (Yu, 2017; Yu et al., 2019).

Active ankle-foot prostheses have normalized biomechanical patterns to some degree, accommodated common activities, decreased metabolic energy cost when compared to passive prostheses, and provided net propulsion work and shock absorption. Despite these improvements, continuous and predictive adaptation to changes in the environment (gait adaptability) is still a major challenge for lower limb amputees due to the limitations in the existing mechanical designs and control algorithms (Kannape & Herr, 2016). Gait adaptability can be improved by incorporating information on user intent (e.g., via EMG activity), allowing users to modify prosthetic joint dynamics in a more natural, and less physically and cognitively demanding way. The following sections describe in depth the advantages and limitations of the current control systems.

1.3.2.1 Finite State Machine Control

The use of FSM control in combination with electromechanical sensors embedded in the prosthesis itself or worn on the residual limb has become an increasingly common approach due to their high precision and reliability. FSM-based control is constrained by a relatively small number of pre-defined, discrete states and locomotion modes, and the need to define switching rules for transitioning between states. User intention is deduced indirectly by prosthetic sensors which introduce undesirable delays and/or requires the user to intentionally switch between modes based on anticipated changes in terrain. Consequently, the system has a limited ability to deal with novel movements and noncyclic activities whereas intentional switching may increase physical and cognitive

load on the user, particularly in complex environments (Culver et al., 2018; Zhang et al., 2015).

Continuous control approaches using intrinsic prosthetic sensors to unify the gait cycle have also been explored. Joint phase-based methods have been developed to control ankle-foot and multi-joint leg prostheses using shank and hip kinematics, respectively (Hitt et al., 2010; Holgate et al., 2009; Quintero et al., 2018). While walking across slopes at varying speeds and running have been demonstrated, phase-based algorithms have limitations responding to noncyclic and novel movements since they need distinguishable phase planes for each ambulation activity. Discrete and continuous approaches designed around intrinsic prosthetic sensors provide high fidelity feedback about past limb state (indirect user intent) but are generally reactive (rather than predictive) to gait and environmental changes, and can introduce delays in the actuation of the prosthesis.

1.3.2.2 Myoelectric Control

Myoelectric control systems involve the detection, classification, and application of EMG signals to understand and control a wide variety of devices such as exoskeletons (Hayashi et al., 2005; Lenzi et al., 2011), wheelchairs (Felzer & Freisleben, 2002; Moon et al., 2005), and multifunction limb prostheses (Kuiken et al., 2009; Light et al., 2002; Tommasi et al., 2013). Myoelectric control has been used commercially in upper limb prostheses for decades (Össur, 2019; Ottobock, 2014). However, implementation in lower limb prostheses has been limited due in part to the development of physical systems that can achieve the power-to-weight demands of walking (e.g., load-bearing conditions) in combination with the challenges in the design of electrode-socket interfaces and the

reliable acquisition of EMG signals through bulkier residual limb soft tissue (e.g., subject to limb volume fluctuations, sweat accumulation, pistoning) (Fleming et al., 2021; Tucker et al., 2015).

In contrast to upper limb prostheses, fewer degrees of freedom must be controlled to restore limb function with lower limb prostheses. For transtibial amputees, most active ankle-foot prostheses focus on restoring motion in the sagittal plane only (e.g., ankle plantarflexion and dorsiflexion), further reducing the requisite degrees of freedom. This maximizes the ratio of myoelectric signal sources to degrees of freedom to several muscle sites (e.g., tibialis anterior, medial and lateral gastrocnemius), making the myoelectric control potentially more feasible and robust. Additionally, advancements in wearable and implantable sensor technology [e.g., knit band sensors (S. Lee et al., 2018), prosthetic liner with embedded electrodes (Reissman et al., 2018), flexible dry electrodes (Kisannagar et al., 2020)] are promising for implementation in real-time myoelectric lower limb prostheses.

For a seamless and intuitive device actuation, prosthetic controllers must recognize the user's locomotive intention given changes in the environment. Although electromechanical prosthetic sensors have high repeatability and reproducibility, they introduce an intrinsic delay and the resulting control must infer human intention through secondary information such as gait events or joint mechanics. As a result, their actuation is reactive to user's biomechanical changes. EMG measurement of muscle activity enables a direct prediction of intended biomechanics. The electrical activity of the muscle precedes force generation, and consequently, limb movement, providing opportunities for an intuitive and volitional control (Cavanagh & Komi, 1979; Merletti & Parker, 2004).

For example, physiological electromechanical delays from onset of surface EMG to the neuromotor drive can range between 4 to 170 ms for lower leg muscles (Go et al., 2018). Additionally, EMG-driven control is particularly useful in responding to sudden changes to the environment. Still, the use of EMG sensors poses challenges in achieving robust control due to low signal quality, variability associated with sensor placement and electrode-skin conductivity, cross-talk between nearby muscles, and signal processing for feature extraction. In spite of these issues, surface EMG have been extensively researched as an alternate, minimally-invasive source of control signals.

1.3.2.2.1 EMG-driven Finite State Machines

Studies have demonstrated that it is possible to record EMG signals within the prosthetic socket of transtibial and transfemoral amputees (Au et al., 2008; S. Huang et al., 2016; Kannape & Herr, 2016; Tkach et al., 2013). Current efforts to incorporate user intent using EMG activity of shank and thigh muscles for myoelectric control have primarily focus on pattern recognition (Au et al., 2008; M. Liu et al., 2017; Spanias et al., 2018; Tkach et al., 2013), and proportional control (J. Wang et al., 2013; Kannape & Herr, 2014, 2016). These hybrid state-based myoelectric approaches use within-socket EMG signals to select discrete locomotion modes, or to modify prosthetic behavior within a single state using proportional control (e.g., motor torque gain) with the prosthesis being controlled by FSM. The combination of direct user intent, via EMG signals, and information about limb state, via electromechanical prosthetic sensors, has been shown to increase robustness and accuracy of locomotion mode detection (B. Chen & Wang, 2015; Tkach & Hargrove, 2013; H. Huang et al., 2011). EMG-driven FSMs can

improve flexibility, allowing amputees to transverse different terrains and adapt to different walking speeds. However, control may not be as intuitive, requiring the user to learn novel muscle activation patterns, and remains constrained to the control of predefined locomotion modes, limiting the amputee's control over the prosthesis.

Spanias et al. used EMG activity from residual thigh muscles (rectus femoris, semitendinosus, tensor fascia latae, and adductor magnus) of transfemoral amputees to control a lower limb prosthesis with actively powered knee and ankle joints (Spanias et al., 2018). By means of deep belief neural networks, the intent recognition algorithm was able to identify gait during level walking, ramps, and stairs over multiple days. Synergistic relationships between the thigh muscles and ankle motion were observed by Tkach et al., who showed that lower classification errors were obtained in transtibial amputees when combining residual shank and *intact* thigh EMG of the prosthetic side to virtually control a three degree-of-freedom ankle-foot prosthesis (Tkach et al., 2013). These results suggest that thigh muscle activity could provide an alternative source to control ankle dynamics. Furthermore, the acquisition of EMG signals outside the socket may reduce within-socket signal disturbances and improve user experience.

1.3.2.2.2 Continuous Proportional Myoelectric Control

Alternate approaches that continuously determine the dynamic changes of the joint and do not require division into discrete states have begun to emerge. Continuous proportional myoelectric control (CPMC) does not rely on a FSM, but instead allows the amputee to actuate the prosthesis based on the amplitude of residual muscle activity. Residual antagonistic muscles of a single transfemoral amputee have been used to

continuously modulate impedance of an active knee prosthesis during level ground walking (Dawley et al., 2013; Hoover et al., 2012). Using CPMC, transtibial amputees were able to control a virtual environment via their residual ankle dorsiflexor and plantarflexor muscles (S. Huang & Huang, 2018, 2019), and control an active ankle-foot prosthesis via a single ankle plantarflexor muscle during level treadmill walking (S. Huang et al., 2016). CPMC, especially for impedance control, is a promising approach; however, it can require extensive user training, increase cognitive processing, and can be affected by muscle fatigue. For robust implementation of CPMC, it is imperative to extensively assess the capabilities and boundaries of an individual amputee's volitional muscle activation (reciprocal and coactivation) prior to use.

1.4 CONTINUOUS GAIT MODELS FOR THE ESTIMATION OF LOWER LIMB STATE

Many methods to estimate joint dynamics continuously (time series) have been proposed to determine the dynamic changes of the hip, knee, and/or ankle joint without the division into discrete locomotion states. In the case of myoelectric control, these continuous gait models could reduce user's cognitive and physical demand and dependency on amputees' ability to generate high quality, independent muscle signals.

Impedance and stiffness control based on joint moment and angle have become an increasingly common approach for actuating active powered lower limb prostheses (**Figure 1.1**) (Au et al., 2008; Culver et al., 2018; Ha et al., 2011; Hoover et al., 2013; Klein & Voglewede, 2018; Spanias et al., 2018). Their development stems from the belief that the central nervous system controls the limbs through impedance control since human movements are robust to perturbations and changes in terrain despite the inherent

delay in signal transmission via neural pathways (Kadiallah et al., 2011; Towhidkhah et al., 1997); therefore, prosthetic impedance control can produce a more natural and smooth actuation. Ankle angle and ankle moment (i.e., torque) are common targets for controlling transtibial prostheses. More generally, limb joint kinematics and kinetics have been continuously estimated from EMG signals (Ardestani et al., 2014; Baby Jephil et al., 2020; J. Chen et al., 2018; Y. Chen et al., 2013; Farmer et al., 2014; Gupta et al., 2020; Hahn & O'Keefe, 2008; Huihui et al., 2018; Keleş & Yucesoy, 2020; J. Lee & Lee, 2005; Li et al., 2015; J. Liu et al., 2020; Meyer et al., 2017; Ngeo et al., 2014; Prasertsakul et al., 2012; Sepulveda et al., 1993; Shao et al., 2009; J. Wang et al., 2020; Zarshenas et al., 2020; Zhang et al., 2012), hip and knee joint dynamics (Dey et al., 2019; Embry et al., 2018; Eslamy & Alipour, 2019; Joshi et al., 2011), force myography (Kumar et al., 2021), and ground reaction forces (Jacobs & Ferris, 2015; Y. Liu et al., 2009), among others. Random forest regression (Huihui et al., 2018), Kalman filters (Brantley et al., 2017), support vector regression (Dey et al., 2019; Li et al., 2015), Gaussian process regression (Eslamy & Alipour, 2019), and various types of artificial neural networks [e.g., feedforward, time delay, recurrent; (Ardestani et al., 2014; J. Chen et al., 2018; Farmer et al., 2014; Hahn & O'Keefe, 2008; Keleş & Yucesoy, 2020; Zarshenas et al., 2020; Zhang et al., 2012)] have been used as modeling techniques for the continuous estimation of gait.

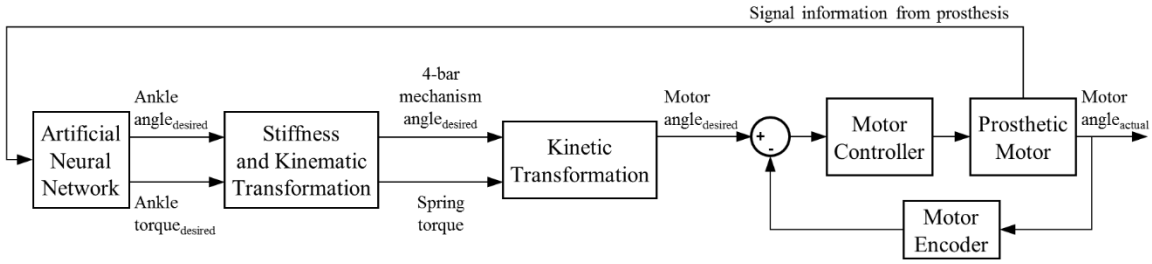

Figure 1.1. Stiffness control for actuating an active ankle-prosthesis using ankle angle and moment as targets (Klein & Voglewede, 2018).

This section gives an overview of different methods for time series (continuous) modelling, including definitions and terms used later in this dissertation. It also reviews continuous gait models developed for the estimation and prediction of ankle dynamics in order to identify areas for improvement. In this dissertation, a distinction between *estimation* and *prediction* is made. *Estimation* refers to the computation of the next time-step value of the time series, commonly known as one-step-ahead prediction (**Figure 1.2**). *Prediction* refers to computation of a future value, several time steps ahead of time (i.e., n-step-ahead prediction).

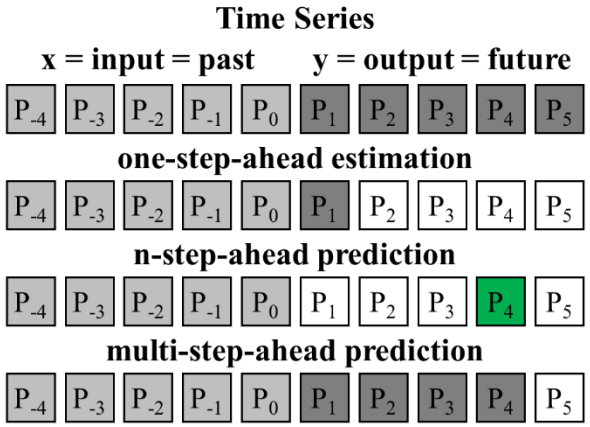

Figure 1.2. Graphical representation of one-step-ahead estimation and n-step-ahead prediction. P: time point.

1.4.1 Time Series Modeling Techniques

Many traditional modeling techniques have been widely used to estimate time series signals. Some examples include AR (autoregressive), ARX (AR model with exogenous, i.e., external, inputs), ARMA (autoregressive with moving average), and ARMAX (ARMA model with exogenous inputs) models, among others. An autoregressive model relates current observations of a variable with past observations of itself and other variables in the system to describe and estimate/predict the time-varying process. These models assume that the underlying signals are linear and stationary (statistical properties constant over time). Due to their linearity, simplicity, and lack of prior information (e.g., initial conditions), they can be outperformed by artificial neural networks in complex (e.g., nonlinear, numerous variables) and noisy problems, especially during long-term prediction (Hu & Hwang, 2001; Mahmoud, 2012).

Artificial neural networks are derived from traditional linear regression methods, and have been expanded to incorporate deep learning and prediction capabilities. Neural networks can deal with time-varying challenges such as variability (noise), nonlinearities, non-stationary data, and lack of prior knowledge. The most common types of neural networks used for continuous estimation of lower limb kinematics and kinetics include multilayer feedforward artificial neural networks (FFANN), time delay neural networks (TDNN), and recurrent neural networks. Similar to traditional linear regression methods, neural networks also characterize the relationship between the inputs and outputs and their temporal relationship at different time steps into the model with the purpose to estimate/predict. The general neural network structure consist of an input layer, one or more hidden layers with nonlinear transfer functions (e.g., sigmoid), and a linear output

layer. Each layer is connected by a series of weights (and a corresponding bias) that represent the strength of the connections between inputs, hidden units (neurons), and outputs. The most popular learning technique used to train neural networks is back-propagation, which uses the errors between the model output and the desired (target) output to readjust the weights and biases in a way that minimizes the overall error across the training data.

Feedforward neural networks are the simplest type of networks, where information flows in one direction and no information is fed back to previous layers or nodes. For continuous gait estimation/prediction, the ability to incorporate a finite memory (e.g., past observations) is particularly useful because timing between EMG activity and kinematics is a key discriminant of gait across different terrains (Lencioni et al., 2019; Wentink et al., 2013, 2014). Time delay networks also have a feedforward information flow; however, they use a tapped delay line to incorporate memory information. In a tapped delay line, the input vector to the hidden layer consists of the current time-step data and past time-step data as individual inputs. In addition to storing memory, TDNN are capable of making ahead of time predictions of the time series (Zarshenas et al., 2020).

Most continuous gait models for the estimation of lower limb state are based on feedforward architectures. These models have proven to be successful within an acceptable level of accuracy. However, the accuracy and stability of feedforward gait models cannot be guaranteed when implemented as part of a feedback control system (Lewis & Parisini, 1998; Menezes & Barreto, 2008). Additionally, feedforward architectures can have limitations identifying complex dynamical systems (sensitive to

noise) and for long-term predictions, require a larger number of hidden units and weights, and may be more susceptible to overfitting (Gençay & Liu, 1997; M. Han et al., 2004; Menezes & Barreto, 2008). These limitations are mainly associated to the lack of direct past values of the model output.

Recurrent neural networks can minimize these problems due to their reliance on past temporal dynamics. Contrary to feedforward models, recurrent networks allow previous values of the output to be used as inputs, creating feedback loops. Such networks are powerful, particularly for long-term prediction, because they incorporate the past history of both inputs and outputs. With the presence of feedback loops (additional input information), recurrent networks tend to be robust to overfitting, can function as noise filters, and have a compact structure (number of hidden units and weights) that outperforms feedforward architectures (Gençay & Liu, 1997; M. Han et al., 2004; Menezes & Barreto, 2008). As a consequence, the complexity and the length of training are increased. An example of a recurrent network is the nonlinear autoregressive neural network with exogenous inputs (NARX) used in this dissertation.

1.4.1.1 The NARX Model

The NARX model is a discrete nonlinear model based on the linear ARX and ARMAX models (S. Chen et al., 1990; Leontaritis & Billings, 1985), and is computationally equivalent to a Turing machine (Siegelmann & Sontag, 1991). The general NARX model output, $y(t)$, can be expressed as,

$$y(t) = f\begin{pmatrix} x(t-1), x(t-2), \dots, x(t-D_x), \\ y(t-1), y(t-2), \dots, y(t-D_y) \end{pmatrix} \tag{1.1}$$

where $x(t)$ is the exogenous model input and $y(t)$ is the model output at discrete time step t, f is a nonlinear function, and D_x and D_y are the input and output memory orders. The net input vector is built through two separate sets of tapped delay lines, one sliding over the input signal and one sliding over the model's output.

In this dissertation, the tapped delay lines define (1) the number of past input values over time (exogenous and output) used in the prediction (D, sampling window) where D_x and D_y are set to be equal, and (2) the time between current inputs (exogenous and output) and future model predictions (τ, prediction interval) (**Figure 1.3**). Given these characteristics, the general NARX model output, $y(t + \tau)$, can be expressed as,

$$y(t+\tau) = f\begin{pmatrix} x(t), x(t-1), x(t-2), \dots, x(t-D), \\ y(t-1), y(t-2), \dots, y(t-D) \end{pmatrix} \quad (1.2)$$

Consequently, $x(t-d)$ and $y(t-d)$, (for $d = 1, \dots, D$), denote the prior values of the exogenous input and output d time steps in the past.

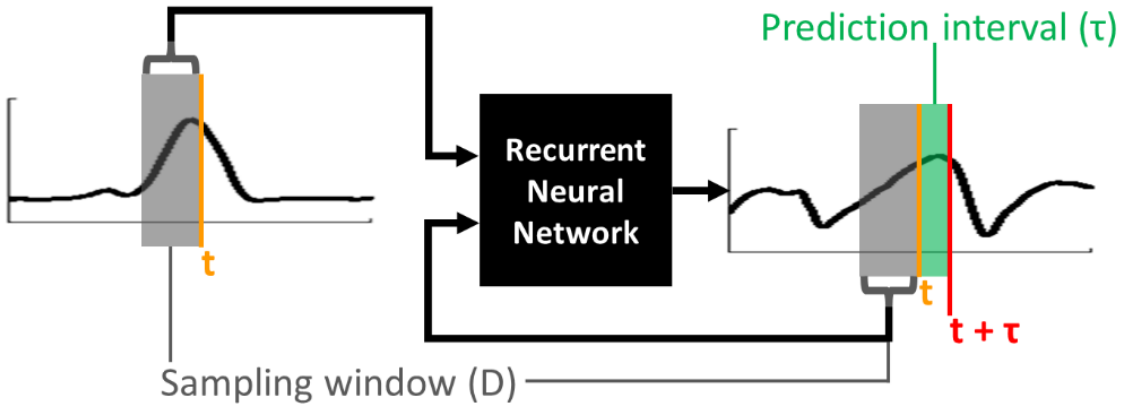

Figure 1.3. Graphical representation of prediction interval and sampling window.

The NARX model can be trained in two modes:

- Open-loop mode (commonly known as *Series-Parallel*): In this mode, the experimentally measured past values of the target, $y(t-d)$, are used in the

input vector of the network, together with the exogenous input, to predict the future output of the model, $\hat{y}(t+\tau)$:

$$\hat{y}(t+\tau) = f\begin{pmatrix} x(t), x(t-1), x(t-2), \dots, x(t-D), \\ y(t), y(t-1), y(t-2), \dots, y(t-D) \end{pmatrix} \quad (1.3)$$

The use of error-free targets results in a highly accurate network. This training mode has a purely feedforward architecture which allows for simpler and faster back-propagation learning algorithms (Menezes & Barreto, 2008). However, as an open-loop network, the NARX model is not suitable for real-time applications since explicit knowledge of the true state (error-free targets) is generally not available. This training mode is used in CHAPTER 2 (Aim 1) of this dissertation. After training, the feedforward (open-loop) NARX model can be converted (without explicit training) to its recurrent (closed-loop) architecture (not done in this dissertation). However, accuracy and stability of the transformed open-loop NARX model cannot be guaranteed because small prediction errors can become amplified, leading to instability and failure.

- Closed-loop mode (commonly known as *Parallel*): In this mode, the predicted past values of the output, $\hat{y}(t-d)$, are fed back to form the input vector of the network, together with the exogenous input, and used to predict the future output of the model, $\hat{y}(t+\tau)$:

$$\hat{y}(t+\tau) = f\begin{pmatrix} x(t), x(t-1), x(t-2), \dots, x(t-D), \\ \hat{y}(t-1), \hat{y}(t-2), \dots, \hat{y}(t-D) \end{pmatrix} \quad (1.4)$$

If the model is trained as closed-loop from the start, the model output error is encoded in the input during training, since output predictions are fed back as recurrent inputs instead of error-free target data. This results in a recurrent

(closed-loop) NARX model architecture that is more robust and stable to model uncertainties (e.g., error accumulation and undesired fluctuations). Closed-loop model performance tends to be inferior (Menezes & Barreto, 2008) to open-loop models, but accuracy can be improved by incorporating additional input signals (Dey et al., 2019; Eslamy & Alipour, 2019; Keleş & Yucesoy, 2020; Gupta et al., 2020). The resulting closed-loop model has the same advantages and disadvantages of recurrent neural networks as described previously. This training mode is used in CHAPTERS 3 and 4 (Aims 2 and 3) of this dissertation.

1.4.2 Continuous Estimation of Ankle Dynamics

The continuous estimation of joint moments has focused on the use of multi-body dynamic musculoskeletal modelling. While effective, it requires constant and time consuming [e.g., 30 min (Meyer et al., 2017)] re-calibration of model parameters that are sensitive to changes in muscle-tendon geometry which may not be well characterized for amputees or orthopedic impaired individuals (Meyer et al., 2017; Shao et al., 2009), and consequently, not suitable for real-time applications. Due to these limitations, regression methods, including artificial neural networks, have been explored to estimate moment continuously for real-time applications. For example, Lui et al. proposed a FFANN to continuously estimate hip, knee, and ankle joint moments using vertical ground reaction forces, vertical displacement of center-of-mass, vertical velocity of center-of-mass, and jump power while performing two different vertical jumps (Y. Liu et al., 2009).

Support vector regression (SVR) and Gaussian process regression (GPR) have been used to continuously estimate ankle angle and moment simultaneously using hip and knee joint kinematics (Dey et al., 2019) and shank kinematics (Eslamy & Alipour, 2019), respectively. Dey et al. used SVR to continuously estimate ankle angle and moment during level overground walking [root mean square error (RMSE) = 2.17° and 0.11 Nm/kg] using two extrinsic inputs (hip and knee angle) of a single healthy participant. The generalized inter-subject GPR method, applied to able-bodied participants, was able to continuously and simultaneously estimate ankle angle and moment during level treadmill walking at varying speeds (0.5, 1, and 1.5 m/s). Using shank kinematics (angle and angular velocity) as the two inputs, angle RMSE and moment RMSE were between 2.2-2.6 degrees and 0.11-0.16 Nm/kg, respectively, with correlations (R^2) greater than 0.82, and 0.86, respectively. Although simultaneous estimation of ankle angle and moment was achieved in both studies, performance was characterized during a single type of terrain, i.e., level walking. The use of kinematic-only inputs can provide an alternative for predicting user intent indirectly but the need for wearable sensors extrinsic (and intrinsic) to the prosthesis poses similar challenges to EMG-based systems.

Classification algorithms have been used together with surface EMG to distinguish among discrete locomotion modes (Gupta & Agarwal, 2017; H. Huang et al., 2009; M. Liu et al., 2017; Young et al., 2014) while other approaches continuously estimate ankle joint kinematics and kinetics (Ardestani et al., 2014; Baby Jephil et al., 2020; J. Chen et al., 2018; Farmer et al., 2014; Gupta et al., 2020; Hahn & O'Keefe, 2008; Huihui et al., 2018; Keleş & Yucesoy, 2020; Prasertsakul et al., 2012; Sepulveda et al., 1993; J. Wang et al., 2020; Zarshenas et al., 2020; Zhang et al., 2012) using EMG

signals. Most approaches characterize performance during a single type of terrain [e.g., level walking; (Ardestani et al., 2014; J. Chen et al., 2018; Farmer et al., 2014; Hahn & O'Keefe, 2008; Keleş & Yucesoy, 2020; Prasertsakul et al., 2012; J. Wang et al., 2020; Zarshenas et al., 2020; Zhang et al., 2012)] or ankle motion (e.g., ankle plantarflexion) while sitting (Baby Jephil et al., 2020; Huihui et al., 2018; Zhang et al., 2012). Models that estimate ankle angle or moment during more than one condition (e.g., speeds) have begun to emerge. In the following paragraphs, the latest published EMG-driven continuous gait models for the estimation of ankle dynamics are reviewed in detail.

Zhang et al. used a three-layer nonlinear FFANN to estimate hip, knee, and ankle angle simultaneously using a combination of muscle activity from one shank and two thigh muscles, including past EMG values (Zhang et al., 2012). Level treadmill walking at different speeds and loads was conducted by able-bodied participants and passive walking by spinal cord injury patients. Zhang et al. obtained a wide range of ankle angle errors (RMSE = 0.82 to 9.3°) during level walking of spinal cord injury patients using subject-specific networks. The large variation in errors was attributed to the wide range of ankle motion of the patients (i.e., restricted motion resulted in lower errors). A deep belief network (DBN) and principal component analysis (PCA) were used separately for EMG dimensionality reduction, and combined with a three-layer nonlinear FFANN to estimate hip, knee, and ankle angle of healthy participants (J. Chen et al., 2018). Trained generalized inter-subject networks continuously estimated changes in speeds during level overground walking using ten EMG signals of the thigh and shank muscles. DBN outperformed PCA, reducing errors by 50% with average correlations (r) greater than 0.86 for ankle angle.

Gupta et al. proposed separate nonlinear autoregressive models (i.e., NARX) for five individual terrain types to estimate ankle angle of healthy participants during gait (Gupta et al., 2020). It is believed that the NARX model was implemented as a feedforward (open-loop) model using error-free targets instead of estimated outputs. Gupta et al. trained and tested separate subject-specific networks and reported errors, using three inputs, during level overground walking (RMSE = 2.44 ± 0.45°, r = 0.97), stair ascent (RMSE = 3.61 ± 1.00°, r = 0.93), stair descent (RMSE = 5.04 ± 1.56°, r = 0.85), ramp ascent (RMSE = 4.52 ± 0.94°, r = 0.82), and ramp descent (RMSE = 5.44 ± 1.64°, r = 0.94). The exogenous inputs of the model consisted of the linear envelopes of two shank EMG signals (tibialis anterior and gastrocnemius), individually, and in combination with knee angle. Time history was incorporated in the model as time tapered delays (equivalent to sampling window) but did not make estimations ahead of time.

Keleş et al. performed a comprehensive analysis of shank, thigh, and gluteal muscle sites and their combinations for use as EMG inputs to estimate ankle angle and moment (Keleş & Yucesoy, 2020). Simultaneous estimation of ankle angle and moment was achieved during level overground walking at various speeds using a TDNN and simulated EMG data of a healthy population, including prior data points. Using ankle plantarflexor and dorsiflexor muscles, they reported ankle angle and moment errors (RMSE) of 2.34 ± 0.15 degrees and 0.041 ± 0.006 Nm/kg with correlations (r) greater than 0.95, although performance was not examined with estimations ahead of time nor across ambulation conditions. Greater errors and lower correlations were reported using EMG from antagonistic thigh (rectus femoris and bicep femoris) muscles (RMSE = 3.60 ± 2.00°, r = 0.90; RMSE = 0.264 ± 0.123 Nm/kg, r = 0.82). Similar to other continuous

gait models (Dey et al., 2019; Eslamy & Alipour, 2019; Gupta et al., 2020), their study revealed that model performance improved by increasing the number of muscle sites (i.e., number of inputs) and the inclusion of shank muscle signals. For the case of minimizing inputs, the combination of tibialis anterior, gastrocnemius medialis and biceps femoris EMG signals yield the best performing model (RMSE = 1.54 ± 0.06°, r = 0.98; RMSE = 0.038 ± 0.007 Nm/kg, r = 0.99). For the case of minimizing within-socket sites, muscles from the shank, thigh, and gluteal area (three signals) were required to achieve acceptable performance (RMSE = 2.25 ± 0.34°, r = 0.96; RMSE = 0.042 ± 0.005 Nm/kg, r = 0.99). The comprehensive analysis supports prior studies indicating that thigh muscle activity contains synergistic gait information about ankle state.

Ardestani et al. used a generalized inter-subject wavelet neural network (WNN) and a three-layer FFANN to estimate ankle plantarflexion moments using a combination of six thigh and two shank EMG signals and two ground reaction forces of patients with unilateral knee replacement (Ardestani et al., 2014). Ardestani et al. obtained ankle moment errors of 4.2% and 8.4% using WNN and FFANN models, respectively, during level walking (single walking condition) when trained on three patients, and tested on a fourth. They obtained higher errors for normal walking (WNN 8.1% and FFANN 12.9%) based on a non-specific inter-subject training paradigm, wherein the network was trained on data from three different patients while performing three rehabilitation therapy walking programs (normal, medial trust, walking pole), and tested on a fourth participant. In their study, the purpose was to create a generalized real-time surrogate inverse dynamic model for gait analysis and was not intended for use in prosthetic control. Another surrogate gait analysis model of sagittal ankle moment was developed for

clinical purposes (Hahn & O'Keefe, 2008). Ankle moment was estimated continuously during normal level overground walking using a FFANN with diverse inputs (demographics: age and gender; anthropometrics: height, mass, foot inertia; kinematics: ankle angle, angular velocity and angular acceleration, and EMG: tibialis anterior and gastrocnemius medialis). Correlations (R^2) greater than 0.95 were obtained using all inputs together with an inter-subject network trained with data from all participants.

Predictive approaches (n-step-ahead prediction, i.e., future estimates) for continuous gait estimation have begun to emerge. Zarshenas et al. utilized a TDNN to predict ankle moment up to 2 seconds (0, 0.5, 1, 1.5, and 2 s) ahead of time (equivalent to prediction interval) during normal level treadmill walking (Zarshenas et al., 2020). EMG signals from four shank muscles (tibialis anterior, gastrocnemius medialis and lateralis, and soleus), together with ankle angle and angular velocity, were used as inputs, including past values. Favorable results occurred up to 1 second with EMG and ankle kinematics ($R^2 > 0.8$) as inputs, and at zero-time with EMG only ($R^2 > 0.84$). Their model exploited the cyclic nature of treadmill walking at a constant speed which resulted in high accuracy over large prediction intervals, although performance was not examined during noncyclic features of gait such as terrain transitions.

Previous work has demonstrated the ability of a feedforward (open-loop) NARX model to continuously predict future ankle kinematics of passive ankle-foot prostheses using within-socket EMG activity from the residual limb of unilateral transtibial amputees (Farmer et al., 2014; Silver-Thorn et al., 2012). The model used the EMG linear envelope of remnant ankle dorsiflexor and plantarflexor as input, together with the prior history of the prosthetic ankle angle (i.e., error-free targets), to predict future ankle

angle during level treadmill walking. It is believed that this was the first study in which a continuous gait model was validated using EMG and kinematic data from transtibial amputees. In the presence of co-contraction between antagonistic muscles, Farmer et al. reported angle errors (RMSE) ranging from 1.2 to 5.4 degrees across participants for prediction intervals of 100 ms ahead of time. The incorporation of natural, yet altered, EMG signals significantly reduced average errors in ankle angle during the gait cycle and phase transitions. However, the subject-specific model was limited to the prediction of a single terrain and did not predict ankle moments needed in stiffness and impedance control.

In summary, these studies support the feasibility of continuously estimating ankle joint angles and moments independently and simultaneously using EMG signals. However, most models have used a feedforward structure to estimate (i.e., excluding future predictions) ankle angle or moment limited to level walking using muscle activity from only the shank, or in combination with thigh EMG, of healthy individuals ($RMSE_\theta$ < 5.3°, R_θ^2 > 0.74; $RMSE_M$ < 0.18 Nm/kg, R_M^2 > 0.83). Simultaneous prediction of both ankle angle and moment across multiple types of terrain (e.g., level walking, stair ascent/descent) including the transitions between terrains has not been demonstrated. Moreover, almost all models characterized ankle dynamics using a reactive (i.e., one-step-ahead estimation) rather than a predictive (i.e., n-step-ahead prediction) approach. A continuous predictive approach could help overcome delays in sensing, processing, and actuation of the mechanical device and help to modify gait proactively in response to upcoming changes in terrain.

1.5 SPECIFIC AIMS

The main goals of this dissertation are (1) to develop a continuous predictive model of lower limb state that uses surface EMG of the lower limb to predict (i.e., future estimates) ankle angle and moment across ambulation conditions (i.e., level overground walking, stair ascent, and stair descent) and the transitions between them (i.e., transitions to/from a staircase), and (2) to determine the feasibility of using natural EMG of the prosthetic side of transtibial amputees for the continuous prediction of normative ankle dynamics. Three specific aims are established to accomplish these goals. Each aim is presented in a separate chapter (CHAPTERS 2-4) and formatted as a standalone manuscript.

1.5.1 Specific Aim 1: Develop a Gait Model That Uses Muscle Activity of the Lower Leg to Continuously Predict Future Ankle Dynamics across Ambulation Conditions

Efforts to use EMG signals to control active lower limb prostheses have mainly focused on discrete approaches that are reactive to changes in terrain, can introduce undesirable discontinuities during gait, and limit the amputee's control over the prosthesis. Here, natural muscle activity of the lower leg (i.e., shank) of able-bodied individuals will be incorporated into a multiple-input multiple-output nonlinear autoregressive model to continuously predict future ankle kinematics and kinetics across ambulation conditions and their transitions. The extent to which EMG signals can be used in model prediction will be assessed. We hypothesize that the autoregressive model can predict the wider ranges of ankle dynamics associated with healthy ambulation across the series of self-powered ambulation conditions, and that the incorporation of EMG signals

can lower prediction errors. This capability is relevant toward the eventual control of prostheses across the range of ankle dynamics in the sound limb needed for restoring symmetric gait. The myoelectric predictive model of able-bodied individuals will provide a best case characterization of normal gait patterns across multiple terrains and transitions.

1.5.2 Specific Aim 2: Determine the Ability of Using Within-Socket Residual EMG Signals of Transtibial Amputees to Continuously Predict Future Ankle Dynamics of the Sound Limb across Ambulation Conditions

Prior work has demonstrated the feasibility of using within-socket residual EMG signals from transtibial amputees together with a NARX model to continuously predict prosthetic ankle angle during treadmill walking. Here, natural patterns of within-socket residual EMG signals of transtibial amputees, in combination with shank kinematics of the sound limb, will be used as exogenous inputs to a NARX model to continuously predict future ankle kinematics and kinetics of the sound limb across ambulation conditions and terrain transitions. We hypothesize that within-socket residual EMG and sound-limb shank kinematics can be used effectively to predict ankle dynamics of the sound limb, and that model prediction errors will not pose a risk of trip-related falls or injury. Continuous predictive models of able-bodied individuals will characterize normal ranges of ankle dynamics using normal shank muscle activity and kinematics, and serve as a normative comparison of model performance and EMG contribution to model prediction of amputee models. We expect that amputee models will have performance comparable to able-bodied models, and that within-socket residual EMG will be used in the model prediction to the same extent as normal ankle dorsiflexor and plantarflexor

muscle activity. Most amputees develop altered lower limb EMG activity, kinematic, and kinetic patterns to compensate for limitations in their prosthesis. The approach of mapping ankle dynamics of the sound limb with residual EMG of the prosthetic side, will take an important step toward establishing a more normal gait by overlaying the dynamics of the sound limb onto the prosthesis to create symmetric gait patterns.

1.5.3 Specific Aim 3: Examine the Feasibility of Using Thigh Muscle Activity to Continuously Predict Future Ankle Dynamics

While thigh muscles do not control ankle motion directly, their synergistic activity and control of the knee and hip joints may provide an alternate source of information to differentiate among multiple terrains. A systematic comparison of gait model performance has not been performed using within-socket residual shank or *intact* thigh muscle activity of the prosthetic side to predict ankle dynamics with transtibial amputees. Here, natural patterns of thigh EMG of the prosthetic side from transtibial amputees, in conjunction with sound-limb shank kinematics, will be used as exogenous inputs to a NARX model to continuously predict future ankle kinematics and kinetics of the sound limb across ambulation conditions and terrain transitions. We hypothesize that prosthetic-side thigh EMG can be used effectively to predict sound-limb ankle dynamics similar to model predictions based on within-socket residual shank EMG. We expect that thigh muscle activity of the prosthetic side will be used in the model prediction, and to the same extent as residual ankle dorsiflexor and plantarflexor muscle activity. Similar to Aim 2, continuous predictive models of able-bodied individuals will be developed. The ability to use thigh muscles to predict ankle dynamics may enhance long-term comfort and improve myoelectric control of ankle-foot prostheses by reducing signal disturbances

(e.g., motion artifacts) that occur within the prosthetic socket during repeated loading and unloading of the prosthesis during gait.

A continuous predictive model of gait that incorporates direct user intent, vis-à-vis EMG signals, could provide a more natural, intuitive, and robust control for a better reproduction of normal human gait of active powered lower limb prostheses, particularly ankle-foot prostheses.

CHAPTER 2: CONTINUOUS MYOELECTRIC PREDICTION OF FUTURE ANKLE ANGLE AND MOMENT ACROSS AMBULATION CONDITIONS AND THEIR TRANSITIONS

This chapter has been previously published:
Zabre-Gonzalez EV, Riem L, Voglewede PA, Silver-Thorn B, Koehler-McNicholas SR and Beardsley SA (2021) Continuous myoelectric prediction of future ankle angle and moment across ambulation conditions and their transitions. Front. Neurosci. 15:709422. doi: 10.3389/fnins.2021.709422

2.1 ABSTRACT

A hallmark of human locomotion is that it continuously adapts to changes in the environment and predictively adjusts to changes in the terrain, both of which are major challenges to lower limb amputees due to the limitations in prostheses and control algorithms. Here, the ability of a single-network nonlinear autoregressive model to continuously predict future ankle kinematics and kinetics simultaneously across ambulation conditions using lower limb surface electromyography (EMG) signals was examined. Ankle plantarflexor and dorsiflexor EMG from ten healthy young adults were mapped to normal ranges of ankle angle and ankle moment during level overground walking, stair ascent, and stair descent, including transitions between terrains (i.e., transitions to/from staircase). Prediction performance was characterized as a function of the time between current EMG/angle/moment inputs and future angle/moment model predictions (prediction interval), the number of past EMG/angle/moment input values over time (sampling window), and the number of units in the network hidden layer that minimized error between experimentally measured values (targets) and model predictions of ankle angle and moment. Ankle angle and moment predictions were robust across ambulation conditions with root mean square errors less than 1 degree and 0.04 Nm/kg, respectively, and cross-correlations (R^2) greater than 0.99 for prediction intervals of 58

ms. Model predictions at critical points of trip-related fall risk fell within the variability of the ankle angle and moment targets (Benjamini-Hochberg adjusted $p > 0.065$). EMG contribution to ankle angle and moment predictions occurred consistently across ambulation conditions and model outputs. EMG signals had the greatest impact on noncyclic regions of gait such as double limb support, transitions between terrains, and around plantarflexion and moment peaks. The use of natural muscle activation patterns to continuously predict variations in normal gait and the model's predictive capabilities to counteract electromechanical inherent delays suggest that this approach could provide robust and intuitive user-driven real-time control of a wide variety of lower limb robotic devices, including active powered ankle-foot prostheses.

2.2 INTRODUCTION

Human locomotion continuously adapts to changes in the environment to maintain balance, reacts to unpredictable perturbations, and predictively adjusts walking patterns to changes in the terrain (Choi & Bastian, 2007; Pearson, 2000). Gait adaptability is a major challenge to lower limb amputees due to the limitations in prostheses and control algorithms (Kannape & Herr, 2016). Accurately and continuously predicting variations in gait, particularly during transitions and noncyclic activities, is limited in commercially available lower limb prostheses. Gait adaptability could be improved by incorporating information on user intent (e.g., myoelectric control), allowing users to modify prosthetic joint dynamics in a more natural, and less physically and cognitively demanding way.

Developing control algorithms for lower limb prostheses is challenging and impacts the level of human adaptation to the device (S. Huang et al., 2016). The use of finite state machines (FSM) in combination with mechanical intrinsic sensors embedded in the prosthesis itself (Cherelle et al., 2014; Culver et al., 2018; Sun et al., 2014) or worn on the residual limb (Au et al., 2008; Kannape & Herr, 2014; Hoover et al., 2013; Spanias et al., 2018) has become an increasingly common approach due to their high precision and reliability. However, FSM-based control is limited by the relatively small number of pre-defined, discrete states, the need to define switching rules for transitioning between states, and the inability to deal with novel movements.

Alternate approaches have been developed that would continuously determine the dynamic changes of the joint and would not require division into discrete states. Impedance and stiffness control based on joint moment and angle have an increasingly common approach for actuating active powered (i.e., able to generate power during propulsion) lower limb prostheses (Au et al., 2008; Culver et al., 2018; Ha et al., 2011; Hoover et al., 2013; Kannape & Herr, 2014; Klein & Voglewede, 2018; Spanias et al., 2018). Specifically, ankle angle and ankle moment are common targets for controlling transtibial prostheses. The continuous estimation of joint moments has focused on the use of multi-body dynamic musculoskeletal modelling. While effective, it requires constant and time consuming [e.g., 30 min (Meyer et al., 2017)] re-calibration of model parameters that are sensitive to changes in muscle-tendon geometry which may not be well characterized for amputees or orthopedic impaired individuals (Meyer et al., 2017; Shao et al., 2009), and consequently, not suitable for real-time applications. Limb joint mechanics and kinematics have been continuously estimated from electromyography

(EMG) signals (Meyer et al., 2017; Shao et al., 2009; J. Liu et al., 2017, 2020; Ngeo et al., 2014; Farmer et al., 2014; Zhang et al., 2012; Gupta et al., 2020; J. Chen et al., 2018; J. Wang et al., 2020; Prasertsakul et al., 2012; Huihui et al., 2018; Keleş & Yucesoy, 2020; Sepulveda et al., 1993; Baby Jephil et al., 2020; Ardestani et al., 2014; Li et al., 2015; Y. Chen et al., 2013; J. Lee & Lee, 2005), hip joint dynamics (Dey et al., 2019; Embry et al., 2018; Eslamy & Alipour, 2019), knee joint dynamics (Embry et al., 2018; Eslamy & Alipour, 2019; Joshi et al., 2011), force myography (Kumar et al., 2021), and ground reaction forces (GRF) (Jacobs & Ferris, 2015; Y. Liu et al., 2009), among others. Support vector regression (SVR) and Gaussian process regression have been used to continuously estimate ankle angle and ankle moment simultaneously using hip and knee joint kinematics (Dey et al., 2019) and shank kinematics (Eslamy & Alipour, 2019), respectively. Although simultaneous estimation of ankle angle and moment was achieved, performance was characterized during a single type of terrain, i.e., level walking, and implementation would require deducing user intent indirectly from mechanical extrinsic or intrinsic prosthetic sensors.

For a seamless and intuitive device actuation, controllers must recognize the user's locomotive intention given changes in the environment. Although mechanical intrinsic sensors have high repeatability and reproducibility, they introduce an intrinsic delay and the resulting control must infer human intention through secondary information such as gait events or joint mechanics. Therefore, their actuation is reactive to user's biomechanical changes. Surface EMG activity enables a direct prediction of intended biomechanics given that muscle activity precedes force generation, and consequently, limb movement, on the order of 10 ms (Cavanagh & Komi, 1979). Still, the use of EMG

sensors poses challenges in achieving robust control due to low signal quality, variability associated with sensor placement and electrode-skin conductivity, cross-talk between nearby muscles, and signal processing for feature extraction.

Classification algorithms have been used together with surface EMG to distinguish among discrete locomotion modes (Gupta & Agarwal, 2017; H. Huang et al., 2009; M. Liu et al., 2017; Young et al., 2014) while other approaches continuously estimate ankle joint kinematics (Farmer et al., 2014; Zhang et al., 2012; Gupta et al., 2020; J. Chen et al., 2018; J. Wang et al., 2020; Prasertsakul et al., 2012; Huihui et al., 2018; Keleş & Yucesoy, 2020; Sepulveda et al., 1993; Baby Jephil et al., 2020) and kinetics (Ardestani et al., 2014; Baby Jephil et al., 2020; Keleş & Yucesoy, 2020; Sepulveda et al., 1993) using EMG signals. Most approaches characterize performance during a single type of terrain [e.g., level walking; (Farmer et al., 2014; Zhang et al., 2012; Gupta et al., 2020; J. Chen et al., 2018; J. Wang et al., 2020; Prasertsakul et al., 2012; Keleş & Yucesoy, 2020; Ardestani et al., 2014)] or ankle motion while sitting (Baby Jephil et al., 2020; Huihui et al., 2018; Zhang et al., 2012). Models that estimate ankle angle or ankle moment during more than one condition (e.g., speeds) have begun to emerge. A deep belief network and principal component analysis, for EMG dimensionality reduction from ten muscle signals, individually combined with a nonlinear back-propagation network have been used to estimate hip, knee, and ankle angle of healthy participants (J. Chen et al., 2018). Trained generalized inter-subject networks continuously estimated changes in speeds during level walking. Gupta et al. proposed separate subject-specific autoregressive models for five individual terrain types (level walking, stair ascent, stair descent, ramp ascent, ramp descent) to estimate ankle

angle using two able-bodied lower limb EMG signals and knee angle (Gupta et al., 2020). A generalized inter-subject wavelet neural network (WNN) and feedforward artificial neural network (FFANN) are capable of estimating ankle moments using EMG activity from eight muscles and two GRFs of patients with unilateral knee replacement while performing three rehabilitation therapy walking programs (Ardestani et al., 2014). Keleş et al. achieved the simultaneous estimation of ankle angle and moment during level walking using a time-delay FFANN and simulated EMG data of a healthy population (Keleş & Yucesoy, 2020). These studies support the feasibility of continuously estimating ankle joint angles and ankle moments independently and simultaneously using EMG signals. However, simultaneous estimation of both ankle angle and moment across multiple types of terrains (e.g., level walking, stair ascent/descent) including transitions between them has not been demonstrated. Moreover, almost all estimations of ankle angle and moment were reactive rather than predictive (i.e., future estimates). A predictive approach would help overcome delays in sensing, processing, and actuation of the mechanical device and also help to modify gait proactively in response to upcoming changes in terrain.

An EMG-driven nonlinear autoregressive neural network with exogenous inputs (NARX) with predictive future states can address these challenges and provide a robust and intuitive control of active powered ankle-foot prostheses. Previous work has demonstrated the ability of a single-output feedforward (open-loop) NARX model to continuously predict future ankle angle of the prosthesis using within-socket EMG activity from the residual limb of transtibial amputees (Farmer et al., 2014; Silver-Thorn et al., 2012). The incorporation of natural, yet abnormal, EMG signals significantly

reduced average errors in ankle angle during the gait cycle and phase transitions. However, the subject-specific model was limited to the prediction of a single ambulation condition (level treadmill walking) and did not estimate ankle moments needed in stiffness and impedance control.

In this study, the feedforward NARX model architecture was expanded to a *multiple*-output model that provided simultaneous estimates of future intended state of ankle angle and ankle moment across *multiple* ambulation conditions using lower limb surface EMG signals as input. Ankle plantarflexor and dorsiflexor EMG signals (antagonistic muscles) from healthy young adults were used to continuously predict normal ranges of ankle angle and moment during level overground walking, stair ascent, and stair descent, including transitions between terrains (i.e., transitions to/from staircase). Prediction performance was quantified using novel data sets and characterized as a function of the model parameters (prediction interval, sampling window, and number of hidden units) to identify optimal subject-specific parameters that minimized error. Models were trained and optimized for each participant to account for individual's specific variations of EMG activity and limb dynamics. The suitability of the model prediction for prosthetic control was then examined by statistically analyzing the prediction variability at critical performance points (Loverro et al., 2013; Protopapadaki et al., 2007; Sinitski et al., 2012) within ambulation conditions where excessive deviations could lead to trips or falls. Gait intention, via lower limb EMG signals, was explored by quantifying the impact of EMG inputs on the model prediction of ankle angle and moment.

2.3 MATERIALS AND METHODS

2.3.1 Participants

Ten healthy young adults (7 males; age = 21.9 ± 1.4; mass = 72.5 ± 8.8 kg; height = 1.8 ± 0.09 m) participated in the study. Participants were excluded if they presented neurologic or orthopedic impairments that would affect their ability to walk or follow instructions. The study was approved by the Institutional Review Board at Marquette University (Milwaukee, Wisconsin), and all participants provided written informed consent.

2.3.2 Experimental Procedure

During a single experimental session, participants ambulated at a self-selected speed wearing athletic shoes in three different ambulation conditions, level overground walking (LW), stair ascent (AS), and stair descent (DS). Twenty-five reflective markers were placed on the participant's key anatomical landmarks (posterior superior iliac spine and bilaterally on the anterior superior iliac spine, greater trochanters, thighs, medial and lateral femoral condyles, shanks, medial and lateral malleoli, calcaneus, second and fifth metatarsal heads, anterior end of first distal phalanx) to define seven lower body segments (pelvis, thighs, shanks, feet) based on a modified Helen Hayes marker set (**Figure 2.1A**). Trigno™ wireless surface EMG electrodes (Delsys, Inc., Natick, MA) were placed bilaterally over the tibialis anterior (dorsiflexor), and the gastrocnemius medialis (plantarflexor). Anthropometric measures (height and weight) were then taken. The walkway was instrumented with two 3-dimensional 6-channel force plates

(Advanced Mechanical Technology, Inc., Watertown, MA) embedded in the floor, a modified 4-step (17.78 cm rise, 60.45 cm width, 29.10 cm run; 1st step: 46.34 cm width, 26.45 cm run) instrumented staircase (Advanced Mechanical Technology, Inc., Watertown, MA) and a landing platform (1.22 x 0.91 m) (**Figure 2.1B**). To minimize session duration and set-up time, ambulation conditions were not randomized (APPENDIX E). Prior to data collection, participants walked on the walkway to get accustomed to the researcher instructions and staircase setup. First, during stair ascent trials, participants traversed the walkway (~3 m), ascended the stairs in a step-over-step fashion, and walked to the end of the landing platform (AS trial). Each stair ascent trial was followed by a subsequent stair descent trial, during which participants turned when instructed, crossed the platform, descended the stairs, step-over-step, and returned to their starting position (DS trial). For level ground walking, the staircase and landing platform were removed and participants walked the entire length of the walkway (~5 m). Participants were encouraged to take breaks as needed to minimize potential fatigue. A minimum of 15 trials were completed for each ambulation condition.

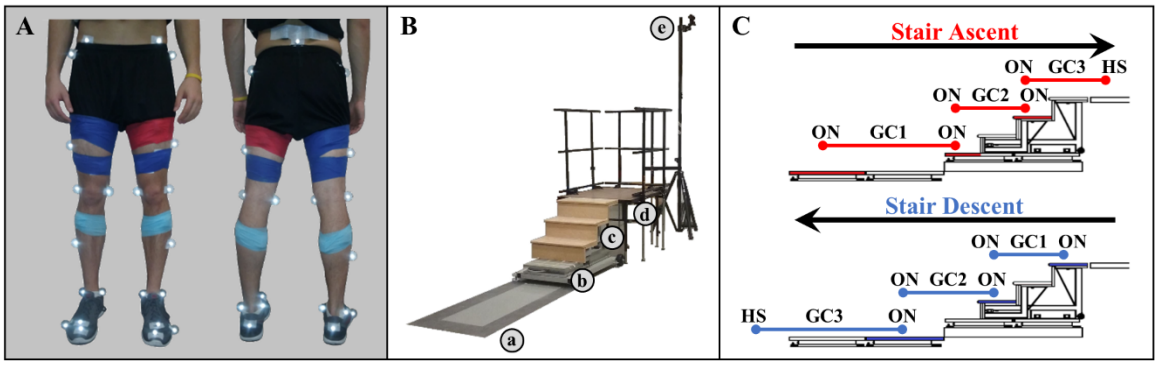

Figure 2.1. Marker and EMG sensor placement and experimental walkway. **(A)** Modified Helen Hayes infrared lower limb marker set and EMG sensor placement. **(B)** Experimental walkway setup including (a) force plates embedded in the floor, (b) stair force plates, (c) staircase, (d) landing platform, and (e) infrared motion cameras (APPENDIX D). **(C)** Schematic of step-over-step stair ambulation gait cycles (GC). Foot contact occurred on the shaded force plates (red, stair ascent; blue, stair descent).

2.3.3 Data Acquisition and Signal Processing

Surface EMG activity, kinetic, and kinematic data were collected and synchronized. Surface differential EMG recordings were amplified (909 V/V), sampled at 1,200 Hz, filtered to obtain linear envelopes, and down sampled to 120 Hz. EMG linear envelopes were obtained using a band-pass filter from 20-499.5 Hz (4^{th} order zero-phase Butterworth), followed by full-wave rectification, and a low-pass filter with a 5.5 Hz cutoff frequency (4^{th} order zero-phase Butterworth). Kinetic data were sampled at 1,200 Hz, low-pass and notch filtered (4^{th} order zero-phase Butterworth) at 15 Hz and 59-61 Hz, respectively, and down sampled to 120 Hz. Kinematic data were sampled at 120 Hz using an OptiTrack (NaturalPoint, Inc., Corvallis, OR) motion capture system (14 to 16 Flex 13 cameras). Markers were manually identified using AMASS (C-Motion, Inc., Germantown, MD) software and processed in Visual 3D (C-Motion, Inc., Germantown, MD) to extract limb kinematic (ankle angle) and foot kinetic (ankle moment, normalized to participant's body mass) time series and gait events. Marker trajectories, and kinematic and kinetic time series were subsequently low-pass filtered (15 Hz, 4^{th} order zero-phase Butterworth) and interpolated (3^{rd} order polynomial, max. gap of 20 frames) in Visual 3D. Ankle angle in the sagittal plane was computed as the motion of the foot segment relative to the shank segment coordinate system using Euler angles. Ankle moment in the sagittal plane was calculated using conventional inverse dynamics and resolved to the shank segment coordinate system (C-Motion, 2015).

Gait events were defined kinematically as HS for heel strike and TO for toe off on floor, and kinetically as ON for first foot contact on force plate, OFF for last foot contact on force plate (threshold 10 N). All trials were temporally normalized and truncated from

225 ms before the first foot contact on the first force plate to the first heel strike before contralateral last foot contact on the last force plate (percent trial). As a result, level walking condition consisted of one gait cycle and each stair ambulation condition consisted of three continuous gait cycles, as of traversing from level walking to stair stepping to level walking (**Figure 2.1C**). Staircase transitions, the short instance when transitioning between terrains, were defined from the start of the swing phase of the limb being investigated to the start of the swing phase of the contralateral limb of the transition step, except during the transition from the platform to the staircase (stair descent) where the transition limb was the contralateral limb.

2.3.4 NARX Neural Network Model

A model of lower limb state was developed to continuously predict simultaneous ankle kinematics and kinetics across ambulation conditions and terrain transitions. Specifically, a feedforward (open-loop) multiple-input multiple-output NARX model (Leontaritis & Billings, 1985; Narendra & Parthasarathy, 1990) was created, trained, and tested in MATLAB (R2017a, The MathWorks Inc., Natick MA) using the Neural Network Toolbox. The feedforward NARX model consisted of an input layer containing the windowed EMG linear envelopes of the ankle dorsiflexor and plantarflexor and the experimentally measured values of ankle angle and ankle moment (targets) passed through separate tapped delay lines, a single hidden layer containing nonlinear units, and a linear output layer containing separate outputs for the predicted (i.e., future estimates) ankle angle and moment in the sagittal plane (**Figure 2.2**).

The feedforward NARX model output, $\hat{y}_j(t+m)$, at each time point was calculated as,

$$v_n(t+m) = f_1\left(\sum_{q=0}^{d}\sum_{i=1}^{2} a_{ni}(q)\, x_i(t-q) - \sum_{q=0}^{d}\sum_{j=1}^{2} c_{nj}(q) y_j(t-q) + b_{1n}\right),$$

$$n = 1, 2, \ldots, N \tag{2.1}$$

$$\hat{y}_j(t+m) = f_2\left(\sum_{n=1}^{N} w_{jn} v_n(t+m) + b_{2j}\right),$$

$$j = 1, 2 \tag{2.2}$$

where $v_n(t+m)$ was the output of nth unit in the hidden layer, N was the total number of hidden units, m was the prediction interval in time steps ($\tau = m\Delta t$), d was the sampling window length ($D = d\Delta t$), $x_i(t-q)$ was the input of the ith EMG linear envelope for the prior q time step, $y_j(t-q)$ was the past jth desired target value (ankle angle and moment), a_{ni}, c_{nj}, and w_{jn} were the weights of EMG inputs, desired target values, and ankle angle and moment outputs, respectively, b_{1n} and b_{2j} were the bias weights at the hidden and output layers, respectively, f_1 was a nonlinear hyperbolic tangent sigmoid function, and f_2 was a linear function with unit slope. The sampling window specified the number of prior input values over time (exogenous and targets) used to calculate future ankle angle and moment. The prediction interval specified the time between the current inputs (exogenous and targets) and the model output predictions of future ankle angle and moment.

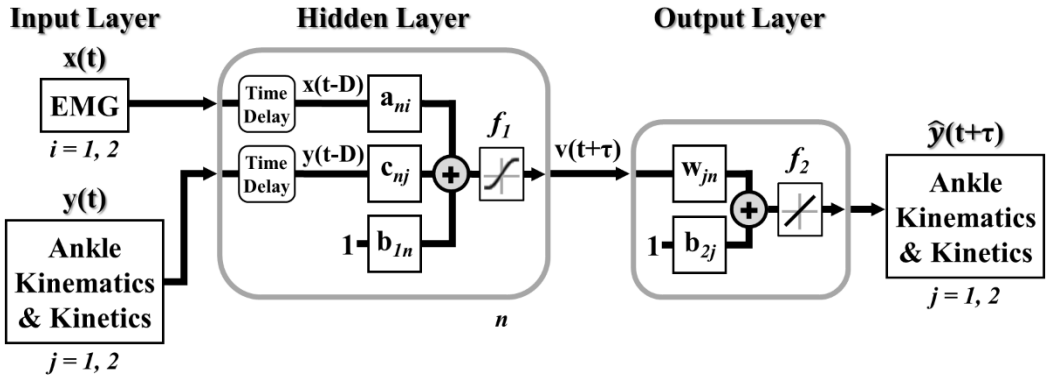

Figure 2.2. Multiple-input multiple-output feedforward (open-loop) NARX model. EMG linear envelopes (ankle dorsiflexor and plantarflexor) and experimentally measured values of ankle angle and ankle moment were weighted and fed via tapped delay lines to a single hidden layer containing nonlinear units with hyperbolic tangent sigmoid transfer functions. Intermediate outputs were weighted and linearly combined to provide continuous and simultaneous predictions of future ankle angle and moment over time.

Separate models were trained for each participant. During training, ten randomized trials from each ambulation condition of a single limb were organized as a concurrent set of sequences and divided into contiguous blocks where 80-percent (8 complete trials/condition) were used for training and 20-percent (2 complete trials/condition) were used for validation. An additional trial of each ambulation condition (novel test trial) was held back and used to separately assess model performance after training using a leave-one-out 10-fold cross-validation. Each model was trained and optimized to minimize the mean squared error (MSE) between the ankle angle and moment targets and the model predictions using a Levenberg-Marquardt backpropagation supervised learning procedure. To fit ankle angle and moment equally, training errors (i.e., MSE) were normalized to the range of [-2, 2] corresponding to normalizing model predictions and targets between -1 and 1 using a min-max mapping of the k-fold training dataset. For each training dataset, ten networks were trained using different initial weights and biases to improve shallow network generalization and avoid overfitting. The network with the lowest MSE averaged across ambulation conditions

was selected as the generalized network for that k-fold dataset. To explore the capabilities of the network, NARX model performance was characterized as a function of the prediction interval (τ: 33, 42, 50, 58, 67, 75, 83, 108, 142 ms), sampling window (D: 8, 17, 33, 50, 67, 83 ms), and number of hidden units (N: 2 to 16 in steps of 2) with error goal bounded to 1-percent of the moment variance of all recorded trials (1% training error goal). Subsequently, while the prediction interval was fixed to 58 ms (7 time steps) to counteract electromechanical inherent delays of the Marquette University's ankle-foot prosthesis (Klein & Voglewede, 2018; Sun et al., 2014; Sun & Voglewede, 2012), minimum MSE averaged over all novel test trials and ambulation conditions (10 complete trials/condition) was used to determine the optimal sampling window and number of hidden units. The training process was then repeated using the fixed prediction interval and the optimal sampling window and number of hidden units with an error goal of zero to maximize network performance for each participant. This optimized subject-specific network structure was used to evaluate model performance after training, unless otherwise specified.

2.3.5 Model Performance Measurements and Statistical Analysis

The number of participants included in the analysis of stair ambulation conditions was reduced to eight because two participants initiated trials with the limb opposite to the one being analyzed. All performance measurements and statistical analysis were averaged across ten novel test trials and then across participants for each ambulation condition (LW, n = 10; AS and DS, n = 8).

Root mean square error (RMSE) and coefficient of determination (R^2) were calculated between the target and model prediction of ankle angle and moment for each test trial to evaluate model performance. The coefficient of determination (R^2), obtained from squaring the cross-correlation peak, was used to quantify the ability of the model to reproduce the temporal profiles of angle and moment for each ambulation condition and their transitions.

Using the first set of models (1% training error goal), simple linear regressions were performed to examine the effects of prediction interval, sampling window, and number of hidden units on model performance. For each model output and ambulation condition, a linear fit (slope and intercept) was performed in MATLAB (R2017a) using the average RMSE collapsed along a single model parameter dimension (i.e., RMSE averaged across two of the three model parameters). Goodness of fit was assessed by the coefficient of determination (R^2), and an ANOVA ($p < 0.001$) was performed for each model parameter and ambulation condition to determine whether the fitted slope was significantly different from zero.

Using the second set of models (optimized subject-specific network structure), RMSE was computed over each trial to characterize maximal model performance across participants. To evaluate the impact of EMG signals on model performance, the instantaneous RMSE over time of NARX model predictions (time-varying EMG) were compared against errors of NARX models having constant EMG inputs. Constant EMG inputs, $x = \bar{x}$, for each participant, were calculated as the average EMG signal over time for each test trial and ambulation condition to provide the same average signal power while omitting the time-varying information. To facilitate analysis across test trials and

participants of instantaneous RMSE, individual trials were interpolated to a common length for each ambulation condition (LW: 145, AS: 430, DS: 400 samples).

Two types of critical performance points, clearance intervals (Loverro et al., 2013) and stance critical points (Protopapadaki et al., 2007; Sinitski et al., 2012), were assessed for each ambulation condition to verify that the NARX model predictions where within the variability of the measured targets. Staircase leg dynamics in this study were matched to the steps from Loverro's et al. 7-step staircase, and clearance intervals were selected corresponding to the locations of minimum foot and toe clearance, i.e., points with the highest tripping risk. Intervals were defined by the range of timings (mean ± standard deviation, i.e., thirty total points) of the minimum clearance angle. Single stance critical points (i.e., nineteen points) were extracted at crucial kinematic (TO, maximum dorsiflexion, maximum plantarflexion) and kinetic (maximum plantarflexion moment) events for prosthetic design. For each critical point, samples were tested for normality using the Shapiro-Wilk test. For normally distributed samples, a paired-samples t-test was used to determine if inter-subject NARX predictions were statistically different from that target. Sign test was performed for non-normally and asymmetric distributed critical points. Statistical analyses were performed using SPSS 22 (SPSS Inc., Chicago, IL) with a significance level of $p < 0.05$. The Benjamini-Hochberg (B-H) procedure was used to adjust p values with a false discovery rate of 0.05 to correct for multiple comparisons (Benjamini & Hochberg, 1995).

2.4 RESULTS

Experimentally measured ankle dorsiflexor and plantarflexor EMGs, ankle angles and ankle moments used to train and test the NARX models of a typical participant (AB4) are illustrated in **Figure 2.3**. EMG activity was variable across trials, occasionally exhibiting co-activation; however, activation patterns were consistent with the reported literature for all ambulation conditions for all participants (Benedetti et al., 2012; Y. Han et al., 2015; Selk Ghafari et al., 2009). Ankle angle was consistent across trials with the greatest ankle range of motion occurring for stair descent, while ankle moment exhibited more variability.

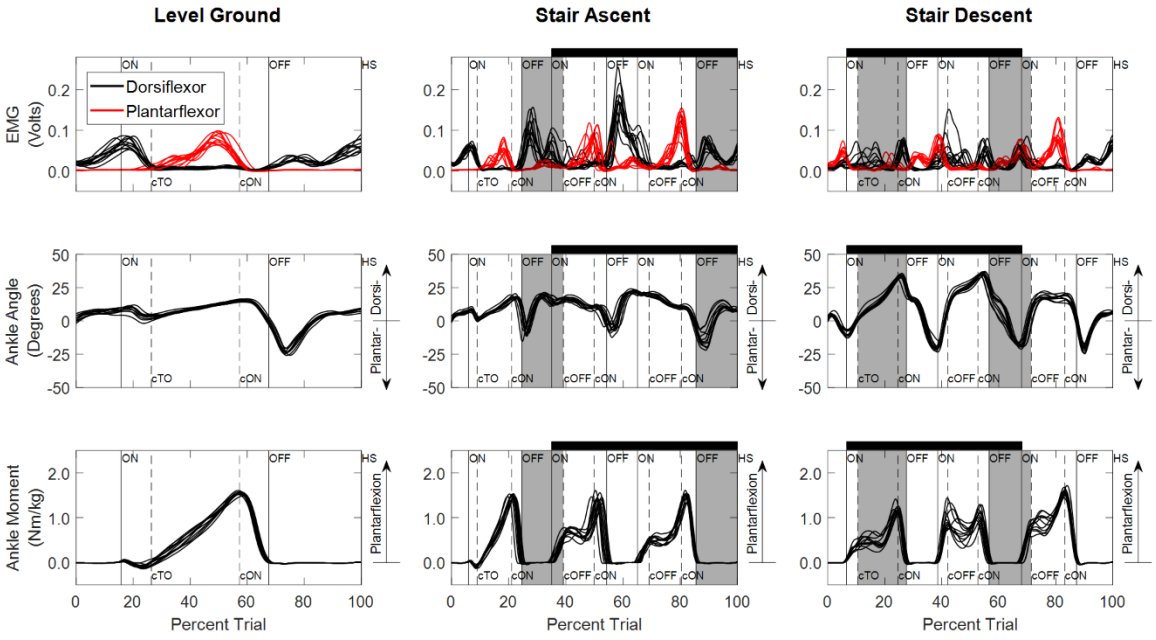

Figure 2.3. Experimentally measured EMG activity, kinetic, and kinematic data. Linear envelope of EMG signals, ankle angle, and ankle moment for level overground walking, stair ascent, and stair descent of a typical participant (AB4) are shown. Percent trial is normalized from 225 ms before the first foot contact on the first force plate to the first heel strike before contralateral last foot contact on the last force plate. Vertical lines denote gait events (solid: limb used to train the model; dashed: contralateral limb) defined based on force plate and floor contact (ON, first contact on force plate; OFF, last contact on force plate; HS, heel strike on floor; TO, toe off on floor). Contralateral gait events are identified by a lowercase 'c' (e.g., cTO, contralateral toe off). Staircase ambulation (black horizontal bar) is defined as the first foot contact on the staircase to the first foot contact on level ground of the limb used during training. Staircase transitions to/from level ground are shaded gray. Double limb support occurs when both feet are in contact with the ground simultaneously (ON to cTO *or* ON to cOFF and cON to OFF).

The performance of the NARX model was comparable across a wide range of sampling windows, and the number of hidden units; however, it was dependent on the size of the prediction interval (**Figure 2.4**). As prediction interval increased, RMSE had a significant linear increase for ankle angle and moment across ambulation conditions (ANOVA $p < < < 0.001$, $R^2 > 0.98$). Model error for predicting ankle angle and moment was largely unaffected by the size of the sampling window across ambulation conditions (ANOVA $p > 0.009$, $R^2 = [0.65, 0.85]$) with error saturating after 33 ms (ANOVA $p > 0.033$, $R^2 = [0.81, 0.94]$). The number of hidden units used in the network showed a small negative correlation with ankle angle and moment RMSE across ambulation conditions (ANOVA $p > 0.008$, $R^2 = [0.54, 0.71]$) that was significant for ankle angle RMSE during level walking and stair ascent (ANOVA $p < 0.001$, $R^2 = 0.88$). After 8 hidden units, RMSE saturated for ankle angle and moment across ambulation conditions (ANOVA $p > 0.003$, $R^2 = [0.61, 0.96]$). There were minimal differences in angle and moment error among ambulation conditions (**Figure 2.4**). When collapsed across model parameters, angle RMSE, averaged across participants and ambulation conditions, ranged from 0.73 to 1.16 degrees for a 33 ms prediction interval, 1.18 to 2.01 degrees for a 58 ms prediction interval, and 2.60 to 4.49 degrees for a 142 ms prediction interval with 1% training error goal. Similarly, moment RMSE ranged from 0.025 to 0.052 Nm/kg, 0.040 to 0.094 Nm/kg, and 0.099 to 0.215 Nm/kg, for 33, 58, and 142 ms prediction intervals, respectively.

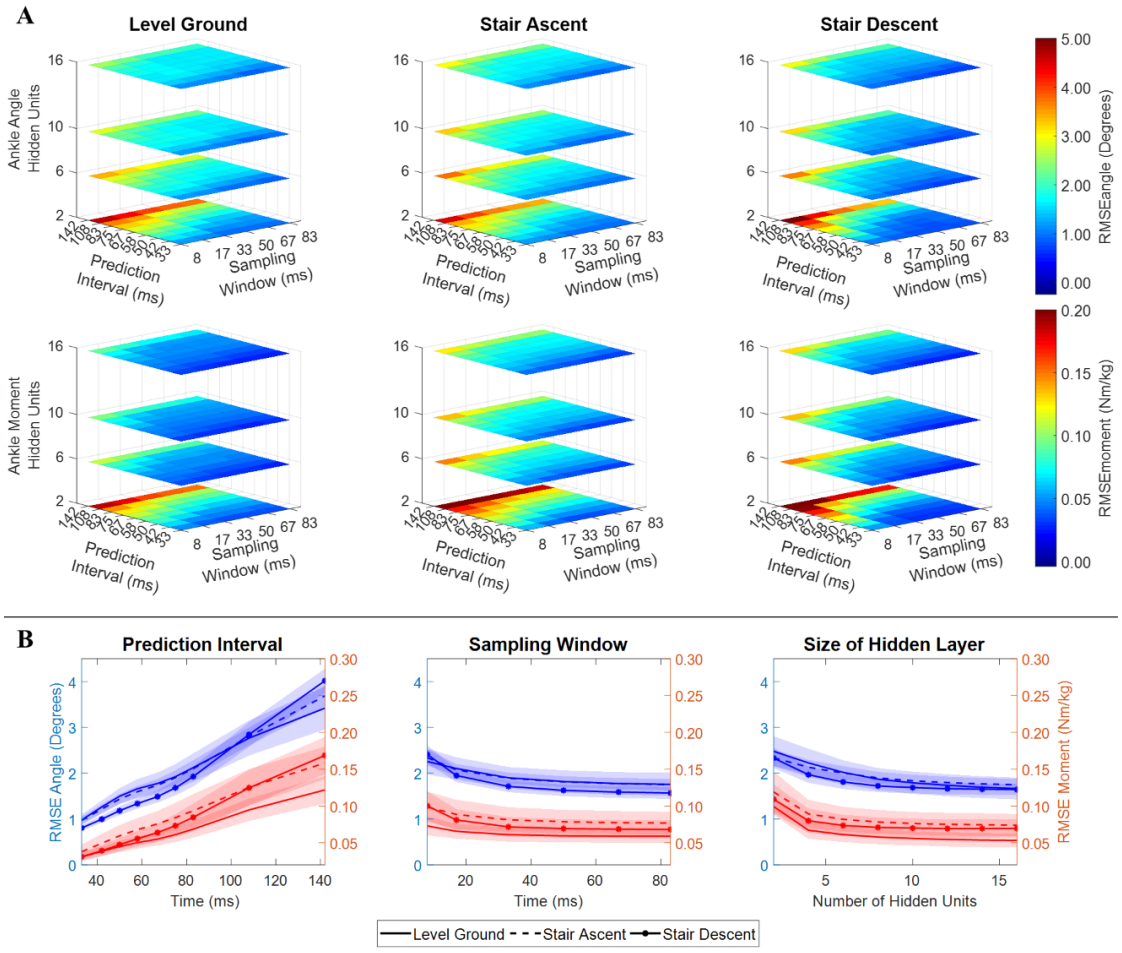

Figure 2.4. Space error based on model parameters. **(A)** RSME between predicted and experimentally measured ankle angle and ankle moment as a function of NARX model prediction interval, sampling window, and number of hidden units, averaged across participants. **(B)** RMSE ankle angle and moment collapsed across model parameters (i.e., averaged across two of the three dimensions). Shaded regions denote ±1 standard deviation. RMSE is shown for the first set of NARX models trained with error goal bounded to 1-percent of the moment variance of all recorded trials.

Joint ankle angle and ankle moment model predictions closely matched the experimentally measured targets in all ambulation conditions and staircase transitions as shown in **Figure 2.5**. The figure shows the comparison of model predictions and targets of a typical participant using optimal model parameters (τ: 58 ms, D: 83 ms, N: 6).

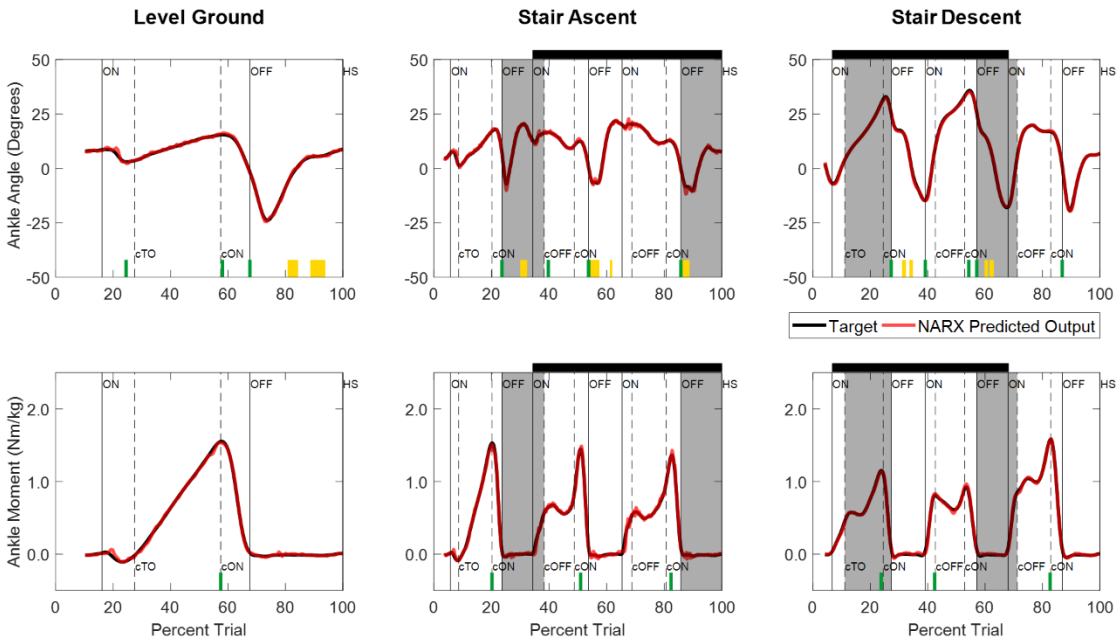

Figure 2.5. Time series of NARX model prediction of ankle angle and ankle moment. Level ground walking and stair ambulation of a typical participant (AB4) using optimal model parameters (τ: 58 ms, D: 83 ms, N: 6) are displayed. NARX model predictions are shown for the k-fold novel test trials with the best accuracy across ambulation conditions and model outputs. Critical performance points used to test for statistically significant differences between the model prediction and experimentally measured targets are denoted by yellow blocks (clearance intervals), and green lines (stance points). No significant differences were found across participants (B-H adjusted $p > 0.05$). Shading and line markers are defined the same as in **Figure 2.3**.

Table 2.1 lists the mean and standard deviations of the correlations (R^2) and errors (RMSE) of the NARX model prediction of ankle angle and moment across participants for all ambulation conditions. The results show high levels of accuracy in all ambulation conditions and model outputs. R^2 ranged between 0.989 and 0.999. All peak cross-correlations occurred at zero time lag. Stair descent had the lowest RMSE and the highest correlations for both ankle angle (RMSE = 0.55 ± 0.13°, R^2 = 0.999 ± 0.001) and moment (RMSE = 0.025 ± 0.007 Nm/kg, R^2 = 0.999 ± 0.001). The maximum error occurred in the prediction of ankle angle during level ground walking (RMSE = 0.84 ± 0.23°, R^2 = 0.989 ± 0.005) and in the prediction of ankle moment during stair ascent (RMSE = 0.036 ± 0.009 Nm/kg, R^2 = 0.997 ± 0.001). Using the Benjamini-Hochberg

multiple comparisons procedure, no significant difference across participants was found between targets and NARX model predictions in any of the critical performance points (B-H adjusted $p > 0.065$). Detailed statistical scores, and mean and standard deviation of ankle angle and moment predictions and targets of all critical points are listed in **Supplementary Table A.1**.

Table 2.1. RMSE and R^2 values of NARX model predictions for each ambulation condition averaged across participants.

Ambulation Condition	Model Output	$\overline{RMSE}$	σ_{RMSE}	Units	$\overline{R^2}$	σ_{R^2}
Level Ground (n = 10)	Angle	0.84	0.23	Degrees	0.989	0.005
	Moment	0.026	0.006	Nm/kg	0.998	0.001
Stair Ascent (n = 8)	Angle	0.78	0.14	Degrees	0.995	0.002
	Moment	0.036	0.009	Nm/kg	0.997	0.001
Stair Descent (n = 8)	Angle	0.55	0.13	Degrees	0.999	0.001
	Moment	0.025	0.007	Nm/kg	0.999	0.001

Comparison of the instantaneous RMSE over time for the NARX models using the participant's time-varying EMG as inputs against models using average EMG showed larger errors and increased variability for the constant-EMG NARX predictions across all ambulation conditions and staircase transitions for both ankle angle and ankle moment (**Figure 2.6, Table 2.2**). The patterns of EMG contribution were consistent among ambulation conditions and model outputs. Removal of the time-varying EMG input had the largest impact during double limb support for both ankle angle and moment. Additionally, the error increased around maximum plantarflexion and going into maximum plantarflexion moment for constant-EMG predictions. The use of time-varying EMG inputs decreased peak errors of ankle angle and moment by approximately 50 and

60% to values less than 1.11 degrees and 0.077 Nm/kg, respectively, across ambulation conditions.

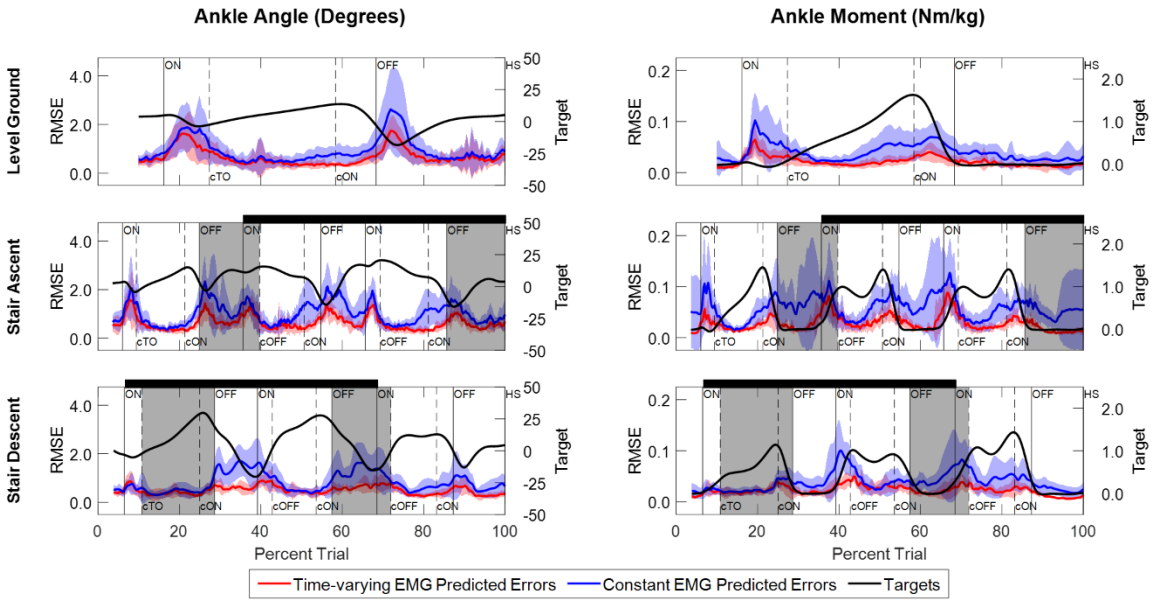

Figure 2.6. Impact of EMG signals on model performance. Instantaneous RMSE between experimentally measured values and NARX model predictions of ankle angle and ankle moment across trials and participants is displayed. Errors are shown for model predictions using the participant's time-varying EMG as input (red trace) and for model predictions using the average EMG signal as a constant input (blue trace). Shaded regions denote ±1 standard deviation. The ankle angle and moment targets averaged across trials and participants are shown for reference (black trace) and scaled accordingly to the right-side vertical axis. Double limb support intervals and gait event markers are defined the same as in **Figure 2.3**.

Table 2.2. Temporal average of the instantaneous RMSE. Error is calculated across participants for the NARX models using the participant's time-varying EMG as input and the NARX models using the average EMG as a constant input.

Ambulation Condition	Model Output	Units	Time-varying EMG		Constant EMG	
			$\overline{RMSE}$	σ_{RMSE}	$\overline{RMSE}$	σ_{RMSE}
Level Ground (n = 10)	Angle	Degrees	0.67	0.35	0.92	0.51
	Moment	Nm/kg	0.022	0.010	0.039	0.017
Stair Ascent (n = 8)	Angle	Degrees	0.64	0.29	1.02	0.44
	Moment	Nm/kg	0.028	0.015	0.058	0.022
Stair Descent (n = 8)	Angle	Degrees	0.50	0.17	0.82	0.40
	Moment	Nm/kg	0.023	0.009	0.039	0.018

2.5 DISCUSSION

An approach was presented for continuous predictive mapping of lower limb state that incorporated user intent, vis-à-vis surface EMG of the lower limb, to predict future ankle joint kinematics and kinetics simultaneously across ambulation conditions, including transitions between terrains. The single-network, feedforward NARX model had the ability to characterize normal gait patterns of ankle angle and ankle moment with predictions that fell within the experimentally measured variability of the kinematic and kinetic targets across trials and participants.

The autoregressive model presented here continuously models the nonlinear dynamic relationships between muscle activation and ankle dynamics to predict ankle kinematics and kinetics across ambulation conditions and terrain transitions. In contrast, EMG-driven FSMs to control active powered lower limb prostheses typically allow the amputee to select a discrete locomotion mode (M. Liu et al., 2017; Spanias et al., 2018) or to control a single parameter (e.g., motor torque gain) during a discrete period of the gait cycle (J. Wang et al., 2013; Kannape & Herr, 2014), and consequently, limit the amputee's control over the prosthesis. Despite proportional myoelectric approaches that enable continuous prosthetic control throughout the gait cycle using volitional muscle contractions, the volitional actuation of the prosthesis can become physically and cognitively demanding over time (S. Huang et al., 2016). Here, the NARX model leverages the user's natural muscle activation patterns to reduce muscle fatigue and the cognitive demand on the user to provide a continuous predictive characterization of gait over time without the need for explicit identification of gait events or selection of ambulation modes. Moreover, the training and optimization of the network structure to

maximize individual performance is relevant for the use in prosthetic applications where amputees may develop abnormal muscle activity and gait patterns to maintain stability and compensate for limitations in their prosthesis (Herr & Grabowski, 2012; S. Huang & Ferris, 2012; Seyedali et al., 2012; Silver-Thorn et al., 2012).

The autoregressive model structure exploits the cyclic process of lower limb motion, to anticipate repetitive components of movement, resulting in a high overall performance ($R^2 > 0.989$) while reducing the model degrees of freedom needed to predict limb kinematics and kinetics during gait. The use of time-varying EMG signals during gait resulted in less error compared to model predictions without time-varying information (**Table 2.2**, **Figure 2.6**). EMG signals provided an important source of information about limb state that was used to differentiate the temporal profiles of ankle dynamics. Although EMG signals contributed to the model prediction of ankle angle and ankle moment across ambulation conditions, the cyclic nature of walking and the open-loop structure of the feedforward model (which used experimentally error-free ankle angle and moment past values) limited the strength of the EMG contribution to the model predictions across ambulation conditions in healthy young adults. Similar to Farmer et al., while using residual within-socket EMG of transtibial amputees (Farmer et al., 2014), EMG signals had the greatest impact on error in regions where the gait profile was noncyclic, such as transitions to and from single limb support, staircase transitions, and around plantarflexion and moment peaks. Contrary to previous studies in transtibial amputees (Farmer et al., 2014) and able-bodied participants (Gupta et al., 2020), ankle angle accuracy and overall level of EMG contribution did not depend on the range of motion of the ankle, yielding similar levels of error across ambulation conditions and

model types tested. These results suggest that EMG signals from the lower leg (ankle dorsiflexor and plantarflexor) can be used to accurately predict noncyclic variations in amplitude and timing of ankle movement intrinsic to human walking across different terrains.

Unlike other nonlinear regressive neural networks (Ardestani et al., 2014; J. Chen et al., 2018; Gupta et al., 2020; Zhang et al., 2012), the current NARX model included temporal relationships (prediction interval, $\tau = m\Delta t$) of inputs and outputs allowing for the prediction of future limb state. A crucial advantage of prediction (i.e., future estimates) for the control of active ankle-foot prostheses is the ability to counteract delays from prosthetic actuation, signal processing (e.g., filtering, sampling), and sensor response inherent to electromechanical systems. In this study, the performance of the optimized NARX models was evaluated using a prediction interval of 58 ms to account for microcontroller and motor actuation delays (max. 50 ms) inherent to Marquette University's active powered ankle prosthesis (Sun et al., 2014; Klein & Voglewede, 2018; Sun & Voglewede, 2012). Other active ankle-foot designs have reported time delays of 40 ms for the system delay between the input and output of a two degrees of freedom cable-driven prosthesis (Ficanha et al., 2016), and maximum 40 ms for the pull-in response time of a bypass restriction valve of an electrohydrostatic-based prosthesis (Yu, 2017). Given the robust performance over a wide range of prediction intervals, sampling windows, and number of hidden units (**Figure 2.4**), models containing larger (or smaller) prediction intervals could be used with comparable results.

Despite variations in ankle moment, walking speed, and muscle activation patterns, the prediction error remained within the range of walking variability measured

across ambulation conditions. The use of two antagonist muscles as inputs, mainly responsible for sagittal ankle motion, resulted in minimal output oscillations that can occur when redundant information is present across multiple inputs (Ardestani et al., 2014; Gupta et al., 2020; Zhang et al., 2012), and simplified the intrinsic [EMG; (Ardestani et al., 2014; J. Chen et al., 2018)] and extrinsic [e.g., knee angle, hip angular velocity; (Ardestani et al., 2014; Dey et al., 2019; Eslamy & Alipour, 2019; Gupta et al., 2020)] inputs needed for implementation in a myoelectric ankle-foot prosthesis.

The NARX model performance complements and extends other feedforward estimation approaches for continuously estimating ankle kinematics and kinetics in healthy individuals (Zhang et al., 2012; Gupta et al., 2020; J. Chen et al., 2018; Keleş & Yucesoy, 2020; Dey et al., 2019; Eslamy & Alipour, 2019) and impaired patients (Ardestani et al., 2014; Farmer et al., 2014; Zhang et al., 2012). Across studies in health individuals, reported errors (RMSE) and correlations (R^2) of ankle angle varied between 2.44 and 5.29 degrees, and between 0.74 and 0.94, respectively, during level walking at different speeds and with various inputs. Specifically, Gupta et al. reported ankle angle errors, across healthy participants, during level walking (RMSE = 2.44 ± 0.45°, r = 0.97), stair ascent (RMSE = 3.61 ± 1.00°, r = 0.93), and stair descent (RMSE = 5.04 ± 1.56°, r = 0.85) using subject-specific NARX models trained and tested separately for each condition (Gupta et al., 2020). In comparison, average angle errors in this study were a factor of five lower for networks trained across the three terrains (RMSE < 0.84°). This may be tied to differences in the data organization (i.e., concurrent set of sequences) and the division of trials (i.e., contiguous blocks) used here during training which minimized discontinuities in the data that would cause inherent training errors, and ensured that

random trials, instead of random points, were used during training. Ardestani et al. obtained ankle moment errors up to 13% and 8% using FFANN and WNN models, respectively, during normal walking in patients with unilateral knee replacement (Ardestani et al., 2014). Interestingly, their results were based on a non-specific inter-subject training paradigm wherein the network was trained on data from three different patients while performing three walking conditions, and tested on a fourth participant. In their study, the purpose was to create a generalized real-time surrogate inverse dynamic model for gait analysis and was not intended for use in prosthetic control. Dey et al. used an SVR approach to continuously estimate ankle angle and moment during level ground walking (RMSE = 2.17° and 0.11 Nm/kg, respectively) using two extrinsic inputs (hip and knee angle) of a single healthy participant (Dey et al., 2019). The use of kinematic-only inputs could provide an alternative for predicting user intent indirectly but the need for wearable sensors extrinsic to the prosthesis poses similar challenges to EMG-based systems. Keleş et al. performed a comprehensive analysis of muscle sites and their combinations for use as EMG inputs to estimate ankle angle and moment during walking in healthy participants (Keleş & Yucesoy, 2020). Using the same ankle plantarflexor and dorsiflexor muscles, they reported ankle angle and moment errors (RMSE) of 2.34 ± 0.15 degrees and 0.041 ± 0.006 Nm/kg, in comparison to 0.84 ± 0.23 degrees and 0.026 ± 0.006 Nm/kg in this study. Correlations were comparable to those reported here, although performance was not examined across ambulation conditions.

The robust performance of the feedforward NARX model across ambulation conditions and terrain transitions suggest that it could provide intuitive user-driven control of an active powered ankle-foot prosthesis, however, additional work is needed.

Implementation in a physical system will require a closed-loop architecture wherein previous values of the predicted (rather than desired) ankle angle and moment are used to estimate changes in ankle dynamics. Feedback of the model predictions is expected to place greater emphasis on the use of EMG inputs to control for errors in the predicted ankle dynamics and to signal user intent during transitions and noncyclic activities (e.g., standing, sitting, obstacle avoidance). While previous studies have demonstrated the feasibility of continuously predicting ankle angle (Farmer et al., 2014; Zhang et al., 2012) and ankle moment (Ardestani et al., 2014), independently from neurological and neuromuscular impaired participants, the simultaneous prediction of ankle angle and moment across ambulation conditions must also be demonstrated with pathological muscle activity and gait data. Lastly, the effects on model performance associated with changes in EMG signal over time caused by variations in sensor placement and electrode-skin conductivity were not evaluated. Future work will characterize closed-loop NARX model performance across ambulation conditions using EMG activity from amputees' residual lower limb muscles as inputs. Furthermore, for real-time implementation in a prosthetic design, the model would be validated with data acquired from commonly used angle and moment sensors [e.g., encoders, inertial measurement units, force sensitive resistors, potentiometers, torque, load cells (Au et al., 2007; Klein & Voglewede, 2018; Sup et al., 2009)] intrinsic to the prosthesis instead of motion capture and force plate data as done in this study.

2.6 CONCLUSION

This study has demonstrated that a single-network nonlinear autoregressive model with exogenous EMG inputs can continuously predict future ankle angle and ankle moment simultaneously during normal walking across ambulation conditions (level ground walking, stair ascent/descent) and transitions between terrains. The natural patterns of muscle activation used to predict variations in normal gait, particularly during transitions, suggests that this approach could be used to create a seamless and intuitive interface for an active powered ankle-foot prosthesis that incorporates user intent and does not require conscious user control. The model's accuracy, robustness, and predictive capabilities (i.e., future estimates) suggest that the approach could be adapted for real-time closed-loop control of a wide variety of lower limb robotic devices, including actuated orthoses and exoskeletons. Further research will characterize the ability of within-socket residual EMG activity from amputees to continuously predict limb kinematics and kinetics across a variety of ambulation conditions.

CHAPTER 3: CLOSED-LOOP FUTURE PREDICTION OF CONTINUOUS ANKLE KINEMATICS AND KINETICS USING RESIDUAL MUSCLE SIGNALS OF TRANSTIBIAL AMPUTEES

This chapter has been submitted by the authors for publication:
Journal: Journal of NeuroEngineering and Rehabilitation
Title: "*Closed-Loop Future Prediction of Continuous Ankle Kinematics and Kinetics Using Residual Muscle Signals of Transtibial Amputees*"
Authors: Erika V. Zabre-Gonzalez, Barbara Silver-Thorn, Thomas Current, Philip A. Voglewede, Sara R. Koehler-McNicholas, and Scott A. Beardsley

3.1 ABSTRACT

Despite performance improvements in active lower limb prostheses, there remains a need for robust and accurate control techniques that incorporate direct user intent (e.g., myoelectric control) to limit the amputee's physical and cognitive demands and provide continuous, natural gait across terrains. Here, the ability of a nonlinear autoregressive neural network with exogenous (i.e., external) inputs (NARX) to continuously predict future (up to 142 ms ahead of time) ankle angle and moment of three transtibial amputees was examined across ambulation conditions (i.e., level overground walking, stair ascent, and stair descent) and terrain transitions. Within-socket residual EMG of the prosthetic side, in conjunction with sound-limb shank velocity, were used as inputs to the single-network NARX model to predict ankle dynamics of the sound limb. By overlaying the ankle dynamics of the sound limb onto the prosthesis, the approach is a step forward to establish a more normal gait by creating symmetric gait patterns between the limbs. The NARX model was trained and tested as a closed-loop network (model predictions fed back as recurrent inputs, rather than error-free targets) to ensure accuracy and stability when implemented in a feedback control system. Models of six able-bodied participants were also analyzed to provide a normative comparison of amputee model performance as

well as the best case characterization of normal gait patterns. Ankle angle and moment predictions of amputee models were accurate across ambulation conditions and terrain transitions with root mean square errors (RMSE) less than 3.7 degrees and 0.22 Nm/kg, respectively, and cross-correlations (R^2) greater than 0.89 and 0.93, respectively, for predictions 58 ms ahead of time. With similar model performance, the closed-loop NARX model had the ability to characterize normal ranges of ankle angle and moment of able-bodied participants ($RMSE_\theta < 2.7°$, $R^2_\theta > 0.95$, $RMSE_M < 0.11$ Nm/kg, $R^2_M > 0.98$ for predictions 58 ms ahead of time). Model performance was stable across a range of different EMG profiles, leveraging both EMG and shank velocity inputs for the prediction of ankle dynamics across ambulation conditions. The use of natural, yet altered in amputees, muscle activity with information about limb state, coupled with the closed-loop predictive design, could provide intuitive user-driven and robust prosthetic control by counteracting delays and proactively modifying gait in response to terrain changes observed by the user. The model takes an important step forward toward continuous real-time feedback control of active ankle-foot prostheses and other lower limb robotic devices.

3.2 INTRODUCTION

Advances in robotic systems and human interface design have facilitated the development of rehabilitation devices, exoskeletons, and limb prostheses, including state-of-the-art active ankle-foot prostheses (Sun et al., 2014; Au et al., 2009; Shultz & Goldfarb, 2018; Q. Wang et al., 2014; Cherelle et al., 2016; Bellman et al., 2008; Grimmer et al., 2016). For successful rehabilitation of lower limb amputees, prostheses

seek to mimic the biomechanical patterns of gait that occur during daily living activities. In spite of these advancements, most lower limb amputees develop altered muscle activity and biomechanical patterns of gait to maintain stability and compensate for limitations in the prosthesis (Herr & Grabowski, 2012; S. Huang & Ferris, 2012; Seyedali et al., 2012; Silver-Thorn et al., 2012). Despite performance improvements in active (i.e., able to generate power during propulsion) lower limb prostheses over passive designs, there remains a need for robust and accurate control techniques that incorporate user intent to limit physical and cognitive demands and provide a more natural gait across terrains (e.g., level ground, stairs, ramps) and environmental conditions.

Controllers for active lower limb prostheses range from closed-loop finite state machines (FSMs) driven by electromechanical sensors intrinsic to the prosthesis [e.g., inertial sensors, position encoders; (Au et al., 2009; Cherelle et al., 2016; Shultz & Goldfarb, 2018; Sun et al., 2014; Q. Wang et al., 2014)], to continuous proportional myoelectric control (Dawley et al., 2013; Hoover et al., 2012; S. Huang et al., 2016; S. Huang & Huang, 2018, 2019), as well as hybrid strategies combining electromechanical and myoelectric signals (Au et al., 2008; M. Liu et al., 2017; Spanias et al., 2018; J. Wang et al., 2013; Kannape & Herr, 2014, 2016). FSMs using intrinsic prosthetic sensors have been widely used to control active ankle-foot prostheses (Au et al., 2009; Cherelle et al., 2016; Shultz & Goldfarb, 2018; Sun et al., 2014; Q. Wang et al., 2014). However, robust control is constrained to a number of predefined locomotion modes. User intention is deduced indirectly by prosthetic sensors and/or requires the amputee to intentionally switch between modes based on anticipated changes in terrain. Consequently, the system has a limited ability to deal with novel movements and noncyclic activities whereas

intentional switching may increase physical and cognitive load on the user, particularly in complex environments (Culver et al., 2018; Zhang et al., 2015).

Continuous control approaches using intrinsic prosthetic sensors to unify the gait cycle have also been explored. Joint phase-based methods have been developed to control ankle-foot and multi-joint leg prostheses using shank and hip kinematics, respectively (Hitt et al., 2010; Holgate et al., 2009; Quintero et al., 2018). Phase-based approaches can accommodate speed changes of cyclic motion (e.g., walking at different speeds), however, they have limitations for noncyclic and novel movements in which phase planes are not well-defined. Discrete and continuous approaches designed around intrinsic prosthetic sensors provide high fidelity feedback about past limb state but are generally reactive (rather than predictive) to gait and environmental changes, and can introduce undesirable delays in the actuation of the prosthesis. In spite of their higher signal variability, surface electromyography (EMG) signals have been widely examined as an alternate, minimally-invasive source of control signals that incorporate direct user intent about intended movement and upcoming changes in terrain.

Hybrid state-based myoelectric approaches have used EMG signals within the prosthetic socket to select discrete locomotion modes (Au et al., 2008; M. Liu et al., 2017; Spanias et al., 2018), or to modify prosthetic behavior within a state [e.g., motor torque gain; (J. Wang et al., 2013; Kannape & Herr, 2014, 2016)]. EMG-driven FSMs can improve flexibility, allowing amputees to transverse different terrains and adapt to different walking speeds. However, control may not be intuitive, requiring the user to learn novel muscle activation patterns, and remains constrained to the control of predefined locomotion modes, limiting the amputee's control over the prosthesis.

Continuous proportional myoelectric control (CPMC) does not rely on a FSM, but instead allows the amputee to actuate the prosthesis based on the amplitude of residual muscle activity. Residual antagonistic muscles of a single transfemoral amputee have been used to continuously modulate impedance of an active knee prosthesis during level ground walking (Dawley et al., 2013; Hoover et al., 2012). Using CPMC, transtibial amputees were able to control a virtual environment via their residual ankle dorsiflexor and plantarflexor muscles (S. Huang & Huang, 2018, 2019), and control an active ankle-foot prosthesis via a single ankle plantarflexor muscle during level treadmill walking (S. Huang et al., 2016). CPMC, especially for impedance control, is a promising approach; however, it can require extensive user training, increase cognitive processing, and can be affected by muscle fatigue.

Many methods to estimate joint dynamics continuously have been proposed to eliminate the need for a discrete state-based control, and in the case of myoelectric control, to reduce user's cognitive and physical demands and to eliminate the need for high quality, independent muscle signals. EMG signals, ground reaction forces, and hip, knee, and shank dynamics have been used as inputs to continuously estimate (i.e., one-step-ahead estimate) (Dey et al., 2019; Eslamy & Alipour, 2019; Keleş & Yucesoy, 2020; J. Chen et al., 2018; Hahn & O'Keefe, 2008; Ardestani et al., 2014; Zhang et al., 2012; Gupta et al., 2020) and predict (i.e., n-step-ahead estimate) (Farmer et al., 2014; Zabre-Gonzalez, Riem, et al., 2021; Zarshenas et al., 2020) ankle kinematics and kinetics. These continuous gait models have proven successful, however, they typically focus on using muscle activity of healthy individuals to estimate ankle angle or moment during a single type of terrain (e.g., level walking).

Autoregressive models, such as nonlinear autoregressive neural network with exogenous (i.e., external) inputs (NARX), have been shown to work well for continuous myoelectric estimation/prediction of limb dynamics (Farmer et al., 2014; Gupta et al., 2020; J. Liu et al., 2017; Zabre-Gonzalez, Riem, et al., 2021). The NARX model can be trained in an open-loop mode (feedforward structure; error-free targets as inputs) or closed-loop mode (recurrent structure; model output estimates fed back as recurrent inputs). In previous work, EMG-driven feedforward (open-loop) NARX models have demonstrated the feasibility of continuously predicting future intended prosthetic ankle angle during level treadmill walking using within-socket residual surface EMG of transtibial amputees (Farmer et al., 2014), and ankle angle and moment across ambulation conditions (i.e., level overground walking, stair ascent, and stair descent) in healthy individuals [see CHAPTER 2 (Zabre-Gonzalez, Riem, et al., 2021)]. However, the accuracy and stability of the open-loop NARX model cannot be guaranteed when implemented in a feedback control system (Lewis & Parisini, 1998; Menezes & Barreto, 2008), commonly used for actuating ankle-foot prostheses. Explicit training as a recurrent (closed-loop) NARX model can overcome these shortcomings. Closed-loop model performance tends to be inferior (Menezes & Barreto, 2008) but model accuracy can be improved by incorporating additional input signals (Dey et al., 2019; Eslamy & Alipour, 2019; Keleş & Yucesoy, 2020; Gupta et al., 2020).

The combination of direct user intent, via EMG signals, and information about limb state, via electromechanical sensor signals, can increase the robustness and accuracy of locomotion mode detection (B. Chen & Wang, 2015; Tkach & Hargrove, 2013; H. Huang et al., 2011) and continuous estimation of lower limb kinematics (Gupta et al.,

2020; López-Delis et al., 2018). EMG and kinematic analyses suggest that timing in the local patterns of EMG activity is a key discriminant of gait while traversing different types of terrains (Lencioni et al., 2019; Wentink et al., 2013, 2014). The integration of EMG signals with information about limb state in a continuous predictive model of gait would provide intuitive and robust prosthetic control by counteracting delays (e.g., sensing, signal processing, and actuation), and proactively modifying gait in response to unexpected perturbations and upcoming changes in terrain.

The purpose of this study was to determine whether within-socket residual EMG of transtibial amputees could be used to continuously predict future ankle kinematics and kinetics across ambulation conditions including transitions between terrains (i.e., transitions to/from a staircase). Unlike previous approaches [see CHAPTER 2 (Farmer et al., 2014; Zabre-Gonzalez, Riem, et al., 2021)], here a recurrent (closed-loop) NARX model was used to predict future ankle angle and ankle moment of the sound limb using residual EMG of the prosthetic side, in conjunction with shank kinematics of the sound limb. By overlaying the ankle dynamics of the sound limb onto the prosthesis, the approach takes an important step toward establishing a more normal gait by creating symmetric gait patterns between the limbs. Prediction variability was statistically analyzed at critical points where excessive deviations in model prediction could lead to falls or injury during prosthetic control. Model performance and EMG contribution to model prediction in amputees were compared to models of able-bodied participants as best case characterization of normal gait patterns.

3.3 MATERIALS AND METHODS

3.3.1 Participants

Three male unilateral transtibial amputees (TTA) (age = 52.9 ± 6.2; with experimental prosthesis donned: mass = 90.9 ± 26.3 kg and height = 1.78 ± 0.08 m; time since amputation = 11.6 ± 4.8 years) and six able-bodied, healthy young adults (AB) (3 females; age = 21.7 ± 1.8; mass = 69.0 ± 9.0 kg; height = 1.77 ± 0.10 m) participated in the study (**Supplementary Table B.1**). For both groups, participants were excluded if they presented a neurologic or orthopedic impairment (other than amputation for TTAs) that would affect their ability to walk or follow instructions. All amputees were K3-K4 ambulators (e.g., variable cadence, community ambulator, independent ambulation without assistive devices), and two actively participated in sports activities. All amputees used energy-storing-and-returning feet with a pin-lock gel liner suspension system, and had volitional control of their remnant ankle flexors and extensors with stable residual volume. The study was approved by the Institutional Review Board at Marquette University (Milwaukee, Wisconsin, United States) and all participants provided written informed consent prior to participation.

3.3.2 Electrode-Socket Integration

A plastic electrode-housing test socket and a modified pin-lock gel liner were designed to integrate wireless surface EMG electrodes and allow the acquisition of EMG signals within the prosthetic socket of amputee participants. Prior to participation in the experimental session, each transtibial amputee was evaluated by a certified prosthetist to

assess the amputee's ability to independently control their residual tibialis anterior and gastrocnemius medialis and lateralis muscles, and to identify the three muscle sites for recording within socket (the gastrocnemius lateralis site was not used in this study). Amputees were instructed to "point up or down" the toes of their phantom limb. Muscle sites were then palpated, verified with a MyoBoy® (Ottobock, Duderstadt, Germany), and marked on the skin. After amputees donned a gel liner, molds of a Trigno™ wireless surface EMG electrode (Delsys, Inc., Natick, MA, United States) were placed inside the liner at the identified sites and marked on the liner's exterior surface. The marked liner was used by the prosthetist to transfer the desired electrode locations to a duplicate socket mold which was used to fabricate an individualized test socket for each amputee (**Figure 3.1A**). At each electrode site, the test socket contained openings with protruding walls sized to the thickness of the Trigno electrode, to provide reliefs that enhanced comfort and minimized electrode motion during ambulation. Similarly, the electrode locations in the marked liner were cut out to produce a small aperture for the electrode to make contact with the skin.

At the beginning and end of the experimental session, a certified prosthetist replaced the amputee's original socket with the duplicate electrode-housing test socket, and vice versa, and verified alignment. The test socket was mounted to the amputee's current prosthetic pylon and ankle-foot, and electrode sites were marked on their residual limb. Cover-Roll® Stretch dressing, with an electrode cut out, was placed over the cleaned skin to delineate electrode sites, and to protect skin from protrusion and pinching between the socket opening and the electrode. Electrodes were then secured on the residual limb and the modified liner was donned. Electrodes were adjusted to fit properly

through the liner holes and EMG signal quality was verified. A prosthetic shrinker was used to apply compression and facilitate donning of the socket. After the test prosthesis was donned, electrodes were adjusted within the socket openings, and electrode molds were placed externally to fill the walled empty space to minimize skin and electrode protrusion. After the donning procedure was completed, the amputee was asked to walk to verify comfort and alignment of the test prosthesis.

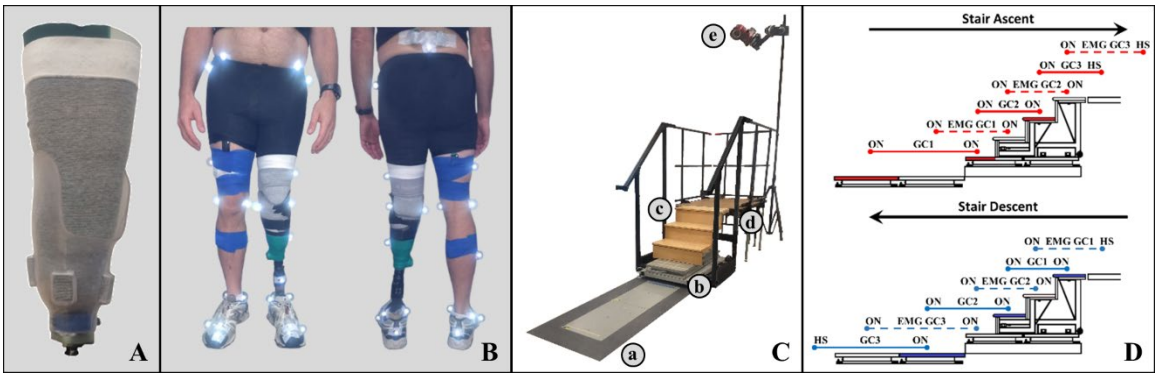

Figure 3.1. Electrode-socket integration and experimental walkway. **(A)** Individualized duplicate electrode-housing test socket and prosthetic shrinker used during amputee testing. **(B)** Modified Helen Hayes infrared lower limb marker set and EMG electrode placement on a transtibial amputee. **(C)** Experimental walkway including (a) embedded floor force plates, (b) stair force plates, (c) staircase, (d) landing platform, and (e) infrared motion cameras (APPENDIX D). **(D)** Schematic of step-over-step stair ambulation gait cycles (GC; red, stair ascent; blue, stair descent) used in the contralateral gait-cycle alignment. Gait cycles of the sound limb (lead limb) whose kinematics (ankle angle, shank velocities) and kinetics (ankle moment) were used as the target movement during training are shown as solid lines. Dashed lines denote consecutive gait cycles of the prosthetic limb (trail limb) whose residual EMG was aligned with the target kinematic/kinetic gait cycles.

3.3.3 Experimental Procedure

Participants ambulated at a comfortable, self-selected speed wearing athletic shoes, in three different ambulation conditions, level overground walking (LW), stair ascent (AS), and stair descent (DS). Ambulation conditions were not randomized to minimize set-up time and session duration (APPENDIX E). The walkway was instrumented with four 3-dimensional 6-channel force plates (Advanced Mechanical

Technology, Inc., Watertown, MA, United States), two embedded in the floor, and two built-in under a modified 4-step (60.5 cm width x 17.8 cm rise x 29.1 cm run; 1st step: 46.3 cm width, 26.5 cm run) staircase (Advanced Mechanical Technology, Inc., Watertown, MA, United States) connected to a landing platform (1.22 x 0.91 m) (**Figure 3.1C**). Prior to data collection, participants walked on the walkway to get accustomed to the staircase setup and task instructions. First, participants traversed the walkway (~3 m), ascended the stairs in a step-over-step fashion, and walked to the end of the platform (stair ascent trial). When instructed, they walked the platform, descended the stairs step-over-step, and returned to their starting position on level ground (stair descent trial). During stair ambulation, amputees had access to handrails for support and protection, however, their use was minimal. For level ground walking trials, the staircase and landing platform were removed, and participants walked the entire length of the walkway (~5 m). Participants completed a minimum of fifteen trials per ambulation condition. Breaks were encouraged to reduce risk of fatigue.

3.3.4 Data Acquisition and Signal Processing

Surface EMG activity, kinematic, and kinetic data were collected and synchronized. Trigno™ wireless surface EMG electrodes were placed on clean skin, bilaterally over the tibialis anterior (dorsiflexor) and the gastrocnemius medialis (plantarflexor) of able-bodied participants. EMG electrode placement on amputees was performed as described previously (Electrode-Socket Integration). Surface EMG recordings were sampled at 1,200 Hz, differentially amplified (909 V/V), filtered and rectified to obtain the linear envelope (band-pass filter: 4th order zero-phase Butterworth

at 20-499.5 Hz, full-wave rectified, low-pass filter: 4th order zero-phase Butterworth at 5.5 Hz), and down sampled to 120 Hz. The band-pass filter removed potential within-socket motion artifacts below 20 Hz similar to Hefferman et al. (Hefferman et al., 2015). Kinetic data was sampled at 1,200 Hz, low-pass (4th order zero-phase Butterworth at 15 Hz) and notch (4th order zero-phase Butterworth at 59-61 Hz) filtered, and down sampled to 120 Hz. Seven lower body segments (pelvis, thighs, shanks, feet) were defined based on a modified Helen Hayes marker set using twenty-five reflective markers placed on the participant's key anatomical landmarks (posterior superior iliac spine and bilaterally on the anterior superior iliac spine, greater trochanters, thighs, medial and lateral femoral condyles, shanks, medial and lateral malleoli, calcaneus, second and fifth metatarsal heads, anterior end of first distal phalanx) (**Figure 3.1B**). Marker locations on the prosthetic limb were approximated based on the sound-limb locations for amputees. Anthropometric measures (height and weight) were taken. Kinematic data were sampled at 120 Hz using an OptiTrack (NaturalPoint, Inc., Corvallis, OR, United States) motion capture system (14 to 16 Flex 13 cameras). AMASS and Visual 3D (C-Motion, Inc., Germantown, MD, United States) were used to extract limb kinematic (shank velocities and sagittal ankle angle) and foot kinetic (sagittal ankle moment, normalized to participant's body mass) time series and gait events. Pre-processing of kinematic and kinetic time series are explained in detail in previous work [see CHAPTER 2 (Zabre-Gonzalez, Riem, et al., 2021)]. Shank segment center of mass linear velocity was obtained in three axes (sagittal, longitudinal, and frontal) relative to the global coordinate system using the finite difference method (C-Motion, 2014). The sagittal axis was

defined along the anterior-posterior (AP) direction, the longitudinal axis in the vertical direction, and the frontal axis in the medial-lateral (ML) direction.

All trials were truncated and temporally normalized from 225 ms before the first foot contact on the first force plate to the first heel strike before contralateral last foot contact on the last force plate (percent trial). Consequently, the level walking trial consisted of one gait cycle, and each stair ambulation trial consisted of three continuous gait cycles including two staircase transitions, as participants traversed from level walking to stair stepping to level walking (**Figure 3.1D**), as detailed in previous work [see CHAPTER 2 (Zabre-Gonzalez, Riem, et al., 2021)]. To overlay the dynamics of the sound limb onto the prosthetic limb to restore symmetric gait using residual EMG, kinematic (ankle angle, shank velocities) and kinetic (ankle moment) trials of the sound limb were temporally aligned with within-socket residual EMG trials of the prosthetic limb to create the dataset for model training and testing. EMG gait cycles of the prosthetic limb (trail limb) were interpolated (piece cubic spline) within a gait cycle to correspond with the length of the gait cycles of the sound limb (lead limb). For stair ambulation, EMG gait cycles were consecutively selected, instead of maximum profile similarities, to avoid introducing error during training associated with discontinuities in the data (**Supplementary Figure B.4**). This method is referred as *contralateral gait-cycle alignment* (**Figure 3.1D**). Similarly, an additional dataset for able-bodied participants was created where EMG signals of the contralateral limb were aligned and interpolated to the gait cycles of the limb used to train the model (i.e., ankle kinematic and kinetic predictions). EMG of this dataset is referred as *contralateral EMG* and the participants as AB_{cEMG}.

3.3.5 NARX Model

A model of future lower limb state was developed to continuously predict (i.e., future estimates) ankle kinematics and kinetics of the sound limb of transtibial amputees, across ambulation conditions and terrain transitions. Specifically, a recurrent (closed-loop) multiple-input multiple-output NARX model (S. Chen et al., 1990; Leontaritis & Billings, 1985) was created, trained, and tested using the Neural Network Toolbox in MATLAB (R2017a, The MathWorks Inc., Natick, MA, United States). The NARX model consisted of an input layer containing windowed time series of five exogenous inputs and two feedback model outputs (i.e., as recurrent inputs) fed via separate tapped delay lines to a single hidden layer containing nonlinear units. The exogenous inputs consisted of the within-socket residual EMG linear envelopes of the ankle dorsiflexor and plantarflexor and the 3-axis shank velocities of the sound limb. The recurrent inputs corresponded to the prior predictions of the sagittal ankle angle and ankle moment of the sound limb fed back from the model output. The hidden layer output was then fed to a linear output layer containing separate outputs of the predicted ankle angle and moment of the sound limb (**Figure 3.2**).

The prediction of the recurrent (closed-loop) NARX model output, $\hat{y}_i(t+m)$, at each time point was calculated by the following equations,

$$v_n(t+m) = f_1\left(\sum_{q=0}^{d}\sum_{i=1}^{5} a_{ni}(q)\, x_i(t-q) - \sum_{q=1}^{d}\sum_{j=1}^{2} c_{nj}(q)\hat{y}_j(t-q) + b_{1n}\right),$$

$$n = 1, 2, \ldots, N \tag{3.1}$$

$$\hat{y}_j(t+m) = f_2\left(\sum_{n=1}^{N} w_{jn} v_n(t+m) + b_{2j}\right),$$

$$j = 1, 2 \tag{3.2}$$

where $v_n(t+m)$ is the output of nth unit in the hidden layer, N is the size of the hidden layer, d is the sampling window length in time steps ($D = d\Delta t$), m is the prediction interval in time steps ($\tau = m\Delta t$), $x_i(t-q)$ is the ith exogenous input (EMG linear envelopes or shank velocities) for the prior q time step, $\hat{y}_j(t+q)$ is the prior prediction of the jth output (ankle angle or moment), a_{ni}, c_{nj}, and w_{jn} are the weights of EMG and shank velocity inputs, feedback outputs, and model outputs, respectively, b_{1n} and b_{2j} are the bias weights of the nth hidden unit and jth output unit respectively, f_1 is a nonlinear hyperbolic tangent sigmoid function, and f_2 is a linear function with unit slope. The prediction interval specified the time relative to the current time step for which future ankle angle and moment were calculated. The length of the sampling window specified the number of prior inputs (exogenous and recurrent) used to predict future ankle angle and moment.

Additional to the amputee models, two NARX models were created using the same set of able-bodied participants (AB model and AB_{cEMG} model). AB models used inputs (EMG and shank velocities) and outputs (ankle angle and moment) of the same limb (i.e., limb used to train the model), whereas AB_{cEMG} models used the aligned contralateral EMG as the EMG input. AB and AB_{cEMG} NARX models served as control

models (1) to determine the ability of a single-network, closed-loop model to continuously predict normal ranges of ankle dynamics associated with healthy ambulation, (2) for a normative comparison of amputee model performance, (3) to determine if using contralateral EMG as inputs was a viable approach, and (4) to determine the influence of the contralateral gait-cycle alignment on model performance.

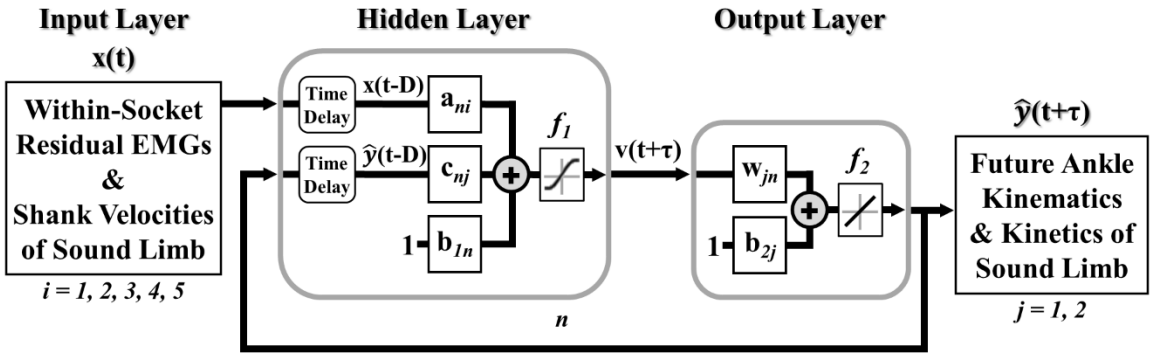

Figure 3.2. Multiple-input multiple-output recurrent (closed-loop) NARX model for transtibial amputees. The linear envelope of within-socket residual EMG (ankle dorsiflexor and plantarflexor), shank linear velocities of the sound limb, and prior predictions of ankle angle and ankle moment of the sound limb were weighted and fed via tapped delay lines to a single hidden layer containing nonlinear units with hyperbolic tangent sigmoid transfer functions. Intermediate outputs were weighted and linearly combined to provide continuous predictions of future ankle angle and moment over time of the sound limb. Models of able-bodied participants (AB and AB_{cEMG} models) differed in the use of inputs and outputs of the same limb (AB), and the use of the aligned contralateral EMG as the EMG input (AB_{cEMG}).

To sample model parameter ranges relevant for the optimization of the model [see CHAPTER 2 (Zabre-Gonzalez, Riem, et al., 2021)], NARX model performance was characterized as a function of prediction interval (τ: 8, 58, 142 ms), sampling window (D: 17, 42, 83 ms), and number of hidden units (N: 16, 30, 50) using a leave-one-out 10-fold cross-validation procedure. The model was optimized using a supervised learning procedure to minimize the mean squared error (MSE) between the experimentally measured ankle angle and moment (targets) and the model predictions where angle and moment errors were fitted equally. For each participant, all trials were randomized and

ten separate model fits, with randomized initial weights, were trained with ten trials of each ambulation condition (80% used for training, 20% for validation). Training trials were organized as concurrent set of sequences and divided into contiguous blocks to avoid discontinuities in the data that would cause inherent training errors, and to ensure that random trials, instead of random points, were used during training. One trial of each ambulation condition was held back (novel test trial) to avoid overfitting and to separately assess model performance after training. All networks were trained and tested in a closed-loop mode whereby model predictions of ankle angle and moment from the output layer were fed back as recurrent inputs rather than the experimentally measured targets. From the ten model fits, the generalized network for that k-fold dataset was determined by the model with the lowest MSE averaged across novel test trials and ambulation conditions. The procedures used for training and testing are explained in detail in previous work [see CHAPTER 2 (Zabre-Gonzalez, Riem, et al., 2021)]. The prediction interval was chosen to be 58 ms (7 time steps) to counteract electromechanical inherent delays (max. 50 ms) of the Marquette University's active ankle-foot prosthesis (Klein & Voglewede, 2018; Sun et al., 2014; Sun & Voglewede, 2012). The optimal sampling window and number of hidden units were determined by the network with the minimum MSE averaged over the ten novel test trials of the stair descent condition. Model performance after training was evaluated using this optimized subject-specific network structure to characterize maximal performance for each participant. For each able-bodied participant, optimal sampling window and number of hidden units were selected for each AB and AB_{cEMG} model.

3.3.6 Model Performance Measurements and Statistical Analysis

All performance measurements and statistical analyses were averaged across ten novel test trials for each ambulation condition and model output (ankle angle and moment), individually for amputees and averaged across able-bodied participants (AB group and AB_{cEMG} group), unless otherwise specified.

Coefficient of determination (R^2; obtained from squaring the cross-correlation peak) and root mean square error (RMSE) were calculated between the model prediction and the experimentally measured target of ankle angle and moment to characterize model performance. R^2 and time lags were used to quantify the model ability to reproduce angle and moment profiles and to identify temporal offsets in the model prediction for each ambulation conditions and their transitions.

The effects of prediction interval, sampling window, and number of hidden units on model performance were examined using the average RMSE collapsed along a single dimension (i.e., RMSE averaged across two of the three model parameters). RMSE was averaged across participants for each participant group (TTA, AB, and AB_{cEMG}). RMSE was also computed using the optimal subject-specific model parameters, individually for amputees, and averaged across participants for able-bodied groups. Model performance was further investigated by analyzing changes in RMSE distribution within the gait cycles of the ambulation conditions. Each gait cycle was divided into the standard seven gait periods based on gait events (Neumann, 2017): loading response (initial foot contact to contralateral toe off), mid-stance (1-50% of single-limb support), terminal stance (50-100% of single-limb support), pre-swing (contralateral initial foot contact to toe off), initial swing, mid-swing, and terminal swing. The three swing periods represented one-

third of the swing phase. RMSE was then computed within each gait period and then averaged across trials.

To evaluate the impact of EMG signals on model prediction, the sum of weighed inputs (SWI) was calculated for each exogenous input using the novel test trials and the trained weights from the input to the hidden layer. The SWI of the ith input, was calculated as,

$$SWI(i,t) = rms\left(\sum_{q=0}^{d} a_{ni}(q)\, x_i(t-q)\right)\Bigg|_N,$$

$$n = 1, 2, \ldots, N \qquad (3.3)$$

where for each time step, the windowed input is multiplied by the associated hidden-layer weights, a_{ni}, and summed across the sampling window to quantify the strength of the ith input to each hidden unit. The root mean square (rms) was then computed across hidden units to characterize the total contribution of the ith input to the model prediction throughout the trial. SWI was averaged over time and across trials for each ambulation condition to quantify the overall contribution of each input. Similar to the analysis of the RMSE distribution within ambulation conditions, the SWI distribution of the inputs (ankle dorsiflexor and plantarflexor EMG and AP shank velocity) were analyzed within the gait cycles for each ambulation condition (gait cycle 2 for stair ambulation). The SWI over time of each gait cycle was divided into the seven gait periods and then averaged across trials.

Several critical performance points, clearance intervals (Loverro et al., 2013) and stance critical points (Protopapadaki et al., 2007; Sinitski et al., 2012), were selected from literature to verify that the NARX model predictions where within the variability of the

targets of each participant at those locations. Leg dynamics of Loverro's et al. staircase steps were matched to the stair steps of this study, and clearance intervals were identified, corresponding to the minimum foot and toe clearance with the highest tripping risk during normal gait (Loverro et al., 2013). For each clearance interval, three critical points were identified corresponding to the range of timings of the minimum clearance angle (mean ± standard deviation, i.e., 30 total points). Crucial kinematic (toe off, maximum dorsiflexion, maximum plantarflexion) and kinetic (maximum plantarflexion moment) events for prosthetic design were defined as single stance critical points (i.e., 19 points). For each participant, a paired-samples t-test was performed for each critical point to determine whether NARX model predictions were statistically different from experimentally measured targets across trials. If the Shapiro-Wilk normality test failed, a nonparametric sign test was performed instead. SPSS 22 (SPSS Inc., Chicago, IL, United States) was used for all statistical analyses with a significance level of $p < 0.05$. For each participant, the p values of the critical points (i.e., 49 total points) were adjusted for multiple comparisons using the Benjamini-Hochberg (B-H) procedure with a false discovery rate of 0.05 (Benjamini & Hochberg, 1995).

3.4 RESULTS

Aligned experimentally measured shank linear velocities, ankle angle and ankle moment of the sound limb, and residual ankle dorsiflexor and plantarflexor EMG used during training and testing are shown for an amputee (TTA3, most active amputee) in **Figure 3.3**. Experimental data of the remaining amputees and a typical able-bodied

participant (AB3) are provided in the Supplementary Material (**Supplementary Figures B.1-B.3**).

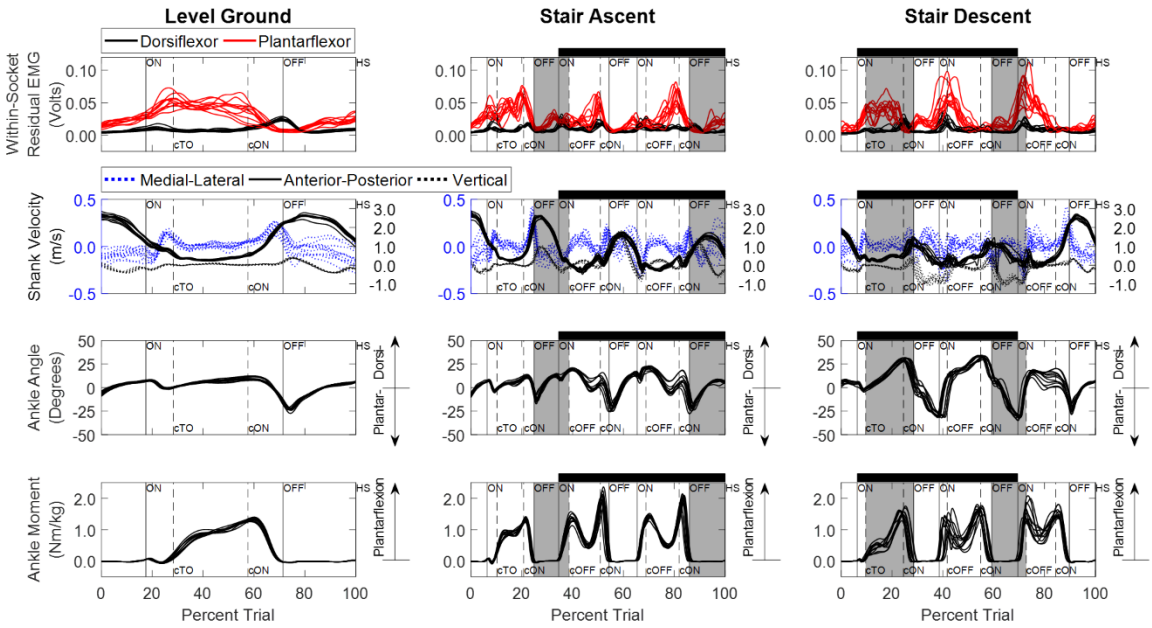

Figure 3.3. Aligned experimentally measured trials used to train and test the NARX model of a transtibial amputee (TTA3). Shank linear velocities, ankle angle, and ankle moment of the sound limb, and the linear envelope of within-socket residual EMG (ankle dorsiflexor and plantarflexor) are shown during level overground walking and stair ambulation. Percent trial is normalized from 225 ms before the first foot contact on the first force plate to the first heel strike before contralateral last foot contact on the last force plate. Vertical lines denote gait events (solid: sound limb; dashed: contralateral limb, i.e., prosthetic limb) defined based on force plate (threshold 10 N) and floor contact (ON, first contact on force plate; OFF, last contact on force plate; HS, heel strike on floor; TO, toe off on floor). Contralateral gait events are identified by a lowercase "c" (e.g., cTO, contralateral toe off). Staircase ambulation (black horizontal bar) is defined as the first foot contact on the staircase to the first foot contact on level ground of the sound limb. Staircase transitions to/from level ground are shaded gray. Single-limb support occurs when only one limb is in contact with the ground (cTO to cON *or* cOFF to cON). Experimental data of the remaining amputees and a typical able-bodied participant (AB3) are provided in the Supplementary Material (APPENDIX B).

All amputees were able to activate both muscles with voluntary sustained contractions. Within-socket residual and able-bodied EMG activation patterns were consistent across trials for each ambulation condition; however, residual EMG showed different temporal profiles among amputees and in comparison to able-bodied participants. EMG activity within the prosthetic socket exhibited different levels of co-contraction between antagonistic muscles (e.g., **Supplementary Figure B.1**). Able-

bodied participants exhibited a phasic pattern of activity within the muscle pair with minimal co-contraction in each ambulation condition (**Supplementary Figure B.3**). When comparing EMG from both limbs of able-bodied participants, the contralateral gait-cycle alignment affected the aligned contralateral EMG patterns (e.g., different shapes), especially during gait cycle 1 and 3 of stair ambulation, but maintained a phased pattern (**Supplementary Figures B.3** and **B.4**). Amputee EMG amplitudes tended to be lower than those of able-bodied participants and tended to have a greater amplitude difference within the muscle pair. Shank velocities and ankle dynamics were also consistent across trials in all ambulation conditions for both amputees' sound limb and able-bodied participants. The largest shank velocity occurred in the AP direction in all ambulation conditions and participant groups. Across participants, the greatest ankle range of motion occurred during stair descent, whereas a qualitative assessment suggested that ankle moment exhibited more trial-wise variability also during stair descent.

Contrary to the feedforward NARX model developed previously [see CHAPTER 2 (Zabre-Gonzalez, Riem, et al., 2021)], closed-loop model error for the prediction of ankle angle and moment varied nonlinearly with prediction interval across ambulation conditions and participant groups (**Figure 3.4** and **Supplementary Figure B.5**). RMSE had a slightly parabolic shape where 8 and 142 ms had similar values but larger than 58 ms. In contrast, RMSE of ankle angle and moment had a small decrease as sampling window increased across ambulation conditions and participant groups. RMSE were similar with 16 and 30 hidden units but increased with 50 units for ankle angle and moment in all ambulation conditions and participant groups. Amputees had similar angle

and moment RMSE to the AB_{cEMG} group, but both groups had slightly larger errors than the able-bodied group (AB) for all model parameters and ambulation conditions. RMSE of the predicted ankle angle and moment were consistently lowest for level walking and largest for stair descent, but with overlapping standard deviations among ambulation conditions, across parameters and participant groups.

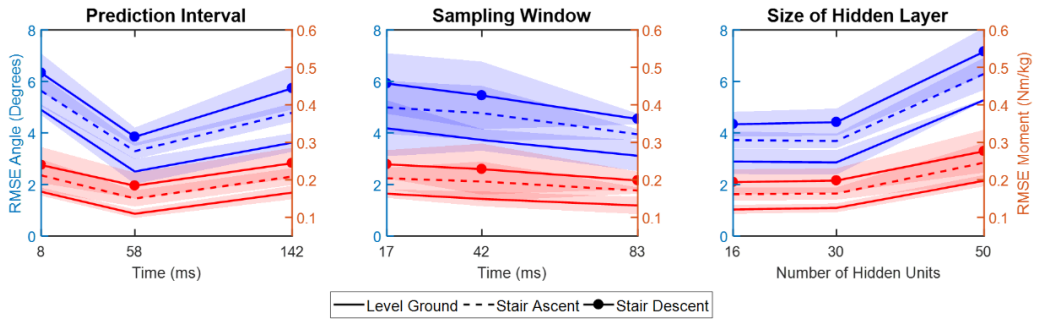

Figure 3.4. Parameter space error of the recurrent (closed-loop) NARX model for transtibial amputees. RSME between predicted and experimentally measured ankle angle and ankle moment is shown as a function of prediction interval, sampling window, and number of hidden units, averaged across amputees. RMSE is collapsed across model parameters (i.e., averaged across two of the three dimensions). Shaded regions denote ±1 standard deviation. Results for able-bodied groups are provided in the Supplementary Material (APPENDIX B).

Closed-loop NARX model predictions of ankle angle and ankle moment closely matched the experimentally measured targets in all ambulation conditions and staircase transitions for all amputees and able-bodied participants (AB and AB_{cEMG} models). **Figure 3.5** shows the comparison of model predictions and targets for each amputee using their optimal model parameters (τ: 58 ms**,** TTA1 - D: 83 ms, N: 50; TTA2 - D: 42 ms, N: 30; TTA3 - D: 83 ms, N: 50). Prediction time series of a typical able-bodied participant trained with same-limb data (AB3) and trained with aligned contralateral EMG as the EMG input ($AB3_{cEMG}$) are provided in the Supplementary Material (**Supplementary Figure B.6**).

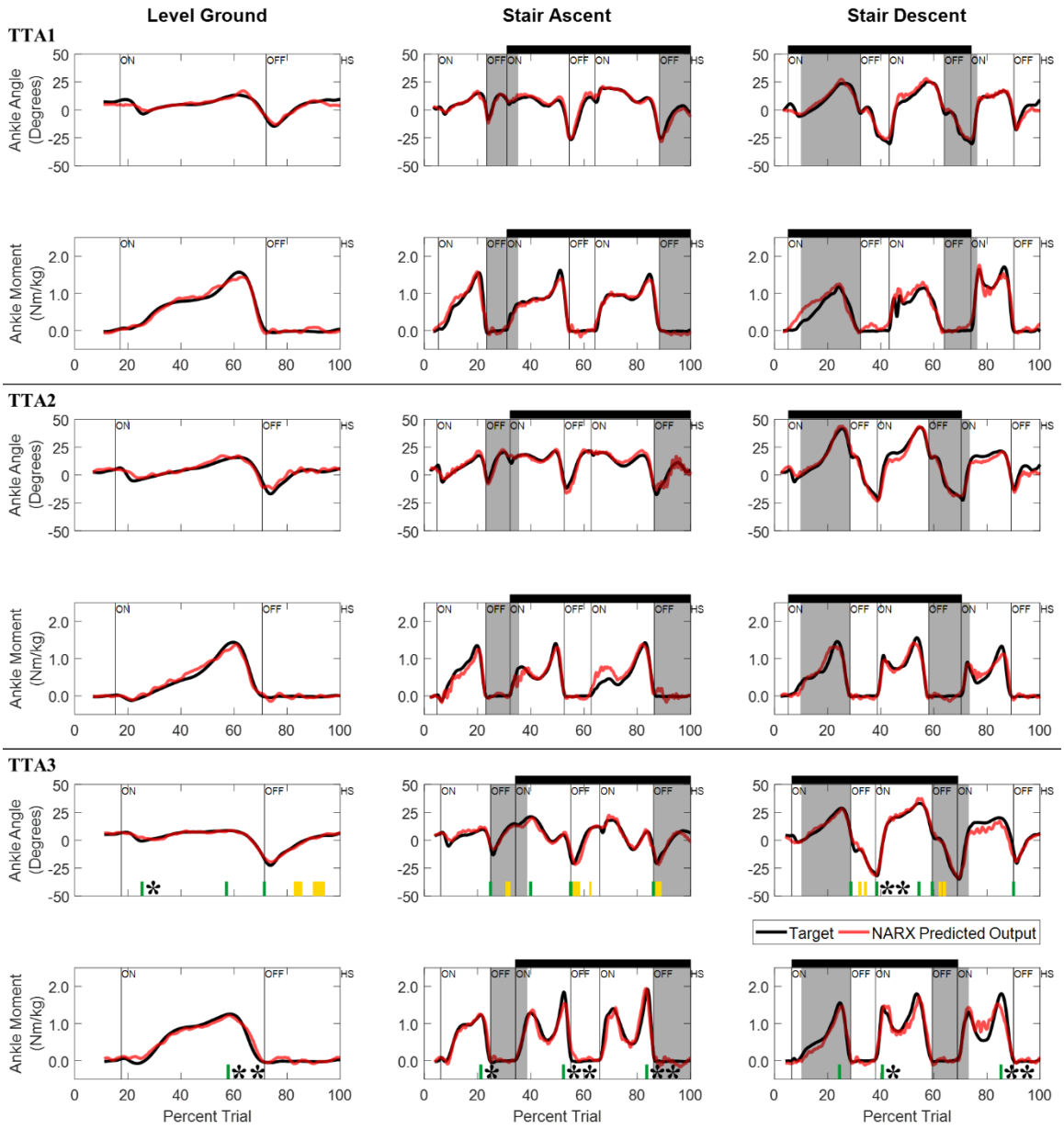

Figure 3.5. Time series of NARX model prediction of ankle angle and ankle moment for all transtibial amputees. Optimal model parameters were used for each amputee (τ: 58 ms**,** TTA1 - D: 83 ms, N: 50; TTA2 - D: 42 ms, N: 30; TTA3 - D: 83 ms, N: 50). Closed-loop NARX model predictions during level overground walking and stair ambulation are shown for the k-fold novel test trials with the best accuracy across ambulation conditions and model outputs. Critical performance points (CPs), used to test for within-subject significant differences (B-H adjusted $p < 0.05$) between the model prediction and experimentally measured targets, are shown under TTA3 plots (clearance intervals as yellow blocks; stance critical points as green lines). Single asterisks (*) indicate CPs with significant difference in at least two amputees. Double asterisks (**) indicate significance differences in at least two amputees as well as in more than 50% of AB_{cEMG} participants. Shading and line markers are defined the same as in **Figure 3.3**. Prediction time series of a typical able-bodied participant trained with same-limb data (AB3) and trained with aligned contralateral EMG as the EMG input ($AB3_{cEMG}$) are provided in the Supplementary Material (APPENDIX B).

Table 3.1 lists average errors (RMSE) and correlations (R^2) of the NARX model predictions of ankle angle (θ) and moment (M) for each ambulation condition, individually for amputees and averaged across able-bodied participants (AB and AB_{cEMG} groups). The results show high levels of accuracy for both ankle angle and moment across participant groups and ambulation conditions and their transitions. For amputees, RMSE and R^2 of ankle angle ranged from 2.06 to 3.74 degrees and from 0.886 to 0.970, respectively, while moment values ranged from 0.096 to 0.213 Nm/kg and from 0.930 to 0.982, respectively. Amputees and the AB_{cEMG} group had similar RMSE and R^2 for both model outputs in all ambulation conditions. Model predictions for the able-bodied group (AB) had lower errors ($RMSE_\theta$ = [2.03, 2.65] °, $RMSE_M$ = [0.071, 0.108] Nm/kg) and higher correlations (R^2_θ = [0.954, 0.971], R^2_M = [0.979, 0.992]) than amputees and the AB_{cEMG} group across ambulation conditions. Model predictions accurately aligned with the ankle angle and moment targets where 91% of time lags were within one time step (8 ms) across all trials (i.e., participants and ambulation conditions). Stair descent had the largest RMSE for both angle and moment across groups; yet, it had the highest R^2 for angle among ambulation conditions. Prediction of ankle moment resulted in higher correlations than angle predictions across ambulation conditions and groups, except TTA2 stair ambulation.

Table 3.1. RMSE and R^2 values of NARX model predictions for each ambulation condition, individually for transtibial amputees (TTA) and averaged across able-bodied participants (AB and AB_{cEMG} groups).

Model Output	Group	Units	Level Ground			Stair Ascent			Stair Descent		
			$\overline{RMSE}$	σ_{RMSE}	$\overline{R^2}$ Unitless	$\overline{RMSE}$	σ_{RMSE}	$\overline{R^2}$ Unitless	$\overline{RMSE}$	σ_{RMSE}	$\overline{R^2}$ Unitless
Angle	**TTA1**	Degrees	2.65	0.59	0.907	3.05	0.64	0.933	3.24	0.47	0.959
	TTA2		2.75	0.54	0.886	3.42	0.46	0.949	3.54	0.56	0.970
	TTA3		2.06	0.59	0.946	3.43	0.74	0.910	3.74	0.69	0.957
	$\overline{AB_{cEMG}}$		2.70	0.66	0.923	3.31	0.22	0.923	3.46	0.41	0.951
	$\overline{AB}$		2.03	0.35	0.957	2.49	0.16	0.954	2.65	0.19	0.971
Moment	**TTA1**	Nm/kg	0.116	0.027	0.977	0.132	0.014	0.974	0.149	0.019	0.962
	TTA2		0.118	0.026	0.967	0.151	0.027	0.948	0.167	0.030	0.938
	TTA3		0.096	0.018	0.982	0.168	0.032	0.959	0.213	0.047	0.930
	$\overline{AB_{cEMG}}$		0.106	0.015	0.987	0.136	0.018	0.966	0.162	0.021	0.951
	$\overline{AB}$		0.071	0.010	0.992	0.094	0.021	0.984	0.108	0.011	0.979

Critical performance points within ambulation conditions are shown in **Figure 3.5**. Statistical analysis revealed several critical points that repeated in at least two amputees (i.e., 8 of 49 points) and in more than 50% of AB_{cEMG} participants (i.e., 9 of 49 points), for which NARX model predictions were statistically different (B-H adjusted $p < 0.05$, asterisks in **Figure 3.5** and **Supplementary Figure B.6**) from the experimentally measured ankle dynamics (see **Supplementary Table B.2** for statistical scores). For models trained with same-limb data, no significant differences were observed at critical points in more than 50% of able-bodied participants (**Supplementary Figure B.6**). Maximum ankle plantarflexion in the stance phase was significantly different during gait cycle 2 of stair descent in at least two amputees as well as in more than 50% of AB_{cEMG} participants (as double asterisks in **Figure 3.5**), whereas level walking was only different for amputees. For ankle moment, six critical points showed significant differences in at least two amputees except gait cycle 1 of stair descent which was only different for TTA3. Similarly, four out of those six peak plantarflexion moments were also statistically

different in more than 50% of AB_{cEMG} participants (as double asterisks in **Figure 3.5**). During level walking in particular, peak moment predictions were significantly different in all AB_{cEMG} participants (n = 6). The percentage difference (absolute difference over mean) between the target and model prediction at all peak plantarflexion moments were up to 19% for level walking, 27% for stair ascent and 24% for stair descent for amputees, 21%, 23% and 28% for AB_{cEMG} participants, and 11%, 10% and 19% for able-bodied participants, respectively. Differences were also observed in four critical points during stair descent in more than 50% of AB_{cEMG} participants but did not occur in at least two amputees (i.e., peak dorsiflexion of gait cycle 2; two angle points in the second clearance interval and peak moment of gait cycle 1; **Supplementary Figure B.6**).

The distribution of RMSE within ambulation conditions showed variations in the accuracy of the predicted ankle angle and moment within and across gait cycles for amputees and able-bodied groups (**Figure 3.6** and **Supplementary Figures B.7** and **B.8**). In able-bodied groups, the largest deviations occurred during initial swing for ankle angle and during pre-swing for ankle moment in every gait cycle and ambulation condition. Ankle angle errors also increased during mid-swing for gait cycle 2 and 3 of stair ascent and during loading response for gait cycle 2 and 3 of stair descent. For both able-bodied groups, the patterns of error were consistent across gait cycles but were generally larger for the AB_{cEMG} group, as well as, more substantial moment error at terminal stance. Amputee RMSE patterns were subject-specific and diverged from able-bodied patterns in several cases. Yet, for the most part, the largest errors occurred during the same gait periods as able-bodied groups, including similar error patterns for a subset of gait cycles (e.g., level walking for TTA2 angle and moment and gait cycle 1 of stair ascent for TTA1

angle in **Supplementary Figure B.7**). All participant groups had minimal moment errors during the swing phase in all gait cycles. Angle RMSE stayed below 3.4 degrees, 4.3 degrees, and 6 degrees during all gait periods for able-bodied, AB_{cEMG}, and amputee participants, respectively, while moment RMSE stayed below 0.155 Nm/kg, 0.255 Nm/kg, and 0.365 Nm/kg, respectively.

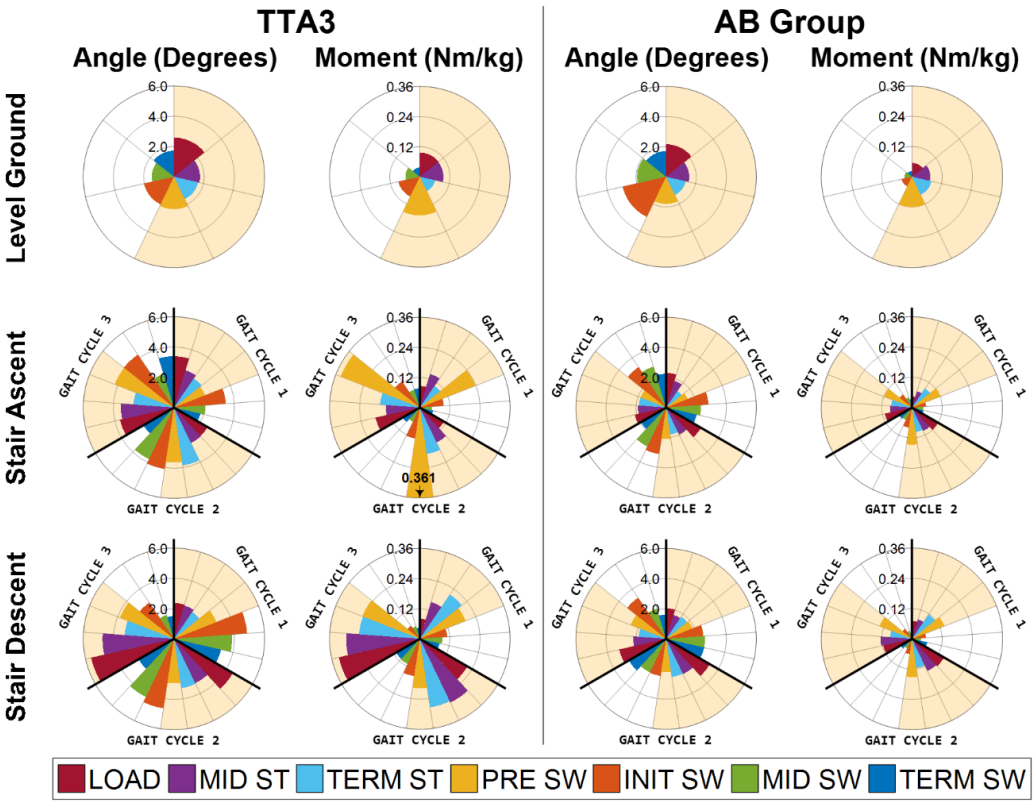

Figure 3.6. RMSE distribution within ambulation conditions for the continuous prediction of ankle angle and moment for a transtibial amputee (TTA3) and the able-bodied group (AB). Each gait cycle is divided into the standard seven gait periods based on gait events: loading response (LOAD; initial foot contact to contralateral toe off), mid-stance (MID ST; 1-50% of single-limb support), terminal stance (TERM ST; 50-100% of single-limb support), pre-swing (PRE SW; contralateral initial foot contact to toe off), initial swing (INIT SW; 1-33% of swing phase), mid-swing (MID SW; 33-66% of swing phase), and terminal swing (TERM SW; 66-100% of swing phase). Stance and swing phases are shaded light orange and white, respectively. RMSE distribution of the remaining amputees and the AB_{cEMG} group are provided in the Supplementary Material (APPENDIX B).

The sum of weighed inputs, averaged over time, showed that both residual ankle dorsiflexor and plantarflexor muscle contribution to the model prediction were

comparable to AP shank velocity, the largest velocity contributor, for each amputee and both able-bodied groups across ambulation conditions (**Figure 3.7A**). Amputees and both able-bodied groups had similar relative contribution of EMG and AP shank velocity across ambulation conditions.

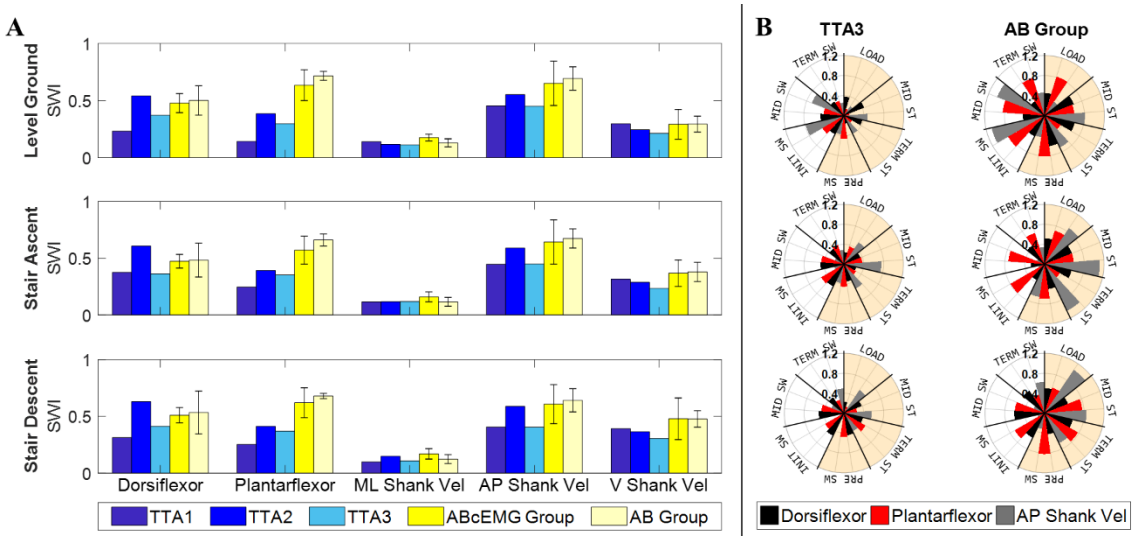

Figure 3.7. Exogenous input contribution to NARX model prediction for each ambulation condition. **(A)** Sum of weighted inputs (SWI) for each input averaged over time. Error bars represents ±1 standard deviation of averaged able-bodied participants. **(B)** SWI distribution of EMG and AP shank velocity inputs within the gait cycle for level ground walking and the second gait cycle of stair ascent and stair descent for a transtibial amputee (TTA3) and the able-bodied group (AB). Because the network bias (offset) was not included in the SWI calculation, SWI absolute values can vary across participants without affecting the relative contribution among inputs. Gait periods and stance and swing phases are defined the same as in **Figure 3.6**. SWI distribution of the remaining amputees and the AB_{cEMG} group are provided in the Supplementary Material (APPENDIX B). Dorsiflexor: tibialis anterior, Plantarflexor: gastrocnemius medialis, ML: medial-lateral, AP: anterior-posterior, V: vertical, Vel: velocity.

SWI distribution within ambulation conditions showed that EMG and AP shank velocity had alternating contributions within the gait cycle for all participant groups (**Figure 3.7A** and **Supplementary Figure B.9**). The contribution of AP shank velocity varied continuously within the gait cycle with a pattern that was consistent across participant groups. EMG contribution predominated during loading response, pre-swing and terminal swing for level walking, swing phase for stair ascent, and during pre-, initial

and mid- swing for stair descent for able-bodied groups. While the patterns of EMG contribution differed for amputees, the largest EMG contribution to the model prediction occurred during similar intervals to the able-bodied groups.

3.5 DISCUSSION

This study demonstrated that the use of within-socket residual EMG of transtibial amputees can be used, in conjunction with shank kinematics of the sound limb, to continuously predict normative ankle kinematics and kinetics of the sound limb across ambulation conditions and terrain transitions. Additionally, the single-network, closed-loop NARX model had the ability to characterize normal gait patterns of ankle angle and moment of able-bodied participants. The need for explicit identification of gait events or selection of locomotion modes was eliminated due to the ability of the autoregressive model to continuously predict ankle dynamics within and across ambulation conditions (i.e., level overground walking, stair ascent, and stair descent), including transitions between terrains.

The proposed NARX model could be used in real-time to generate continuous ankle angle and ankle moment commands for the control of an active ankle-foot prosthesis using impedance, stiffness, or similar control schemes (Au et al., 2008; Kannape & Herr, 2014; Klein & Voglewede, 2018; Shultz & Goldfarb, 2018). It is believed that this work is the first in which a fully closed-loop model with predictive capabilities (i.e., future estimates) has been developed to continuously predict ankle state. In the closed-loop NARX model, prior model error was directly encoded during training because output predictions were fed back as recurrent inputs instead of using error-free

target data (as in open-loop models). A closed-loop structure would make the system robust to model uncertainties (e.g., error accumulation and undesired fluctuations), thus ensuring accuracy and stability when implemented in a feedback control system. Moreover, the prediction of future limb state enables a control system to counteract control and actuation delays, and allows gait changes to be modified proactively in response to terrain changes perceived by the user. Results show that similar performance can be achieved for prediction intervals ranging from 8 to 142 ms (**Figure 3.4** and **Supplementary Figure B.5**) which would accommodate prosthetic delays [e.g., 40-50 ms response time of ankle-foot prostheses (Ficanha et al., 2016; Sun et al., 2014; Yu, 2017)] and enable future predictions given the physiological electromechanical delay from onset of surface EMG to the neuromotor drive [4-170 ms for lower leg muscles (Go et al., 2018)], while keeping ankle angle error less than 5 degrees [see CHAPTER 2 (Zabre-Gonzalez, Riem, et al., 2021)]. These features make the recurrent (closed-loop) NARX model appealing for real-time feedback control in a wide variety of lower limb robotic devices, including actuated orthoses and exoskeletons.

In lower limb amputees, gait asymmetries between the sound and prosthetic limb are primary attributed to limitations in the prostheses, even active prostheses, and are a major concern in achieving normal gait (Bateni & Olney, 2002; Pröbsting et al., 2020; Schmalz et al., 2007; Sinitski et al., 2012). The practical need to adapt to such asymmetries often leads to differences in kinematics and kinetics of the sound limb when compared to able-bodied controls (Grabowski & D'Andrea, 2013; Rábago & Wilken, 2016). The approach presented here, mapping ankle dynamics of the sound limb with residual EMG of the prosthetic side (i.e., aligned), takes an important step toward

establishing a more normal gait by overlaying the dynamics of the sound limb onto the prosthesis to create symmetric gait patterns. However, the long-term impact on gait is dependent on the interaction between the model prediction and the human user as they adapt and react to changes (e.g., muscle recruitment, environment, and control errors). In previous work, a human-in-the-loop model was developed to simulate the user's EMG in response to changes in ankle dynamics (Zabre-Gonzalez, Amieva-Alvarado, et al., 2021). Real-time performance of the autoregressive model during human-in-the-loop control is needed to ensure safety and stability of the physical prosthetic system prior human testing.

Despite amputees in this study having a wide array of residual ankle dorsiflexor and plantarflexor profiles with different levels of EMG activation and co-activation, walking patterns, and foot placement strategies during stair ambulation, the closed-loop NARX model performance was accurate and robust across amputees and ambulation conditions, including terrain transitions (R^2 = [0.886, 0.982]), suggesting that the model can be used consistently across amputees. The strength of the model lies in its ability to account for individual's specific variations of limb dynamics and muscle activity by training and optimizing the model to maximize performance for each amputee. Similarities in ankle angle and moment RMSE (across gait cycles and ambulation conditions) between individual amputees and the AB_{cEMG} group suggest that the combination of antagonistic residual EMG along with sound-limb shank motion can effectively predict normative ankle dynamics. Importantly, the contribution of natural residual EMG signals of amputees, to the prediction of ankle dynamics across ambulation conditions, was consistent with normal muscle activity of able-bodied participants

(**Figure 3.7** and **Supplementary Figure B.9**). In contrast to proportional myoelectric control systems, the ability to use natural, yet altered, amputee muscle activation profiles, eliminates the need for conscious, intentional muscle contraction, extensive user training, and high quality, independent muscle signals. When implemented in a prosthesis, the cognitive and physical demand on the user is expected to be less than current myoelectric control systems (S. Huang et al., 2016; S. Huang & Huang, 2019; Kannape & Herr, 2014, 2016).

The use of shank kinematics and antagonistic surface EMG signals allowed for accurate and robust model performance that included information about limb state and direct user intention. While the model developed here used shank linear velocity, other measures of shank kinematics (e.g., angle, angular velocity) could be used as well (B. Chen & Wang, 2015; Eslamy & Alipour, 2019; Holgate et al., 2009; Stolyarov et al., 2018). A benefit of using shank kinematics in transtibial amputees is that the motion of the residual shank is still governed by the central nervous system and contains information about the limb state in relation to the gait cycle. Furthermore, in real-time application, shank kinematics could be obtained intrinsically from sensors embedded in the prosthesis (e.g., inertial measurement units, gyroscopes, accelerometers), similar to within-socket EMG, minimizing design complexity and facilitating donning and doffing of the prosthesis.

Ankle angle and moment predictions closely matched the experimentally measured targets in all ambulation conditions for all participants. However, deviations in the predicted values were still present, particularly at local minima and maxima. Analyses revealed a number of critical points where predictions of amputee and AB_{cEMG} models

repeatedly fell outside the variability of the targets. While sample size may have been a contributing factor, differences in model predictions may not necessarily correlate with practical disruptions of gait. For example, ankle angle predictions deviated from the targets at one critical point during the stance phase of level walking and stair descent. Studies suggest that foot placement during stair use is not a factor that contributes to a stumble or fall (Ramstrand & Nilsson, 2009), especially if the obstacle is seen beforehand (Schulz, 2011). Since the foot was already in contact with the surface, trip-related fall risk or injury from such prediction errors would be minimal. However, more generally, the impact of critical point errors on prosthetic control during gait remains an underdeveloped area of study in the field, particularly during human-in-the-loop control of an active prosthesis.

While the influence of push-off has not been linked to fall risk (Müller et al., 2019), limb asymmetry and offsets in the timing of push-off have been associated with increased metabolic rates, excessive limb loading, osteoarthritis, and back pain among lower limb amputees (Hill & Herr, 2013; Kulkarni et al., 2005; Miller et al., 2001; Montgomery & Grabowski, 2018; Morgenroth et al., 2011) and controls (Malcolm et al., 2015). Although significant differences were also found at peak moments for the amputees, the peak percentage differences across ambulation conditions were lower than those present in commercially available ankle-foot prostheses (i.e., active to SACH) compared to able-bodied individuals [LW: 28% (Ferris et al., 2012; Pröbsting et al., 2020; Rábago & Wilken, 2016; Sinitski et al., 2012), AS: 41% (Aldridge et al., 2012; Schmalz et al., 2007; Sinitski et al., 2012; Vack et al., 1999), DS: 50% (Schmalz et al., 2007; Sinitski et al., 2012)]. Moreover, timing differences relative to the desired profile

were present in the peak moments of those commercial prostheses, unlike the prediction peaks in this study (>84% of moment predictions in amputees were within one time step of the targets). It is known that push-off timing is a key factor to maintain gait stability and stride variability (Malcolm et al., 2015). The ability of lower limb amputees to adapt to these limitations in their own prostheses (Hak et al., 2013) suggests that the moment prediction errors of the NARX model may not negatively impact the robust control of a prosthesis.

The recurrent (closed-loop) NARX model predicted ankle angles and moments over a wider range of conditions at levels comparable to, and in some instances better than, other continuous gait models (Ardestani et al., 2014; J. Chen et al., 2018; Dey et al., 2019; Eslamy & Alipour, 2019; Gupta et al., 2020; Hahn & O'Keefe, 2008; Keleş & Yucesoy, 2020; Zhang et al., 2012). Most models have used a feedforward structure to estimate (i.e., one-step-ahead estimate) ankle dynamics of healthy individuals limited to level walking [$RMSE_\theta < 4.7°$, $R^2_\theta > 0.74$; $RMSE_M < 0.16$ Nm/kg, $R^2_M > 0.86$; (J. Chen et al., 2018; Dey et al., 2019; Eslamy & Alipour, 2019; Hahn & O'Keefe, 2008; Keleş & Yucesoy, 2020)]. In impaired populations, ankle angle errors (RMSE) ranging from 1.2 to 5.4 degrees and from 0.82 to 9.3 degrees have been reported for transtibial amputees (Farmer et al., 2014) and spinal cord injury patients (Zhang et al., 2012), respectively, during level treadmill walking. For the errors of transtibial amputees, ankle angle of their passive prostheses was predicted 100 ms ahead of time using two antagonistic within-socket residual EMG (i.e., same limb) as inputs to an open-loop NARX model (Farmer et al., 2014). In the current study, even with a greater model complexity, similar errors were achieved in transtibial amputees during level ground walking (RMSE < 2.8° for $\tau = 58$

ms) with the inclusion of shank kinematics as inputs. In comparison to the 2-input open-loop NARX model developed previously [see CHAPTER 2 (Zabre-Gonzalez, Riem, et al., 2021)], while ankle angle and moment errors increased by at least a factor of two across ambulation conditions for the closed-loop model, they remained less than 2.7 degrees and 0.11 Nm/kg for able-bodied participants with correlations greater than 0.95 for both models. Zarshenas et al. obtained favorable results ($R^2 > 0.8$) using a time delay neural network with ankle kinematics and EMG inputs to predict ankle moment of healthy participants up to 1 second ahead of time (Zarshenas et al., 2020). Their model exploited the cyclic nature of treadmill walking at a constant speed which resulted in high accuracy over large prediction intervals, although performance was not examined during noncyclic features of gait such as terrain transitions. Gupta et al. estimated (i.e., excluding future predictions) ankle angle of able-bodied individuals during level ground walking (RMSE = 2.44 ± 0.45°, $r = 0.97$), stair ascent (RMSE = 3.61 ± 1.00°, $r = 0.93$), and stair descent (RMSE = 5.04 ± 1.56°, $r = 0.85$) using NARX models trained for each terrain individually (Gupta et al., 2020). It is believed that the NARX model was implemented as an open-loop model using error-free targets. The closed-loop model presented here had better performance, possibly due to the use of more relevant inputs (shank versus knee kinematics) and the absence of discontinuities in the training data, with the added benefit of being implemented in a single-network model capable of continuous prediction across ambulation conditions and terrain transitions.

The use of contralateral EMG to align residual EMG from the prosthetic side with sound-limb dynamics was a viable approach that yielded accurate predictions of ankle dynamics. While this approach provides a path toward the implementation of sound-limb

ankle dynamics in the prosthetic limb, there remains room for improvement. When comparing able-bodied groups, where the only training difference was the use of aligned contralateral EMG instead of data from the same limb (EMG, ankle angle and moment, and shank velocities), the AB_{cEMG} group had worse performance in all metrics (e.g., higher errors, lower correlations, model predictions that fell outside the variability of targets) than the able-bodied group (AB). Assuming limb symmetry in able-bodied participants (Sadeghi et al., 2000), large discrepancies in EMG profiles and ankle dynamics were observed during transition steps onto and off the staircase due to differences in step limb dynamics between the lead limb (i.e., limb of ankle kinematic and kinetic predictions) and the aligned trail limb (i.e., limb of contralateral EMG) (**Supplementary Figure B.4**). The limiting factor was the lack of EMG trials from both legs as the lead limb. The use of contralateral EMG collected as the lead limb would be expected to improve model performance by more accurately matching step dynamics with EMG signals.

In this study, the impact of post-processing motion artifacts on model performance was not analyzed in depth for the electrode-housing test socket design. Given the consistency of trial-wise variability and the absence of high-frequency, large amplitudes in the EMG linear envelopes across amputees, the potential impact on the current results was considered minimal. Additionally, it has been shown that a similar design using the same EMG electrodes and filtering techniques (i.e., band-pass filter at 20-450 Hz) in a transfemoral amputee produced negligible motion artifacts during level walking and stair ambulation, and produced a high level of user comfort when compared to other designs and electrodes (Hefferman et al., 2015). Furthermore, the effects of

variations in EMG signal due to changes in electrode placement and electrode-skin interface were not evaluated. Although studies suggest that these factors can adversely affect myoelectric pattern recognition (L. Chen et al., 2011; Hargrove et al., 2006; Radmand et al., 2014), preliminary testing of trained NARX models with EMG from subsequent days suggests the impact may be more limited. However, further research is needed to validate robustness over time. Finally, while the current results demonstrate the feasibility to continuously predict ankle angle and moment across a subset of common ambulation conditions and transitions, additional work is needed to validate the model training and performance with a larger cohort of participants under additional ambulation conditions (e.g., ramps, cadence modulation, noncyclic activities) and in response to untrained situations such as recovering from an unexpected perturbation.

3.6 CONCLUSION

This work demonstrated the ability of an autoregressive model to continuously predict (i.e., future estimates up to 142 ms) desired ankle kinematics and kinetics of the sound limb of transtibial amputees using within-socket residual EMG and sound-limb shank kinematics. The recurrent (closed-loop) NARX model successfully predicted ankle angle and ankle moment during multiple ambulation conditions (i.e., level overground walking and stair ambulation) including terrain transitions. Models of able-bodied participants were presented as a reference for the model performance possible under the same training methodology as amputees, as well as the maximum accuracy possible when predicting normal gait patterns. Model performance was stable and accurate across a range of different EMG profiles, leveraging both EMG and shank velocity inputs for the

prediction of ankle dynamics across ambulation conditions. The use of natural, yet altered, muscle activation as inputs could facilitate the design of intuitive and robust control strategies that reduce the cognitive and physical demands associated with volitional actuation of an ankle-foot prosthesis. This closed-loop predictive model is a step forward for continuous feedback control of lower limb robotic devices, particularly active ankle-foot prostheses, and has the potential to improve prosthetic function for lower limb amputees toward establishing a more normal, symmetric gait patterns. Further research is needed to validate the model on a larger cohort of amputees, characterize the impact of EMG signal changes on model performance, and evaluate real-time performance during human-in-the-loop control.

CHAPTER 4: CONTINUOUS PREDICTION OF FUTURE ANKLE DYNAMICS USING THIGH EMG: IMPLICATIONS FOR THE CONTROL OF ACTIVE POWERED LOWER LIMB PROSTHESES

This chapter will be submitted for peer review:
Journal: Journal of Neural Engineering
Title: "*Continuous Prediction of Future Ankle Dynamics Using Thigh EMG: Implications for the Control of Active Powered Lower Limb Prostheses*"
Authors: Erika V. Zabre-Gonzalez, Barbara Silver-Thorn, Philip A. Voglewede, Sara R. Koehler-McNicholas, and Scott A. Beardsley

4.1 ABSTRACT

While thigh muscles do not control ankle motion directly, their synergistic activity and control of the knee and hip may provide an alternate source of locomotion intent to differentiate among terrains. The feasibility of using thigh electromyography (EMG) signals to continuously predict future ankle dynamics was examined to address some of the current challenges with the reliable acquisition of within-socket EMG signals from residual shank muscles. Thigh EMG of the prosthetic side, in conjunction with sound-limb shank kinematics, were used as inputs to an nonlinear autoregressive model to continuously predict ankle kinematics and kinetics of the sound limb in three transtibial amputees. Ankle angle and moment were predicted 58 ms ahead of time across three ambulation conditions (level walking, stair ascent, and stair descent) and terrain transitions. Model performance and EMG contribution to model prediction was then compared to models trained using within-socket residual shank EMG and to models of six able-bodied participants. Amputee models trained with thigh EMG accurately predicted ankle angle and moment across ambulation conditions and terrain transitions with root mean square errors (RMSE) less than 3.7 degrees and 0.21 Nm/kg, respectively, and cross-correlations (R^2) greater than 0.91 and 0.94, respectively. Model performance

was similar to model predictions based on within-socket residual shank EMG without significant RMSE differences (within-subject ANOVA, $p > 0.05$). Thigh EMG was used in the model prediction to the same extent as residual ankle dorsiflexor and plantarflexor EMG as well as normal thigh EMG of able-bodied participants. The continuous predictive model provides opportunities for counteracting prosthetic delays, proactively modifying gait, and intuitively controlling ankle dynamics using different muscle groups. The ability to use natural thigh muscle activity to predict ankle dynamics may improve myoelectric control of ankle-foot prostheses by reducing within-socket signal disturbances and enhancing long-term user comfort.

4.2 INTRODUCTION

Surface electromyography (EMG) has been extensively researched for the non-invasive control of robotic devices such as prosthetic limbs (Moon et al., 2005; Hayashi et al., 2005; Asghari Oskoei & Hu, 2007; Fleming et al., 2021). Generation of EMG activity precedes limb motion which allows the direct interpretation of the user's intended biomechanics providing an intuitive and volitional control (Cavanagh & Komi, 1979; Go et al., 2018; Merletti & Parker, 2004). Additionally, EMG-driven control is particularly useful in responding to sudden changes to the environment. Myoelectric control has been used commercially in upper limb prostheses for decades (Össur, 2019; Ottobock, 2014). However, implementation in lower limb prostheses has been limited due in part to the development of physical systems that can achieve the power-to-weight demands of walking (e.g., load-bearing conditions) in combination with the challenges in the design of electrode-socket interfaces and the reliable acquisition of EMG signals through bulkier

residual limb soft tissue (e.g., subject to limb volume fluctuations, sweat accumulation, pistoning) (Fleming et al., 2021; Tucker et al., 2015).

Recent studies have demonstrated that it is possible to record EMG signals within the prosthetic socket of transtibial and transfemoral amputees to control lower limb prostheses (Au et al., 2008; Kannape & Herr, 2014; S. Huang et al., 2016; Spanias et al., 2018; Tkach et al., 2013). Active powered (i.e., able to generate power during propulsion) ankle-foot prostheses have been controlled using neural networks as locomotion classifiers (Au et al., 2008) and proportional control (S. Huang et al., 2016; Kannape & Herr, 2014) during level walking using within-socket EMG signals from residual shank muscles of transtibial amputees. While amputees are able to activate their residual muscles, EMG patterns differed from healthy individuals, and are highly variable across amputees, (S. Huang & Ferris, 2012; Seyedali et al., 2012) due to atrophy and changes in muscular attachment points after amputation (Brown et al., 2014; Clites et al., 2018). Within-socket EMG signal variability is also sensitive to physiological and skin-electrode interface changes (e.g., motion artifacts, electrode location variation, fatigue), which can impact performance (Hargrove et al., 2006; Young et al., 2012), while the use of embedded electrodes in the socket or liner can compromise socket suspension and user comfort (Wagner et al., 2020; Hefferman et al., 2015; Nakamura & Hahn, 2017).

Human locomotion is achieved by anticipatory changes in EMG activation and the subsequent joint and segment movements by means of coordinated synergies of the upper limbs, trunk, and lower limbs (Dietz et al., 1987; Hirschfeld & Forssberg, 1991). This suggests that EMG activity from thigh muscles could be used to inform ankle motion. Spanias et al. used within-socket EMG signals from residual thigh muscles

(rectus femoris, semitendinosus, tensor fascia latae, and adductor magnus) of transfemoral amputees to control a lower limb prosthesis with actively powered knee and ankle joints (Spanias et al., 2018). By means of deep belief neural networks, the intent recognition algorithm was able to identify gait during level walking, ramps, and stairs over multiple days. Synergistic relationships between the thigh muscles and ankle motion were also observed by Tkach et al., who showed that lower classification errors were obtained in transtibial amputees when combining residual shank and *intact* thigh EMG of the prosthetic side to virtually control a three degree-of-freedom ankle-foot prosthesis (Tkach et al., 2013). For transtibial amputees, *intact* thigh muscle activity of the prosthetic side has been shown to be less variable than residual muscles and more similar to normal muscle activation patterns (S. Huang & Ferris, 2012; Seyedali et al., 2012). From a practical standpoint, the acquisition of EMG signals outside the socket may reduce within-socket signal disturbances and improve user experience. These studies suggest that thigh muscle activity of the prosthetic side could provide an alternative source of locomotion intent for controlling ankle dynamics in transtibial amputees.

The present study addresses the feasibility of using muscle activity of the upper leg (i.e., thigh) to predict (i.e., generate future estimates of) gait continuously. A continuous predictive approach to characterize gait over time, as opposed to discrete locomotion classifiers to differentiate joint motion and terrains (e.g., level, stairs, ramps), would provide more natural and robust prosthetic control for restoring normal human gait (Zabre-Gonzalez, Riem, et al., 2021; Farmer et al., 2014; Zarshenas et al., 2020). Studies have shown that myoelectric signals in combination with neural networks (e.g., autoregressive, time delay, feedforward, wavelet) provide a promising solution for the

continuous estimation of ankle kinematics and kinetics (Zabre-Gonzalez, Riem, et al., 2021; Farmer et al., 2014; Zarshenas et al., 2020; Zhang et al., 2012; Ardestani et al., 2014; Keleş & Yucesoy, 2020; Gupta et al., 2020; J. Chen et al., 2018; Hahn & O'Keefe, 2008). Most approaches have characterized ankle dynamics (angle or moment) using muscle activity of the lower leg (i.e., shank) of healthy participants during a single type of terrain (e.g., level walking) in a reactive (i.e., one-step-ahead estimate) rather than a predictive (i.e., n-step-ahead estimate) approach. In previous work, a nonlinear autoregressive neural network with exogenous (i.e., external) inputs (NARX) has been used to continuously predict future prosthetic ankle angle using within-socket residual EMG of transtibial amputees during level treadmill walking (Farmer et al., 2014), and ankle angle and moment across multiple terrains using lower-leg EMG of healthy individuals [see CHAPTER 2 (Zabre-Gonzalez, Riem, et al., 2021)]. Continuous prediction of ankle angle and moment across multiple terrains has not been demonstrated using muscle activity from only the upper leg of healthy individuals or transtibial amputees.

The purpose of this study was to determine whether natural patterns of thigh EMG activity can used as exogenous inputs to a NARX model to effectively predict future ankle kinematics and kinetics across ambulation conditions (i.e., level walking, stair ascent, and stair descent) including terrain transitions. The upper-leg NARX model was developed using thigh muscle activity of the prosthetic side from transtibial amputees, in conjunction with sound-limb shank kinematics, to continuously predict ankle angle and moment of the sound limb. To train the system, prosthetic-side EMG signals were mapped with sound-limb ankle dynamics with the intention of creating

symmetric gait patterns and establishing a more normal gait by overlaying the ankle dynamics of the sound limb onto the prosthesis. The performance of upper-leg NARX models was statistically compared to models trained with within-socket EMG activity from residual shank muscles. The extent in which thigh muscle activity was used in the model prediction was examined and compared to within-socket residual EMG activity, which is primarily used for the control of ankle-foot prostheses due to its biomechanical coupling and proximity to the ankle. Normal ranges of ankle angle and moment of able-bodied participants were characterized using either upper-leg or lower-leg muscle activity as inputs as a normative comparison to amputee model performance, and to determine whether the use of contralateral EMG to predict ankle dynamics of the opposite limb was a viable approach for controlling a lower limb prosthesis.

4.3 MATERIALS AND METHODS

Surface EMG, kinematic, and kinetic data were collected previously from three unilateral transtibial amputees (TTA) and six able-bodied young adults (AB) during three ambulation conditions (LW, level overground walking; AS, stair ascent; DS, stair descent). Written informed consent was provided by each participant, and the experimental protocol was approved by Marquette University Institutional Review Board. Additional participant and methodology details can be found in CHAPTERS 2 and 3 (Zabre-Gonzalez et al., 2022; Zabre-Gonzalez, Riem, et al., 2021).

4.3.1 Experimental Protocol

During a single session, each participant ambulated along an instrumented walkway at a self-selected speed. Ambulation conditions were not randomized to minimize session length (APPENDIX E). First, during stair ascent (AS trial), participants traversed part of the walkway (~3 m) and over two floor-embedded force plates, ascended step-over-step a 4-step instrumented staircase with two additional force plates, and walked to the end of a landing platform (1.2 x 0.9 m) (**Supplementary Figure C.1C**). Participants then turned, and when instructed, walked the platform, descended the stairs, and returned to their starting position (DS trial). During stair ambulation, staircase handrails were available to amputees, with minimal use, for protection and support. During level ground walking, the staircase and platform were removed, and participants traversed the entire walkway length (~ 5 m; LW trial). A minimum of fifteen trials per condition were completed. Breaks were encouraged to minimize potential fatigue.

4.3.2 Data Acquisition and Processing

Trigno™ wireless electrodes (Delsys, Inc., Natick, MA) were used to record bilateral surface EMG activity (sampled at 1200 Hz) from thigh muscles (rectus femoris and semitendinosus, i.e., upper leg) and shank muscles (tibialis anterior and gastrocnemius medialis, i.e., lower leg). Amputees demonstrated volitional control of their residual ankle flexors and extensors, and residual myosites were identified (MyoBoy®, Ottobock, Duderstadt, Germany) prior to testing. For each amputee, a duplicate electrode-housing test socket and a modified pin-lock gel liner were fabricated to allow EMG acquisition from within-socket residual shank muscles and *intact* thigh

muscles (i.e., under the gel liner) from the prosthetic side (**Supplementary Figure C.1B**). The test socket was attached to the amputee's current pylon and energy-storing-and-returning foot. Residual myosite selection, test socket fabrication, and within-socket electrode placement are described in more detail in CHAPTER 3 (Zabre-Gonzalez et al., 2022). EMG signals were band-pass filtered (4th-order zero-phase Butterworth at 20-499.5 Hz), full-wave rectified, and low-pass filtered (4th-order zero-phase Butterworth at 5.5 Hz) to obtain the low-frequency EMG linear envelope.

Kinetic data, recorded from the force plates embedded in the floor and integrated under the staircase (Advanced Mechanical Technology, Inc., Watertown, MA), were sampled at 1,200 Hz. EMG linear envelopes and force plate data were subsequently down sampled to 120 Hz and time-locked with the kinematic data. Kinematic data were sampled at 120 Hz using an OptiTrack motion capture system (NaturalPoint, Inc., Corvallis, OR). Lower limb motion was tracked using a modified Helen Hayes twenty-five marker set (**Supplementary Figure C.1A**). For amputees, marker locations on the prosthetic limb were approximated based on sound-limb locations. Kinetic and kinematic data were processed using AMASS and Visual3D software (C-Motion, Inc., Germantown, MD) to extract gait events and time series of ankle angle (sagittal plane), shank segment center-of-mass linear velocity (AP, anterior-posterior; ML, medial-lateral; V, vertical directions), and ankle moment (sagittal plane; normalized to the participant's body mass). EMG, kinetic, and kinematic time series were temporally normalized as a percentage of the trial that contained data from 225 ms before the first foot contact on the first force plate to the last time point where force data were available for the lead limb (i.e., limb of first foot contact on first force plate). Consequently, the level walking

condition contained one full gait cycle, and each stair ambulation condition contained three continuous gait cycles and two transitions between terrains, i.e., from level ground to the stair step, and vice versa (**Supplementary Figures C.1C-D** and **C.2**).

To overlay the dynamics of the sound limb onto the prosthesis with the intention of restoring symmetric gait using EMG activity of the prosthetic side, upper-leg and lower-leg EMG gait cycles of the prosthetic limb were temporally interpolated (piece cubic spline) to correspond with the length of the gait cycles of the sound limb. This *contralateral gait-cycle alignment* generated an amputee dataset for model training and testing that contained EMG trials from the prosthetic limb (trail limb) aligned with kinematic/kinetic (shank velocities, ankle angle and moment) trials from the sound limb (lead limb). **Supplementary Figure C.1D** depicts the EMG gait cycles and the kinematic/kinetic gait cycles during stair ascent and stair descent. Similarly, an additional dataset was created for able-bodied participants in which EMG signals of the contralateral limb (trail limb) were aligned and interpolated to the gait cycles of the limb used to train the model (lead limb). EMG signals in this dataset are referred as *contralateral EMG* and the participants as AB_{cEMG}. Processing of EMG, kinetic, and kinematic trials, and description of ambulation conditions and staircase transitions are described in more detail in CHAPTERS 2 and 3 (Zabre-Gonzalez et al., 2022; Zabre-Gonzalez, Riem, et al., 2021).

4.3.3 NARX Model

Nonlinear autoregressive models were developed to continuously predict future ankle kinematics and kinetics across ambulation conditions and staircase transitions using

either upper-leg or lower-leg muscle activity as inputs. Multiple-input multiple-output recurrent (closed-loop) NARX models (S. Chen et al., 1990; Leontaritis & Billings, 1985) were implemented in MATLAB (R2017a, The MathWorks Inc., Natick, MA, United States) using the Neural Network Toolbox.

The general network structure consisted of an input layer in which windowed exogenous inputs and feedback model outputs (as recurrent inputs) were passed through separate tapped delay lines, a single nonlinear hidden layer, and a linear output layer containing separate outputs corresponding to predictions (i.e., future estimates) of ankle angle and moment (**Figure 4.1**). The tapped delay lines defined the time between current inputs (exogenous and recurrent) and future model predictions (τ, prediction interval), and the number of past input values over time (exogenous and recurrent) used in the prediction (D, sampling window). Given these characteristics, the general recurrent (closed-loop) NARX model output, $\hat{y}(t+\tau)$, can be expressed as,

$$\hat{y}(t+\tau) = f\begin{pmatrix} x(t), x(t-1), x(t-2), \dots, x(t-D), \\ \hat{y}(t-1), \hat{y}(t-2), \dots, \hat{y}(t-D) \end{pmatrix} \quad (4.1)$$

where $x(t)$ and $\hat{y}(t)$ are the exogenous input and the model output, respectively, at discrete time step t, f is a nonlinear '*tansig*' function, and $x(t-d)$ and $\hat{y}(t-d)$, (for $d = 1, \dots, D$), denote prior values of the exogenous input and model output at d time steps in the past. Further details on the structure of the recurrent (closed-loop) NARX model and the prediction of the model output can be found in CHAPTER 3 (Zabre-Gonzalez et al., 2022).

For models of amputees, the exogenous inputs consisted of the shank velocities of the sound limb in all directions and aligned EMG linear envelopes of the prosthetic side corresponding to either the rectus femoris and semitendinosus muscles for upper-leg

NARX models, or the tibialis anterior and gastrocnemius medialis muscles for lower-leg NARX models. Ankle angle and moment (sagittal plane) of the sound limb were the target outputs in both model types (UL: upper-leg model and LL: lower-leg model). For each model type, two models were created using the same set of able-bodied participants (AB model and AB_{cEMG} model). Models differed in the source of EMG inputs (AB: same-limb inputs and outputs; AB_{cEMG}: aligned contralateral EMG), and were used as control models to determine the ability a single-network, closed-loop model to continuously predict normal ranges of ankle dynamics associated with healthy ambulation using thigh muscle activity as inputs, and to determine whether the use of contralateral EMG was a viable approach to predict dynamics of the opposite limb.

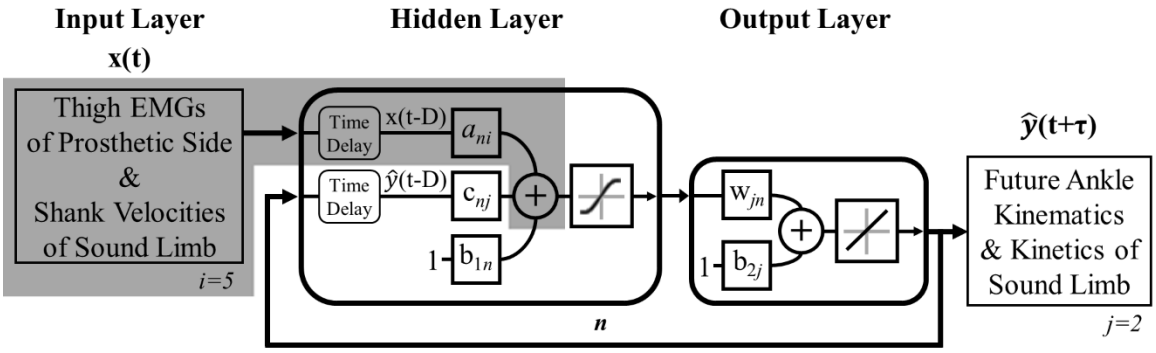

Figure 4.1. Multiple-input multiple-output recurrent (closed-loop) upper-leg NARX model for transtibial amputees. Inputs consisted of sound-limb shank velocities (medial-lateral, anterior-posterior, vertical) and the EMG linear envelopes of the prosthetic-side thigh (rectus femoris and semitendinosus) for upper-leg models. Within-socket residual EMG from the tibialis anterior and gastrocnemius medialis muscles were used for lower-leg models. Future predictions of sound-limb ankle angle and moment (sagittal plane) were the target outputs in both model types. Models of able-bodied participants differed in the use of same-limb EMG (AB models), or aligned contralateral EMG (AB_{cEMG} models). The sum of weighted inputs for each exogenous input was calculated using the trained weights from the input to the hidden layer (a_{ni}; shaded gray area). Experimentally measured input and output data of one amputee (TTA1) and a representative able-bodied participant (AB4) are provided in the Supplementary Material (APPENDIX C).

For each participant, upper-leg and lower-leg NARX models were trained independently using the same order of randomized trials. The models were optimized for a prediction interval of 58 ms (7 time steps) to counteract electromechanical delays (i.e.,

microcontroller and motor actuation) inherent to the Marquette University active ankle-foot prosthesis (Sun et al., 2014; Sun & Voglewede, 2012). For each model type, performance was evaluated as a function of sampling window (D: 17, 42, 83 ms) and the number of hidden units (N: 16, 30, 50) using a supervised learning procedure to minimize the mean squared error (MSE) between the experimentally measured ankle angle and moment (targets) and the model predictions. During training, ten complete trials per ambulation condition (80% training, 20% validation) were grouped as concurrent sequences (for discontinuity minimization) and divided into contiguous blocks (to use random trials, instead of random points). Using a leave-one-out 10-fold cross-validation procedure, one trial of each ambulation condition (novel test trial) was held back to prevent overfitting and to separately assess model performance after training. For each k-fold dataset, a generalized network was selected from ten model fits based on the smallest MSE averaged across novel test trials and ambulation conditions. All models were trained and tested in a closed-loop mode such that the model output (rather than the error-free target) was fed back to the input layer. The optimal sampling window and number of hidden units for each model type (upper-leg and lower-leg) were determined by the minimum averaged MSE of the stair descent novel test trials since it had the lowest performance among the ambulation conditions. Independent sets of optimal model parameters were selected between AB and AB_{cEMG} models. Training procedures are explained in more detail in CHAPTER 3 (Zabre-Gonzalez et al., 2022). The optimized subject-specific networks were then used to evaluate the effects of EMG source (upper leg or lower leg) on the model prediction of ankle dynamics.

4.3.4 Analysis of the Effects of EMG sources on Model Performance

Pairwise cross-correlations between pairs of trials used to train and test the NARX models were calculated for each input and output to examine within-subject trial-wise variability. Individual trials were interpolated to a common length for each ambulation condition (LW: 145, AS: 430, DS: 400 samples) to facilitate analysis across trials. Upper-leg and lower-leg EMG signals of amputees (i.e., prosthetic side) and able-bodied participants (i.e., both limbs) were normalized by the ensemble peak average across trials (for a given participant, EMG, and ambulation condition) to allow comparisons (Sinclair et al., 2015). In addition to the trial-wise variability of EMG signals, the upper-leg and lower-leg EMG patterns of amputees (i.e., prosthetic side) and contralateral EMG of able-bodied participants (AB_{cEMG}) were compared to the group averaged muscle activation pattern of able-bodied participants (AB, i.e., normal pattern). Group averaged EMG signals were created by averaging trials for each muscle and ambulation condition. Pairwise cross-correlations were then calculated between the group averaged AB EMG signal and trials of amputee EMG and able-bodied contralateral EMG (AB_{cEMG}). All pairwise cross-correlations are reported as the coefficient of determination (R^2, obtained from squaring the cross-correlation peak), averaged across trials, ambulation conditions, and participants within the group.

The strength and patterns of the contribution of upper-leg and lower-leg EMG inputs to the model prediction of ankle angle and moment was evaluated using the sum of weighed inputs (SWI) [see CHAPTER 3 (Zabre-Gonzalez et al., 2022)]. For each upper-leg and lower-leg NARX model, the $SWI(i,t)$ of each exogenous input was computed using novel test trials such that,

$$SWI(i,t) = rms\left(\sum_{q=0}^{d} a_{ni}(q)\, x_i(t-q)\right)\Bigg|_N,$$

$$n = 1, 2, \ldots, N \qquad (4.2)$$

where $x_i(t-q)$ is the ith input (EMG or shank velocity) for the prior q time step, and a_{ni}, is the trained weight connecting the ith input and the nth unit of the hidden layer, which represents the input strength. The root mean square (rms) was then computed across hidden units (N) to characterize the total contribution of the ith input to the model prediction throughout the trial. SWI was averaged over time and across test trials for each ambulation condition, individually for amputees and averaged across able-bodied participants (AB and AB_{cEMG} groups), to quantify the overall contribution of each exogenous input. To compare the impact of upper-leg and lower-leg EMG signals on model performance, a ratio of the SWI of the EMG input divided by the SWI of the AP shank velocity input was calculated for each muscle, and then averaged for each muscle pair ($ratio_{UL}$ for upper-leg muscles and $ratio_{LL}$ for lower-leg muscles) to determine the relative contribution of the EMG inputs. Ratios were calculated for each ambulation condition, individually for amputees and averaged across able-bodied participants (AB and AB_{cEMG} groups). The contribution patterns of EMG and anterior-posterior shank velocity inputs were evaluated within the gait cycles of each ambulation condition (gait cycle 2 for stair ambulation). Each gait cycle of SWI over time was divided into the standard seven gait periods based on gait events (Neumann, 2017): loading response (initial foot contact to contralateral toe off), mid-stance (1-50% of single-limb support), terminal stance (50-100% of single-limb support), pre-swing (contralateral initial foot contact to toe off), initial swing (1-33% of swing phase), mid-swing (33-66% of swing

phase), and terminal swing (66-100% of swing phase). The SWI of each period was then averaged across test trials, individually for amputees and averaged across able-bodied participants (AB and AB_{cEMG} groups).

The performance of upper-leg and lower-leg NARX models was evaluated using root mean square error (RMSE) and the coefficient of determination (R^2; from squaring the cross-correlation peak), calculated between the experimentally measured ankle angle and moment and the corresponding model prediction for the novel test trials. RMSE and R^2 were averaged across test trials for each ambulation condition, model output, and model type, individually for amputees and averaged across able-bodied participants (AB and AB_{cEMG} groups). Similar to the analysis of the SWI across gait periods, model performance was further investigated by analyzing ankle angle and moment RMSE within the gait cycles for each ambulation condition. RMSE was computed within each gait period and then averaged across test trials for each amputee and able-bodied participant (AB and AB_{cEMG}). Separate within-subject three-way ANOVA analyses were used to identify significant differences ($p < 0.05$) in angle RMSE and moment RMSE when using either upper-leg or lower-leg muscle activity as inputs. The factors in the analysis were muscle group (upper leg and lower leg), ambulation condition (as seven gait cycles: 1-LW, 3-AS, and 3-DS), and gait period (loading response, mid-stance, terminal stance, pre-swing, initial swing, mid-swing, and terminal swing). Prior the ANOVA tests, normality of the data was confirmed using the Kolmogorov–Smirnoff test. Tukey's honest significant difference criterion ($p < 0.05$) was used in multiple comparison tests. Statistical analyses were performed in MATLAB (R2017a).

4.4 RESULTS

Experimentally measured inputs and outputs of the NARX models were highly consistent across trials and ambulation conditions for amputees and able-bodied participants with the exception of medial-lateral shank velocity ($\bar{R}^2 > 0.46$) (**Supplementary Table C.1**). Input and output data used to train and test the NARX models of an amputee (TTA1) and a representative able-bodied participant (AB4) are provided in the Supplementary Material (**Supplementary Figures C.2** and **C.3**). For amputees and able-bodied participants, pairwise cross-correlations between trials ($\bar{R}^2$), averaged across ambulation conditions and participants within the group, were greater than 0.91, 0.94, 0.90 for ankle angle, ankle moment, and shank velocities (AP and vertical directions), respectively. EMG patterns presented minimal within-subject trial-wise variability ($\bar{R}^2 > 0.80$) for upper-leg and lower-leg muscles of amputees (i.e., prosthetic side) and able-bodied participants (i.e., both limbs). When comparing to the group averaged AB EMG pattern, amputees had lower pairwise cross-correlations (mean, [min max]) across conditions ($\bar{R}^2_{TA}$ = 0.58, [0.47, 0.78], $\bar{R}^2_{MG}$ = 0.64, [0.51, 0.86]) than the AB_{cEMG} group ($\bar{R}^2_{TA}$ = 0.81, [0.66, 0.92]; $\bar{R}^2_{MG}$ = 0.75, [0.49, 0.98]) for lower-leg muscles, and had comparable values for upper-leg muscles (TTA: $\bar{R}^2_{RF}$ = 0.74, [0.57, 0.92], $\bar{R}^2_{ST}$ = 0.63, [0.48, 0.82]; AB_{cEMG}: $\bar{R}^2_{RF}$ = 0.76, [0.61, 0.95], $\bar{R}^2_{ST}$ = 0.69, [0.54, 0.91]).

NARX models trained with upper-leg muscle activity showed comparable performance to models trained with lower-leg muscle activity across ambulation conditions and staircase transitions. **Figure 4.2** shows a comparison of predicted ankle angle (θ) and ankle moment (M) across ambulation conditions for upper-leg and lower-leg NARX models of an amputee (TTA1, τ: 58 ms, D: 83 ms, UL - N: 16; LL - N: 50)

and a representative able-bodied participant (AB4, τ: 58 ms, UL - D: 83 ms, N: 16; LL - D: 42 ms, N: 30). Model predictions of the remaining amputees and the same representative able-bodied participant trained with aligned contralateral EMG as the EMG input ($AB4_{cEMG}$) are provided in the Supplementary Material (**Supplementary Figures C.4** and **C.5**). The predicted outputs of both model types accurately aligned with the experimentally measured ankle angle and moment across ambulation conditions and participant groups ($\bar{R}^2_{UL,\theta}$= [0.908, 0.966], $\bar{R}^2_{UL,M}$= [0.935, 0.989]; $\bar{R}^2_{LL,\theta}$= [0.886, 0.971], $\bar{R}^2_{LL,M}$= [0.930, 0.992]; **Supplementary Table C.2**). Cross-correlation time lags were within one time step (8 ms) for more than 87% of upper-leg (TTA: 94%, AB_{cEMG}: 87%, AB: 88%) and lower-leg (TTA: 89%, AB_{cEMG}: 87%, AB: 96%) model predictions. Both upper-leg and lower-leg models provided stable and robust prediction across ambulation conditions and participant groups ($\overline{RMSE}_{UL}$= [1.98, 3.69] °, [0.097, 0.213] Nm/kg; $\overline{RMSE}_{LL}$= [2.03, 3.74] °, [0.071, 0.213] Nm/kg; **Supplementary Table C.2**). Amputees and the AB_{cEMG} group had minimal differences in RMSE and R^2 between upper-leg and lower-leg models (**Supplementary Table C.2**). The able-bodied group (AB) had the largest error differences between model types with a less than 1 degree and 0.05 Nm/kg difference and less than 3.5% reduction in R^2 for upper-leg models in all ambulation conditions (**Figure 4.3** and **Supplementary Table C.2**).

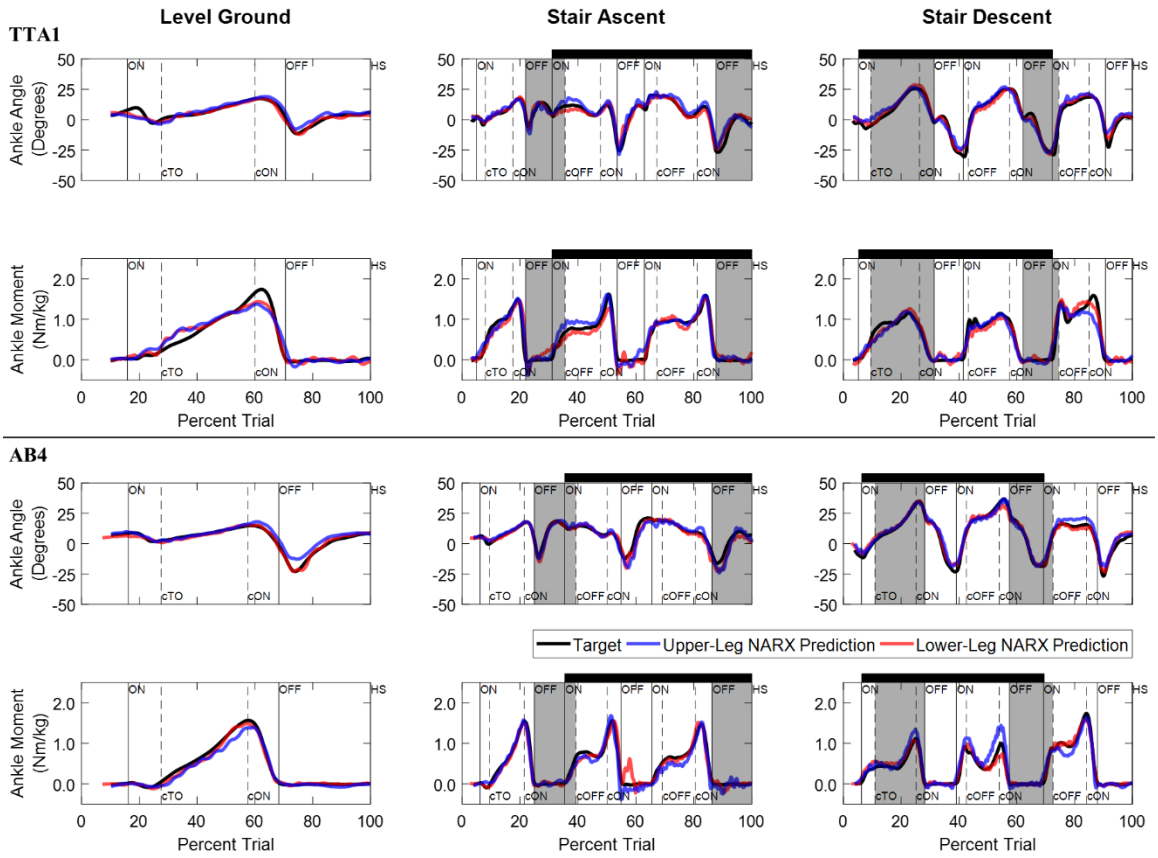

Figure 4.2. Comparison of ankle angle and moment NARX model predictions using either upper-leg or lower-leg muscle activity as inputs. Experimentally measured targets and the model predictions of a transtibial amputee (TTA1, τ: 58 ms, D: 83 ms, UL - N: 16; LL - N: 50) and a representative able-bodied participant (AB4, τ: 58 ms, UL - D: 83 ms, N: 16; LL - D: 42 ms, N: 30) are displayed during level overground walking, stair ascent, and stair descent. Model predictions are shown for the k-fold novel test trials with an average performance (mid-point performance) across ambulation conditions, model outputs (angle, moment), and model types (upper-leg and lower-leg). Staircase ambulation (black horizontal bar) is defined as the first foot contact on the staircase to the first foot contact on level ground of the lead limb (i.e., sound limb for amputees). Staircase transitions to/from level ground are shaded gray. Percent trial is normalized from 225 ms before the first foot contact on the first force plate to the first heel strike before contralateral last foot contact on the last force plate. Vertical lines denote gait events (solid: lead limb; dashed: contralateral limb, i.e., prosthetic limb) defined based on force plate (threshold 10 N) and floor contact (ON, first contact on force plate; OFF, last contact on force plate; HS, heel strike on floor; TO, toe off on floor). Contralateral gait events are identified by a lowercase 'c' (e.g., cTO, contralateral toe off). Single-limb support occurs when only one foot is in contact with the ground (cTO *or* cOFF to cON). Model predictions of the remaining amputees and the same representative able-bodied participant trained with aligned contralateral EMG as the EMG input ($AB4_{cEMG}$) are provided in the Supplementary Material (APPENDIX C).

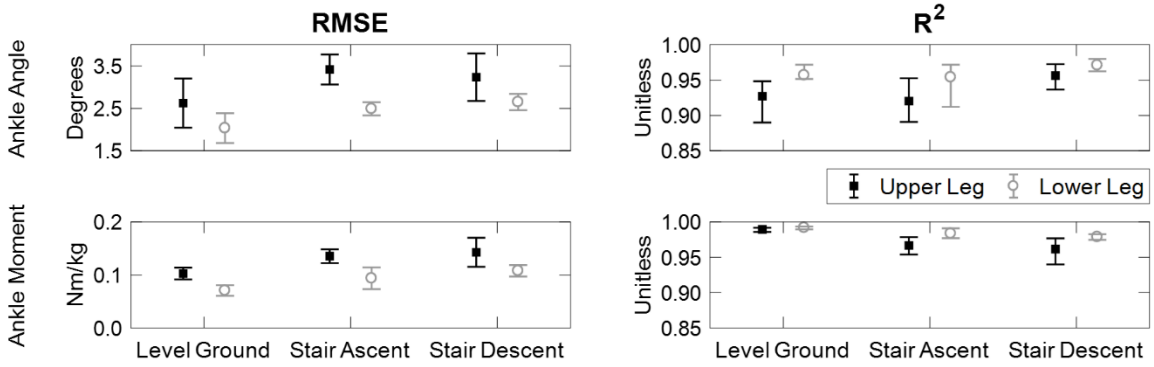

Figure 4.3. RMSE and R^2 values of upper-leg and lower-leg NARX model predictions for the able-bodied group trained with same-limb data (AB). Values are averaged across trials and participants. Error bars denote ±1 standard deviation for RMSE, and minimum and maximum values for R^2. Amputees and the AB_{cEMG} group exhibited smaller differences between model types than the data shown.

Upper-leg (rectus femoris and semitendinosus) and lower-leg (tibialis anterior and gastrocnemius medialis) muscle activity had contributions to the prediction of ankle dynamics that were similar to the largest shank velocity contributor (AP direction) for each amputee and able-bodied group (AB and AB_{cEMG}) in all ambulation conditions (sum of weighted inputs averaged over time, **Figure 4.4A** and **Supplementary Figure C.6**). Both able-bodied groups had similar EMG contributions (i.e., ratio of SWI of EMG to AP shank velocity, **Figure 4.4B**) of upper-leg ($ratio_{UL} > 0.67$) and lower-leg ($ratio_{LL} > 0.64$) muscles across ambulation conditions. Amputees also had similar relative contributions between upper-leg ($ratio_{UL} = [0.62, 0.89]$) and lower-leg ($ratio_{LL} = [0.41, 0.96]$) EMG and were comparable to the able-bodied groups.

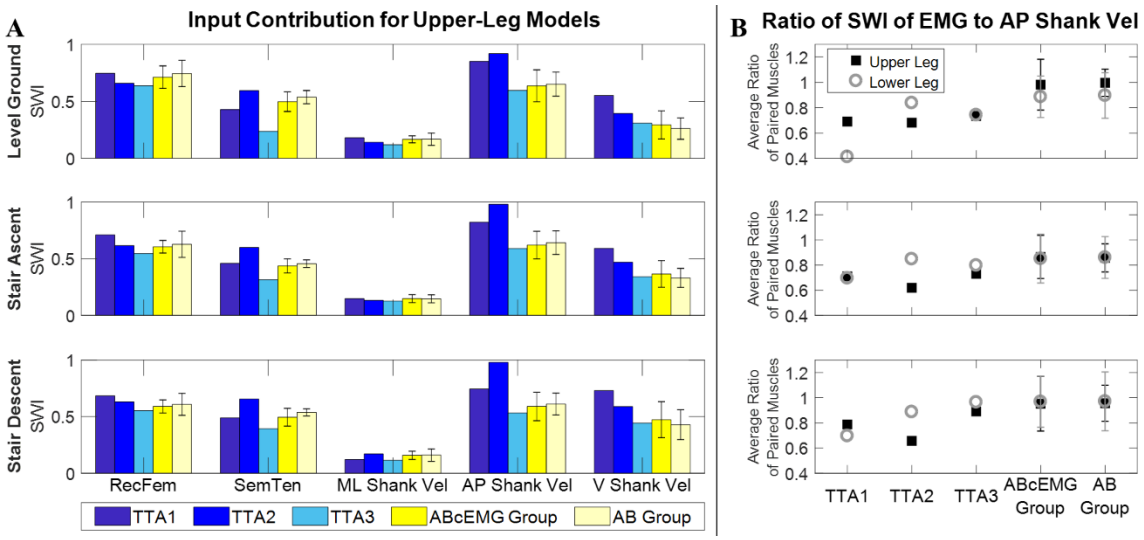

Figure 4.4. Exogenous input contribution to model prediction for upper-leg NARX models for each ambulation condition. **(A)** Sum of weighted inputs (SWI) for each input averaged over time. SWI for lower-leg models is provided in the Supplementary Material (APPENDIX C). **(B)** Comparison of EMG relative contribution between upper-leg and lower-leg models expressed as a ratio of SWI of EMG to AP shank velocity. The average between paired muscle ratios (UL - RecFem: rectus femoris and SemTen: semitendinosus; LL - tibialis anterior and gastrocnemius medialis) is shown. Error bars represents ±1 standard deviation of averaged able-bodied participants. ML: medial-lateral, AP: anterior-posterior, V: vertical, Vel: velocity, UL: upper leg, LL: lower leg.

The SWI distribution within ambulation conditions showed that EMG and AP shank velocity had an alternating contribution within the gait cycle in amputees and able-bodied groups for both upper-leg and lower-leg models. **Figure 4.5** highlights the alternation among the inputs for the second gait cycle of stair ascent of amputees and the able-bodied group (AB). Additional ambulation conditions and the AB_{cEMG} group are provided in the Supplementary Material (**Supplementary Figure C.7**). The patterns of EMG contribution between amputees and able-bodied groups tended to be more similar when using upper-leg EMG versus lower-leg EMG; whereas AP shank velocity had consistent contribution patterns between model types across participant groups. Input contribution patterns of upper-leg and lower-leg models were different across amputees. Both able-bodied groups had the same relative contribution patterns (EMG and AP shank velocity) between groups in both model types (**Supplementary Figure C.7**).

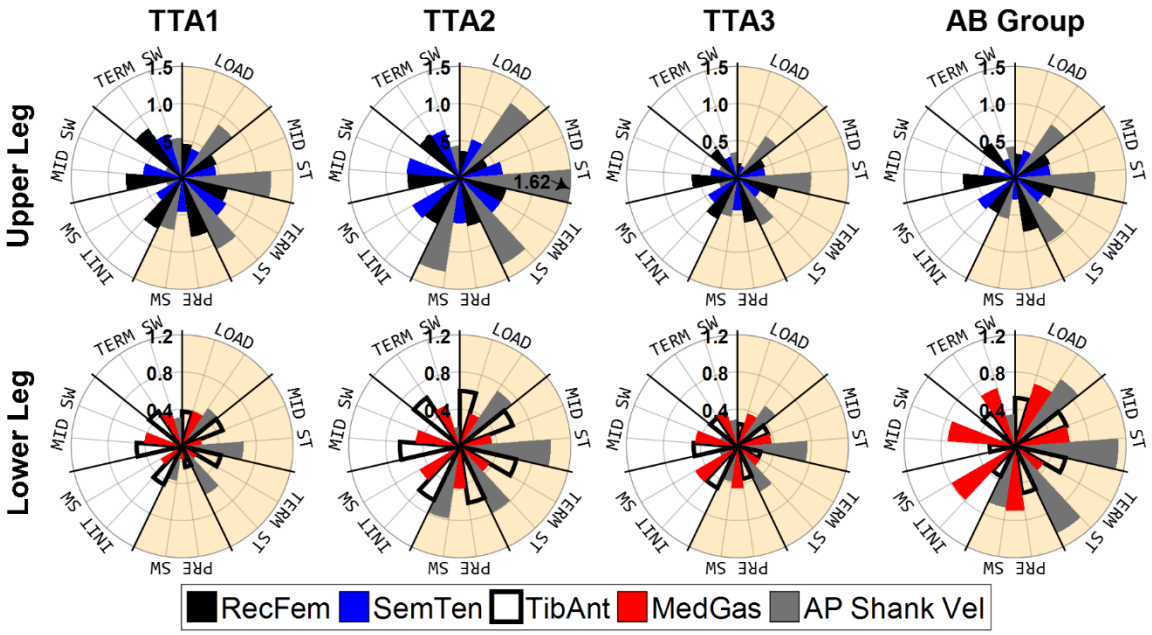

Figure 4.5. Comparison of sum of weighted inputs (SWI) distribution within the gait cycle between upper-leg and lower-leg NARX models. SWI of EMG and AP shank velocity inputs for the second gait cycle of stair ascent are shown for transtibial amputees and the able-bodied group (AB). Because the network bias (offset) was not included in the SWI calculation, SWI absolute values can vary across participants without affecting the relative contribution among inputs. Each gait cycle is divided into the standard seven gait periods based on gait events: loading response (LOAD; initial foot contact to contralateral toe off), mid-stance (MID ST; 1-50% of single-limb support), terminal stance (TERM ST; 50-100% of single-limb support), pre-swing (PRE SW; contralateral initial foot contact to toe off), initial swing (INIT SW; 1-33% of swing phase), mid-swing (MID SW; 33-66% of swing phase), and terminal swing (TERM SW; 66-100% of swing phase). Stance and swing phases are shaded light orange and white, respectively. RecFem: rectus femoris, SemTen: semitendinosus, TibAnt: tibialis anterior, MedGas: gastrocnemius medialis, AP: anterior-posterior, Vel: velocity. SWI distribution of additional ambulation conditions and the AB_{cEMG} group are provided in the Supplementary Material (APPENDIX C).

In the further analysis of the RMSE across gait periods, RMSE of ankle angle and moment varied within and across gait cycles in upper-leg and lower-leg NARX models for each amputee and able-bodied participant (AB and AB_{cEMG}) (**Figure 4.6** and **Supplementary Figures C.8-C.11**). Angle and moment error patterns within the gait cycle were similar between model types in every participant. In each able-bodied participant (AB and AB_{cEMG}), the largest error mostly occurred, in both model types, during initial swing for level walking and stair ascent and during loading response for stair descent for ankle angle, and during pre-swing for ankle moment across ambulation

conditions. For the most part, maximum errors for amputees occurred during the same periods as able-bodied participants. RMSE stayed below 6 degrees and 0.36 Nm/kg during all gait periods in both upper-leg and lower-leg amputee models. Able-bodied participants (AB) had errors less than 7 degrees and 0.32 Nm/kg and 5 degrees and 0.27 Nm/kg for upper-leg and lower-leg models, respectively. Able-bodied participants trained with contralateral EMG (AB_{cEMG}) had maximum moment errors of 0.38 and 0.31 Nm/kg in upper-leg and lower-leg models, respectively, and up to 8 degrees in both model types.

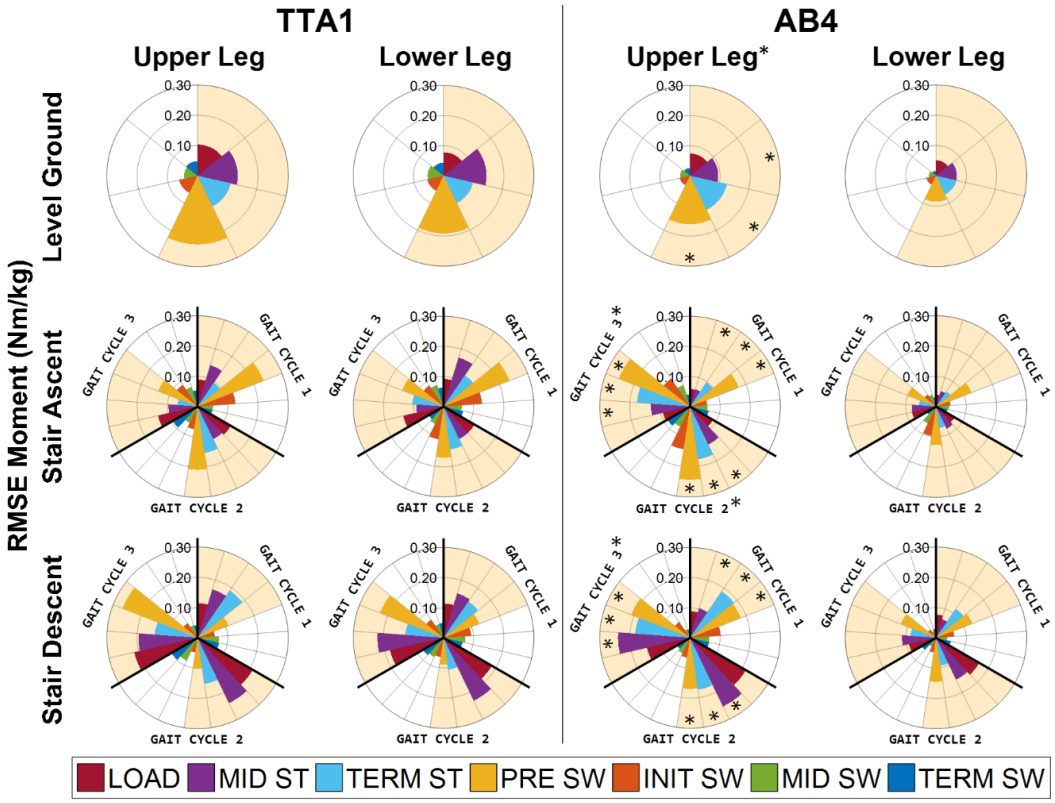

Figure 4.6. RMSE distribution within ambulation conditions of upper-leg and lower-leg NARX models for the continuous prediction of ankle moment. All gait cycles for each ambulation condition of a transtibial amputee (TTA1) and a representative able-bodied participant (AB4) are shown. Asterisks (*) indicate within-subject significant (ANOVA, $p < 0.05$) main effect for muscle group (upper leg versus lower leg) and significant interactions between muscle group and ambulation-condition gait cycle, or between muscle group and gait period (Tukey's for multiple comparisons, $p < 0.05$) that are present in the displayed participant and in more than 50% of the able-bodied participants (AB). Gait periods and stance and swing phases are defined the same as in **Figure 4.5**. RMSE distribution of ankle angle, the remaining amputees, and the same representative able-bodied participant trained with aligned contralateral EMG as the EMG input ($AB4_{cEMG}$) is provided in the Supplementary Material (APPENDIX C).

Within-subject three-way ANOVA revealed no significant differences in angle and moment RMSE when using either upper-leg or lower-leg muscle activity of amputees as inputs (ANOVA, $p > 0.10$; **Figure 4.6** and **Supplementary Figures C.8** and **C.10**) expect for TTA2 where upper-leg models had lower moment errors [$F(1,882) = 4.6$, $p = 0.03$; **Supplementary Figure C.9**]. Detailed ANOVA scores are listed in the Supplementary Material (**Supplementary Table C.3**). All able-bodied participants trained with same-limb data (AB) had significantly higher angle (ANOVA, $p << 0.05$; **Supplementary Figure C.8**) and moment (ANOVA, $p << 0.05$; **Figure 4.6**) errors using upper-leg muscles as inputs. On the contrary, only two able-bodied participants trained with contralateral EMG ($AB2_{cEMG}$ and $AB6_{cEMG}$) had significantly higher upper-leg angle errors (ANOVA, $p < 0.02$); and one participant trained with contralateral EMG ($AB2_{cEMG}$) had significantly higher upper-leg moment errors, $F(1,882) = 5.74$, $p = 0.02$. There were no significant three-way interactions, or interactions between muscle group and either ambulation-condition gait cycle or gait period for angle (ANOVA, $p > 0.12$) and moment (ANOVA, $p > 0.08$) RMSE for amputees and able-bodied participants trained with contralateral EMG (AB_{cEMG}), except for $AB1_{cEMG}$ which had a significant interaction between muscle group and gait period in moment RMSE, $F(6,882) = 3.22$, $p = 0.004$. For models trained with same-limb data, a significant interaction was found between muscle group and ambulation-condition gait cycle in more than 50% of the able-bodied participants (AB) for both angle (n = 3, ANOVA, $p < 0.01$; **Supplementary Figure C.8**) and moment (n = 4, ANOVA, $p < 0.02$; **Figure 4.6**) RMSE. There was also a significant interaction between muscle group and gait period in moment RMSE in all able-bodied participants (AB; ANOVA, $p < 0.05$), but only in two participants (AB4 and

AB6) in angle RMSE (ANOVA, $p < 0.03$). There were no significant three-way interactions (ANOVA, $p > 0.17$) for angle or moment across able-bodied participants (AB). When significant ANOVA interactions were found in more than 50% of the participants (i.e., AB participants only), *post hoc* Tukey's test identified significant differences in angle RMSE between upper-leg and lower-leg models during the last gait cycle of stair ascent (Tukey's, $p < 0.02$; **Supplementary Figure C.8**), and in moment RMSE during stair ascent (GC 2 and 3, Tukey's, $p << 0.05$) and the last gait cycle of stair descent (Tukey's, $p < 0.02$) (**Figure 4.6**). Additionally, upper-leg models had higher moment errors than lower-leg models during mid-stance (Tukey's, $p <<< 0.05$), terminal stance (Tukey's, $p < 0.01$) and pre-swing (Tukey's, $p <<< 0.05$) (**Figure 4.6**).

4.5 DISCUSSION

The autoregressive neural network presented here continuously modelled the nonlinear synergistic relationships between muscle activation of the upper leg and ankle dynamics. The NARX model demonstrated the feasibility of using natural patterns of thigh muscle activity of the prosthetic side from transtibial amputees, in conjunction with sound-limb shank kinematics, to predict future ankle kinematics and kinetics of the sound limb across ambulation conditions (i.e., level walking, stair ascent, and stair descent) and terrain transitions. It is believed that this work is the first to perform a systematic comparison of gait model performance using either *intact* thigh or within-socket residual shank EMG of the prosthetic side to continuously predict ankle dynamics across a variety of terrains.

The NARX model had the ability to characterize normal ranges of ankle angle and moment of able-bodied participants using either upper-leg or lower-leg muscle activity as inputs. Importantly, the model was able to use contralateral EMG, suggesting that the prediction of the opposite-limb ankle dynamics may be a viable approach toward replicating sound-limb dynamics onto the prosthesis tied to thigh muscle activity of the prosthetic side. By overlaying the ankle dynamics of the sound limb onto the prosthesis, the approach is a step forward to establish a more normal gait by creating symmetric gait patterns. The single-network, closed-loop NARX model with predictive capabilities (i.e., future estimates) was robust and stable to prediction errors due to its closed-loop training (use of predicted values rather than error-free targets), and allowed for the estimation of future limb state. These characteristics are useful to avoid undesired fluctuations and instability when introduced to feedback control systems, and to proactively modify gait in response to observed changes in terrain and overcome prosthetic delays (e.g., signal processing and actuation).

The NARX model takes advantage of the cyclic nature of gait, the need for constant signals (low variability) rather than high amplitudes, and the use of past output values, to accurately predict ankle angle and moment across ambulation conditions and terrain transitions using upper-leg EMG activity and shank kinematics as inputs. *Intact* thigh muscle activity of the prosthetic side was used in the model prediction to the same extent as residual ankle dorsiflexor and plantarflexor EMG as well as normal thigh muscle activity of able-bodied participants (**Figure 4.4B**). For the small sample of amputees tested, thigh musculature changes of the prosthetic side that could have occurred after amputation did not impede the continuous prediction of ankle dynamics

since amputees (e.g., $\bar{R}^2_{UL} > 0.91$) had comparable upper-leg model performance as able-bodied participants (e.g., AB and AB_{cEMG}: $\bar{R}^2_{UL} > 0.92$) despite having different gait patterns [e.g., EMG profiles (pairwise correlation to normal pattern $R^2 > 0.48$), foot placement]. This suggests that the upper-leg NARX model can be used consistently across transtibial amputees. Prosthetic-side thigh muscle activity was used effectively to predict sound-limb ankle dynamics similar to model predictions based on within-socket residual shank EMG without significant deterioration on model performance (**Supplementary Table C.3**). In CHAPTER 3 (Zabre-Gonzalez et al., 2022), it was shown that predictions of lower-leg amputee models fell outside the range of variability of the experimentally measured targets in a few instances. However, the timing of the errors were not located at regions that could contribute to trip-related falls or injury. This suggests that the robust control of a prosthesis would not be negatively impacted by prediction errors of the upper-leg NARX models. These results support that while thigh muscles do not control ankle motion directly, their synergistic activity and control of the knee and hip joints provided an alternate source of information to differentiate ambulation conditions and terrain transitions to the same extent as ankle dorsiflexor and plantarflexor muscles.

With the use of shank kinematics and two antagonistic EMG signals as inputs, the upper-leg NARX model provided robust performance that included information about limb state and direct information of user intent. Given the similarities in performance of the upper-leg and lower-leg models in transtibial amputees, the ability to use *intact* thigh muscles from the prosthetic side to predict ankle dynamics may enhance long-term comfort and improve EMG-driven prostheses by reducing signal disturbances (e.g.,

motion artifacts) that occur within the prosthetic socket during repeated loading and unloading of the prosthesis during gait. When implemented in a physical system, shank kinematics could be reliably measured from sensors (e.g., gyroscopes, accelerometers) within the prosthesis, reducing design complexity and facilitating prosthetic donning and doffing. EMG from the prosthetic-side thigh would require wearable sensors, extrinsic to the prosthesis, to obtain the required inputs signals. Advancements in wearable and implantable sensor technology [e.g., knit band sensors (S. Lee et al., 2018), prosthetic liner with embedded electrodes (Reissman et al., 2018), flexible dry electrodes (Kisannagar et al., 2020)] are promising for implementation in real-time myoelectric lower limb prostheses.

The NARX model proposed here can be used to generate real-time continuous ankle angle and moment commands needed for closed-loop control [e.g., impedance, stiffness (Au et al., 2008; Klein & Voglewede, 2018; Spanias et al., 2018)] of myoelectric lower limb devices such as transtibial and transfemoral prostheses. Current efforts to incorporate direct user intent using EMG activity from thigh and shank muscles for myoelectric control have primarily focused on pattern recognition for discrete locomotion identification (Au et al., 2008; Spanias et al., 2018; Tkach et al., 2013) and proportional control [i.e., discrete (Kannape & Herr, 2014) and continuous (S. Huang et al., 2016)], which limit the user's control over the device. In contrast, the NARX model uses natural muscle activity to provide a continuous gait prediction without explicitly identifying modes or gait events. The use of natural EMG signals of the upper leg, while different in transtibial amputees (pairwise correlation to normal pattern $R^2 > 0.48$), as inputs to the model could facilitate the design of intuitive and direct controllers that reduce the

amputee's cognitive and physical effort associated with intentional muscle contraction for actuating a prosthesis. Additionally, the optimized subject-specific networks maximized individual performance by taking into account individual variations in limb dynamics and EMG activity, reducing the need for extensive muscle training and high quality, independent muscle signals.

The upper-leg NARX model, coupled with its closed-loop structure, predicted future ankle angle and moment across multiple terrains to a similar level to other EMG-driven continuous gait models (Zabre-Gonzalez, Riem, et al., 2021; Farmer et al., 2014; Zarshenas et al., 2020; Zhang et al., 2012; Ardestani et al., 2014; Keleş & Yucesoy, 2020; Gupta et al., 2020; J. Chen et al., 2018; Hahn & O'Keefe, 2008). However, those models mostly focused on using lower-leg EMG, or in combination with upper-leg EMG, of healthy individuals to estimate (i.e., one-step-ahead estimate) ankle angle or moment limited to level walking using a feedforward structure ($RMSE_\theta$ < 5.3°, R_θ^2 > 0.74; $RMSE_M$ < 0.18 Nm/kg, R_M^2 > 0.83). In contrast to the feedforward (open-loop) NARX model previously developed using two lower-leg EMG signals as the only inputs [see CHAPTER 2 (Zabre-Gonzalez, Riem, et al., 2021)], peak errors of ankle angle and moment of able-bodied participants increased by a factor of two for level walking and stair ascent and by a factor of four for stair descent for the upper-leg (closed-loop) model. While correlations remained high for both models ($R_{UL,closed}^2$ > 0.92, $R_{LL,open}^2$ > 0.99), the open-loop structure (which used error-free targets during training rather than output predictions) resulted in minimal errors for the lower-leg (open-loop) model (e.g., $RMSE_{LL,open}$ = 0.55 ± 0.13°, 0.03 ± 0.01 Nm/kg). Farmer et al. utilized an open-loop NARX model to predict prosthetic ankle angle during level treadmill walking using

antagonistic within-socket residual EMG (i.e., same limb) of transtibial amputees, and reported errors between 1.2 to 5.4 degrees for predictions 100 ms ahead of time (Farmer et al., 2014). In comparison, using prosthetic-side upper-leg EMG to predict sound-limb ankle dynamics resulted in comparable errors (RMSE < 3.7° for τ = 58 ms) across ambulation conditions with the inclusion of shank kinematic inputs and improved training paradigm (e.g., concurrent sequence organization and contiguous block division). Zhang et al. obtained a wide range of ankle angle errors (RMSE = 0.82 to 9.3°) during level walking when estimating (i.e., excluding future predictions) hip, knee, and ankle angles of spinal cord injury patients using a combination of two upper-leg and one lower-leg EMG signals (Zhang et al., 2012). The large variation in errors was attributed to the wide range of ankle motion of the patients (i.e., restricted motion resulted in lower errors). Ardestani et al. also used a combination of six upper-leg and two lower-leg EMG signals and two ground reaction forces to estimate ankle plantarflexion moment during level walking in patients with unilateral knee replacement (Ardestani et al., 2014). Ankle moment errors of 4 and 8% were reported using wavelet and feedforward neural networks, respectively. Similar performance (TTA_{UL}: 7.8%, AB_{UL}: 6.2%) was achieved here for level walking with networks trained across three terrains. Keleş et al. used combinations of upper-leg, lower-leg, and gluteal muscles sites from a healthy population to estimate ankle angle and moment during level walking at various speeds (Keleş & Yucesoy, 2020). Greater error differences were reported, especially for ankle moment ($RMSE_{UL}$ = 0.26 ± 0.12 Nm/kg, $RMSE_{LL}$ = 0.04 ± 0.01 Nm/kg), using similar antagonistic upper-leg and lower-leg EMG signals as the only inputs to a time delay feedforward neural network. Although they reported the pair of upper-leg muscles as

inaccurate models (R_{θ}^{2} = 0.81, R_{M}^{2} = 0.67), the results support that thigh muscle activity contains some degree of synergistic gait information about ankle state.

Model performance may have been influenced by limitations in the present study. EMG electrode placement of the posterior thigh muscle (approximated as semitendinosus) varied in amputees and able-bodied participants, although locations were identified by consistent placement techniques (i.e., most prominent muscle belly when flexing the knee in the presence of resistance). The subject-specific NARX model accounted for the antagonistic muscle activity generated by each participant, limiting the effect of electrode placement inconsistencies on the current results. An in-depth motion artifact analysis was not conducted on EMG signals collected using the electrode-housing test prosthesis. The potential impact on model performance was considered minimal given the low trial-wise variability (pairwise correlation $\bar{R}_{EMG}^{2}$ > 0.80) and the absence of spike amplitudes in the EMG linear envelopes, and the filtering techniques used (De Luca et al., 2010; Hefferman et al., 2015). The model results suggest that the contralateral gait-cycle alignment was a viable approach for using contralateral EMG as inputs. However, it may have introduced a source of variability, for example, the resulting discrepancies in EMG and ankle dynamic profiles between the lead limb and the aligned trail limb (i.e., limb of contralateral EMG) during transition steps onto and off the staircase [**Supplementary Figure C.3**; see CHAPTER 3 for detailed explanation (Zabre-Gonzalez et al., 2022)]. In able-bodied individuals, the coupling between shank muscle activation and ankle dynamics is biomechanically stronger than thigh muscles due to the increased number of degrees of freedom associated with the knee joint. Supporting these differences in coupling levels, errors within ambulation conditions of upper-leg able-

bodied models trained with same-limb data were statistically higher than lower-leg models (**Supplementary Table C.3**). In contrast, the strong shank-ankle coupling was disrupted by the contralateral gait-cycle alignment in the AB_{cEMG} dataset resulting in larger errors in the lower-leg AB_{cEMG} models causing no statistical differences with upper-leg models. For the transtibial amputees, the effects of the contralateral gait-cycle alignment on model performance cannot be differentiated in upper-leg and lower-leg models because the degree of ankle coupling to the thigh muscles and the residual shank muscles due to amputation is not known. Regardless of the possible influence on the current results, errors and correlations of the upper-leg amputee models were comparable to upper-leg able-bodied models trained with same-limb data.

Despite the ability of the model to effectively map ankle dynamics of the sound limb with EMG activity from the prosthetic-side thigh muscles, establishing a normal, symmetric gait brings additional challenges. It is unknown how model performance and control stability would be impacted by having a user in the feedback control loop, one that is continuously adapting and reacting to changes in the environment (e.g., perturbations, terrain) and prosthetic control errors. Model performance may need to be maintained by iterative training as a result of the user's adaptation (e.g., changes in muscle recruitment). Preliminary work had examined the feasibility of predicting user's EMG responses to changes of ankle dynamics for simulating human-in-the-loop control (Zabre-Gonzalez, Amieva-Alvarado, et al., 2021). Forward stability of the autoregressive model presented here and its interaction with a closed-loop prosthetic controller, in conjunction with the human-in-the loop model, will be evaluated in future studies to ensure stability and safety of the system prior human testing. With a larger cohort of

participants, prediction of ankle dynamics in response to external perturbations and additional conditions (e.g., varying speeds, ramps, noncyclic activities) is also needed to explicitly model user's EMG corrective actions of both muscle groups in response to changes in gait. Further research will also assess model performance to changes in EMG signals over time due to variations in the electrode-skin interface, and systematically evaluate the benefits (e.g., user comfort, motion artifacts, signal variability) of using either *intact* thigh or residual shank muscle activity as inputs given the differences in electrode placement methodologies (i.e., under the gel liner with variable position versus within-socket with fixed position).

4.6 CONCLUSION

Natural muscle activity from the thigh muscles can be used together with a NARX model to continuously predict (up to 58 ms) ankle dynamics across ambulation conditions and terrain transitions. The predictive closed-loop model could prove useful for counteracting delays, proactively modifying gait in response to observed changes in terrain, and maintaining its stability when introduced to a feedback control system. The use of natural thigh muscle activity of transtibial amputees could provide an alternative for intuitively controlling ankle dynamics, especially when acquisition of residual EMG signals is not possible (e.g., lack of muscle control, short residual limb, dermatological problems). Alternatively, when coupled with the ability to use within-socket EMG signals, the model could be adapted to control a robotic leg (i.e., above the knee) using residual thigh muscle activity within the prosthetic socket of transfemoral amputees. The nonlinear autoregressive model provides opportunities for continuous myoelectric control

using different muscle groups and takes an important step toward user-driven real-time control of lower limb robotic systems including actuated orthoses and exoskeletons.

CHAPTER 5: SIGNIFICANCE OF RESEARCH AND FUTURE DIRECTIONS

5.1 CONCLUDING REMARKS

The purpose of this dissertation was to develop a continuous predictive model of lower limb state that uses lower limb surface EMG signals to predict future ankle dynamics across multiple terrains and the transitions between them. A continuous myoelectric predictive approach that incorporates user intent could provide a more natural, intuitive, and robust control for a better reproduction of normal human gait using active powered lower limb prostheses, particularly ankle-foot prostheses. To that end, a single-network nonlinear autoregressive model was developed to continuously predict (i.e., future estimates) ankle angle and ankle moment simultaneously across three ambulation conditions (i.e., level overground walking, stair ascent, and stair descent) and four terrain transitions (i.e., to/from staircase). This dissertation is the first study to develop a single-network continuous gait model that accounts for multiple terrains and transitions.

The work in Aim 1 (CHAPTER 2) demonstrated the feasibility of using EMG as the only exogenous inputs to an open-loop NARX model to continuously predict the normal ranges of ankle angle and moment associated with healthy locomotion across ambulation conditions. A network training paradigm was developed to minimize discontinuities in the training data and to ensure that random trials, instead of random points, were used during training. Prediction performance was extensively characterized across model parameters (i.e., prediction interval, sampling window, and the number of hidden units) to optimize model structure within and across ambulation conditions. The

training paradigm resulted in improved prediction performance in comparison to other continuous gait models (Ardestani et al., 2014; J. Chen et al., 2018; Dey et al., 2019; Eslamy & Alipour, 2019; Farmer et al., 2014; Gupta et al., 2020; Hahn & O'Keefe, 2008; Keleş & Yucesoy, 2020; Zarshenas et al., 2020; Zhang et al., 2012). Moreover, the model yielded robust performance over a relatively wide range of prediction intervals that can overcome delays of the prosthesis.

The work in the subsequent aims demonstrated that natural patterns of within-socket residual shank EMG (Aim 2, CHAPTER 3) and prosthetic-side *intact* thigh EMG (Aim 3, CHAPTER 4) from transtibial amputees can be used in conjunction with the NARX model to accurately predict ankle dynamics, similar to normal muscle activity of able-bodied individuals. To accommodate EMG sensing from the prosthetic side, a custom electrode-housing test socket was designed to allow EMG acquisition from within the prosthetic socket using commercially available wireless surface EMG sensors. It is believed that this dissertation is the first study to characterize the ability of using muscle activity (within-socket residual shank or thigh) from transtibial amputees to continuously predict future ankle kinematics and kinetics across a variety of ambulation conditions. The remainder of this section summarizes key results of the final model (developed in Aims 2 and 3), and describes its properties and their significance toward the development of an intuitive user interface for prosthetic control.

The final model consisted of a recurrent (closed-loop) MIMO (five-input, two-output) NARX model to continuously predict (i.e., future estimates) ankle angle and moment of the sound limb of transtibial amputees using prosthetic-side EMG and sound-limb shank velocities as exogenous inputs. The prediction of the intended future limb

state is crucial for the control of lower limb prostheses to counteract prosthetic delays (e.g., sensing, signal processing, and actuation), and to modify gait proactively (not reactively as in current prostheses) in response to upcoming terrain changes and unexpected perturbations. The model implementation as a closed-loop network structure eliminated the need for explicit knowledge of the true limb state and is an important characteristic for real-time feedback applications within physical prosthetic systems.

The NARX model effectively mapped muscle activity of the prosthetic side (within-socket residual shank or thigh) with ankle kinematics and kinetics of the sound limb of each amputee. Although the sound limb of lower limb amputees may have kinematic and kinetic differences when compared to able-bodied individuals (Grabowski & D'Andrea, 2013; Rábago & Wilken, 2016), the approach of mapping prosthetic-side EMG (i.e., aligned) with sound-limb ankle dynamics is the first step toward establishing a more normal gait by overlaying the dynamics of the sound limb onto the prosthesis to create symmetric gait patterns between the limbs. However, to individualize the model to restore gait for each user and be widely accessible, simpler equipment [e.g., inertial sensors, instrumented foot insoles (Gupta et al., 2020; Jacobs & Ferris, 2015; Sivakumar et al., 2019)] is required to obtain the kinematic and kinetic data needed to train the algorithm in a clinical setting.

The strength of the autoregressive model developed here lies in its ability to account for individual's specific variations of limb dynamics and muscle activity patterns. Amputees may develop abnormal and variable muscle activity and gait patterns (S. Huang & Ferris, 2012; Pröbsting et al., 2020; Seyedali et al., 2012; Sinitski et al., 2012). The use of natural, yet altered, muscle activation eliminates the need for conscious

muscle contraction, extensive muscle training, and high quality, independent muscle signals. In doing so, the system enables seamless and intuitive control strategies and reduces the cognitive and physical demands of the user by removing the need to volitionally actuate the prosthesis, a shortcoming of current myoelectric control systems. The proposed NARX model can be used to generate real-time continuous ankle angle and moment commands needed for the control of lower limb devices (e.g., impedance, stiffness). Unlike EMG-driven pattern recognition and FSM-based proportional control systems (Au et al., 2008; Kannape & Herr, 2014; M. Liu et al., 2017; Spanias et al., 2018; J. Wang et al., 2013), the NARX model characterizes gait over time without the need for explicit identification of gait events and terrains, or selection of locomotion modes.

The incorporation of shank velocity together with EMG signals (within-socket residual shank or thigh) as inputs to the model resulted in robust and accurate model performance that included information about limb state and direct information of user's intention. The combination of only two antagonistic EMG signals with intrinsic electromechanical signals could simplify implementation in a real-time system. Shank velocities could be reliably obtained from embedded sensors within the prosthesis making them readily available as inputs, minimizing design complexity and facilitating prosthetic donning and doffing. Other shank kinematic signals (e.g., angle, angular velocity) could also be used, however, model performance might differ from this study.

The resulting autoregressive model accurately predicted (prediction interval, τ = 58 ms) ankle angle and moment across ambulation conditions and terrain transitions using either within-socket residual shank or prosthetic-side thigh EMG as inputs, in conjunction with shank kinematics. The closed-loop NARX model had the ability to

characterize normal ranges of ankle dynamics of able-bodied participants using either shank or thigh muscle activity, including the use of contralateral EMG as the EMG input which determined that predicting ankle dynamics of the opposite limb was a viable approach. For the small sample of amputees tested, the trained models had similar angle and moment prediction errors and correlations to able-bodied models despite amputees having different gait patterns (e.g., EMG profiles, contraction levels, foot placement). This suggests that the model can be used consistently across transtibial amputees. In a few instances, predictions of amputee lower-leg models fell outside the range of variability of the experimentally measured targets. However, the timing of the errors were not located at regions that could contribute to trip-related falls or injury. The impact of critical point errors on prosthetic control during gait remains an underdeveloped area of study in the field.

The contribution to the model prediction of muscle activity of the prosthetic side (within-socket residual shank or thigh) and anterior-posterior shank velocity of the sound limb were generally equal on average and throughout the gait cycle (alternating contribution). Importantly, prosthetic-side muscle activity (within-socket residual shank or thigh) of the amputees was used in the model prediction to the same extent as normal muscle activity of able-bodied participants. These results support that EMG changes in the prosthetic side of transtibial amputees do not hinder the continuous prediction of ankle dynamics across ambulation conditions.

The results of this research provide opportunities for continuous myoelectric control of lower limb prostheses using two different muscle groups that is intuitive for the user and robust to changes in the type of ambulation. While implementation has signal

quality and user comfort considerations, the use of thigh muscle activity of transtibial amputees could provide an alternative to control ankle dynamics, without significant deterioration on model performance, when acquisition of residual EMG signals is not possible (e.g., lack of muscle control, short residual limb, dermatological problems). Alternatively, when coupled with the ability to use within-socket EMG signals, the model could be adapted to use within-socket thigh muscle activity of transfemoral amputees to control a robotic leg (i.e., above the knee). While the focus of this dissertation has been toward active powered ankle-foot prostheses, the autoregressive model developed here could provide robust and intuitive user-driven real-time control of a wide variety of lower limb robotic devices including exoskeletons and actuated orthoses.

5.2 FUTURE DIRECTIONS

The integration of the autoregressive model into a real-time prosthetic controller brings additional challenges that would need to be addressed in future studies. Despite the NARX model's ability to successfully predict ankle dynamics continuously during level walking, stair ascent, and stair descent, the model would need to be expanded to include additional conditions and transitions encountered in every day ambulation (e.g., ramps, cadence modulation, noncyclic activities). While the NARX model took advantage of the cyclic nature of gait to accurately predict ankle dynamics, the ability to also predict transitions from level walking to/from stair stepping of the stair conditions suggests it is also capable of predicting changes in ankle movement during noncyclic activities (e.g., sit-to-stand, turning, jumping, avoiding obstacles). Since the model cannot be trained in every scenario, it will be important to assess the model's capability to extrapolate

untrained situations (such as recovering from an unexpected perturbation), and to determine whether the model fails gracefully before it is integrated into the myoelectric controller of a physical system. Catastrophic prediction errors are not anticipated due to the generalization capabilities of neural networks (Ardestani et al., 2014; Keleş & Yucesoy, 2020; Q. Liu et al., 2020), especially if the model has been trained with activities that encompass the complete spectrum of ankle and leg motion and muscle contraction.

Donning and doffing of the prosthesis is a daily activity for lower limb amputees. For myoelectric control, this action introduces disturbances (e.g., changes in socket alignment, electrode position, pressure distribution) that could impact the acquisition of EMG signals and the performance of the predictive model. Additionally, muscles of the prosthetic side, particularly residual muscles, are subject to continuous weight bearing forces, socket pistoning, limb volume fluctuations, sweat accumulation, and impedance variations at the electrode-skin interface, which increase EMG signal variability, consequently, affecting model performance (Hargrove et al., 2006; Radmand et al., 2014; Young et al., 2012). For these reasons, the robustness of NARX model needs to be investigated during a longitudinal study across days to determine how performance is affected by the changes in EMG signal quality over time. In a preliminary analysis, a *single*-output NARX model was trained with data from an able-bodied participant across ambulation conditions obtained in a single experimental session (e.g., Day 1). The model had similar average ankle angle errors for novel test trials from the same session ($RMSE_{ascent} = 2.8 \pm 0.1°$) and from trials collected in sessions on two additional days

(e.g., Day 2 and 3, $RMSE_{ascent} = 2.4 \pm 0.1°$). Further research is needed to validate these results.

During the gait experiments, it was observed that the custom-design test socket increased the repeatability of the sensor placement on the residual muscles in comparison to prosthetic-side thigh muscles. However, the electrode-socket interface caused greater skin irritation and discomfort than having the sensors placed on the thigh under the prosthetic liner. For the case of transtibial amputees, additional work should systematically evaluate the benefits (e.g., user comfort, motion artifacts, signal variability) of using either residual shank or *intact* thigh muscle activity as inputs given the differences in electrode placement methodologies (i.e., under the gel liner with variable position versus within-socket with fixed position). In addition to obtaining robust EMG signals, the model needs to be validated using shank and ankle data acquired from sensors [e.g., encoders, inertial measurement units, force sensitive resistors, potentiometers, torque, load cells (Au et al., 2007; Klein & Voglewede, 2018; Sup et al., 2009)] intrinsic to the prosthesis instead of motion capture and force plate data as was done in the current series of experiments. In this dissertation, data were acquired from only three amputees with similar characteristics (e.g., age, gender, cause of amputation) but different level of ambulation activity (e.g., athletes and non-athletes), muscle control awareness, and staircase foot placement. Although the small number of participants did not affect the good performance of each amputee model, the improvements and studies mentioned above will require a larger cohort of participants with diverse characteristics to validate model performance across the amputee population.

While the NARX model had favorable performance in transtibial amputees offline, it is unknown how model accuracy and control stability would be impacted by having a user in the feedback control loop, one that is continuously adapting and reacting to changes in the environment (e.g., perturbations, terrains) and limitations in prosthetic control (e.g., errors). The user's adaptation (e.g., change in muscle recruitment) to the system will likely require iterative training to maintain robust and stable model performance. In a study outside the aims of this dissertation, the feasibility of predicting user's EMG responses to changes of ankle angle dynamics for simulating human-in-the-loop control was demonstrated (Zabre-Gonzalez, Amieva-Alvarado, et al., 2021). The NARX-based user response model predicted ankle plantarflexor and dorsiflexor EMG continuously across ambulation conditions (i.e., level walking, stair ascent, stair descent) using variable inputs (i.e., ankle kinetics, and shank and/or ankle kinematics). Forward stability of the autoregressive model presented here and its interaction with a closed-loop prosthetic controller, in conjunction with the human-in-the loop model, must be evaluated in future studies (e.g., in MATLAB Simulink) to ensure the safety and stability of the physical system prior human testing.

The end goal of the project, beyond this dissertation, is to integrate the autoregressive model developed here into the controller and hardware of existing research and commercially available active powered lower limb prostheses, for example, Marquette University's active ankle-foot (Sun et al., 2014; Sun & Voglewede, 2012). Once the physical system is fully implemented, it would be tested with human participants to determine whether the NARX model predictions of continuous ankle angle and moment can be applied to real-time control of the stiffness (or impedance) of the

ankle joint. The continuous and predictive qualities of the EMG-driven NARX model has the potential to accelerate the development of myoelectric controlled devices, especially to improve prosthetic function for lower limb amputees by returning the user to a more normal gait pattern and enabling them to live more active lives.

BIBLIOGRAPHY

Ahmad, N., Thomas, G. N., Gill, P., Chan, C., & Torella, F. (2014). Lower limb amputation in England: Prevalence, regional variation and relationship with revascularisation, deprivation and risk factors. A retrospective review of hospital data. *Journal of the Royal Society of Medicine*, *107*(12), 483–489. https://doi.org/10.1177/0141076814557301

Aldridge, J. M., Sturdy, J. T., & Wilken, J. M. (2012). Stair ascent kinematics and kinetics with a powered lower leg system following transtibial amputation. *Gait & Posture*, *36*(2), 291–295. https://doi.org/10.1016/j.gaitpost.2012.03.013

Ardestani, M. M., Zhang, X., Wang, L., Lian, Q., Liu, Y., He, J., Li, D., & Jin, Z. (2014). Human lower extremity joint moment prediction: A wavelet neural network approach. *Expert Systems with Applications*, *41*(9), 4422–4433. https://doi.org/10.1016/j.eswa.2013.11.003

Asghari Oskoei, M., & Hu, H. (2007). Myoelectric control systems–A survey. *Biomedical Signal Processing and Control*, *2*(4), 275–294. https://doi.org/10.1016/j.bspc.2007.07.009

Au, S. K., Berniker, M., & Herr, H. M. (2008). Powered ankle-foot prosthesis to assist level-ground and stair-descent gaits. *Neural Networks*, *21*(4), 654–666. https://doi.org/10.1016/j.neunet.2008.03.006

Au, S. K., Herr, H. M., Weber, J., & Martinez-Villalpando, E. C. (2007). Powered ankle-foot prosthesis for the improvement of amputee ambulation. *29th Annual International Conference of the IEEE Engineering in Medicine and Biology Society*, 3020–3026. https://doi.org/10.1109/IEMBS.2007.4352965

Au, S. K., Weber, J., & Herr, H. M. (2009). Powered ankle-foot prosthesis improves walking metabolic economy. *IEEE Transactions on Robotics*, *25*(1), 51–66. https://doi.org/10.1109/TRO.2008.2008747

Baby Jephil, P., Acharaya, P., Xu, L., Guo, K., Yu, H., Watsford, M., Rong, S., & Su, S. (2020). Estimation of ankle joint torque and angle based on s-EMG signal for assistive rehabilitation robots. In G. Naik (Ed.), *Biomedical Signal Processing* (pp. 31–47). Springer. https://doi.org/10.1007/978-981-13-9097-5_2

Bateni, H., & Olney, S. J. (2002). Kinematic and kinetic variations of below-knee amputee gait. *JPO Journal of Prosthetics and Orthotics*, *14*(1), 2–10.

Bellman, R. D., Holgate, M. A., & Sugar, T. G. (2008). SPARKy 3: Design of an active robotic ankle prosthesis with two actuated degrees of freedom using regenerative kinetics. *2nd IEEE RAS & EMBS International Conference on Biomedical Robotics and Biomechatronics*, 511–516. https://doi.org/10.1109/BIOROB.2008.4762887

Benedetti, M. G., Agostini, V., Knaflitz, M., & Bonato, P. (2012). Muscle activation patterns during level walking and stair ambulation. In C. Steele & C. Steele (Eds.), *Applications of EMG in Clinical and Sports Medicine*. InTechOpen. https://doi.org/10.5772/25792

Benjamini, Y., & Hochberg, Y. (1995). Controlling the false discovery rate: A practical and powerful approach to multiple testing. *Journal of the Royal Statistical Society: Series B (Methodological)*, *57*(1), 289–300. https://doi.org/10.1111/j.2517-6161.1995.tb02031.x

Brantley, J. A., Luu, T. P., Nakagome, S., & Contreras-Vidal, J. L. (2017). Prediction of lower-limb joint kinematics from surface EMG during overground locomotion. *IEEE International Conference on Systems, Man, and Cybernetics*, 1705–1709. https://doi.org/10.1109/SMC.2017.8122861

Brown, B. J., Iorio, M. L., Klement, M., Conti Mica, M. R., El-Amraoui, A., O'Halloran, P., & Attinger, C. E. (2014). Outcomes after 294 transtibial amputations with the posterior myocutaneous flap. *The International Journal of Lower Extremity Wounds*, *13*(1), 33–40. https://doi.org/10.1177/153473461452070

Cavanagh, P. R., & Komi, P. V. (1979). Electromechanical delay in human skeletal muscle under concentric and eccentric contractions. *European Journal of Applied Physiology and Occupational Physiology*, *42*(3), 159–163. https://doi.org/10.1007/BF00431022

Chen, B., & Wang, Q. (2015). Combining human volitional control with intrinsic controller on robotic prosthesis: A case study on adaptive slope walking. *37th Annual International Conference of the IEEE Engineering in Medicine and Biology Society*, 4777–4780. https://doi.org/10.1109/EMBC.2015.7319462

Chen, J., Zhang, X., Cheng, Y., & Xi, N. (2018). Surface EMG based continuous estimation of human lower limb joint angles by using deep belief networks. *Biomedical Signal Processing and Control*, *40*, 335–342. https://doi.org/10.1016/j.bspc.2017.10.002

Chen, L., Geng, Y., & Li, G. (2011). Effect of upper-limb positions on motion pattern recognition using electromyography. *4th International Congress on Image and Signal Processing*, 139–142. https://doi.org/10.1109/CISP.2011.6100025

Chen, S., Billings, S. A., & Grant, P. M. (1990). Non-linear system identification using neural networks. *International Journal of Control*, *51*(6), 1191–1214. https://doi.org/10.1080/00207179008934126

Chen, Y., Hu, J., Zhang, F., Li, P., & Hou, Z.-G. (2013). EMG-based estimation of knee joint angle under functional electrical stimulation using an artificial neural network. *Proceedings of the 32nd Chinese Control Conference*, 4661–4665.

Cherelle, P., Grosu, V., Cestari, M., Vanderborght, B., & Lefeber, D. (2016). The AMP-Foot 3, new generation propulsive prosthetic feet with explosive motion characteristics: Design and validation. *BioMedical Engineering OnLine*, *15*(Suppl 3), 145. https://doi.org/10.1186/s12938-016-0285-8

Cherelle, P., Grosu, V., Matthys, A., Vanderborght, B., & Lefeber, D. (2014). Design and validation of the ankle mimicking prosthetic (AMP-) foot 2.0. *IEEE Transactions on Neural Systems and Rehabilitation Engineering*, *22*(1), 138–148. https://doi.org/10.1109/TNSRE.2013.2282416

Choi, J. T., & Bastian, A. J. (2007). Adaptation reveals independent control networks for human walking. *Nature Neuroscience*, *10*(8), 1055–1062. https://doi.org/10.1038/nn1930

Clites, T. R., Herr, H. M., Srinivasan, S. S., Zorzos, A. N., & Carty, M. J. (2018). The Ewing amputation: The first human implementation of the agonist-antagonist myoneural interface. *Plastic and Reconstructive Surgery - Global Open*, *6*(11), e1997. https://doi.org/10.1097/GOX.0000000000001997

C-Motion. (2014). *First derivative*. https://c-motion.com/v3dwiki/index.php/First_Derivative

C-Motion. (2015). *Inverse dynamics*. https://c-motion.com/v3dwiki/index.php/Inverse_Dynamics

Culver, S., Bartlett, H., Shultz, A., & Goldfarb, M. (2018). A stair ascent and descent controller for a powered ankle prosthesis. *IEEE Transactions on Neural Systems and Rehabilitation Engineering*, *26*(5), 993–1002. https://doi.org/10.1109/TNSRE.2018.2819508

Dawley, J. A., Fite, K. B., & Fulk, G. D. (2013). EMG control of a bionic knee prosthesis: Exploiting muscle co-contractions for improved locomotor function. *IEEE 13th International Conference on Rehabilitation Robotics*, 1–6. https://doi.org/10.1109/ICORR.2013.6650389

De Luca, C. J., Donald Gilmore, L., Kuznetsov, M., & Roy, S. H. (2010). Filtering the surface EMG signal: Movement artifact and baseline noise contamination. *Journal of Biomechanics*, *43*(8), 1573–1579. https://doi.org/10.1016/j.jbiomech.2010.01.027

Dey, S., Eslamy, M., Yoshida, T., Ernst, M., Schmalz, T., & Schilling, ArndtF. (2019). A support vector regression approach for continuous prediction of ankle angle and moment during walking: An implication for developing a control strategy for active ankle prostheses. *IEEE 16th International Conference on Rehabilitation Robotics*, 727–733. https://doi.org/10.1109/ICORR.2019.8779445

Dietz, V., Quintern, J., & Sillem, M. (1987). Stumbling reactions in man: Significance of proprioceptive and pre-programmed mechanisms. *The Journal of Physiology*, *386*, 149–163. https://doi.org/10.1113/jphysiol.1987.sp016527

Dillingham, T. R., Pezzin, L. E., & Mackenzie, E. J. (2002). Limb amputation and limb deficiency: Epidemiology and recent trends in the United States. *Southern Medical Journal*, *95*(8), 875–883. https://doi.org/10.1097/00007611-200208000-00018

Embry, K. R., Villarreal, D. J., Macaluso, R. L., & Gregg, R. D. (2018). Modeling the kinematics of human locomotion over continuously varying speeds and inclines. *IEEE Transactions on Neural Systems and Rehabilitation Engineering*, *26*(12), 2342–2350. https://doi.org/10.1109/TNSRE.2018.2879570

Eslamy, M., & Alipour, K. (2019). Synergy-based Gaussian process estimation of ankle angle and torque: Conceptualization for high level controlling of active robotic foot prostheses/orthoses. *Journal of Biomechanical Engineering*, *141*(2), 021002. https://doi.org/10.1115/1.4041767

Farmer, S., Silver-Thorn, B., Voglewede, P. A., & Beardsley, S. A. (2014). Within-socket myoelectric prediction of continuous ankle kinematics for control of a powered transtibial prosthesis. *Journal of Neural Engineering*, *11*(5), 056027. https://doi.org/10.1088/1741-2560/11/5/056027

Felzer, T., & Freisleben, B. (2002). HaWCoS: The "hands-free" wheelchair control system. *Proceedings of the Fifth International ACM Conference on Assistive Technologies*, 127–134. https://doi.org/10.1145/638249.638273

Ferris, A. E., Aldridge, J. M., Rábago, C. A., & Wilken, J. M. (2012). Evaluation of a powered ankle-foot prosthetic system during walking. *Archives of Physical Medicine and Rehabilitation*, *93*(11), 1911–1918. https://doi.org/10.1016/j.apmr.2012.06.009

Ficanha, E. M., Ribeiro, G. A., Dallali, H., & Rastgaar, M. (2016). Design and preliminary evaluation of a two DOFs cable-driven ankle-foot prosthesis with active dorsiflexion-plantarflexion and inversion-eversion. *Frontiers in Bioengineering and Biotechnology*, *4*(36). https://doi.org/10.3389/fbioe.2016.00036

Fleming, A., Stafford, N., Huang, S., Hu, X., Ferris, D. P., & Huang, H. (2021). Myoelectric control of robotic lower limb prostheses: A review of electromyography interfaces, control paradigms, challenges and future directions. *Journal of Neural Engineering*, *18*(4), 041004. https://doi.org/10.1088/1741-2552/ac1176

Gençay, R., & Liu, T. (1997). Nonlinear modelling and prediction with feedforward and recurrent networks. *Physica D: Nonlinear Phenomena*, *108*(1–2), 119–134. https://doi.org/10.1016/S0167-2789(97)82009-X

Go, S. A., Litchy, W. J., Evertz, L. Q., & Kaufman, K. R. (2018). Evaluating skeletal muscle electromechanical delay with intramuscular pressure. *Journal of Biomechanics*, *76*, 181–188. https://doi.org/10.1016/j.jbiomech.2018.05.029

Grabowski, A. M., & D'Andrea, S. (2013). Effects of a powered ankle-foot prosthesis on kinetic loading of the unaffected leg during level-ground walking. *Journal of NeuroEngineering and Rehabilitation*, *10*, 49. https://doi.org/10.1186/1743-0003-10-49

Grimmer, M., Holgate, M., Holgate, R., Boehler, A., Ward, J., Hollander, K., Sugar, T., & Seyfarth, A. (2016). A powered prosthetic ankle joint for walking and running. *BioMedical Engineering OnLine*, *15*(Suppl 3), 141. https://doi.org/10.1186/s12938-016-0286-7

Grimmer, M., Holgate, M., Ward, J., Boehler, A., & Seyfarth, A. (2017). Feasibility study of transtibial amputee walking using a powered prosthetic foot. *International Conference on Rehabilitation Robotics*, 1118–1123. https://doi.org/10.1109/ICORR.2017.8009399

Gupta, R., & Agarwal, R. (2017). sEMG interface design for locomotion identification. *The World Academy of Science, Engineering and Technology*, *11*(2), 133–142.

Gupta, R., Dhindsa, I. S., & Agarwal, R. (2020). Continuous angular position estimation of human ankle during unconstrained locomotion. *Biomedical Signal Processing and Control*, *60*, 101968. https://doi.org/10.1016/j.bspc.2020.101968

Ha, K. H., Varol, H. A., & Goldfarb, M. (2011). Volitional control of a prosthetic knee using surface electromyography. *IEEE Transactions on Biomedical Engineering*, *58*(1), 144–151. https://doi.org/10.1109/TBME.2010.2070840

Hahn, M. E., & O'Keefe, K. B. (2008). A neural network model for estimation of net joint moments during normal gait. *Journal of Musculoskeletal Research*, *11*(03), 117–126. https://doi.org/10.1142/S0218957708002036

Hak, L., van Dieën, J. H., van der Wurff, P., Prins, M. R., Mert, A., Beek, P. J., & Houdijk, H. (2013). Walking in an unstable environment: Strategies used by transtibial amputees to prevent falling during gait. *Archives of Physical Medicine and Rehabilitation*, *94*(11), 2186–2193. https://doi.org/10.1016/j.apmr.2013.07.020

Han, M., Xi, J., Xu, S., & Yin, F.-L. (2004). Prediction of chaotic time series based on the recurrent predictor neural network. *IEEE Transactions on Signal Processing*, *52*(12), 3409–3416. https://doi.org/10.1109/TSP.2004.837418

Han, Y., Song, A., Gao, H., & Zhu, S. (2015). The muscle activation patterns of lower limb during stair climbing at different backpack load. *Acta of Bioengineering and Biomechanics*, *17*(4), 13–20. https://doi.org/10.5277/ABB-00155-2014-06

Hargrove, L., Englehart, K., & Hudgins, B. (2006). The effect of electrode displacements on pattern recognition based myoelectric control. *28th Annual International Conference of the IEEE Engineering in Medicine and Biology Society*, 2203–2206. https://doi.org/10.1109/IEMBS.2006.260681

Hayashi, T., Kawamoto, H., & Sankai, Y. (2005). Control method of robot suit HAL working as operator's muscle using biological and dynamical information. *IEEE/RSJ International Conference on Intelligent Robots and Systems*, 3063–3068. https://doi.org/10.1109/IROS.2005.1545505

Hefferman, G. M., Zhang, F., Nunnery, M. J., & Huang, H. (2015). Integration of surface electromyographic sensors with the transfemoral amputee socket: A comparison of four differing configurations. *Prosthetics and Orthotics International*, *39*(2), 166–173. https://doi.org/10.1177/0309364613516484

Herr, H. M., & Grabowski, A. M. (2012). Bionic ankle-foot prosthesis normalizes walking gait for persons with leg amputation. *Proceedings of the Royal Society B: Biological Sciences*, *279*(1728), 457–464. https://doi.org/10.1098/rspb.2011.1194

Hill, D., & Herr, H. M. (2013). Effects of a powered ankle-foot prosthesis on kinetic loading of the contralateral limb: A case series. *IEEE 13th International Conference on Rehabilitation Robotic*, 1–6. https://doi.org/10.1109/ICORR.2013.6650375

Hirschfeld, H., & Forssberg, H. (1991). Phase-dependent modulations of anticipatory postural activity during human locomotion. *Journal of Neurophysiology*, *66*(1), 12–19. https://doi.org/10.1152/jn.1991.66.1.12

Hitt, J., Merlo, J., Johnston, J., Holgate, M., Boehler, A., Hollander, K., & Sugar, T. (2010, November). Bionic running for unilateral transtibial military amputees [Conference presentation]. *27th Army Science Conference*.

Holgate, M. A., Sugar, T. G., & Bohler, A. W. (2009). A novel control algorithm for wearable robotics using phase plane invariants. *IEEE International Conference on Robotics and Automation*, 3845–3850. https://doi.org/10.1109/ROBOT.2009.5152565

Hoover, C. D., Fulk, G. D., & Fite, K. B. (2012). The design and initial experimental validation of an active myoelectric transfemoral prosthesis. *Journal of Medical Devices*, *6*(1), 011005. https://doi.org/10.1115/1.4005784

Hoover, C. D., Fulk, G. D., & Fite, K. B. (2013). Stair ascent with a powered transfemoral prosthesis under direct myoelectric control. *IEEE/ASME Transactions on Mechatronics*, *18*(3), 1191–1200. https://doi.org/10.1109/TMECH.2012.2200498

Hu, Y. H., & Hwang, J.-N. (Eds.). (2001). *Handbook of neural network signal processing* (1st edition). CRC Press.

Huang, H., Kuiken, T. A., & Lipschutz, R. D. (2009). A strategy for identifying locomotion modes using surface electromyography. *IEEE Transactions on Biomedical Engineering*, *56*(1), 65–73. https://doi.org/10.1109/TBME.2008.2003293

Huang, H., Zhang, F., Hargrove, L. J., Dou, Z., Rogers, D. R., & Englehart, K. B. (2011). Continuous locomotion-mode identification for prosthetic legs based on neuromuscular-mechanical fusion. *IEEE Transactions on Biomedical Engineering*, *58*(10), 2867–2875. https://doi.org/10.1109/TBME.2011.2161671

Huang, S., & Ferris, D. P. (2012). Muscle activation patterns during walking from transtibial amputees recorded within the residual limb-prosthetic interface. *Journal of NeuroEngineering and Rehabilitation*, *9*, 55. https://doi.org/10.1186/1743-0003-9-55

Huang, S., & Huang, H. (2018). Voluntary control of residual antagonistic muscles in transtibial amputees: Feedforward ballistic contractions and implications for direct neural control of powered lower limb prostheses. *IEEE Transactions on Neural Systems and Rehabilitation Engineering*, *26*(4), 894–903. https://doi.org/10.1109/TNSRE.2018.2811544

Huang, S., & Huang, H. (2019). Voluntary control of residual antagonistic muscles in transtibial amputees: Reciprocal activation, coactivation, and implications for direct neural control of powered lower limb prostheses. *IEEE Transactions on Neural Systems and Rehabilitation Engineering*, *27*(1), 85–95. https://doi.org/10.1109/TNSRE.2018.2885641

Huang, S., Wensman, J. P., & Ferris, D. P. (2016). Locomotor adaptation by transtibial amputees walking with an experimental powered prosthesis under continuous myoelectric control. *IEEE Transactions on Neural Systems and Rehabilitation Engineering*, *24*(5), 573–581. https://doi.org/10.1109/TNSRE.2015.2441061

Huihui, C., Farong, G., Chao, C., & Taixing, T. (2018). Estimation of ankle angle based on multi-feature fusion with random forest. *37th Chinese Control Conference*, 5549–5553. https://doi.org/10.23919/ChiCC.2018.8482982

Imam, B., Miller, W. C., Finlayson, H. C., Eng, J. J., & Jarus, T. (2017). Incidence of lower limb amputation in Canada. *Canadian Journal of Public Health*, *108*(4), e374–e380. https://doi.org/10.17269/CJPH.108.6093

Jacobs, D. A., & Ferris, D. P. (2015). Estimation of ground reaction forces and ankle moment with multiple, low-cost sensors. *Journal of NeuroEngineering and Rehabilitation*, *12*, 90. https://doi.org/10.1186/s12984-015-0081-x

Joshi, D., Mishra, A., & Anand, S. (2011). ANFIS based knee angle prediction: An approach to design speed adaptive contra lateral controlled AK prosthesis. *Applied Soft Computing*, *11*(8), 4757–4765. https://doi.org/10.1016/j.asoc.2011.07.007

Kadiallah, A., Liaw, G., Kawato, M., Franklin, D. W., & Burdet, E. (2011). Impedance control is selectively tuned to multiple directions of movement. *Journal of Neurophysiology*, *106*(5), 2737–2748. https://doi.org/10.1152/jn.00079.2011

Kannape, O. A., & Herr, H. M. (2014). Volitional control of ankle plantar flexion in a powered transtibial prosthesis during stair-ambulation. *34th Annual International Conference of the IEEE Engineering in Medicine and Biology Society*, 1662–1665. https://doi.org/10.1109/EMBC.2014.6943925

Kannape, O. A., & Herr, H. M. (2016). Split-belt adaptation and gait symmetry in transtibial amputees walking with a hybrid EMG controlled ankle-foot prosthesis. *38th Annual International Conference of the IEEE Engineering in Medicine and Biology Society*, 5469–5472. https://doi.org/10.1109/EMBC.2016.7591964

Keleş, A. D., & Yucesoy, C. A. (2020). Development of a neural network based control algorithm for powered ankle prosthesis. *Journal of Biomechanics*, *113*, 110087. https://doi.org/10.1016/j.jbiomech.2020.110087

Kisannagar, R. R., Jha, P., Navalkar, A., Maji, S. K., & Gupta, D. (2020). Fabrication of silver nanowire/polydimethylsiloxane dry electrodes by a vacuum filtration method for electrophysiological signal monitoring. *ACS Omega*, *5*(18), 10260–10265. https://doi.org/10.1021/acsomega.9b03678

Klein, J. G., & Voglewede, P. A. (2018). Stiffness control of an active transtibial prosthesis. *Proceedings of the ASME 2018 International Design Engineering Technical Conferences and Computers and Information in Engineering Conference*, *5A*, V05AT07A060. https://doi.org/10.1115/DETC2018-85455

Kuiken, T. A., Li, G., Lock, B. A., Lipschutz, R. D., Miller, L. A., Stubblefield, K. A., & Englehart, K. B. (2009). Targeted muscle reinnervation for real-time myoelectric control of multifunction artificial arms. *JAMA*, *301*(6), 619–628. https://doi.org/10.1001/jama.2009.116

Kulkarni, J., Gaine, W. J., Buckley, J. G., Rankine, J. J., & Adams, J. (2005). Chronic low back pain in traumatic lower limb amputees. *Clinical Rehabilitation*, *19*(1), 81–86. https://doi.org/10.1191/0269215505cr819oa

Kumar, A., Godiyal, A. K., Joshi, P., & Joshi, D. (2021). A new force myography-based approach for continuous estimation of knee joint angle in lower limb amputees and able-bodied subjects. *IEEE Journal of Biomedical and Health Informatics*, *25*(3), 701–710. https://doi.org/10.1109/JBHI.2020.2993697

Lee, J., & Lee, G.-K. (2005). Gait angle prediction for lower limb orthotics and prostheses using an EMG signal and neural networks. *International Journal of Control, Automation, and Systems*, *3*(2), 152–158.

Lee, S., Kim, M.-O., Kang, T., Park, J., & Choi, Y. (2018). Knit band sensor for myoelectric control of surface EMG-based prosthetic hand. *IEEE Sensors Journal*, *18*(20), 8578–8586. https://doi.org/10.1109/JSEN.2018.2865623

Lencioni, T., Carpinella, I., Rabuffetti, M., Marzegan, A., & Ferrarin, M. (2019). Human kinematic, kinetic and EMG data during different walking and stair ascending and

descending tasks. *Scientific Data*, *6*, 309. https://doi.org/10.1038/s41597-019-0323-z

Lenzi, T., De Rossi, S. M. M., Vitiello, N., & Carrozza, M. C. (2011). Proportional EMG control for upper-limb powered exoskeletons. *33rd Annual International Conference of the IEEE Engineering in Medicine and Biology Society*, 628–631. https://doi.org/10.1109/IEMBS.2011.6090139

Leontaritis, I. J., & Billings, S. A. (1985). Input-output parametric models for non-linear systems Part I: Deterministic non-linear systems. *International Journal of Control*, *41*(2), 303–328. https://doi.org/10.1080/0020718508961129

Lewis, F. L., & Parisini, T. (1998). Guest editorial: Neural network feedback control with guaranteed stability. *International Journal of Control*, *70*(3), 337–339. https://doi.org/10.1080/002071798222262

Li, Q., Song, Y., & Hou, Z.-G. (2015). Estimation of lower limb periodic motions from sEMG using least squares support vector regression. *Neural Processing Letters*, *41*(3), 371–388. https://doi.org/10.1007/s11063-014-9391-4

Light, C. M., Chappell, P. H., Hudgins, B., & Engelhart, K. (2002). Intelligent multifunction myoelectric control of hand prostheses. *Journal of Medical Engineering & Technology*, *26*(4), 139–146. https://doi.org/10.1080/03091900210142459

Liu, J., Kang, S. H., Xu, D., Ren, Y., Lee, S. J., & Zhang, L.-Q. (2017). EMG-based continuous and simultaneous estimation of arm kinematics in able-bodied individuals and stroke survivors. *Frontiers in Neuroscience*, *11*, 480. https://doi.org/10.3389/fnins.2017.00480

Liu, J., Ren, Y., Xu, D., Kang, S. H., & Zhang, L.-Q. (2020). EMG-based real-time linear-nonlinear cascade regression decoding of shoulder, elbow, and wrist movements in able-bodied persons and stroke survivors. *IEEE Transactions on Biomedical Engineering*, *67*(5), 1272–1281. https://doi.org/10.1109/TBME.2019.2935182

Liu, M., Zhang, F., & Huang, H. H. (2017). An adaptive classification strategy for reliable locomotion mode recognition. *Sensors*, *17*(9), 2020. https://doi.org/10.3390/s17092020

Liu, Q., Chen, W., Hu, H., Zhu, Q., & Xie, Z. (2020). An optimal NARX neural network identification model for a magnetorheological damper with force-distortion behavior. *Frontiers in Materials*, *7*, 10. https://doi.org/10.3389/fmats.2020.00010

Liu, Y., Shih, S.-M., Tian, S.-L., Zhong, Y.-J., & Li, L. (2009). Lower extremity joint torque predicted by using artificial neural network during vertical jump. *Journal of Biomechanics*, *42*(7), 906–911. https://doi.org/10.1016/j.jbiomech.2009.01.033

López-Delis, A., Miosso, C. J., Carvalho, J. L. A., da Rocha, A. F., & Borges, G. A. (2018). Continuous estimation prediction of knee joint angles using fusion of electromyographic and inertial sensors for active transfemoral leg prostheses. *Advances in Data Science and Adaptive Analysis*, *10*(02), 1840008. https://doi.org/10.1142/S2424922X18400089

Loverro, K. L., Mueske, N. M., & Hamel, K. A. (2013). Location of minimum foot clearance on the shoe and with respect to the obstacle changes with locomotor task. *Journal of Biomechanics*, *46*(11), 1842–1850. https://doi.org/10.1016/j.jbiomech.2013.05.002

Mahmoud, S. M. (2012). *Identification and prediction of abnormal behaviour activities of daily living in intelligent environments* [Doctoral, Nottingham Trent University]. http://irep.ntu.ac.uk/id/eprint/60/

Malcolm, P., Quesada, R. E., Caputo, J. M., & Collins, S. H. (2015). The influence of push-off timing in a robotic ankle-foot prosthesis on the energetics and mechanics of walking. *Journal of NeuroEngineering and Rehabilitation*, *12*(1), 21. https://doi.org/10.1186/s12984-015-0014-8

McDonald, C. L., Westcott-McCoy, S., Weaver, M. R., Haagsma, J., & Kartin, D. (2021). Global prevalence of traumatic non-fatal limb amputation. *Prosthetics and Orthotics International*, *45*(2), 105–114. https://doi.org/10.1177/0309364620972258

Menezes, J. M. P., & Barreto, G. A. (2008). Long-term time series prediction with the NARX network: An empirical evaluation. *Neurocomputing*, *71*(16), 3335–3343. https://doi.org/10.1016/j.neucom.2008.01.030

Merletti, R., & Parker, P. (Eds.). (2004). *Electromyography: Physiology, engineering, and non-invasive applications*. Wiley-IEEE Press.

Meyer, A. J., Patten, C., & Fregly, B. J. (2017). Lower extremity EMG-driven modeling of walking with automated adjustment of musculoskeletal geometry. *PLoS ONE*, *12*(7), e0179698. https://doi.org/10.1371/journal.pone.0179698

Miller, W. C., Speechley, M., & Deathe, B. (2001). The prevalence and risk factors of falling and fear of falling among lower extremity amputees. *Archives of Physical Medicine and Rehabilitation*, *82*(8), 1031–1037. https://doi.org/10.1053/apmr.2001.24295

Montgomery, J. R., & Grabowski, A. M. (2018). Use of a powered ankle-foot prosthesis reduces the metabolic cost of uphill walking and improves leg work symmetry in people with transtibial amputations. *Journal of the Royal Society Interface*, *15*(145). https://doi.org/10.1098/rsif.2018.0442

Moon, I., Lee, M., Chu, J., & Mun, M. (2005). Wearable EMG-based HCI for electric-powered wheelchair users with motor disabilities. *Proceedings of the 2005 IEEE*

International Conference on Robotics and Automation, 2649–2654. https://doi.org/10.1109/ROBOT.2005.1570513

Morgenroth, D. C., Segal, A. D., Zelik, K. E., Czerniecki, J. M., Klute, G. K., Adamczyk, P. G., Orendurff, M. S., Hahn, M. E., Collins, S. H., & Kuo, A. D. (2011). The effect of prosthetic foot push-off on mechanical loading associated with knee osteoarthritis in lower extremity amputees. *Gait & Posture*, *34*(4), 502–507. https://doi.org/10.1016/j.gaitpost.2011.07.001

Müller, R., Tronicke, L., Abel, R., & Lechler, K. (2019). Prosthetic push-off power in trans-tibial amputee level ground walking: A systematic review. *PLoS ONE*, *14*(11), e0225032. https://doi.org/10.1371/journal.pone.0225032

Nakamura, B. H., & Hahn, M. E. (2017). Myoelectric activation pattern changes in the involved limb of individuals with transtibial amputation during locomotor state transitions. *Archives of Physical Medicine and Rehabilitation*, *98*(6), 1180–1186. https://doi.org/10.1016/j.apmr.2016.12.003

Narendra, K. S., & Parthasarathy, K. (1990). Identification and control of dynamical systems using neural networks. *IEEE Transactions on Neural Networks*, *1*(1), 4–27. https://doi.org/10.1109/72.80202

Neumann, D. A. (2017). *Kinesiology of the musculoskeletal system: Foundations for rehabilitation* (3rd edition). Elsevier.

Ngeo, J. G., Tamei, T., & Shibata, T. (2014). Continuous and simultaneous estimation of finger kinematics using inputs from an EMG-to-muscle activation model. *Journal of NeuroEngineering and Rehabilitation*, *11*, 122. https://doi.org/10.1186/1743-0003-11-122

Össur. (2019). *I-Limb® Quantum*. https://www.ossur.com/en-us/prosthetics/arms/i-limb-quantum

Ottobock. (2014). *Myoelectric prosthetics*. https://www.ottobockus.com/prosthetics/upper-limb-prosthetics/solution-overview/myoelectric-prosthetics/

Owings, M. F., & Kozak, L. J. (1998). Ambulatory and inpatient procedures in the United States, 1996. *Vital and Health Statistics. Series 13, Data from the National Health Survey*, *139*, 1–119.

Pearson, K. G. (2000). Neural adaptation in the generation of rhythmic behavior. *Annual Review of Physiology*, *62*(1), 723–753. https://doi.org/10.1146/annurev.physiol.62.1.723

Prasertsakul, T., Poonsiri, J., & Charoensuk, W. (2012). Prediction gait during ascending stair by using artificial neural networks. *The 5th 2012 Biomedical Engineering International Conference*, 1–5. https://doi.org/10.1109/BMEiCon.2012.6465464

Pröbsting, E., Bellmann, M., Schmalz, T., & Hahn, A. (2020). Gait characteristics of transtibial amputees on level ground in a cohort of 53 amputees–Comparison of kinetics and kinematics with non-amputees. *Canadian Prosthetics & Orthotics Journal*, *2*(2), 1. https://doi.org/10.33137/cpoj.v2i2.32955

Protopapadaki, A., Drechsler, W. I., Cramp, M. C., Coutts, F. J., & Scott, O. M. (2007). Hip, knee, ankle kinematics and kinetics during stair ascent and descent in healthy young individuals. *Clinical Biomechanics*, *22*(2), 203–210. https://doi.org/10.1016/j.clinbiomech.2006.09.010

Quintero, D., Villarreal, D. J., Lambert, D. J., Kapp, S., & Gregg, R. D. (2018). Continuous-phase control of a powered knee-ankle prosthesis: Amputee experiments across speeds and inclines. *IEEE Transactions on Robotics*, *34*(3), 686–701. https://doi.org/10.1109/TRO.2018.2794536

Rábago, C. A., & Wilken, J. M. (2016). The prevalence of gait deviations in individuals with transtibial amputation. *Military Medicine*, *181*(Suppl 4), 30–37. https://doi.org/10.7205/MILMED-D-15-00505

Radmand, A., Scheme, E., & Englehart, K. (2014). A characterization of the effect of limb position on EMG features to guide the development of effective prosthetic control schemes. *36th Annual International Conference of the IEEE Engineering in Medicine and Biology Society*, 662–667. https://doi.org/10.1109/EMBC.2014.6943678

Ramstrand, N., & Nilsson, K.-Å. (2009). A comparison of foot placement strategies of transtibial amputees and able-bodied subjects during stair ambulation. *Prosthetics and Orthotics International*, *33*(4), 348–355. https://doi.org/10.3109/03093640903074891

Reissman, T., Halsne, E., Lipschutz, R., Miller, L., & Kuiken, T. (2018). A novel gel liner system with embedded electrodes for use with upper limb myoelectric prostheses. *PLoS ONE*, *13*(6), e0198934. https://doi.org/10.1371/journal.pone.0198934

Rouhani, A., & Mohajerzadeh, S. (2013). An epidemiological and etiological report on lower extremity amputation in northwest of Iran. *The Archives of Bone and Joint Surgery*, *1*(2), 103–106.

Sadeghi, H., Allard, P., Prince, F., & Labelle, H. (2000). Symmetry and limb dominance in able-bodied gait: A review. *Gait & Posture*, *12*(1), 34–45. https://doi.org/10.1016/S0966-6362(00)00070-9

Schmalz, T., Blumentritt, S., & Marx, B. (2007). Biomechanical analysis of stair ambulation in lower limb amputees. *Gait & Posture*, *25*(2), 267–278. https://doi.org/10.1016/j.gaitpost.2006.04.008

Schulz, B. W. (2011). Minimum toe clearance adaptations to floor surface irregularity and gait speed. *Journal of Biomechanics*, *44*(7), 1277–1284. https://doi.org/10.1016/j.jbiomech.2011.02.010

Selk Ghafari, A., Meghdari, A., & Vossoughi, G. R. (2009). Contribution of the muscles at the ankle joint during daily activities. *17th Annual (International) Conference on Mechanical Engineering*. https://doi.org/10.13140/2.1.3687.4243

Sepulveda, F., Wells, D. M., & Vaughan, C. L. (1993). A neural network representation of electromyography and joint dynamics in human gait. *Journal of Biomechanics*, *26*(2), 101–109. https://doi.org/10.1016/0021-9290(93)90041-C

Seyedali, M., Czerniecki, J. M., Morgenroth, D. C., & Hahn, M. E. (2012). Co-contraction patterns of trans-tibial amputee ankle and knee musculature during gait. *Journal of NeuroEngineering and Rehabilitation*, *9*, 29. https://doi.org/10.1186/1743-0003-9-29

Shao, Q., Bassett, D. N., Manal, K., & Buchanan, T. S. (2009). An EMG-driven model to estimate muscle forces and joint moments in stroke patients. *Computers in Biology and Medicine*, *39*(12), 1083–1088. https://doi.org/10.1016/j.compbiomed.2009.09.002

Shaw, J., Challa, S., Conway, D., Liu, M., Haonga, B., Eliezer, E., Morshed, S., & Shearer, D. (2018). Quality of life and complications in lower limb amputees in Tanzania: Results from a pilot study. *The Lancet Global Health*, *6*, S18. https://doi.org/10.1016/S2214-109X(18)30147-5

Shultz, A. H., & Goldfarb, M. (2018). A unified controller for walking on even and uneven terrain with a powered ankle prosthesis. *IEEE Transactions on Neural Systems and Rehabilitation Engineering*, *26*(4), 788–797. https://doi.org/10.1109/TNSRE.2018.2810165

Shultz, A. H., Lawson, B. E., & Goldfarb, M. (2016). Variable cadence walking and ground adaptive standing with a powered ankle prosthesis. *IEEE Transactions on Neural Systems and Rehabilitation Engineering*, *24*(4), 495–505. https://doi.org/10.1109/TNSRE.2015.2428196

Siegelmann, H. T., & Sontag, E. D. (1991). Turing computability with neural nets. *Applied Mathematics Letters*, *4*(6), 77–80. https://doi.org/10.1016/0893-9659(91)90080-F

Silver-Thorn, B., Current, T., & Kuhse, B. (2012). Preliminary investigation of residual limb plantarflexion and dorsiflexion muscle activity during treadmill walking for trans-tibial amputees. *Prosthetics and Orthotics International*, *36*(4), 435–442. https://doi.org/10.1177/0309364612443379

Sinclair, J., Taylor, P. J., Hebron, J., Brooks, D., Hurst, H. T., & Atkins, S. (2015). The reliability of electromyographic normalization methods for cycling analyses. *Journal of Human Kinetics*, *46*, 19–27. https://doi.org/10.1515/hukin-2015-0030

Sinitski, E. H., Hansen, A. H., & Wilken, J. M. (2012). Biomechanics of the ankle-foot system during stair ambulation: Implications for design of advanced ankle-foot prostheses. *Journal of Biomechanics*, *45*(3), 588–594. https://doi.org/10.1016/j.jbiomech.2011.11.007

Sivakumar, S., Gopalai, A. A., Lim, K. H., & Gouwanda, D. (2019). Artificial neural network based ankle joint angle estimation using instrumented foot insoles. *Biomedical Signal Processing and Control*, *54*, 101614. https://doi.org/10.1016/j.bspc.2019.101614

Spanias, J. A., Simon, A. M., Finucane, S. B., Perreault, E. J., & Hargrove, L. J. (2018). Online adaptive neural control of a robotic lower limb prosthesis. *Journal of Neural Engineering*, *15*(1), 016015. https://doi.org/10.1088/1741-2552/aa92a8

Stolyarov, R., Burnett, G., & Herr, H. M. (2018). Translational motion tracking of leg joints for enhanced prediction of walking tasks. *IEEE Transactions on Biomedical Engineering*, *65*(4), 763–769. https://doi.org/10.1109/TBME.2017.2718528

Sun, J., Fritz, J. M., Del Toro, D. R., & Voglewede, P. A. (2014). Amputee subject testing protocol, results, and analysis of a powered transtibial prosthetic device. *Journal of Medical Devices*, *8*(4), 0410071–0410076. https://doi.org/10.1115/1.4027497

Sun, J., & Voglewede, P. A. (2012). Controller design and preliminary testing of a powered below-knee prosthetic device. *Proceedings of the ASME 2012 International Design Engineering Technical Conferences and Computers and Information in Engineering Conference*, *4*, 1465–1472. https://doi.org/10.1115/DETC2012-71010

Sup, F., Varol, H. A., Mitchell, J., Withrow, T. J., & Goldfarb, M. (2009). Preliminary evaluations of a self-contained anthropomorphic transfemoral prosthesis. *IEEE/ASME Transactions on Mechatronics*, *14*(6), 667–676. https://doi.org/10.1109/TMECH.2009.2032688

Tkach, D. C., & Hargrove, L. J. (2013). Neuromechanical sensor fusion yields highest accuracies in predicting ambulation mode transitions for trans-tibial amputees. *35th Annual International Conference of the IEEE Engineering in Medicine and Biology Society*, 3074–3077. https://doi.org/10.1109/EMBC.2013.6610190

Tkach, D. C., Lipschutz, R. D., Finucane, S. B., & Hargrove, L. J. (2013). Myoelectric neural interface enables accurate control of a virtual multiple degree-of-freedom foot-ankle prosthesis. *IEEE 13th International Conference on Rehabilitation Robotics*, 1–4. https://doi.org/10.1109/ICORR.2013.6650499

Tommasi, T., Orabona, F., Castellini, C., & Caputo, B. (2013). Improving control of dexterous hand prostheses using adaptive learning. *IEEE Transactions on Robotics*, *29*(1), 207–219. https://doi.org/10.1109/TRO.2012.2226386

Towhidkhah, F., Gander, R. E., & Wood, H. C. (1997). Model predictive impedance control: A model for joint movement. *Journal of Motor Behavior*, *29*(3), 209–222. https://doi.org/10.1080/00222899709600836

Tucker, M. R., Olivier, J., Pagel, A., Bleuler, H., Bouri, M., Lambercy, O., Millán, J. del R., Riener, R., Vallery, H., & Gassert, R. (2015). Control strategies for active lower extremity prosthetics and orthotics: A review. *Journal of NeuroEngineering and Rehabilitation*, *12*, 1. https://doi.org/10.1186/1743-0003-12-1

Vack, H. J., Nielsen, D. H., & Shurp, D. G. (1999). Kinetic patterns during stair ascent in patients with transtibial amputations using three different prostheses. *JPO Journal of Prosthetics and Orthotics*, *11*(3), 57–62.

Wagner, K. E., Nolasco, L. A., Morgenroth, D. C., Gates, D. H., & Silverman, A. K. (2020). The effect of lower-limb prosthetic alignment on muscle activity during sit-to-stand. *Journal of Electromyography and Kinesiology*, *51*, 102398. https://doi.org/10.1016/j.jelekin.2020.102398

Wang, J., Kannape, O. A., & Herr, H. M. (2013). Proportional EMG control of ankle plantar flexion in a powered transtibial prosthesis. *IEEE 13th International Conference on Rehabilitation Robotics*, 1–5. https://doi.org/10.1109/ICORR.2013.6650391

Wang, J., Wang, L., Xi, X., Miran, S. M., & Xue, A. (2020). Estimation and correlation analysis of lower limb joint angles based on surface electromyography. *Electronics*, *9*(4), 556. https://doi.org/10.3390/electronics9040556

Wang, Q., Yuan, K., Zhu, J., & Wang, L. (2014). Finite-state control of a robotic transtibial prosthesis with motor-driven nonlinear damping behaviors for level ground walking. *IEEE 13th International Workshop on Advanced Motion Control*, 155–160. https://doi.org/10.1109/AMC.2014.6823274

Ward, J., Schroeder, K., Vehon, D., Holgate, R., Boehler, A., & Grimmer, M. (2015, August). A rugged microprocessor controlled ankle-foot prosthesis for running [Conference presentation]. *39th Annual Meeting of the American Society of Biomechanics*.

Wentink, E. C., Beijen, S. I., Hermens, H. J., Rietman, J. S., & Veltink, P. H. (2013). Intention detection of gait initiation using EMG and kinematic data. *Gait & Posture*, *37*(2), 223–228. https://doi.org/10.1016/j.gaitpost.2012.07.013

Wentink, E. C., Schut, V. G. H., Prinsen, E. C., Rietman, J. S., & Veltink, P. H. (2014). Detection of the onset of gait initiation using kinematic sensors and EMG in

transfemoral amputees. *Gait & Posture*, *39*(1), 391–396. https://doi.org/10.1016/j.gaitpost.2013.08.008

World Health Organization. (2017). *WHO standards for prosthetics and orthotics, Part 1: Standards*. https://apps.who.int/iris/handle/10665/259209

World Health Organization, US Department of Defense, & MossRehab Amputee Rehabilitation Program. (2004). *The rehabilitation of people with amputations*. https://www.medbox.org/document/the-rehabilitation-of-people-with-amputations#GO

Young, A. J., Hargrove, L. J., & Kuiken, T. A. (2012). Improving myoelectric pattern recognition robustness to electrode shift by changing interelectrode distance and electrode configuration. *IEEE Transactions on Biomedical Engineering*, *59*(3), 645–652. https://doi.org/10.1109/TBME.2011.2177662

Young, A. J., Kuiken, T. A., & Hargrove, L. J. (2014). Analysis of using EMG and mechanical sensors to enhance intent recognition in powered lower limb prostheses. *Journal of Neural Engineering*, *11*(5), 056021. https://doi.org/10.1088/1741-2560/11/5/056021

Yu, T. (2017). *Actuation and control of lower limb prostheses* [Doctoral, University of Bath]. https://researchportal.bath.ac.uk/en/studentTheses/actuation-and-control-of-lower-limb-prostheses

Yu, T., Plummer, A. R., Iravani, P., Bhatti, J., Zahedi, S., & Moser, D. (2019). The design, control, and testing of an integrated electrohydrostatic powered ankle prosthesis. *IEEE/ASME Transactions on Mechatronics*, *24*(3), 1011–1022. https://doi.org/10.1109/TMECH.2019.2911685

Zabre-Gonzalez, E. V., Amieva-Alvarado, D., & Beardsley, S. A. (2021). Prediction of EMG activation profiles from gait kinematics and kinetics during multiple terrains. *43rd Annual International Conference of the IEEE Engineering in Medicine and Biology Society*, 6326–6329. https://doi.org/10.1109/EMBC46164.2021.9630067

Zabre-Gonzalez, E. V., Riem, L., Voglewede, P. A., Silver-Thorn, B., Koehler-McNicholas, S. R., & Beardsley, S. A. (2021). Continuous myoelectric prediction of future ankle angle and moment across ambulation conditions and their transitions. *Frontiers in Neuroscience*, *15*, 709422. https://doi.org/10.3389/fnins.2021.709422

Zabre-Gonzalez, E. V., Silver-Thorn, B., Current, T., Voglewede, P. A., Koehler-McNicholas, S. R., & Beardsley, S. A. (2022). Closed-loop future prediction of continuous ankle kinematics and kinetics using residual muscle signals of transtibial amputees. *Journal of NeuroEngineering and Rehabilitation*. https://doi.org/10.21203/rs.3.rs-2200146/v1

Zarshenas, H., Ruddy, B. P., Kempa-Liehr, A. W., & Besier, T. F. (2020). Ankle torque forecasting using time-delayed neural networks. *42nd Annual International Conference of the IEEE Engineering in Medicine and Biology Society*, 4854–4857. https://doi.org/10.1109/EMBC44109.2020.9175376

Zhang, F., Li, P., Hou, Z.-G., Lu, Z., Chen, Y., Li, Q., & Tan, M. (2012). sEMG-based continuous estimation of joint angles of human legs by using BP neural network. *Neurocomputing*, *78*(1), 139–148. https://doi.org/10.1016/j.neucom.2011.05.033

Zhang, F., Liu, M., & Huang, H. (2015). Investigation of timing to switch control mode in powered knee prostheses during task transitions. *PLoS ONE*, *10*(7), e0133965. https://doi.org/10.1371/journal.pone.0133965

Zheng, H., & Shen, X. (2015). Design and Control of a Pneumatically Actuated Transtibial Prosthesis. *Journal of Bionic Engineering*, *12*(2), 217–226. https://doi.org/10.1016/S1672-6529(14)60114-1

Ziegler-Graham, K., MacKenzie, E. J., Ephraim, P. L., Travison, T. G., & Brookmeyer, R. (2008). Estimating the prevalence of limb loss in the United States: 2005 to 2050. *Archives of Physical Medicine and Rehabilitation*, *89*(3), 422–429. https://doi.org/10.1016/j.apmr.2007.11.005

APPENDIX A: SUPPLEMENTARY MATERIAL FOR CHAPTER 2

Supplementary Table A.1. Statistical scores for CHAPTER 2. Model predictions and targets of ankle angle and ankle moment at critical performance points across participants for each ambulation condition. Significant differences between experimentally measured targets and the model predictions were assessed using a paired-samples t-test (normally distributed samples) and Sign test (non-normally and asymmetric distributed samples). Bold numbers indicate significance using the Benjamini-Hochberg (B-H) multiple comparisons procedure with a false discovery rate of 0.05. Shaded areas represent staircase transition gait cycles during stair ambulation.

Critical Performance Points	Units	Mean ± SD		*t* (df)	*p* value	B-H *p* value
		Target	Prediction			
				Level Ground (n = 10)		
				Gait Cycle 1		
Clearance Intervals during swing phase						
Interval 1: MTC (Mean - SD)	Degrees	-6.03 ± 3.93	-6.03 ± 3.72	*t*(9) = -0.010	0.992	*0.992*
Interval 1: MTC (Mean)	Degrees	-3.56 ± 3.73	-3.67 ± 3.79	*t*(9) = 1.507	0.166	*0.407*
Interval 1: MTC (Mean - SD)	Degrees	-1.04 ± 3.55	-0.92 ± 3.56	*t*(9) = -1.463	0.178	*0.414*
Interval 2: MFC (Mean + SD)	Degrees	2.44 ± 3.15	2.34 ±3.10	*t*(9) = 1.203	0.260	*0.471*
Interval 2: MFC (Mean)	Degrees	3.33 ± 2.89	3.09 ± 2.66	Sign Test	0.344	*0.581*
Interval 2: MFC (Mean + SD)	Degrees	3.80 ± 3.09	3.53 ± 2.74	*t*(9) = 2.163	0.059	*0.213*
Stance Phase Critical Points						
Flexion at Toe Off	Degrees	-2.00 ± 2.10	-1.97 ± 1.94	*t*(9) = -0.186	0.857	*0.893*
Dorsiflexion	Degrees	13.93 ± 1.94	13.99 ± 1.88	*t*(9) = -1.303	0.225	*0.455*
Plantarflexion	Degrees	-4.56 ± 4.59	-4.77 ± 4.76	*t*(9) = 1.518	0.163	*0.407*
Plantarflexor moment	Nm/kg	1.64 ± 0.11	1.62 ± 0.10	*t*(9) = 4.577	0.001	*0.065*
				Stair Ascent (n = 8)		
				Gait Cycle 1		
Clearance Intervals during swing phase						
Interval 1: MTC (Mean - SD)	Degrees	12.35 ± 4.77	12.20 ± 4.77	*t*(7) = 2.825	0.026	*0.125*
Interval 1: MTC (Mean)	Degrees	13.70 ± 4.35	13.55 ± 4.45	*t*(7) = 1.408	0.202	*0.450* [b]
Interval 1: MTC (Mean - SD)	Degrees	14.37 ± 4.12	14.33 ± 3.97	*t*(7) = 0.348	0.738	*0.803* [b]
Interval 2: MFC (Mean + SD)	Degrees	13.70 ± 4.35	13.55 ± 4.45	*t*(7) = 1.408	0.202	*0.450* [b]
Interval 2: MFC (Mean)	Degrees	14.37 ± 4.12	14.33 ± 3.97	t(7) = 0.348	0.738	*0.803* [b]
Interval 2: MFC (Mean + SD)	Degrees	14.15 ± 4.18	14.02 ± 4.24	*t*(7) = 1.247	0.252	*0.471*
Stance Phase Critical Points						
Flexion at Toe Off	Degrees	6.17 ± 2.77	6.37 ± 2.58	Sign Test	0.727	*0.803*
Dorsiflexion	Degrees			d		
Plantarflexion	Degrees			d		
Plantarflexor moment	Nm/kg	1.58 ± 0.11	1.58 ± 0.12	*t*(7) = 0.616	0.557	*0.759*
				Stair Descent (n = 8)		
				Gait Cycle 1		
Clearance Intervals during swing phase						
Interval 1: MTC (Mean - SD)	Degrees	9.03 ± 5.05	9.09 ± 4.97	*t*(7) = -0.812	0.444	*0.639*
Interval 1: MTC (Mean)	Degrees	6.82 ± 4.79	7.04 ± 4.79	*t*(7) = -3.574	0.009	*0.065*
Interval 1: MTC (Mean - SD)	Degrees	2.89 ± 4.89	3.26 ± 5.06	*t*(7) = -4.502	0.003	*0.065*
Interval 2: MFC (Mean + SD)	Degrees	-4.99 ± 5.91	-4.54 ± 6.05	*t*(7) = -3.391	0.012	*0.068*
Interval 2: MFC (Mean)	Degrees	-8.53 ± 6.17	-8.13 ± 6.23	*t*(7) = -3.706	0.008	*0.065*
Interval 2: MFC (Mean + SD)	Degrees	-10.96 ± 6.28	-10.61 ± 6.39	*t*(7) = -3.339	0.012	*0.068*
Stance Phase Critical Points						
Flexion at Toe Off	Degrees	19.89 ± 4.47	19.94 ± 4.45	*t*(7) = -0.506	0.629	*0.786*
Dorsiflexion	Degrees			d		
Plantarflexion	Degrees			d		
Plantarflexor moment	Nm/kg	1.24 ± 0.21	1.24 ± 0.21	*t*(7) = -0.550	0.600	*0.773*

Supplementary Table A.1. cont.

Critical Performance Points	Units	Mean ± SD		*t* (df)	*p* value	B-H *p* value
		Target	Prediction			
				Stair Ascent (n = 8) Gait Cycle 2		
Clearance Intervals during swing phase						
Interval 1: MTC (Mean - SD)	Degrees	11.57 ± 6.19	11.60 ± 6.25	*t*(7) = -0.301	0.772	*0.823* [b]
Interval 1: MTC (Mean)	Degrees	13.22 ± 5.78	13.34 ± 5.82	*t*(7) = -1.349	0.219	*0.455* [b]
Interval 1: MTC (Mean - SD)	Degrees	14.73 ± 5.29	14.78 ± 5.39	Sign Test	0.727	*0.803* [b]
Interval 2: MFC (Mean + SD)	Degrees	-8.61 ± 5.69	-8.84 ± 5.56	*t*(7) = 2.231	0.061	*0.213*
Interval 2: MFC (Mean)	Degrees	-15.03 ± 4.70	-15.75 ± 4.52	*t*(7) = 3.551	0.009	*0.065*
Interval 2: MFC (Mean + SD)	Degrees	-9.83 ± 5.81	-9.91 ± 5.76	*t*(7) = 0.413	0.692	*0.803*
Stance Phase Critical Points						
Flexion at Toe Off	Degrees	-6.95 ± 5.64	-7.12 ± 5.43	*t*(7) = 1.683	0.136	*0.393* [c]
Dorsiflexion	Degrees	16.10 ± 3.00	16.04 ± 3.00	*t*(7) = 1.078	0.317	*0.555*
Plantarflexion	Degrees	-6.95 ± 5.64	-7.12 ± 5.43	*t*(7) = 1.683	0.136	*0.393* [c]
Plantarflexor moment	Nm/kg	1.59 ± 0.20	1.59 ± 0.21	*t*(7) = -0.674	0.522	*0.730*
				Stair Descent (n = 8) Gait Cycle 2		
Clearance Intervals during swing phase						
Interval 1: MTC (Mean - SD)	Degrees	10.37 ± 4.29	10.20 ± 4.44	*t*(7) = 2.090	0.075	*0.245*
Interval 1: MTC (Mean)	Degrees	9.29 ± 3.98	9.20 ± 4.07	*t*(7) = 0.935	0.381	*0.600*
Interval 1: MTC (Mean - SD)	Degrees	7.45 ± 3.64	7.44 ± 3.66	*t*(7) = 0.162	0.876	*0.894*
Interval 2: MFC (Mean + SD)	Degrees	5.26 ± 3.75	5.33 ± 3.73	*t*(7) = -0.487	0.641	*0.786*
Interval 2: MFC (Mean)	Degrees	2.15 ± 4.46	2.33 ± 4.41	*t*(7) = -1.308	0.232	*0.455*
Interval 2: MFC (Mean + SD)	Degrees	-2.06 ± 5.65	-1.75 ± 5.64	*t*(7) = -1.834	0.109	*0.335*
Stance Phase Critical Points						
Flexion at Toe Off	Degrees	21.14 ± 3.83	21.25 ± 3.88	*t*(7) = -1.606	0.152	*0.407*
Dorsiflexion	Degrees	32.94 ± 4.05	32.79 ± 4.10	*t*(7) = 2.644	0.033	*0.148*
Plantarflexion	Degrees	-23.01 ± 1.88	-22.82 ± 1.77	*t*(7) = -2.487	0.042	*0.170*
Plantarflexor moment	Nm/kg	1.20 ± 0.23	1.22 ± 0.22	*t*(7) = -4.035	0.005	*0.065*

MTC, Minimum Toe Clearance; MFC, Minimum Foot Clearance; SD, Standard Deviation; df. Degrees of Freedom

[a] No MTC or MFC was reported for an equivalent step in literature reference

[b] Overlapped MTC and MFC intervals

[c] Point overlaps with another critical point

[d] Only stair step analyzed

Supplementary Table A.1. cont.

Critical Performance Points	Units	Mean ± SD		*t* (df)	*p* value	B-H *p* value
		Target	Prediction			
		Stair Ascent (n = 8) Gait Cycle 3				
Clearance Intervals during swing phase						
Interval 1: MTC (Mean - SD)	Degrees			a		
Interval 1: MTC (Mean)	Degrees			a		
Interval 1: MTC (Mean - SD)	Degrees			a		
Interval 2: MFC (Mean + SD)	Degrees	-7.98 ± 5.01	-8.05 ± 4.85	$t(7) = 0.584$	0.578	*0.765* [c]
Interval 2: MFC (Mean)	Degrees	-15.06 ± 4.56	-14.90 ± 4.41	$t(7) = -0.902$	0.397	*0.600*
Interval 2: MFC (Mean + SD)	Degrees	-14.98 ± 5.27	-14.85 ± 5.43	$t(7) = -0.887$	0.404	*0.600*
Stance Phase Critical Points						
Flexion at Toe Off	Degrees	-7.98 ± 5.01	-8.05 ± 4.85	$t(7) = 0.584$	0.578	*0.765* [c]
Dorsiflexion	Degrees			d		
Plantarflexion	Degrees			d		
Plantarflexor moment	Nm/kg	1.55 ± 0.21	1.55 ± 0.20	$t(7) = -0.975$	0.362	*0.591*
		Stair Descent (n = 8) Gait Cycle 3				
Clearance Intervals during swing phase						
Interval 1: MTC (Mean - SD)	Degrees			a		
Interval 1: MTC (Mean)	Degrees			a		
Interval 1: MTC (Mean - SD)	Degrees			a		
Interval 2: MFC (Mean + SD)	Degrees			a		
Interval 2: MFC (Mean)	Degrees			a		
Interval 2: MFC (Mean + SD)	Degrees			a		
Stance Phase Critical Points						
Flexion at Toe Off	Degrees	-1.37 ± 4.22	-1.05 ± 4.23	$t(7) = -3.722$	0.007	*0.065*
Dorsiflexion	Degrees			d		
Plantarflexion	Degrees			d		
Plantarflexor moment	Nm/kg	1.71 ± 0.17	1.70 ± 0.18	$t(7) = 0.382$	0.714	*0.803*

MTC, Minimum Toe Clearance; MFC, Minimum Foot Clearance; SD, Standard Deviation; df. Degrees of Freedom
[a] No MTC or MFC was reported for an equivalent step in literature reference
[b] Overlapped MTC and MFC intervals
[c] Point overlaps with another critical point
[d] Only stair step analyzed

APPENDIX B: SUPPLEMENTARY MATERIAL FOR CHAPTER 3

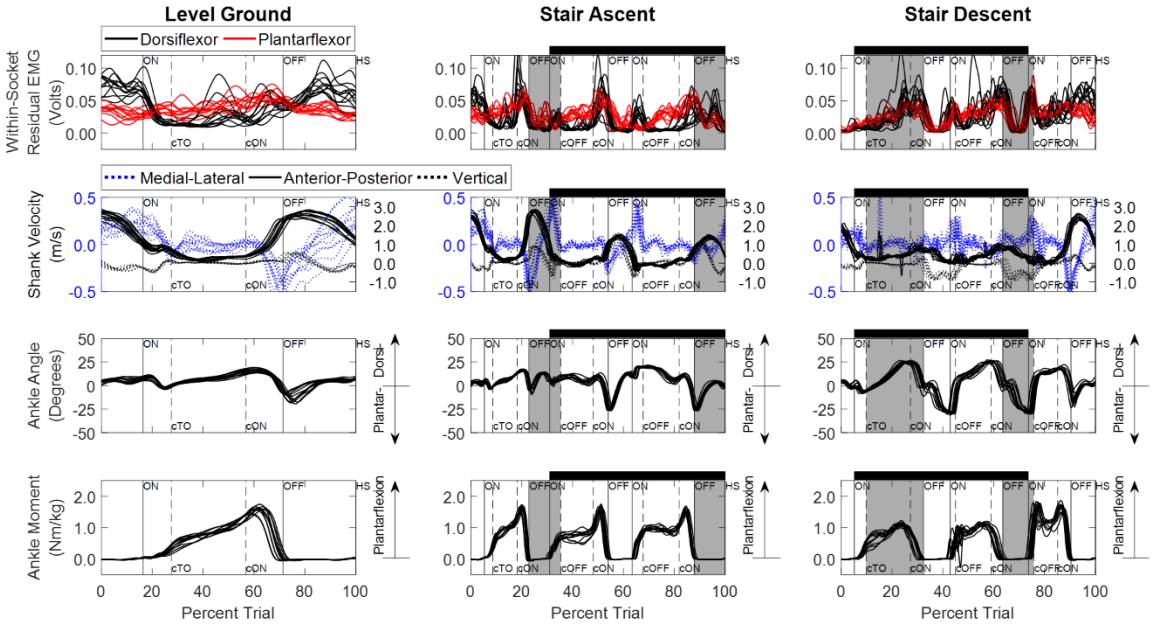

Supplementary Figure B.1. Aligned experimentally measured training and testing trials for TTA1. Shank linear velocities, ankle angle, and ankle moment of the sound limb, and the linear envelope of within-socket residual EMG (ankle dorsiflexor and plantarflexor) are shown. Shading and line markers are defined the same as in **Figure 3.3**.

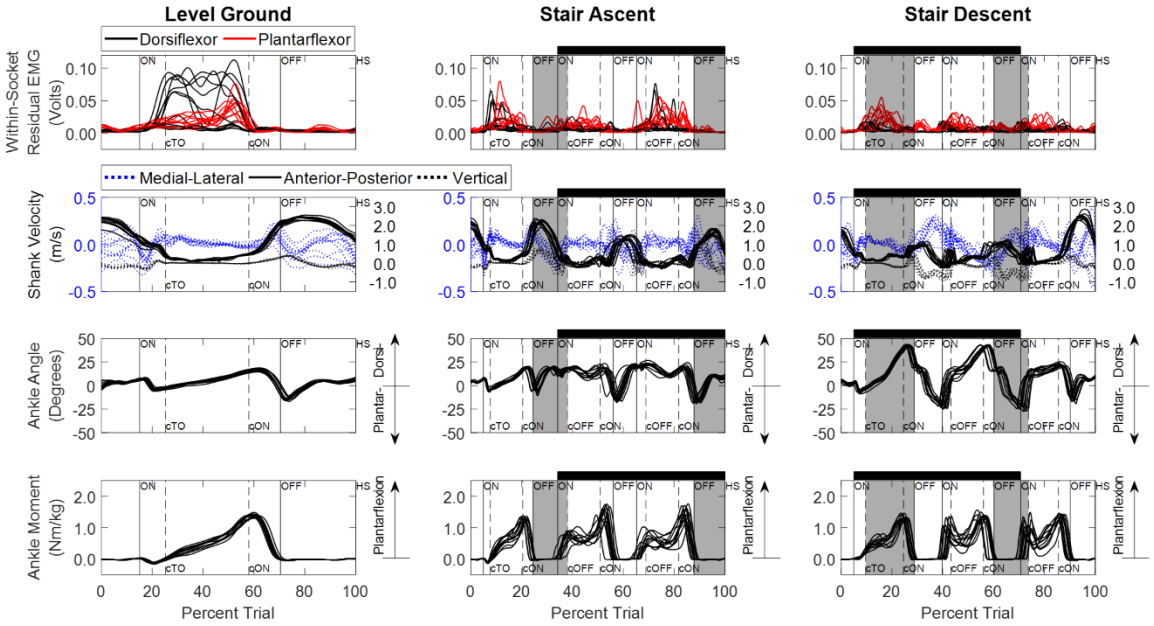

Supplementary Figure B.2. Aligned experimentally measured training and testing trials for TTA2. Shank linear velocities, ankle angle, and ankle moment of the sound limb, and the linear envelope of within-socket residual EMG (ankle dorsiflexor and plantarflexor) are shown. Shading and line markers are defined the same as in **Figure 3.3**.

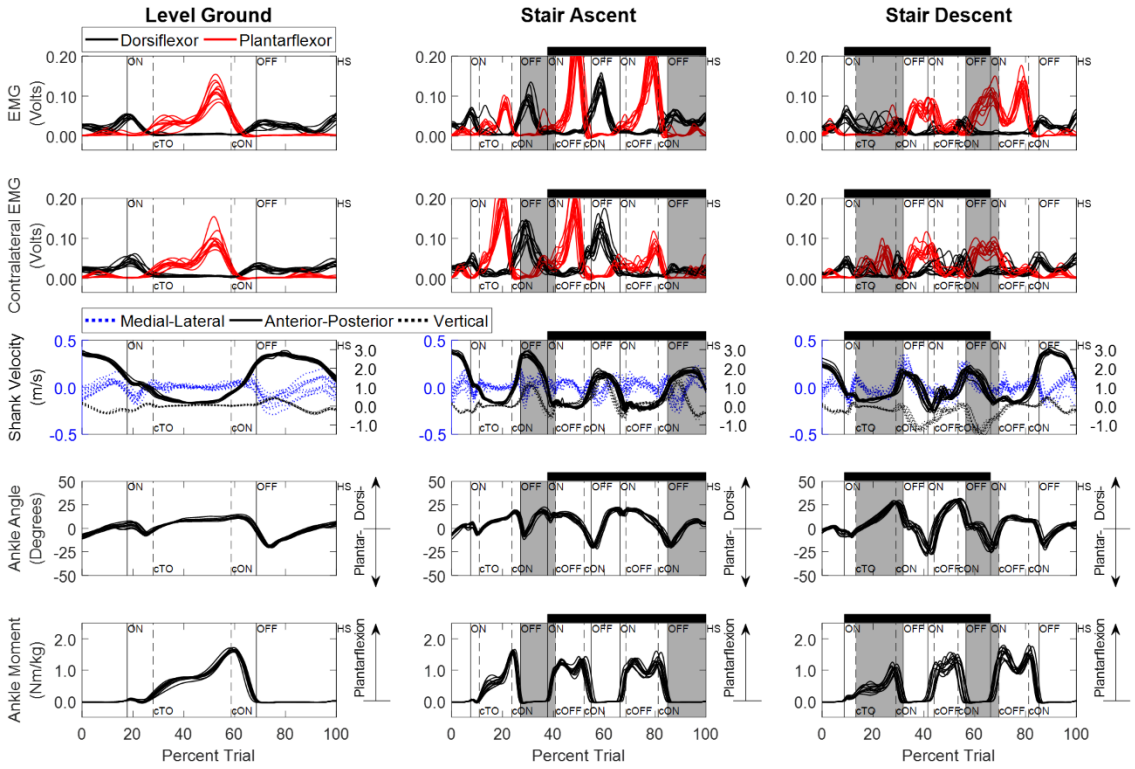

Supplementary Figure B.3. Experimentally measured training and testing trials for a typical able-bodied participant (AB3). EMG linear envelopes, shank linear velocities, ankle angle, and ankle moment of the limb used to train the model, and aligned contralateral EMG signals are shown. Shading and line markers are defined the same as in **Figure 3.3** except the following elements. Vertical lines denote gait events of the limb used to train the model as solid lines and the contralateral limb as dashed lines. Staircase ambulation is based on the limb used during training.

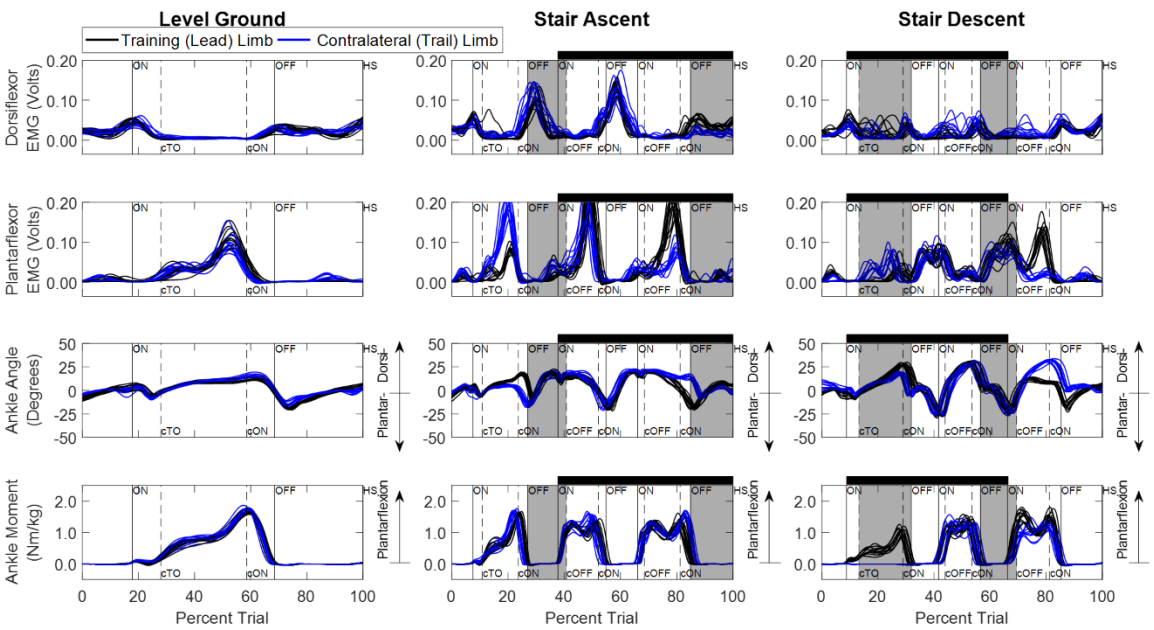

Supplementary Figure B.4. Comparison of experimentally measured EMG profiles and ankle dynamics of the consecutively aligned gait cycles of a typical able-bodied participant (AB3). Large discrepancies are present during gait cycle 1 and 3 of stair ambulation. Force plate data of the contralateral limb during gait cycle 1 of stair descent is not available; however, analysis was unaffected because ankle dynamics of the contralateral limb (blue traces) were not used during training. Shading and line markers are defined the same as in **Figure 3.3** and **Supplementary Figure B.3**.

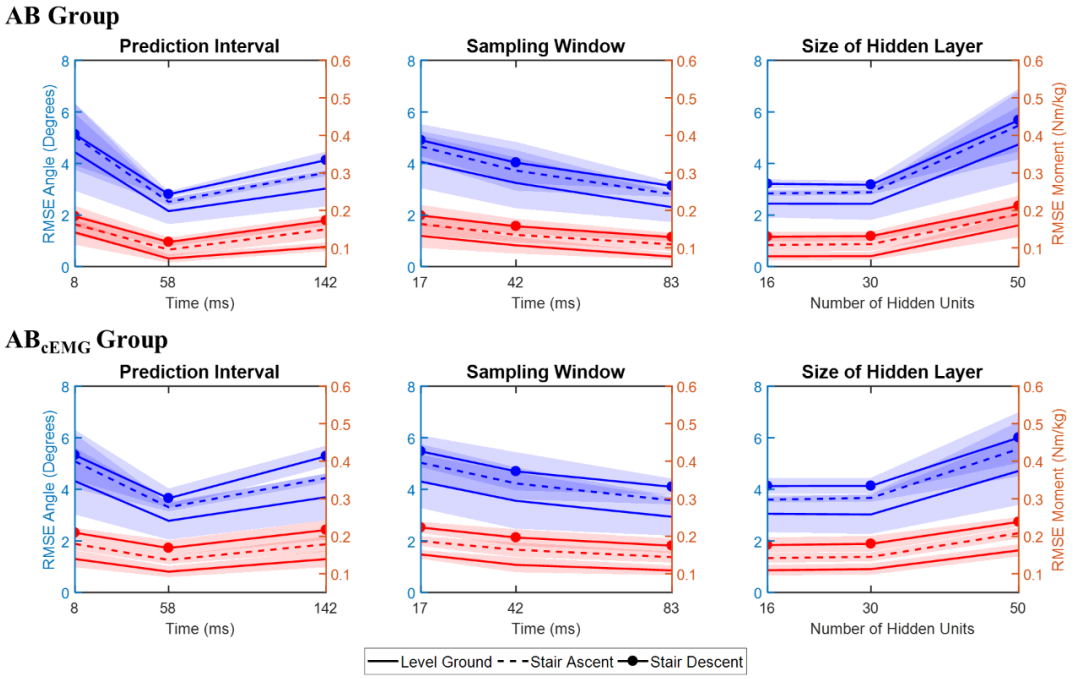

Supplementary Figure B.5. Parameter space error of the closed-loop NARX model for able-bodied participants. RMSE, averaged across participants (AB and AB_{cEMG} groups), is collapsed across model parameters (i.e., averaged across two of the three dimensions). Shaded regions denote ±1 standard deviation.

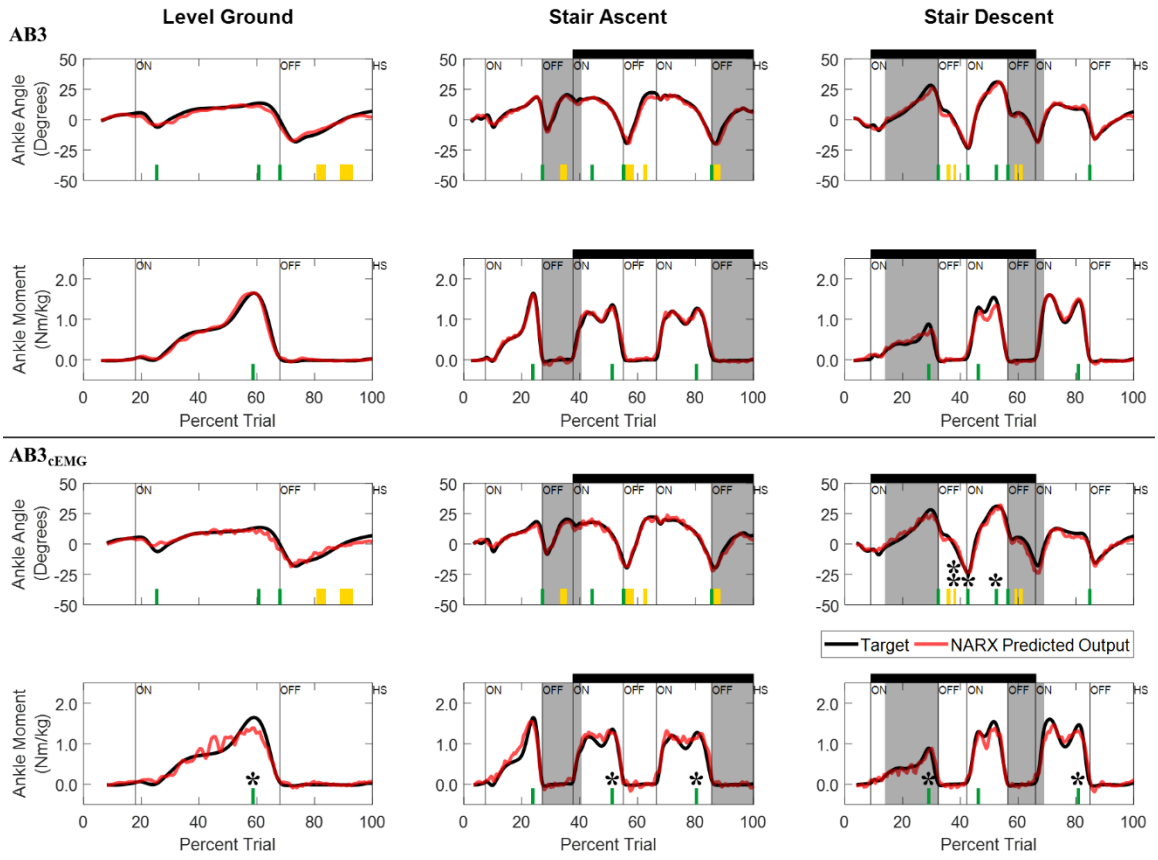

Supplementary Figure B.6. Time series of closed-loop NARX model prediction of normal ranges of ankle angle and moment for a typical able-bodied participant trained with same-limb data (AB3 - τ: 58 ms, D: 17 ms, N: 16) and trained with aligned contralateral EMG as the EMG input ($AB3_{cEMG}$ - τ: 58 ms, D: 42 ms, N: 16). NARX model predictions of AB and AB_{cEMG} models are shown for the k-fold novel test trials of the AB model with the best accuracy across ambulation conditions and model outputs. Critical performance points (CPs), used to test for within-subject significant differences (B-H adjusted $p < 0.05$) between the model prediction and experimentally measured targets, are denoted by yellow blocks (clearance intervals) and green lines (stance points). Each asterisk (*) represent a critical point with significant differences in more than 50% of AB_{cEMG} participants. For models trained with same-limb data, no significant differences were observed at critical points in more than 50% of able-bodied participants (AB). Shading and line markers are defined the same as in **Figure 3.3** and **Supplementary Figure B.3**.

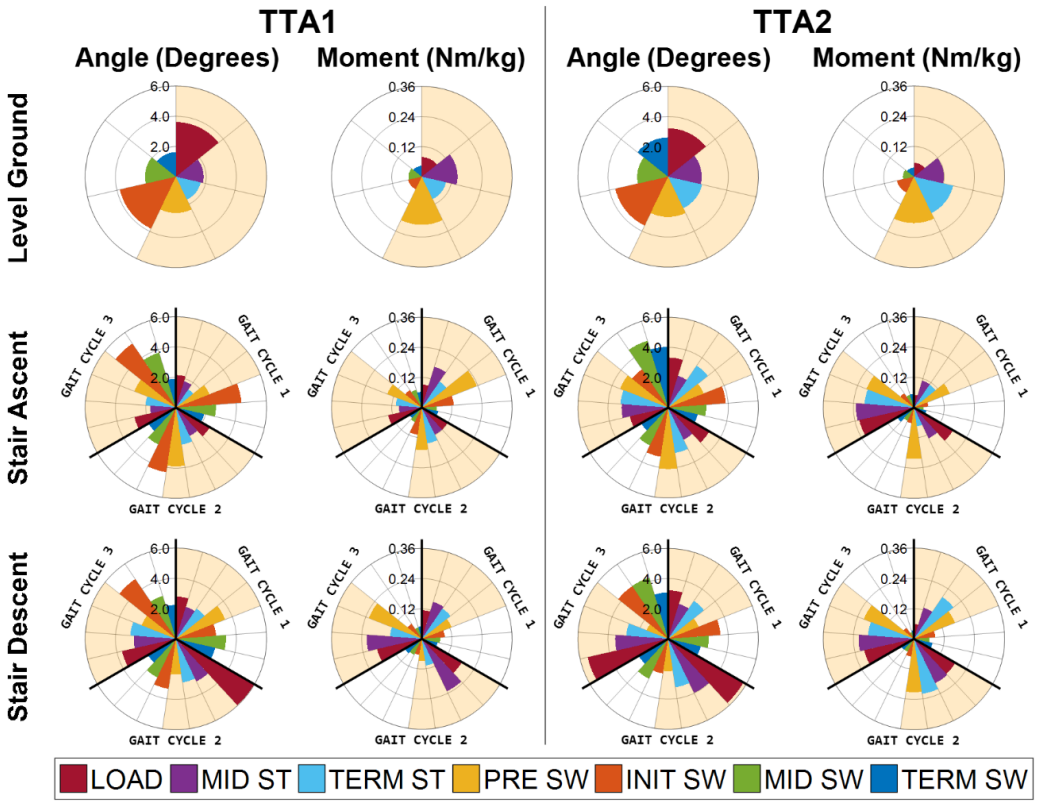

Supplementary Figure B.7. RMSE distribution within ambulation conditions for TTA1 and TTA2 for the continuous prediction of ankle angle and moment. Gait periods and stance and swing phases are defined the same as in **Figure 3.6**.

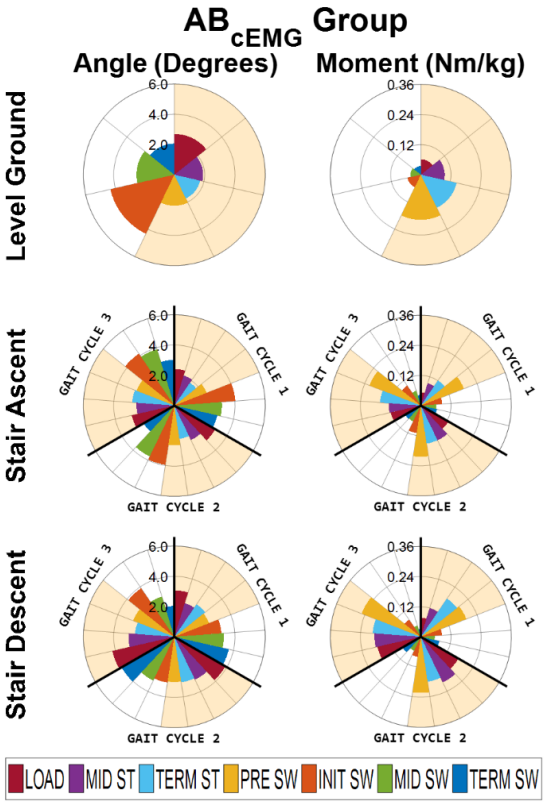

Supplementary Figure B.8. RMSE distribution within ambulation conditions for the able-bodied group trained with aligned contralateral EMG (AB_{cEMG} group) for the continuous prediction of ankle angle and moment. Gait periods and stance and swing phases are defined the same as in **Figure 3.6**.

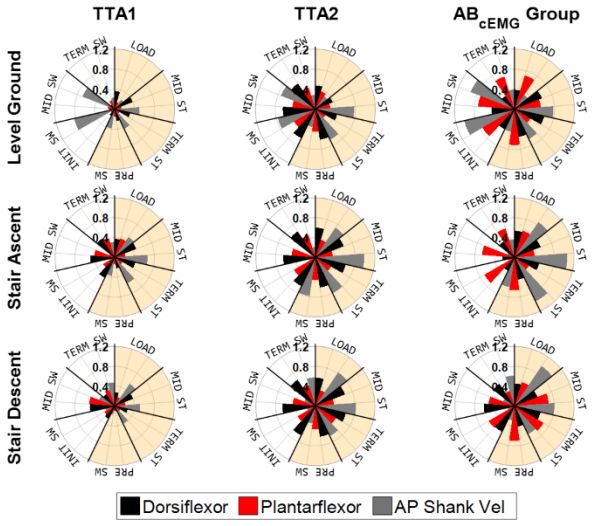

Supplementary Figure B.9. Sum of weighted inputs (SWI) distribution for TTA1, TTA2, and the able-bodied group trained with aligned contralateral EMG (AB_{cEMG} group) of EMG and anterior-posterior shank velocity inputs within the gait cycle for level ground walking and the second gait cycle of stair ascent and stair descent. Because the network bias (offset) was not included in the SWI calculation, SWI absolute values can vary across participants without affecting the relative contribution among inputs. Gait periods, stance and swing phases, and labels are defined the same as in **Figures 3.6** and **3.7**.

Supplementary Table B.1. Characteristics of transtibial amputees and able-bodied participants.

Group	Sex	Age (years)	Mass (kg)	Height (m)	Time since Amputation (years)	Affected Side	Cause of Amputation	Prosthetic Foot	Level of Activity
Transtibial Amputees									
TTA1	M	57	120.2	1.85	8.2	R	Trauma	Ossur Pro-Flex®	K4, golfing, construction worker
TTA2	M	56	69.3	1.70	9.5	L	Trauma	RUSH LoPro	K3
TTA3	M	46	83.3	1.80	17	L	Trauma	Ohio Willow Wood Fusion™	K4, triathlete, mountain climbing
Mean (SD)		52.9 (6.2)	90.9 (26.3)	1.78 (0.08)	11.6 (4.8)				
Able-Bodied Participants									
AB1	M	22	81.7	1.85	-	-	-	-	-
AB2	M	21	72.4	1.87	-	-	-	-	-
AB3	F	24	55.7	1.68	-	-	-	-	-
AB4	M	21	70.6	1.75	-	-	-	-	-
AB5	F	19	62.1	1.61	-	-	-	-	-
AB6	F	23	71.5	1.83	-	-	-	-	-
Mean (SD)		21.7 (1.8)	69.0 (9.0)	1.77 (0.10)					

Supplementary Table B.2. Statistical scores for CHAPTER 3. Significant differences between targets and model predictions were assessed using a paired-samples t-test (normally distributed samples) and sign test (non-normally and asymmetric distributed samples). For each participant, *p* values of all critical points (49 total points) were adjusted for multiple comparisons using the Benjamini-Hochberg (B-H) procedure with a false discovery rate of 0.05. Numbers indicate the first critical point that crossed the significance threshold.

Participant	*t* (df = 9)	*p* value	B-H *p* value
TTA1	3.405	0.008	0.048
TTA2	3.646	0.005	0.024
TTA3	3.859	0.004	0.031
AB1$_{cEMG}$	3.520	0.007	0.032
AB2$_{cEMG}$	3.995	0.003	0.038
AB3$_{cEMG}$	4.170	0.002	0.039
AB4$_{cEMG}$	4.008	0.003	0.030
AB5$_{cEMG}$	-3.702	0.005	0.040
AB6$_{cEMG}$	3.062	0.014	0.039
AB1	4.831	0.001	0.046
AB2	4.211	0.002	0.037
AB3	5.590	0.000	0.008
AB4	4.858	0.001	0.022
AB5	ns	ns	ns
AB6	-5.367	0.000	0.022

ns: no significant differences were found
df: degrees of freedom

APPENDIX C: SUPPLEMENTARY MATERIAL FOR CHAPTER 4

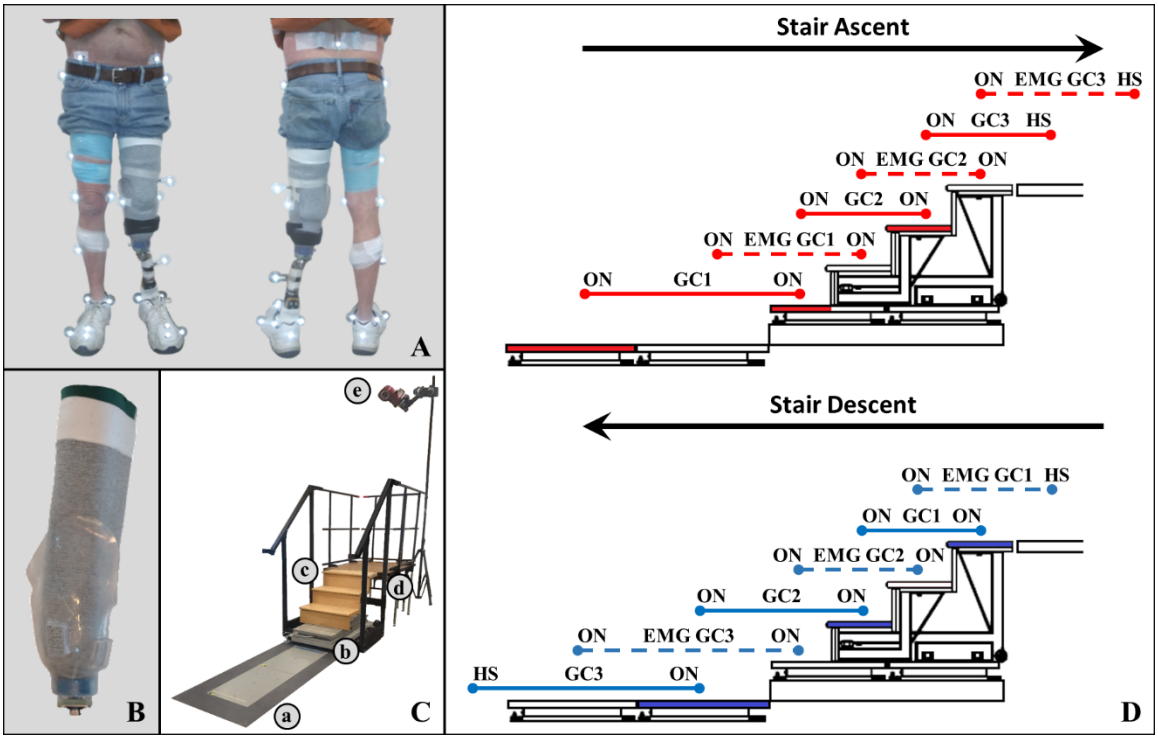

Supplementary Figure C.1. Electrode-socket integration and instrumented walkway. **(A)** EMG electrode placement and modified Helen Hayes infrared lower limb marker set on a transtibial amputee. **(B)** Individualized duplicated electrode-housing test socket and prosthetic shrinker used during amputee testing. **(C)** Instrumented walkway including (a) embedded floor force plates, (b) stair force plates, (c) staircase, (d) landing platform, and (e) infrared motion cameras. **(D)** Schematic of step-over-step stair ambulation gait cycles (GC; red, stair ascent; blue, stair descent) used in the contralateral gait-cycle alignment. Dashed lines denote consecutive gait cycles of the prosthetic limb (trail limb) whose residual upper-leg and lower-leg EMG was aligned with the target kinematic/kinetic gait cycles. Gait cycles of the sound limb (lead limb) whose kinematics (ankle angle, shank velocities) and kinetics (ankle moment) were used as the target movement during training are shown as solid lines.

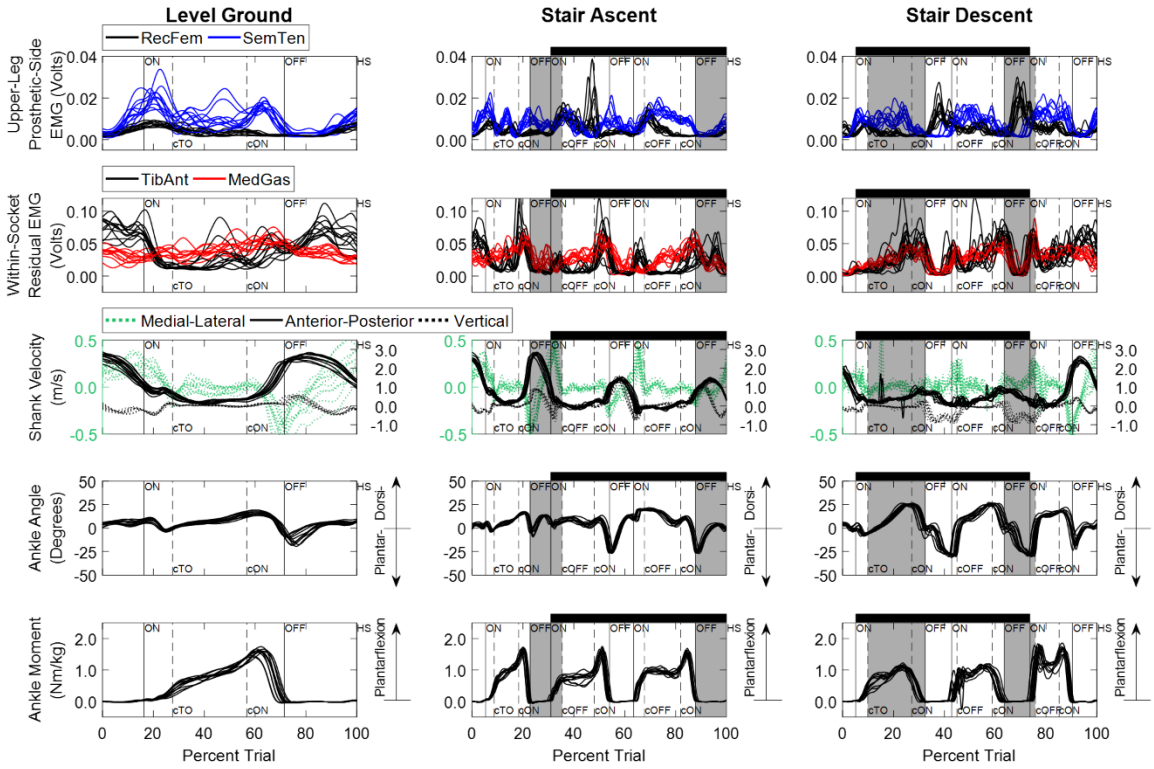

Supplementary Figure C.2. Aligned experimentally measured input and output trials used to train and test upper-leg and lower-leg NARX models of TTA1. Inputs consists of shank linear velocities of the sound limb (medial-lateral, anterior-posterior, vertical) and EMG linear envelope of the prosthetic-side thigh (rectus femoris and semitendinosus) for upper-leg NARX models, and instead, within-socket residual EMG (tibialis anterior and gastrocnemius medialis) for lower-leg NARX models. Ankle angle and moment of the sound limb (sagittal plane) are the outputs of both model types. Shading and line markers are defined the same as in **Figure 4.2**.

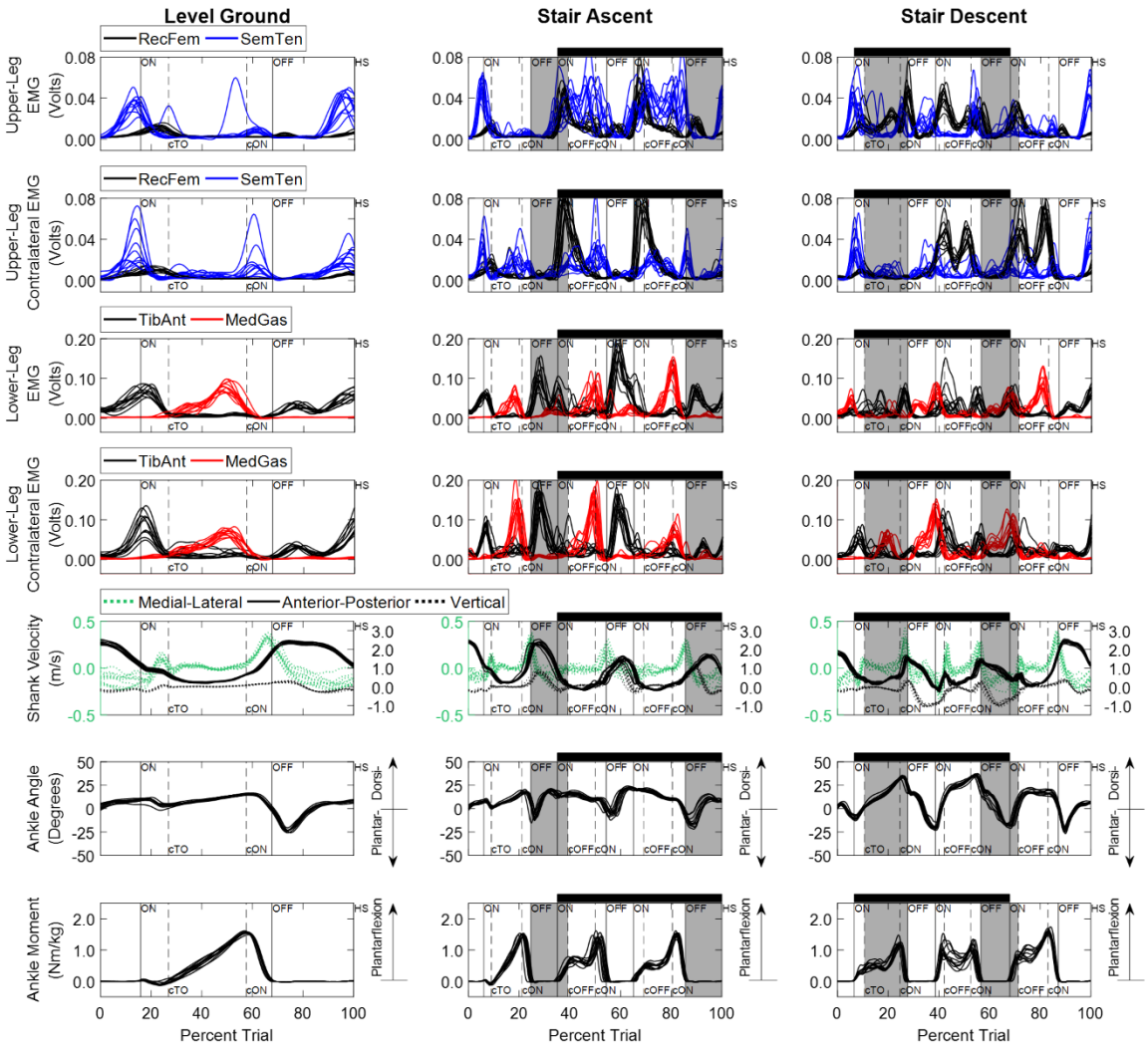

Supplementary Figure C.3. Experimentally measured training and testing trials used in upper-leg and lower-leg models of a representative able-bodied participant (AB4). Upper-leg and lower-leg EMG linear envelopes, shank linear velocities, ankle angle, and ankle moment of the lead limb (i.e., limb used to train the models), and aligned contralateral EMG signals are shown. Differences in EMG shapes can be observed when comparing signals to their aligned contralateral EMG (e.g., rectus femoris during the first gait cycle of stair descent). These differences are the effects of the contralateral gait-cycle alignment. Shading and line markers are defined the same as in **Figure 4.2** except the following elements. Vertical lines denote gait events of the limb used to train the model as solid lines and the contralateral limb as dashed lines. Staircase ambulation is based on the limb used during training.

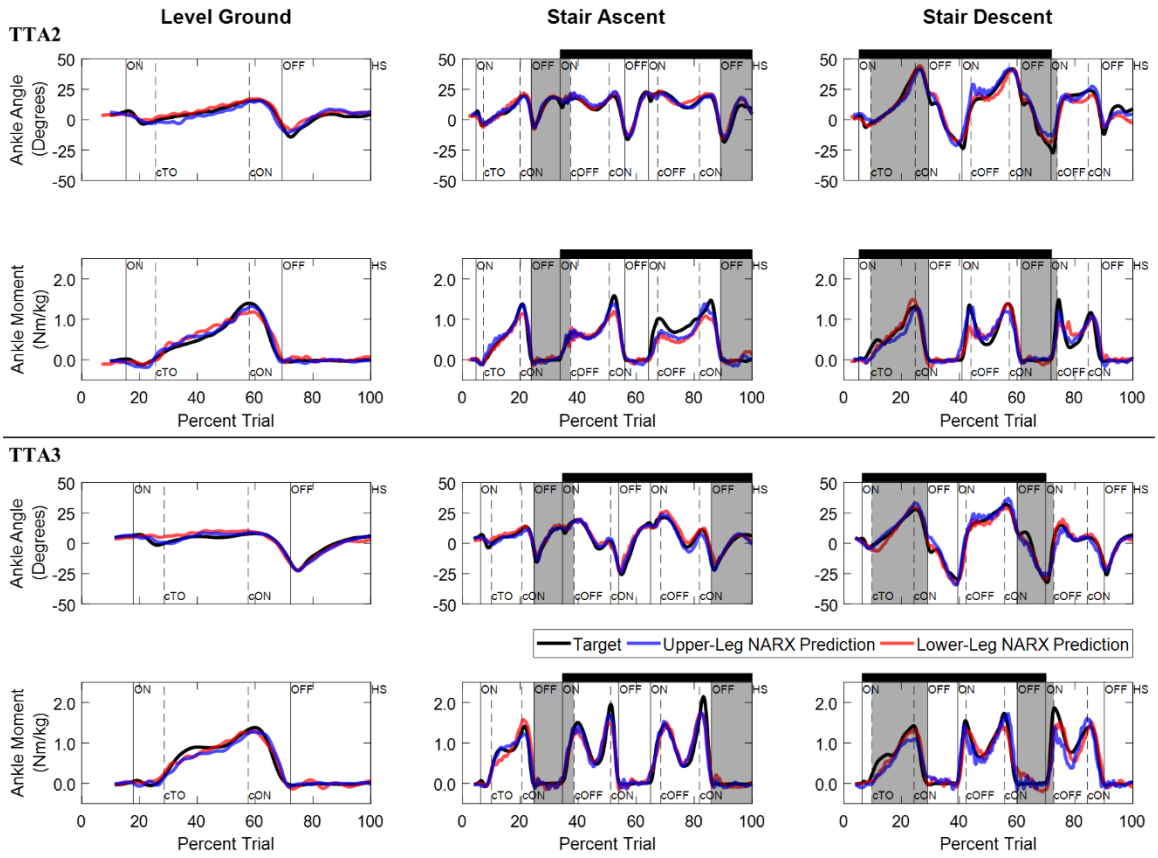

Supplementary Figure C.4. Comparison of upper-leg and lower-leg NARX model predictions for the remaining transtibial amputees. Model predictions and experimentally measured targets of TTA2 (τ: 58 ms, UL - D: 83 ms, N: 16; LL - D: 42 ms, N: 30) and TTA3 (τ: 58 ms, D: 83 ms, UL - N: 30; LL - N: 50) are displayed. Model predictions are shown for the k-fold novel test trials with an average performance (mid-point performance) across ambulation conditions, model outputs (angle, moment) and model types (upper-leg and lower-leg). Shading and line markers are defined the same as in **Figure 4.2**.

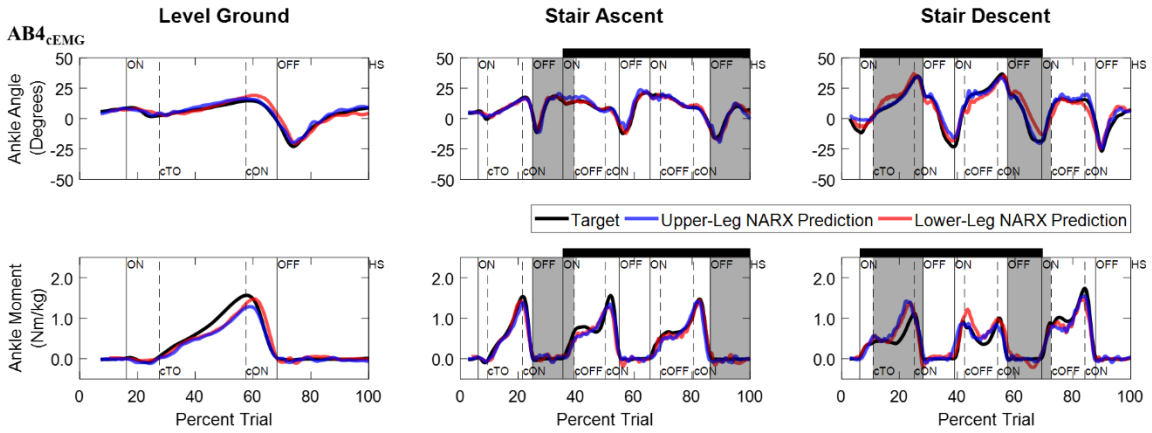

Supplementary Figure C.5. Comparison of upper-leg and lower-leg NARX model predictions for a representative able-bodied participant trained with aligned contralateral EMG ($AB4_{cEMG}$, τ: 58 ms, N: 30, UL - D: 42 ms; LL - D: 83 ms). Model predictions and experimentally measured targets are shown for the same k-fold novel test trials as AB4 in **Figure 4.2**. Shading and line markers are defined the same as in **Figure 4.2** and **Supplementary Figure C.3**.

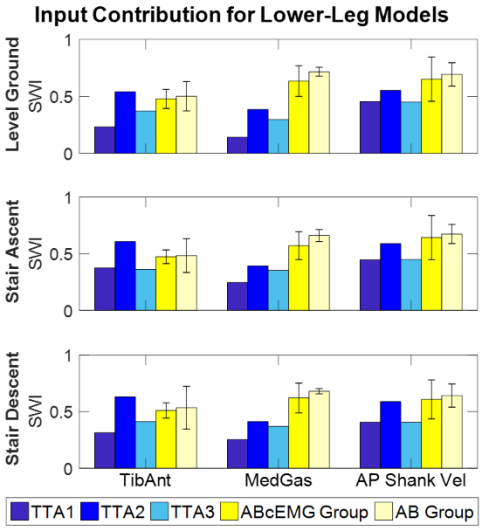

Supplementary Figure C.6. Sum of weighted inputs (SWI) for selected lower-leg exogenous inputs averaged over time. Error bars represents ±1 standard deviation of averaged able-bodied participants. TibAnt: tibialis anterior, MedGas: gastrocnemius medialis, AP: anterior-posterior, Vel: velocity.

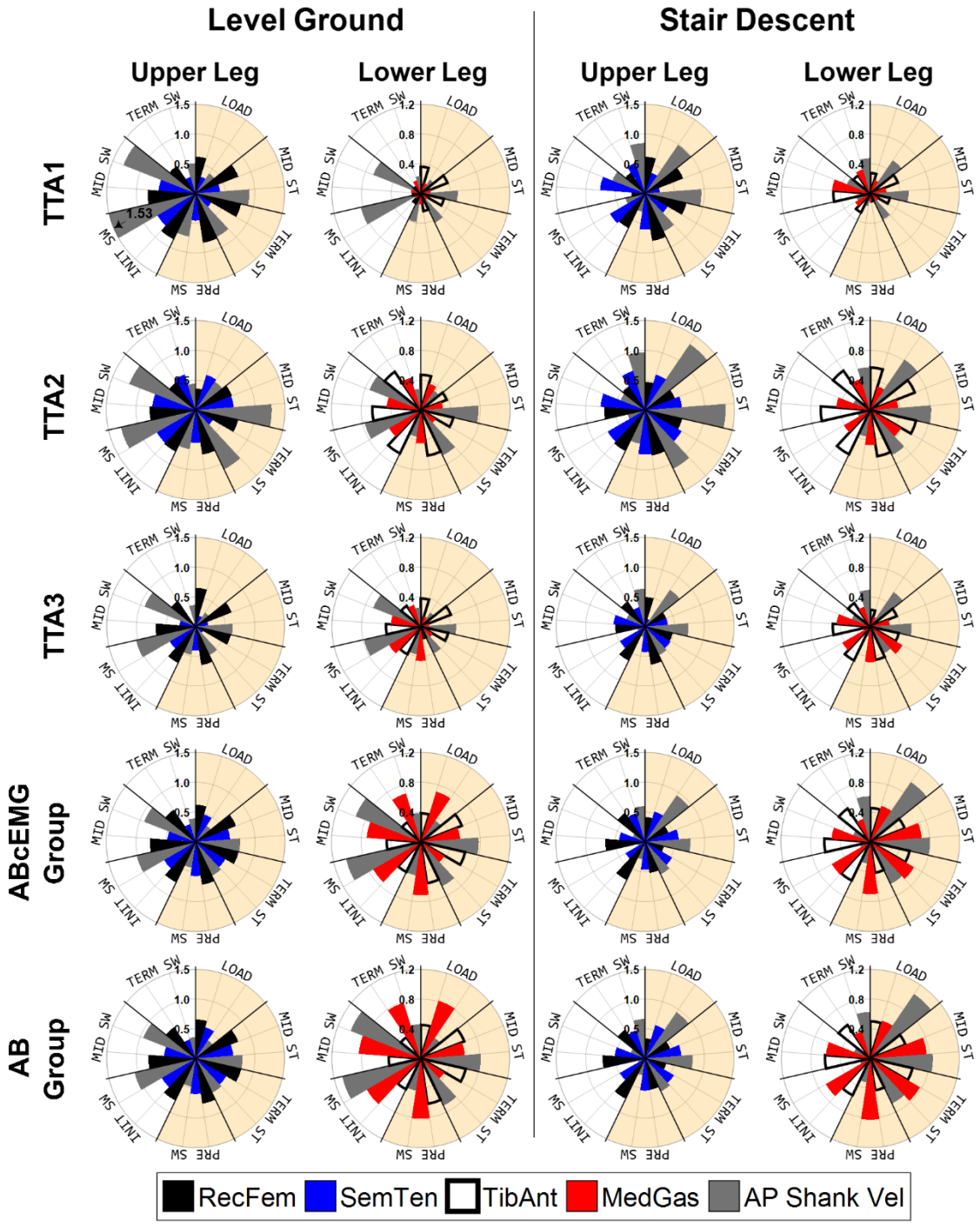

Supplementary Figure C.7. Comparison of sum of weighted inputs (SWI) distribution within the gait cycle between upper-leg and lower-leg NARX models for level ground walking and second gait cycle of stair descent. Gait periods, stance and swing phases, and labels are defined the same as in **Figure 4.5**.

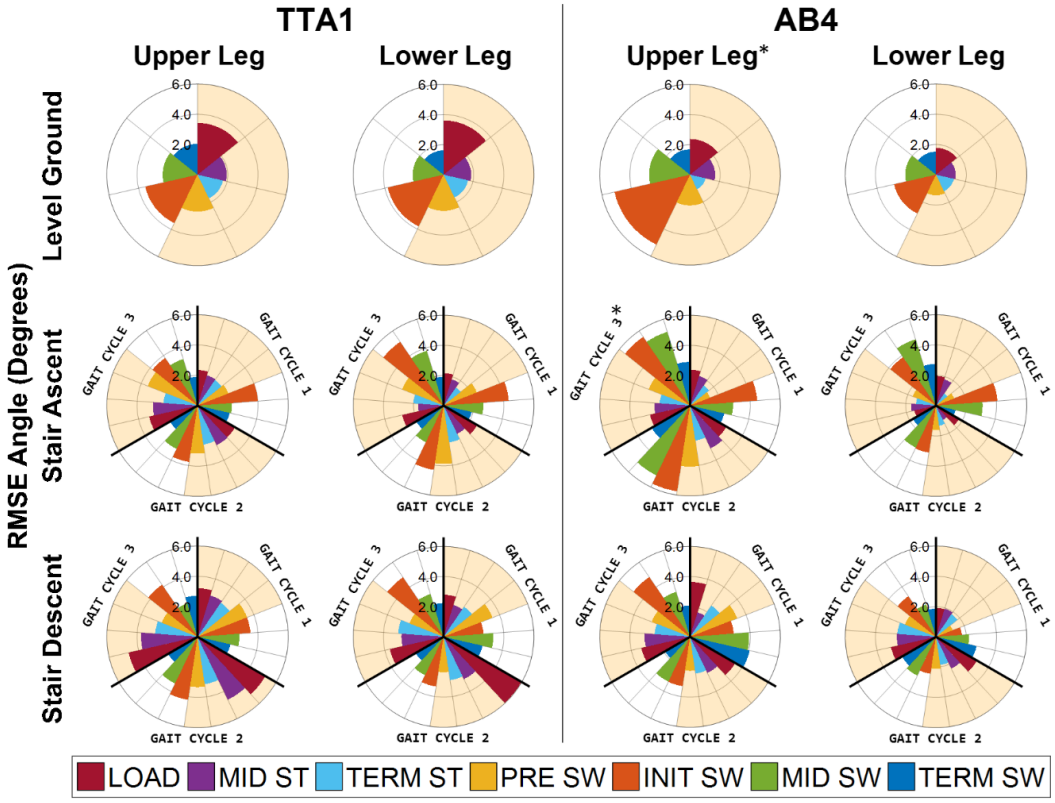

Supplementary Figure C.8. RMSE distribution within ambulation conditions of upper-leg and lower-leg NARX models for TTA1 and a representative able-bodied participant (AB4) for the continuous prediction of ankle angle. Asterisks (*) indicate within-subject significant (ANOVA, $p < 0.05$) main effect for muscle group (upper leg versus lower leg) and significant interaction between muscle group and ambulation-condition gait cycle (Tukey's for multiple comparisons, $p < 0.05$) that are present in the displayed participant and in more than 50% of the able-bodied participants (AB). Gait periods and stance and swing phases are defined the same as in **Figure 4.5**.

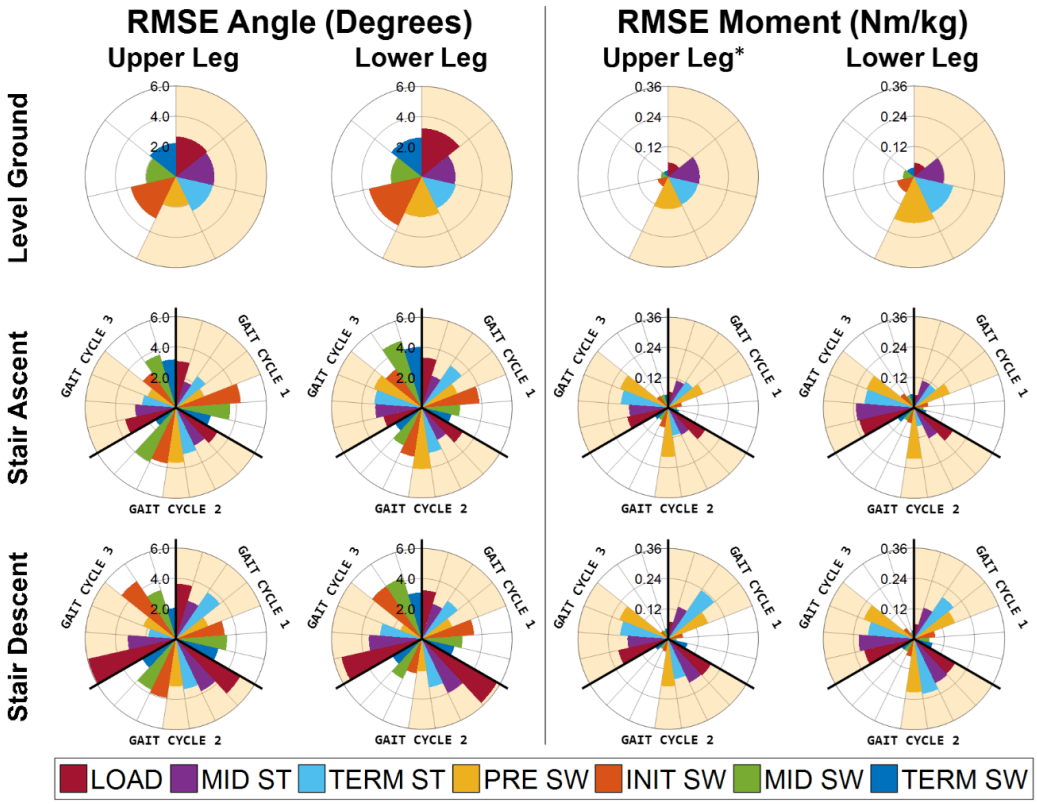

Supplementary Figure C.9. RMSE distribution within ambulation conditions of upper-leg and lower-leg NARX models for TTA2 for the continuous prediction of ankle angle and moment. Asterisk (*) indicate significantly lower moment error when using upper-leg muscle activity as inputs (ANOVA, $p < 0.05$). Gait periods and stance and swing phases are defined the same as in **Figure 4.5**.

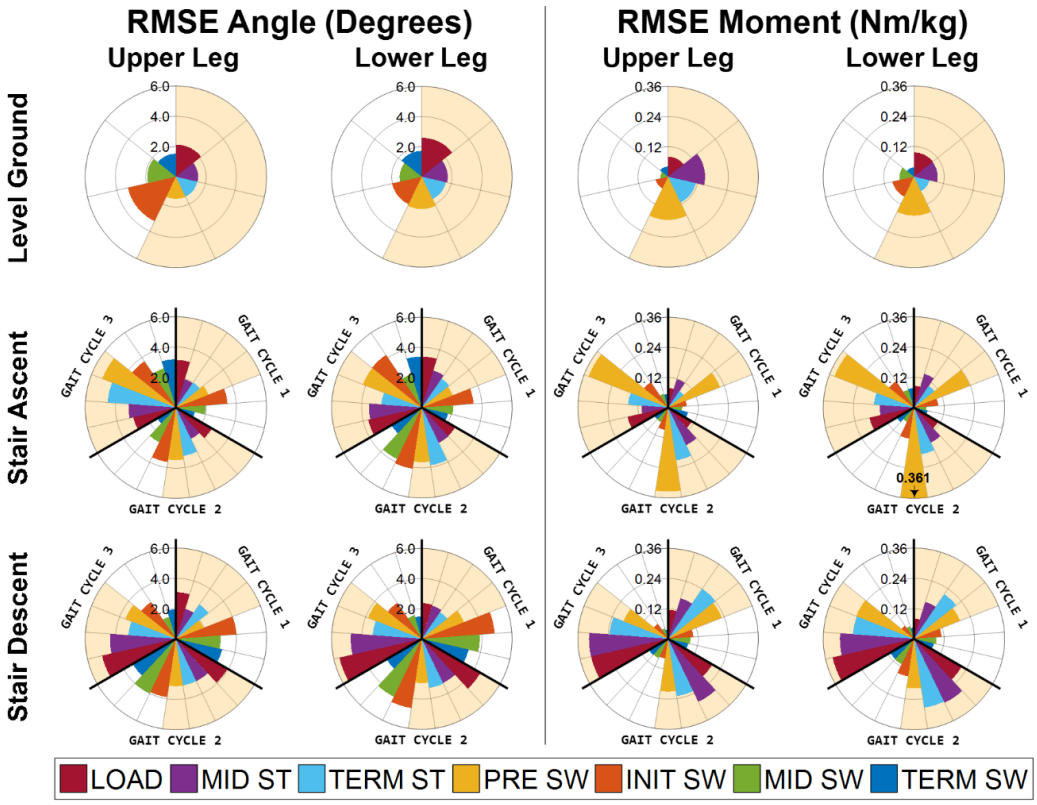

Supplementary Figure C.10. RMSE distribution within ambulation conditions of upper-leg and lower-leg NARX models for TTA3 for the continuous prediction of ankle angle and moment. Gait periods and stance and swing phases are defined the same as in **Figure 4.5**.

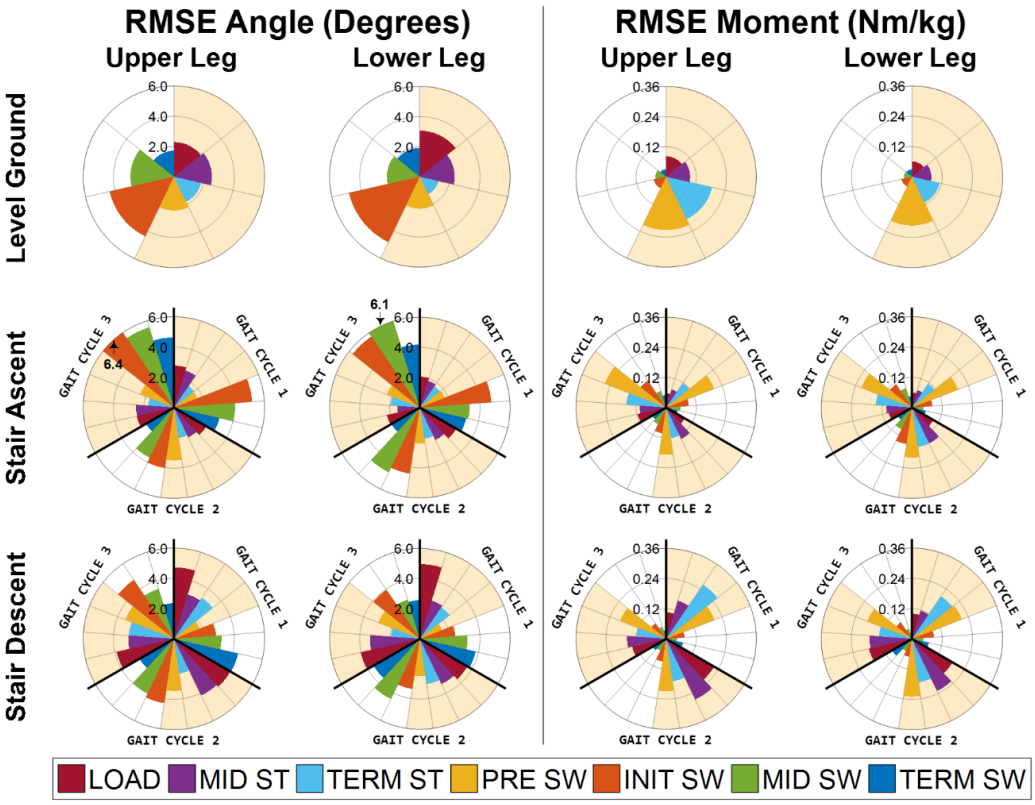

Supplementary Figure C.11. RMSE distribution within ambulation conditions of upper-leg and lower-leg NARX models for a representative able-bodied participant trained with aligned contralateral EMG ($AB4_{cEMG}$) for the continuous prediction of ankle angle and moment. Gait periods and stance and swing phases are defined the same as in **Figure 4.5**.

Supplementary Table C.1. Pairwise cross-correlations (R^2) for input and output trials (averaged across trials, participants, and ambulation conditions). Shank velocity and output trials for the AB_{cEMG} group are the same as the AB group.

		Within-Subject Trial-Wise Variability											
		TTA Group				**AB_{cEMG} Group**				**AB Group**			
		LW	**AS**	**DS**	$\overline{R^2}$	**LW**	**AS**	**DS**	$\overline{R^2}$	**LW**	**AS**	**DS**	$\overline{R^2}$
Input	**TibAnt**	0.87	0.75	0.79	0.80	0.90	0.90	0.79	0.86	0.91	0.89	0.75	0.85
	MedGas	0.92	0.83	0.82	0.86	0.93	0.90	0.86	0.90	0.95	0.89	0.87	0.90
	RecFem	0.92	0.86	0.83	0.87	0.94	0.89	0.91	0.91	0.92	0.87	0.87	0.89
	SemTen	0.88	0.84	0.80	0.84	0.89	0.84	0.80	0.85	0.89	0.85	0.81	0.85
	ML Shank Vel	0.51	0.48	0.4	0.46	na				0.65	0.53	0.49	0.56
	AP Shank Vel	0.99	0.96	0.95	0.97	na				0.99	0.98	0.98	0.98
	Vertical Shank Vel	0.91	0.92	0.87	0.90	na				0.94	0.95	0.95	0.95
Output	**Ankle Angle**	0.93	0.89	0.91	0.91	na				0.93	0.91	0.93	0.93
	Ankle Moment	0.99	0.94	0.91	0.94	na				0.99	0.96	0.95	0.97

		Correlation to Normal Pattern											
		TTA Group						**AB_{cEMG} Group**					
		LW	**AS**	**DS**	$\overline{R^2}$	R^2_{min}	R^2_{max}	**LW**	**AS**	**DS**	$\overline{R^2}$	R^2_{min}	R^2_{max}
EMG	**TibAnt**	0.59	0.53	0.61	0.58	0.47	0.78	0.89	0.83	0.71	0.81	0.66	0.92
	MedGas	0.70	0.63	0.59	0.64	0.51	0.86	0.93	0.73	0.58	0.75	0.49	0.98
	RecFem	0.84	0.73	0.65	0.74	0.57	0.92	0.86	0.74	0.69	0.76	0.61	0.95
	SemTen	0.67	0.69	0.53	0.63	0.48	0.82	0.81	0.65	0.62	0.69	0.54	0.91
Output	**Ankle Angle**	0.83	0.75	0.82	0.80	0.69	0.92	na					
	Ankle Moment	0.97	0.85	0.86	0.89	0.82	0.99	na					

na: not applicable

Supplementary Table C.2. RMSE and R^2 values of upper-leg and lower-leg NARX model predictions for each ambulation condition, individually for transtibial amputees (TTA) and averaged across able-bodied participants (AB and AB_{cEMG} groups). Values were calculated between experimentally measured targets and model predictions of ankle angle and moment using optimal model parameters for each model type.

Model Output	Units	Participant	Level Ground									
			Upper Leg				Lower Leg					
			$\overline{RMSE}$	σ_{RMSE}			$\overline{RMSE}$	σ_{RMSE}				
Angle	Degrees	**TTA1**	2.60	0.73			2.65	0.59				
		TTA2	2.53	0.68			2.75	0.54				
		TTA3	1.98	0.72			2.06	0.59				
		$\overline{AB}_{cEMG}$	2.63	0.54			2.70	0.66				
		$\overline{AB}$	2.62	0.58			2.03	0.35				
Moment	Nm/kg	**TTA1**	0.128	0.026			0.116	0.027				
		TTA2	0.097	0.032			0.118	0.026				
		TTA3	0.110	0.023			0.096	0.018				
		$\overline{AB}_{cEMG}$	0.112	0.016			0.106	0.015				
		$\overline{AB}$	0.103	0.011			0.071	0.010				
			$\overline{R^2}$	R^2_{min}	R^2_{max}		$\overline{R^2}$	R^2_{min}	R^2_{max}			
Angle	Unitless	**TTA1**	0.914	0.837	0.959		0.907	0.832	0.951			
		TTA2	0.908	0.784	0.965		0.886	0.707	0.934			
		TTA3	0.948	0.910	0.980		0.946	0.886	0.980			
		$\overline{AB}_{cEMG}$	0.929	0.895	0.948		0.923	0.868	0.940			
		$\overline{AB}$	0.927	0.890	0.948		0.957	0.952	0.972			
Moment		**TTA1**	0.968	0.936	0.989		0.977	0.946	0.989			
		TTA2	0.970	0.911	0.993		0.967	0.928	0.985			
		TTA3	0.978	0.952	0.994		0.982	0.970	0.990			
		$\overline{AB}_{cEMG}$	0.985	0.980	0.989		0.987	0.986	0.991			
		$\overline{AB}$	0.989	0.986	0.992		0.992	0.989	0.993			

Supplementary Table C.2. cont.

Model Output	Units	Participant	Stair Ascent								Stair Descent							
			Upper Leg				Lower Leg				Upper Leg				Lower Leg			
			$\overline{RMSE}$	σ_{RMSE}			$\overline{RMSE}$	σ_{RMSE}			$\overline{RMSE}$	σ_{RMSE}			$\overline{RMSE}$	σ_{RMSE}		
Angle	Degrees	**TTA1**	3.06	0.48			3.05	0.64			3.64	0.66			3.24	0.47		
		TTA2	3.24	0.67			3.42	0.46			3.69	0.79			3.54	0.56		
		TTA3	3.34	0.66			3.43	0.74			3.49	0.56			3.74	0.69		
		$\overline{AB}_{cEMG}$	3.42	0.31			3.31	0.22			3.61	0.48			3.46	0.41		
		$\overline{AB}$	3.42	0.35			2.49	0.16			3.23	0.56			2.65	0.19		
Moment	Nm/kg	**TTA1**	0.131	0.022			0.132	0.014			0.163	0.020			0.149	0.019		
		TTA2	0.141	0.024			0.151	0.027			0.161	0.018			0.167	0.030		
		TTA3	0.160	0.032			0.168	0.032			0.213	0.035			0.213	0.047		
		$\overline{AB}_{cEMG}$	0.142	0.021			0.136	0.018			0.157	0.025			0.161	0.021		
		$\overline{AB}$	0.135	0.013			0.094	0.020			0.143	0.027			0.108	0.011		
			$\overline{R^2}$	R^2_{min}	R^2_{max}		$\overline{R^2}$	R^2_{min}	R^2_{max}		$\overline{R^2}$	R^2_{min}	R^2_{max}		$\overline{R^2}$	R^2_{min}	R^2_{max}	
Angle	Unitless	**TTA1**	0.930	0.902	0.957		0.933	0.879	0.960		0.947	0.898	0.967		0.959	0.940	0.969	
		TTA2	0.947	0.899	0.971		0.949	0.928	0.963		0.966	0.935	0.988		0.970	0.951	0.980	
		TTA3	0.908	0.845	0.952		0.910	0.857	0.959		0.963	0.938	0.980		0.957	0.928	0.976	
		$\overline{AB}_{cEMG}$	0.919	0.877	0.948		0.923	0.880	0.946		0.946	0.927	0.965		0.951	0.942	0.964	
		$\overline{AB}$	0.920	0.891	0.953		0.954	0.912	0.972		0.956	0.937	0.973		0.971	0.963	0.980	
Moment		**TTA1**	0.974	0.958	0.985		0.974	0.961	0.982		0.957	0.934	0.969		0.962	0.938	0.974	
		TTA2	0.951	0.923	0.974		0.948	0.919	0.970		0.942	0.925	0.959		0.938	0.906	0.969	
		TTA3	0.962	0.921	0.984		0.959	0.928	0.977		0.935	0.870	0.960		0.930	0.836	0.972	
		$\overline{AB}_{cEMG}$	0.961	0.952	0.976		0.966	0.957	0.977		0.954	0.930	0.972		0.951	0.928	0.965	
		$\overline{AB}$	0.967	0.954	0.979		0.984	0.977	0.991		0.961	0.940	0.977		0.979	0.975	0.983	

Supplementary Table C.3. Within-subject three-way ANOVA. The factors are muscle group (upper leg and lower leg), ambulation condition (as seven gait cycles: 1-LW, 3-AS, and 3-DS), and gait period (loading response, mid-stance, terminal stance, pre-swing, initial swing, mid-swing, and terminal swing). Asterisk (*) indicate significance ($p < 0.05$) of higher upper-leg errors except TTA2 moment main effect.

Model Output	Participant	Main Effect muscle		
		$F(1,882)$ =	p value	
Angle	**TTA1**	2.67	0.103	
	TTA2	0.04	0.841	
	TTA3	2.39	0.123	
	AB1$_{cEMG}$	4E-03	0.949	
	AB2$_{cEMG}$	9.95	1.66E-03	*
	AB3$_{cEMG}$	0.34	0.558	
	AB4$_{cEMG}$	2.56	0.110	
	AB5$_{cEMG}$	0.60	0.439	
	AB6$_{cEMG}$	5.30	0.022	*
	AB1	17.28	3.54E-05	*
	AB2	16.91	4.29E-05	*
	AB3	36.31	2.47E-09	*
	AB4	78.30	4.77E-18	*
	AB5	9.41	2.22E-03	*
	AB6	152.15	2.31E-32	*
Moment	**TTA1**	0.68	0.410	
	TTA2	4.60	0.032	*
	TTA3	1.39	0.238	
	AB1$_{cEMG}$	0.83	0.363	
	AB2$_{cEMG}$	5.74	0.017	*
	AB3$_{cEMG}$	0.96	0.326	
	AB4$_{cEMG}$	1.10	0.296	
	AB5$_{cEMG}$	0.46	0.499	
	AB6$_{cEMG}$	0.02	0.876	
	AB1	52.48	9.56E-13	*
	AB2	32.09	1.99E-08	*
	AB3	63.50	4.93E-15	*
	AB4	167.02	4.09E-35	*
	AB5	10.65	1.14E-03	*
	AB6	191.61	1.41E-39	*

Supplementary Table C.3. cont.

Model Output	Participant	Interactions					
		muscle*gait cycle		muscle*gait period		muscle*gait cycle*gait period	
		$F(6,882)$ =	p value	$F(6,882)$ =	p value	$F(36,882)$ =	p value
Angle	**TTA1**	0.38	0.893	1.52	0.168	0.64	0.951
	TTA2	1.68	0.123	0.58	0.745	0.79	0.802
	TTA3	0.64	0.698	0.31	0.929	0.72	0.886
	AB1$_{cEMG}$	0.66	0.680	0.67	0.671	0.88	0.673
	AB2$_{cEMG}$	1.02	0.410	0.82	0.557	0.74	0.867
	AB3$_{cEMG}$	0.53	0.789	0.91	0.487	0.81	0.780
	AB4$_{cEMG}$	0.37	0.897	0.41	0.870	0.53	0.991
	AB5$_{cEMG}$	0.82	0.558	0.51	0.803	0.69	0.918
	AB6$_{cEMG}$	1.10	0.360	0.81	0.564	0.37	0.999
	AB1	1.38	0.220	1.05	0.391	0.55	0.986
	AB2	2.82	1.01E-02 *	0.57	0.754	1.10	0.323
	AB3	1.47	0.18	1.20	0.305	0.84	0.735
	AB4	4.63	1.21E-04 *	2.32	3.12E-02 *	0.68	0.927
	AB5	2.91	8.12E-03 *	0.99	0.432	1.05	0.384
	AB6	1.37	0.22	4.99	4.90E-05 *	1.23	0.170
Moment	**TTA1**	1.29	0.258	1.29	0.258	0.62	0.960
	TTA2	0.90	0.493	0.39	0.886	0.67	0.932
	TTA3	1.10	0.362	0.68	0.667	0.52	0.992
	AB1$_{cEMG}$	1.78	0.100	3.22	3.91E-03 *	0.56	0.984
	AB2$_{cEMG}$	0.84	0.537	0.80	0.568	1.00	0.476
	AB3$_{cEMG}$	0.60	0.728	0.47	0.829	0.79	0.812
	AB4$_{cEMG}$	1.58	0.151	0.35	0.911	0.50	0.995
	AB5$_{cEMG}$	1.41	0.208	0.86	0.526	0.65	0.947
	AB6$_{cEMG}$	1.90	0.078	1.10	0.361	0.89	0.659
	AB1	2.42	2.49E-02 *	3.37	2.75E-03 *	0.92	0.603
	AB2	2.74	1.21E-02 *	3.21	4.05E-03 *	1.19	0.205
	AB3	1.65	0.129	2.14	0.047 *	1.07	0.360
	AB4	3.00	6.65E-03 *	9.94	1.23E-10 *	1.21	0.185
	AB5	1.73	0.111	3.77	1.02E-03 *	1.11	0.303
	AB6	3.42	2.44E-03 *	5.46	1.47E-05 *	1.03	0.429

APPENDIX D: SYSTEM INTEGRATION AND CONNECTIONS FOR GAIT ANALYSIS

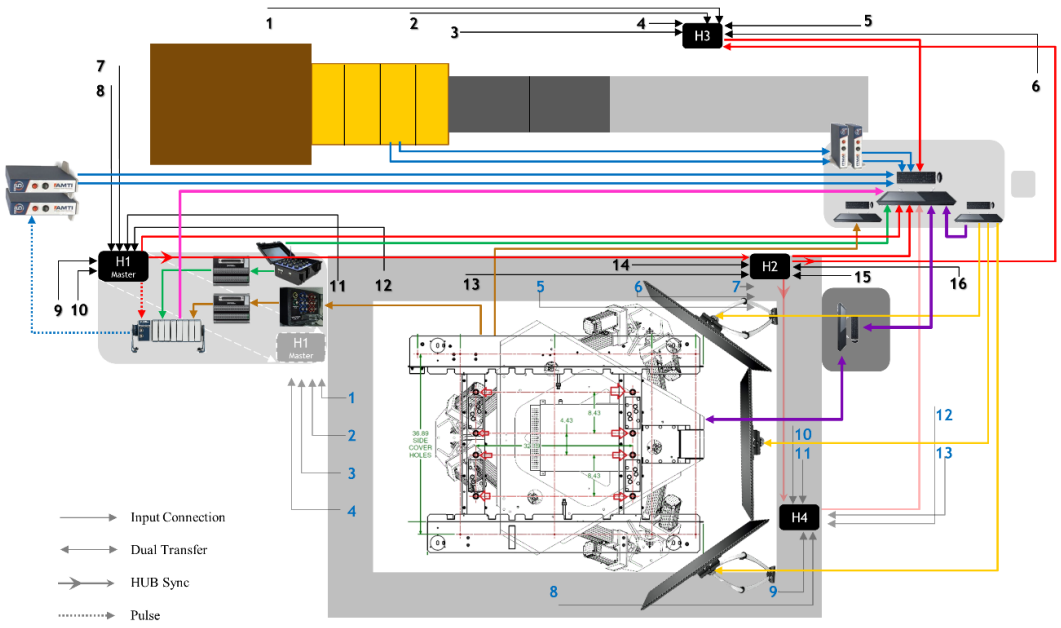

Supplementary Figure D.1. Instrumented walkway and motion base systems.

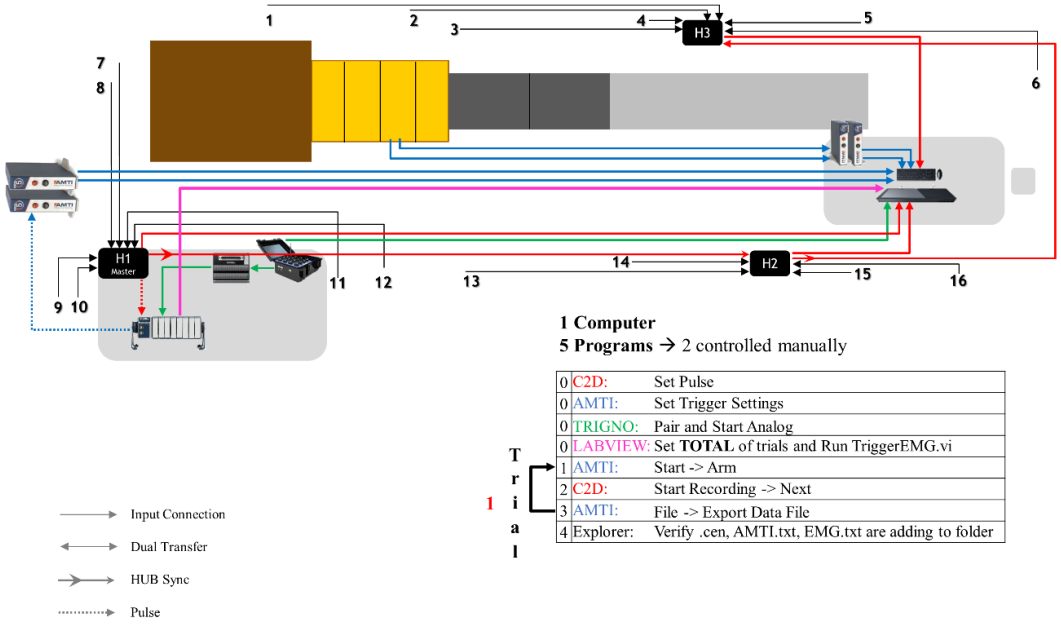

Supplementary Figure D.2. Data collection workflow for level overground walking and stair ambulation on the instrumented walkway.

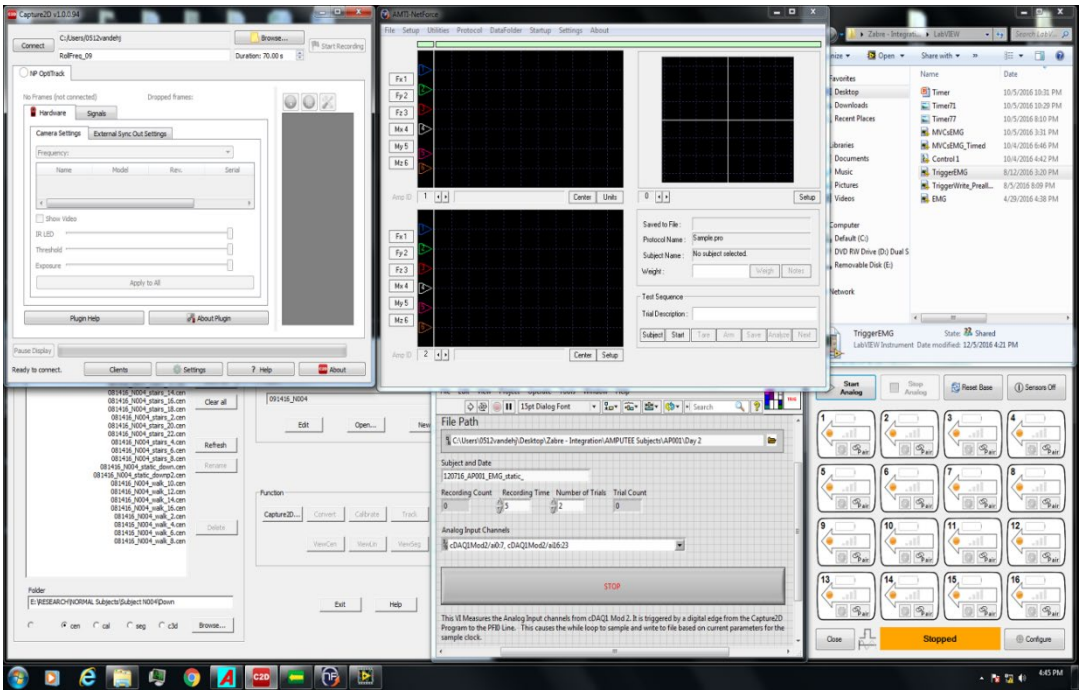

Supplementary Figure D.3. Software for data collection on the instrumented walkway. Caputre2D, AMTI NetForce, AMASS, LabVIEW, and Trigno Utility Control are shown.

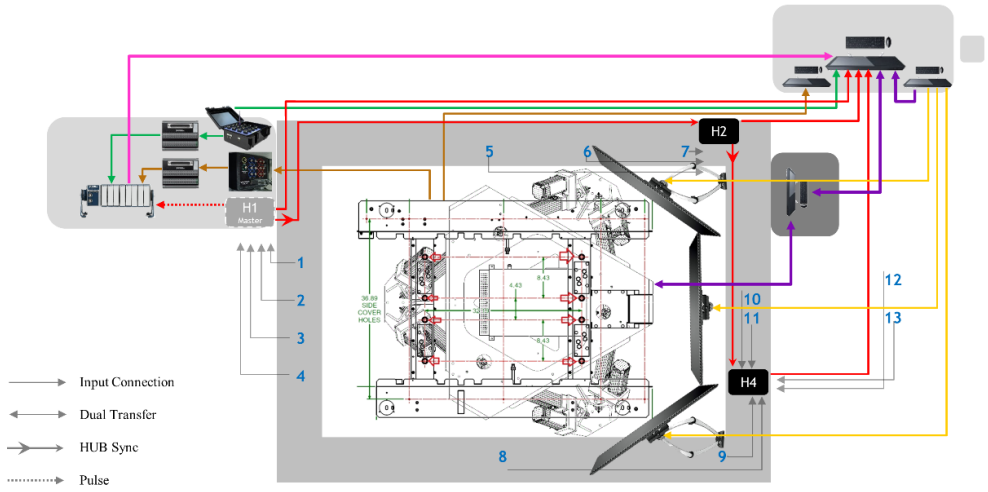

Supplementary Figure D.4. Motion base system with visual feedback for ramp incline, ramp decline and level treadmill walking conditions.

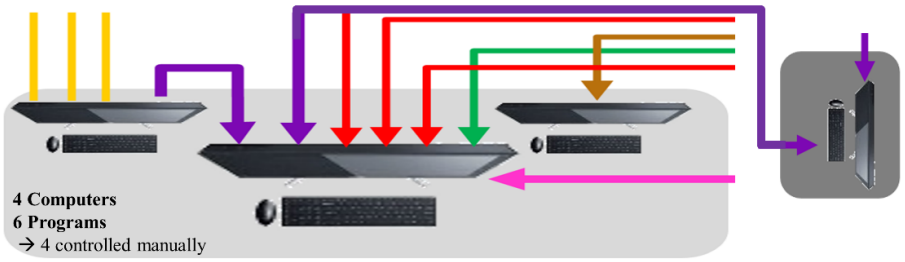

	0		Turn on MOOG Computer and Run App	
	0		C2D: Set Pulse, Time, Folder, Filename	
	0		TRIGNO: Pair and Start Analog	
	0			Treadmill: Set Speed and Pause belts
Only 1 Trial	1		LABVIEW: 1.1: Recording time as C2D, set 2 trials, update filename and folder 1.2: Click: TEST ON 1.3: Run IV (Base will engage)	
	2	Unity: Input Speed and Run		
	3		LABVIEW: Click: Unity Yes	
	4			Treadmill: Unpause belts
	5		C2D: Start Recording (Trial 1) -> Next	
	6			Treadmill: Pause belts
	7		C2D: Start Recording (Trial 2) -> Stop -> Delete	
	8		LABVIEW: 8.1: Stop VI with Halt (Base will disengage) 8.2: Close LabVIEW 8.3: Reopen VI and repeat from 1	

Supplementary Figure D.5. Data collection workflow for motion base system with visual feedback.

APPENDIX E: TESTING CHECKLIST – GAIT ANALYSIS PROTOCOL

Protocol including all ambulation conditions (Instrumented Walkway and Motion Base with Visual Feedback).

Before Testing Day

- ☐ Send confirmation email with date, time, and location to test subject. Remind of tight shorts and t-shirt, athletic shoes (same as previous sessions if applicable), no recent injuries

Before Testing Day or Before Subject Arrival (30-45 mins)

- ☐ Rewire and reorient cameras and HUBs to Walkway Mode. Use detailed connection diagram (**HPL System.pdf**, **Supplementary Figure D.2**) and photos with reflective markers on walkway as a guide. Put retractable barriers in place
- ☐ Verify treadmill sensors offsets and force-voltage calibration

Testing Day – Before Subject Arrival (30-45 mins)

- ☐ Turn on master computer, motion base, treadmill, motion base computer (MBC), treadmill computer, TV displays, and Unity computer
- ☐ On Master Computer, create a main New Folder for subject using subject's ID number. Create a subfolder called Day # to refer to the session number
- ☐ Cameras Calibration for Walkway Mode
  - Clear walkway for calibration by removing chairs, landing platform, and staircase
  - Launch **AMASS**, create a New Project (*MMDDYY_SubjectID#)* in subject's main folder, and update settings (see list below)
  - Launch **Capture2D** from **AMASS**
  - Place L-frame on floor force plates with the arrow pointing north as going "up the stairs". Use L-frame screw and levels as alignment guide
  - Verify that all cameras have the L-frame in view and cover any reflective areas
  - Update filename to *MMDDYY_SubjectID#_cal_up* and complete 140 seconds of wanding calibration with proper technique
  - In **AMASS**, calibrate file. Aim for >90% Image for every camera. If lower, verify field of view or retake calibration. If satisfied, close window
  - Repeat with L-frame facing south as going "down the stairs". Name file as *MMDDYY_SubjectID#_cal_down*
- ☐ Set equipment for Stair Ambulation Condition
  - Without touching, moving tripods and cameras, wheel staircase to align legs with floor marks and floor force plate edge with 1st stair step. Avoid wheeling staircase over floor force plates
  - Wheel landing platform. Use floor marks and black spacers for alignment. Lower and secure legs and check stability by walking on landing platform
  - For able-bodied subjects, remove staircase handrails and landing platform guardrails
  - Pull the AMTI GEN5s (#1&2) from the wall, connect USB and Pulse cable, and zero plates
  - Connect staircase cables to AMTI GEN5s (#3&4), zero plates, and pull cables out of space
  - Verify staircase level and remove handles
- ☐ Put all instruments, materials, and consumables containers needed for testing on a table
- ☐ Prepare 25 reflective markers with adhesive and cover-roll stretch tape
- ☐ Clean 16 EMG sensors with alcohol wipes, dry and apply adhesive, turn on and start running **Trigno Utility Control**, verify signal and battery
- ☐ Print out Consent, EMG Questionnaire, Participant Record, and Payment Verification forms
- ☐ In the last session, have payment available
- ☐ Open software and update settings

- **AMASS**: Calibrate: Reference marker file; Track: Error: 5, Residual: 3, Cameras: 2, Diam: 14, Calibration File; Identify: Leave empty Marker and Link files
- **AMTI Netforce**: Hardware Installation; Export and File Options; Set/View Protocol: Data Rate: 1200; Data Folder; Hardware Zero; Acquisition Settings; Trigger Settings: Event Type: [x] by External Source, Edge: Rising, Trigger Position: 5%, Amp ID 1&3
- **Capture2D**: Countdown: 2 s
- **Trigno Utility Control**
- **TriggerEMG.vi**
- **Explorer** Data Folder
- **MVCsEMG_Timed.vi**
- **NI Max**

Testing Day – Subject Arrival and Preparation (60 mins)

- Greet subject and ask to change clothing if necessary
- Explain testing protocol briefly and answer any question or concerns
- Subject will fill out and sign (4) forms if required
- During any time of the testing, allow subject to rest and offer water
- Take subject measurements: ○ Knee diameter ○ ankle diameter
- Place markers on skin (except greater trochanter)
  - 2nd and 5th metatarsal
  - Heel: leveled with 2nd metatarsal
  - Lateral and medial malleolus
  - Tip of shoe: in line with 2nd metatarsal
  - Shank: in line with lateral knee and ankle markers at widest shank width
  - Lateral and medial femur epicondyles
  - Thigh: in line with lateral knee and greater trochanter markers, below hand plane
  - Greater trochanter: over shorts
  - Middle point of PSIS and ASIS
- Take subject measurements:
  ○ ASIS distance ○ASIS to lateral malleoli ○ Heel to shoe tip ○ 2nd metatarsal to shoe tip
- To place EMG (16) electrodes, wipe skin over muscle belly with alcohol wipe, follow Participant Record Form for number order, place electrodes with arrow pointing up and in line with muscle belly
- Test EMG signals using **NI Max** software by instructing subject to contract the specific muscle
- Wrap EMG electrodes with COBAN
- MVCs Data Collection
  - Pull testing bed closer to computer desk
  - In **MVCsEMG_Timed.vi,** update testing information and select muscle group (9)
  - Instruct subject about experiment (3 series of maximal contraction with resting states) and run VI
    - Tibialis anterior: *subject*: standing up, dorsiflexes; *tester*: holds foot down against floor
    - M/L Gastrocnemius: *tester*: adjust aluminum bar to shoulder's subject height, place wedge on floor against aluminum frame; *subject*: with locked knee, contracts calf by pushing up against the aluminum bar
    - Quadriceps: *subject*: lying down facing up with plastic tube underneath knee, extends knee; *tester*: holds shank down
    - Hamstrings: *subject*: lying down facing down with plastic tube underneath ankle, flexes knee; *tester*: holds shank down
    - Lower back: *subject*: lying down facing down with straps around shanks and thighs, extends back upward; *tester*: holds upper back down
- Remove testing bed and check marker and electrode placement

Testing Day – Walking and Stair Ascent/Descent Conditions (50 mins)

- In **Capture2D**, set pulse parameters in External Sync Out Settings

- ○ Mode: On during recording ○ Duration: Recording level
- ○ Pulse Phase: In phase ○ [x] Invert pulse polarity

- Run Static Trials
  - Place 16 reflective markers on each corner of the 4 force plates
  - In **AMTI NetForce**, zero unloaded plates
  - Set filenames to:
    - **Capture2D**: *MMDDYY_SubjectID#_static_up*
    - **AMTI NetForce**: *MMDDYY_SubjectID#_Force_static*
    - **TriggerEMG.vi**: *MMDDYY_SubjectID#_EMG_static*
  - Set settings to:
    - **Capture2D**: Duration: 5 s
    - **AMTI NetForce**: Duration: 5 s; File Seed No.: 00000
    - **TriggerEMG.vi**: Recording Time: 5 s; Number of Trials: 1
  - Ask subject to stand on plate #1 facing north with anatomical position (or arms crossed across chest) and not to move for 5 seconds when signaled
  - Take Static Up trial and save EMG and Force baseline files
    - Run **TriggerEMG.vi**, Start and Arm in **AMTI NetForce**, Start Recording in **Capture2D,** signal subject not to move
    - Next **Capture2D,** Export Data File in **AMTI NetForce.** Verify EMG and force data files
  - Take Static Down trial
    - Ask subject to face south. Take only kinematic data in **Capture2D** by changing filename to *MMDDYY_SubjectID#_static_down*
  - Ensure that at least one static trial has all (41) markers visible by tracking in **AMASS**. Look for noise, and dropped and ghost markers. Verify also in Dynamic files and Motion Base files
  - Remove force plate markers (16)
- Run Stair Ascent/Descent Dynamic Trials
  - Instruct subject on how to ambulate during trial, which signals to expect, and from where to start
  - Set filenames to:
    - **Capture2D**: *MMDDYY_SubjectID#_stairs_*
    - **AMTI NetForce**: *MMDDYY_SubjectID#_Force_stairs_*
    - **TriggerEMG.vi**: *MMDDYY_SubjectID#_EMG_stairs_*
  - Set settings to:
    - **Capture2D**: Duration: 10 s
    - **AMTI NetForce**: Duration: 10.5 s; File Seed No.: 00000
    - **TriggerEMG.vi**: Recording Time: 10 s; Number of Trials: 30
  - Take Dynamic trials and save files
    - Run **TriggerEMG.vi**
    - 1. Start and Arm in **AMTI NetForce**, Start Recording in **Capture2D**
    - 2. Stair Ascent or Descent: signal subject "Ready, Go, Turn around"
    - 3. Next **Capture2D,** Export Data File in **AMTI NetForce**
    - On the Participant Record Form, record successful/unsuccessful hits on each force plate
    - After 2 or 4 trials, verify content of kinematic, EMG, and force data files. Subsequently, only verify that files are being created in data folder
    - Repeat until all stair ascent/descent trials are collected
- Run Walking Dynamic Trials
  - Disconnect staircase cables and turn off AMTI GEN5s (#3&4)
  - In **AMTI NetForce**, update Hardware Installation and Amp ID to 1&2
  - Without touching, moving tripods and cameras, remove landing platform and staircase from walkway. If cameras are even slightly moved, new calibrations (up and down) must be recorded
  - Set filenames to:
    - **Capture2D**: *MMDDYY_SubjectID#_walk_*

        - **AMTI NetForce**: *MMDDYY_SubjectID#_Force_walk_*
        - **TriggerEMG.vi**: *MMDDYY_SubjectID#_EMG_walk_*
    - Set settings to:
        - **Capture2D**: Duration: 8 s
        - **AMTI NetForce**: Duration: 8.4 s; File Seed No.: 00000
        - **TriggerEMG.vi**: Recording Time: 8 s; Number of Trials: 16
    - Take Dynamic trials as described previously under Stair Ascent/Descent

Testing Day – Motion Base with Visual Feedback Mode: Ramp Incline/Decline Condition (60 mins)

- Disconnect and return AMTI GEN5s (#1&2) to the wall
- Rewire cameras and HUBs to Motion Base with Visual Feedback Mode. Use detailed connection diagram (**HPL System.pdf**, **Supplementary Figure D.4**)
- On Master Computer, close **AMTI NetForce** and **TriggerEMG.vi,** open **HostController.vi,** set LabVIEW priority to 'Real Time' under Task Manager
- On MBC, ensure system is running
- On Unity Computer, open Unity simulation. Turn on TV displays
- On Treadmill Computer, open treadmill control software
- Run motion base and unity program to ensure no immediate errors
- Cameras Calibration for Motion Base Mode
    - Engage motion base and remove velcro treadmill (4) markers
    - Place L-frame on middle of the treadmill with the arrow pointing south (TV displays)
    - Verify that all cameras have the L-frame in view and cover any reflective areas
    - Update filename as *MMDDYY_SubjectID#_cal_MOOG* and complete 120 seconds of wanding calibration with proper technique
    - In **AMASS**, calibrate file. Aim for >90% Image for every camera. If lower, verify field of view or retake calibration. If satisfied, apply and close
- Fit subject with safety harness and verify marker placement
- In **Capture2D**, set pulse parameters in External Sync Out Settings
  ○ Mode: On during recording ○ Duration: Recording level
  ○ Pulse Phase: In phase ○ [x] Invert pulse polarity
- Run Static trial and save EMG and Force baseline files
    - Place velcro treadmill (4) markers
    - Engage motion base and secure subject to fall-arrest system. Point out emergency stop
    - Ask subject to cross arms across chest and stand still
    - In **Capture2D,** change filename to *MMDDYY_SubjectID#_static_MOOG* and record 5 s
        - ADD/Verify **HostController.vi** can record EMG and Force baseline files
    - Ensure static trial is valid by tracking in **AMASS**
- Run Ramp Incline/Decline Dynamic Trials
    - Verify treadmill Reverse mode. Begin treadmill and increase speed gradually until subject's self-selected speed (SSS) is reached. Pause belts and record speed on Participant Record Form
    - Follow **Motion Base System with Visual Feedback Data Collection** in **HPL System.pdf** (**Supplementary Figure D.5**) to collect and save data in each of the following runs:
        - Run a single trial of 35 s at SSS. Verify content of kinematic and EMG&Force files
            - Set filenames to:
                - **Capture2D**: *MMDDYY_SubjectID#_MOOG_single*
                - **HostController.vi**: *MMDDYY_SubjectID#_EMG&Force_MOOG_single*
            - Set settings to:
                - **Capture2D**: Duration: 5 s
                - **HostController.vi**: Recording Time: 5 s; Number of Trials: 2

        - Run 2 multiple trial simulation (7s-8 trials) of ~5 mins each at SSS. Change filename from _1 to _2 to avoid overwriting files. Verify content of files at the end of each run
            - Set filenames to:
                - **Capture2D**: *MMDDYY_SubjectID#_MOOG_multi_1*
                - **HostController.vi**: *MMDDYY_SubjectID#_EMG&Force_MOOG_multi_1*
            - Set settings to:
                - **Capture2D**: Duration: 290 s
                - **HostController.vi**: Recording Time: 290 s; Number of Trials: 2
        - If required, run multiple trial simulation (7s – 8 trials) of ~5 mins each at different speeds
    - After all trials are collected, disengage motion base and remove subject fall-arrest harness system

Testing Day – Subject Dismissal (15 mins)

- Remove EMG electrodes and markers from subject
- If last session, sign Payment Verification Form and make payment
- Thank and escort subject out of the room/building

After Subject Dismissal (30-45 mins)

- Organize files to subfolders labeled MOOG: MVCs and Walkway: UP, DOWN, MVCs. If necessary, rename files to match kinematic, EMG, and force names and numbers
- Copy and rename AMASS project file into subfolders MOOG: *MMDDYY_SubjectID#_MOOG*, UP: *MMDDYY_SubjectID#_up*, and DOWN: *MMDDYY_SubjectID#_down*
- Compile all information on Participant Record Form
- Clean 16 EMG sensors with alcohol wipes and place them in the Trigno box
- Turn off equipment and computers
- Put all instruments, materials, and consumables containers in cabinet
- Prepare lab for class
    - Wheel in staircase and landing platform
    - Disconnect cameras and move tripods and retractable barriers
    - Move chairs back around tables